Improving iron oxide-based adsorbents for phosphate recovery from surface water using Mössbauer spectroscopy as main analytical tool

Belloni, C.

DOI
10.4233/uuid:53e46ea5-5802-42cf-814f-4bb2bf76aadc

Publication date
2023

Document Version
Final published version

Citation (APA)
Belloni, C. (2023). *Improving iron oxide-based adsorbents for phosphate recovery from surface water using Mössbauer spectroscopy as main analytical tool*. https://doi.org/10.4233/uuid:53e46ea5-5802-42cf-814f-4bb2bf76aadc

Important note
To cite this publication, please use the final published version (if applicable).
Please check the document version above.

IMPROVING IRON OXIDE-BASED ADSORBENTS FOR PHOSPHATE RECOVERY FROM SURFACE WATER

USING MÖSSBAUER SPECTROSCOPY AS MAIN ANALYTICAL TOOL

CARLO BELLONI

M.Sc. Carlo Belloni,

Improving iron oxide-based adsorbents for phosphate recovery from surface water, using Mössbauer spectroscopy as main analytical tool,

280 pages,

This work was performed in the cooperation framework of Wetsus and Delft University of Technology. This work is part of the "Phosphate Recovery Theme" at Wetsus. This research received funding from the Netherlands Organization for Scientific Research (NWO) in the framework of the Innovation Fund for Chemistry, and from the Ministry of Economic Affairs and Climate Policy in the framework of the TKI/PPS-Toeslagregeling.

Printed by: **Ridder**print

Cover concept: Carlo Belloni

Cover design: Carlo Belloni, Laura Silvestri, Andrea Belloni

ISBN/EAN: 978-90-8593-559-9

An electronic version of this dissertation is available at: http://repository.tudelft.nl/

IMPROVING IRON OXIDE-BASED ADSORBENTS FOR PHOSPHATE RECOVERY FROM SURFACE WATER

USING MÖSSBAUER SPECTROSCOPY AS MAIN ANALYTICAL TOOL

Dissertation

for the purpose of obtaining the degree of doctor
at Delft University of Technology
by the authority of the Rector Magnificus, Prof. dr. ir. T.H.J.J. van der Hagen
chair of the Board for Doctorates
to be defended publicly on
Monday 12th of June 2023 at 17:30

By

Carlo BELLONI

Master of Science in Physics
Università degli Studi di Padova, Italia
Born in Camposampiero (PD), Italia

This dissertation has been approved by the promotors:

promotor:	Prof. dr. E.H. Brück
promotor:	Prof. dr. G.J. Witkamp
copromotor:	dr. A.I. Dugulan

Composition of the doctoral committee:

Rector Magnificus,	chairperson
Prof. dr. E.H. Brück	Technische Universiteit Delft
Prof. dr. G.J. Witkamp	Technische Universiteit Delft
dr. A.I. Dugulan	Technische Universiteit Delft

Independent members:

Prof. dr. ir. A. Soares	Cranfield University
dr. P.S. Kumar	Plaksha University
Prof. dr. ir. D. van Halem	Technische Universiteit Delft
Prof. dr. S.J. Picken	Technische Universiteit Delft

Ir. L. Korving of Wetsus has contributed greatly to the preparation of this dissertation.

TU Delft, Reactor Institute, TNW-RST, FAME group
Casimir PhD series, Delft-Leiden, 2023-11

To everyone who

supported me throughout this journey,

and myself.

Popular summary of this thesis

This thesis focuses on recycling resources while preserving water quality and availability. This concept is at the basis of a healthy and sustainable society yet works needs to be done. Water scarcity will be a growing challenge that humanity will have to face in the coming years, due to poor resource management and the climate change crisis. Waters cover 70 % of our planet, but only 3 % of it is freshwater, and only 1 % is easily accessible. Already more than 2 billion people live in water-stressed countries.

Moreover, in some ways, this thesis will show how there is a thin line between resources and waste, nutrients and pollutants, impurity and added value. This thin line is both defined by our everyday life choices, the name we give to things, and their related connotation.

Food is fundamental for life. From humans to bacteria, from animals to plants and fungi, we all consume food, although in different forms. This is because food contains different compounds, or nutrients, which are necessary to the organism to carry out the vital functions. Among these nutrients, phosphorus is one of the most important. Phosphorus is involved in many vital functions of living beings. In humans, it is present in the DNA, bones, teeth, and so on. We assume phosphorus through food, both animal- and plant-based, in the form of phosphate. Phosphate is a molecule containing one atom of phosphorus (P) and four atoms of oxygen (O). As a product, we make many uses of phosphate, in many industries, including pharmaceutical, construction, electronics, and many others, with the main one being agriculture. In agriculture, phosphate is used as an essential and irreplaceable component of fertilizers. It is necessary to produce fruits, vegetables, and animal feedstock, and hence to sustain the world population and its growth. We get phosphate from phosphate rock mines, which are present only in a few countries, and its extraction is also cause of pollution (as for any mining activity).

Once we excrete food, this goes to municipal wastewater treatment plants. Here, pollutants are removed, while nutrients, like phosphate, are partially removed (and possibly recovered). This means that some phosphate will eventually end up in surface waters.

At the same time, overuse of fertilizers causes phosphate to accumulate in soil, eventually leaching into water streams and bodies.

In surface waters, phosphate can accumulate becoming a pollutant. In fact, phosphate serves as nutrient to organisms living in water, such as algae. However, an overload of nutrients in water, called eutrophication, can lead to algae population overgrowth, called algae blooms. This results in the dirty, greenish, and slimy layer that we sometimes see covering canals, rivers, and lakes. An algae bloom can have a detrimental impact on many levels. Environmentally, it can lead to the death of a water body, while for human health, some algae can be highly toxic. From a socioeconomic perspective, an algae bloom can strongly affect the tourism, housing, and fishing industries, among

others. Interestingly, through this consumption chain, phosphate transformed from a resource to waste, from a nutrient to a pollutant.

Therefore, two concurrent actions are necessary: removing phosphate from water, to avoid pollution, and recovering such an important yet finite resource, to be reused, for example, as a fertilizer. This would lead to a circular use of phosphate. As previously said, this is already partially done in wastewater treatment plants, but not to the extent to prevent surface water eutrophication. For this, phosphate needs to be removed from water down to the so called ultra-low concentrations, below 0.01 mg/L or 10 ppb (parts per billion). It means a concentration equivalent to a serving spoon of salt dissolved in an Olympic swimming pool. Alternatively, for those who prefer comparison to distances, the distance between your ears compared to the diameter of the Earth, or the length of a B-segment (subcompact car) compared to the average Earth-Moon distance.

To achieve these goals, one of the most promising technologies is adsorption. Compared to the better-known absorption, in which substances pass through or enter a larger material (e.g., when we dry water with absorbing kitchen paper), during adsorption a compound adhere to the surface of another material. This material is called an adsorbent. Adsorption is potentially able to reach ultra-low concentrations, and once the adsorbent is fully covered with phosphate, this can be separated (desorbed) and recovered. To do so, the adsorbent surface needs to be able to selectively attract phosphate, even when there is little of it in water. This property is called affinity and tell us how much an adsorbent and phosphate like each other (like for human relationships). At the same time, adsorption must not be too strong to prevent phosphate recovery. In this sense, a promising category of adsorbent are iron oxides, generally referred to as rust.

One last important point to make this technology economically affordable is that the adsorbent needs to be reused multiple times. This means that it needs to be able to go through multiple phosphate adsorption and phosphate desorption/recovery cycles. This is fundamental to be able to apply this technology in the real world. Without this regeneration of the adsorbent, it would be too expensive and require too much use of materials: it would not be worth it.

This thesis work focused on improving the properties and performances of iron oxide-based adsorbents for phosphate removal and recovery from surface waters. The main goal was to identify strategies to increase the affinity of iron oxide-based adsorbents for phosphate, while improving their stability and durability.

The strategy adopted to manipulate iron oxides and their surface properties is doping. Doping is a technique which consists of adding some impurities into a material to change its properties. Excluding the infelicitous unethical (and illegal) sport-related practices, doping is widely applied to electronics, like the circuits in our smartphones and computers. Like adding chocolate droplets to biscuits to make them more appetizing or adding salt to a chocolate bar to dramatically change the flavor, doping can improve iron oxides to make them more performing, for instance increasing their affinity for

phosphate. Surprisingly, an impurity can prove resourceful and valuable, and added value to iron oxides.

This investigation was carried out using iron oxide nanoparticles (about 100 nm x 20 nm), meaning particles of ten-to-hundred thousand times smaller than a millimeter. A nanometer is a billionth of a meter, ten-to-hundred thousand times smaller than the width of our hair, or the thickness of a paper sheet. If a person would be one nanometer tall, a millimeter would be longer than the whole of Italy, precisely, from Capo delle Correnti to München. Even longer than driving from Padova to Delft and then to Leeuwarden. This jump into such small scales allowed to better investigate the interaction between phosphate and iron oxide, while providing some flexibility on their manipulation through doping.

Moreover, in this work, a particular technique was used to study these iron oxides and the effect of doping: Mössbauer spectroscopy. Mössbauer spectroscopy is a nuclear technique, which uses nuclear gamma radiation to study the properties of iron compounds. This can be thought off as when we do X-rays at the hospital. There, we irradiate a part of our body, for example to obtain a "picture" of our bones and comparing it with how a bone should look like, we (or better, doctors) can draw conclusions. With Mössbuaer spectroscopy, we can take sort of "pictures" (called spectra) of iron oxides. Comparing spectra between each other and with reference spectra, we can see for instance the effect of doping, or the effect of prolonged use, on the iron oxides.

This thesis consists of a journey throughout adsorbent development, from doping of iron oxide nanoparticles to implementation of such nanoparticles into a commercial-like adsorbent. It is shown how doping can constitute a promising strategy to improve the surface properties of an adsorbent to effectively recover phosphate from water. In this sense, zinc seems to be a promising dopant. Also, this thesis provides improved understanding on the characteristics and phosphate adsorption/desorption mechanism on a specific category of (commercial) adsorbents. The experimental conditions which can mainly influence the results and interpretations have been highlighted. At the end, based on experimental observations and the experience gained, perspectives and recommendations for future research are provided. More focus should be spent on affinity and surface properties rather than the surface magnitude, and tests should be performed at conditions as close as possible to those of the application.

Populaire samenvatting van dit proefschrift

Dit proefschrift richt zich op zowel het recyclen van grondstoffen als het verbeteren van de waterkwaliteit en de beschikbaarheid van water. Dit is cruciaal voor een gezonde en duurzame samenleving, maar er moet nog veel gebeuren. Door slecht beheer van onze hulpbronnen en klimaatverandering, is waterschaarste een groeiende uitdaging waarmee de mensheid de komende jaren wordt geconfronteerd. Water bedekt 70 % van onze planeet, maar slechts 3 % daarvan is zoet water en slechts 1 % is gemakkelijk toegankelijk. Nu al leven meer dan 2 miljard mensen in landen met watertekorten.

Bovendien is er, zoals zal blijkt uit dit proefschrift, een dunne lijn tussen grondstoffen en afval, voedingsstoffen en verontreinigende stoffen, onzuiverheid en toegevoegde waarde. Deze dunne lijn wordt bepaald door onze dagelijkse keuzes, de naam die we aan dingen geven en de bijbehorende connotatie.

Voedsel is fundamenteel voor het leven. Van mensen tot bacteriën, van dieren tot planten en schimmels, we consumeren allemaal voedsel, zij het in verschillende vormen. Dat komt omdat voedsel verschillende verbindingen (nutriënten) bevat die het organisme nodig heeft om zijn vitale functies uit te voeren. Van deze nutriënten is fosfor één van de belangrijkste. Fosfor is betrokken bij vele vitale functies van levende wezens. Bij de mens is het aanwezig in het DNA, de botten, de tanden, enz. Wij nemen fosfor op via ons voedsel, zowel dierlijk als plantaardig, in de vorm van fosfaat. Fosfaat is een molecuul met één atoom fosfor (P) en vier atomen zuurstof (O). Als product wordt fosfaat in vele sectoren gebruikt, zoals de farmaceutische industrie, de bouw en de elektronica, maar de belangrijkste is de landbouw. In de landbouw wordt fosfaat gebruikt als een essentieel en onvervangbaar bestanddeel van meststoffen. Het is nodig om fruit, groenten en veevoeder te produceren en zo de wereldbevolking en haar groei in stand te houden. We halen fosfaat uit fosfaaterts, dat slechts in enkele landen aanwezig is. De winning ervan beïnvloedt het landschap en veroorzaakt vervuiling (zoals bij elke mijnbouwactiviteit).

Zodra we voedsel uitscheiden, gaat dit naar gemeentelijke waterzuiveringsinstallaties. Hier worden verontreinigende stoffen evenals nutriënten, zoals fosfaat, grotendeels worden verwijderd. In sommige gevallen wordt fosfaat ook al teruggewonnen. Dit betekent desondanks dat toch nog een deel van het fosfaat uiteindelijk in het oppervlaktewater terechtkomt.

Tegelijkertijd zorgt overmatig gebruik van meststoffen ervoor dat fosfaat zich ophoopt in de bodem en uiteindelijk uitspoelt in waterstromen en -lichamen.

In oppervlaktewateren kan fosfaat zich ophopen en een verontreinigende stof worden. In feite dient fosfaat als voedingsstof voor organismen die in het water leven, zoals algen. Een overvloed aan voedingsstoffen in het water, eutrofiëring genoemd, kan echter leiden tot overmatige groei van algen, algenbloei genoemd. Dit resulteert in de vieze, groenige en slijmerige laag die we soms zien op kanalen, rivieren en meren. Een algenbloei kan op vele niveaus schadelijke gevolgen hebben. Op milieugebied kan het leiden

tot de dood van een waterlichaam, terwijl voor de menselijke gezondheid sommige algen zeer giftig kunnen zijn. Vanuit sociaaleconomisch oogpunt kan een algenbloei sterke gevolgen hebben voor onder meer het toerisme, de woningbouw en de visserij. Interessant is dat fosfaat via deze consumptieketen verandert van een hulpbron in afval, van een nutriënt in een verontreinigende stof.

Daarom zijn twee gelijktijdige acties nodig: allereerst het verwijderen van fosfaat uit het water, om vervuiling te voorkomen, en daarna het terugwinnen van deze belangrijke maar eindige hulpbron, om deze bijvoorbeeld als meststof te hergebruiken. Dit zou leiden tot een circulair gebruik van fosfaat. Zoals eerder gezegd gebeurt dit al gedeeltelijk in waterzuiveringsinstallaties, maar niet in die mate dat eutrofiëring van oppervlaktewater wordt voorkomen. Daartoe moet fosfaat uit het water worden verwijderd tot de zogenaamde ultra lage concentraties, beneden 0,01 mg/L of 10 ppb (parts per billion, ofwel delen per miljard). Dit betekent een concentratie die overeenkomt met een theelepel zout opgelost in een Olympisch zwembad. Of, voor wie liever vergelijkingen maakt met afstanden, de afstand tussen je oren vergeleken met de diameter van de aarde, of de lengte van een middenklasse auto vergeleken met de gemiddelde afstand van de aarde tot de maan.

Om deze doelstellingen te bereiken is adsorptie een van de meest belovende technologieën. Vergeleken met de bekendere absorptie, waarbij stoffen een groter materiaal passeren of binnendringen (bijvoorbeeld wanneer we water drogen met absorberend keukenpapier), hecht een verbinding zich bij adsorptie aan het oppervlak van een ander materiaal. Dit materiaal wordt een adsorptiemiddel genoemd. Bij adsorptie kunnen ultra lage concentraties worden bereikt, en zodra het adsorbens volledig bedekt is met fosfaat, kan dit weer worden losgemaakt (gedesorbeerd) en teruggewonnen. Daartoe moet het oppervlak van het adsorbens selectief fosfaat kunnen aantrekken, zelfs wanneer er weinig van in het water aanwezig is. Deze eigenschap wordt affiniteit genoemd en vertelt ons hoeveel een adsorptiemiddel en fosfaat van elkaar houden (zoals bij menselijke relaties). Tegelijkertijd mag de adsorptie niet te sterk zijn om de terugwinning van fosfaat te verhinderen. IJzeroxide verbindingen, in de volksmond beter bekend als roest, vormen een veelbelovende categorie van adsorptiemiddelen.

Een laatste belangrijk punt om deze technologie economisch betaalbaar te maken is dat het adsorbens meerdere malen moet kunnen worden hergebruikt. Dit betekent dat het meerdere fosfaatadsorptie- en fosfaatdesorptie/herstelcycli moet kunnen doorlopen. Dit is van fundamenteel belang om deze technologie in de echte wereld te kunnen toepassen. Zonder deze regeneratie van het adsorbens zou het te duur zijn en te veel materiaal vergen: het zou nutteloos zijn.

Dit proefschrift is gericht op het verbeteren van de eigenschappen en prestaties van op ijzeroxide gebaseerde adsorbentia voor de verwijdering en terugwinning van fosfaat uit oppervlaktewater. Het hoofddoel was het identificeren van strategieën om de

affiniteit van op ijzeroxide gebaseerde adsorbentia voor fosfaat te verhogen en tegelijkertijd hun stabiliteit en duurzaamheid te verbeteren.

De gekozen strategie om ijzeroxiden en hun oppervlakte-eigenschappen te manipuleren is doping. Doping is een techniek waarbij onzuiverheden aan een materiaal worden toegevoegd om de eigenschappen ervan te veranderen. Afgezien van de ongeoorloofde, onethische (en illegale) sport gerelateerde praktijken, wordt doping op grote schaal toegepast in de elektronica, bijvoorbeeld in de chips in onze smartphones en computers. Net zoals het toevoegen van chocoladedruppels aan koekjes om ze smakelijker te maken of het toevoegen van zout aan een chocoladereep om de smaak drastisch te veranderen, kan doping ijzeroxiden verbeteren om ze beter te laten presteren, bijvoorbeeld door hun affiniteit voor fosfaat te vergroten. Verrassend genoeg kan een onzuiverheid dus vernuftig en waardevol blijken en waarde toevoegen aan ijzeroxiden.

Bij dit onderzoek is gebruik gemaakt van nanodeeltjes van ijzeroxide (ongeveer 100 nm x 20 nm), dat wil zeggen deeltjes die tien- tot honderdduizendmaal kleiner zijn dan een millimeter. Een nanometer is een miljardste meter, tien- tot honderdduizendmaal kleiner dan de breedte van ons haar, of de dikte van een papierblad. Als een mens één nanometer groot zou zijn, zou een millimeter langer zijn dan heel Italië, precies, van Capo delle Correnti tot München. Zelfs langer dan rijden van Padua naar Delft en dan naar Leeuwarden. Deze sprong naar zulke kleine schalen maakte het mogelijk om de interactie tussen fosfaat en ijzeroxide beter te onderzoeken en tegelijkertijd enige flexibiliteit te bieden bij de manipulatie ervan door middel van doping.

In dit werk werd een bijzondere techniek gebruikt om deze ijzeroxiden en het effect van doping te bestuderen: Mössbauer spectroscopie. Mössbauer spectroscopie is een nucleaire techniek, die gebruik maakt van nucleaire gammastraling om de eigenschappen van ijzerverbindingen te bestuderen. Dit kan worden vergeleken met röntgenstraling in het ziekenhuis. Daar bestralen we een deel van ons lichaam, bijvoorbeeld om een "plaatje" van onze botten te krijgen en door dat te vergelijken met hoe een bot eruit hoort te zien, kunnen wij (of beter, artsen) conclusies trekken. Met Mössbauer spectroscopie kunnen we een soort "foto's" (spectra genoemd) maken van ijzeroxiden. Door spectra onderling en met referentiespectra te vergelijken, kunnen we bijvoorbeeld het effect van doping, of het effect van langdurig gebruik, op de ijzeroxiden zien.

Dit proefschrift bestaat uit een reis door de ontwikkeling van een adsorbens, van de doping van ijzeroxide nanodeeltjes tot de implementatie van dergelijke nanodeeltjes in een commercieel adsorbens. Er wordt aangetoond hoe doping een veelbelovende strategie kan zijn om de oppervlakte-eigenschappen van een adsorptiemiddel te verbeteren, zodat fosfaat effectief uit water kan worden teruggewonnen. In dit opzicht lijkt zink een veelbelovende stof voor doping te zijn. Ook geeft dit proefschrift een beter inzicht in de kenmerken en het mechanisme van fosfaatadsorptie/desorptie op een specifieke categorie van (commerciële) adsorbentia. In het proefschrift worden de experimentele omstandigheden die de resultaten en interpretaties kunnen beïnvloeden in detail besproken. Aan

het eind worden op basis van de experimentele waarnemingen en de opgedane ervaringen, perspectieven en aanbevelingen voor toekomstig onderzoek gegeven. Er moet bijvoorbeeld meer aandacht worden besteed aan affiniteit en oppervlakte-eigenschappen dan aan de grootte van het oppervlak, en de proeven moeten worden uitgevoerd onder omstandigheden die zo dicht mogelijk bij die van de toepassing liggen.

Riassunto divulgativo di questa tesi

In questa tesi viene trattato il riciclo di risorse, pulendo l'acqua e preservandone la disponibilità. Nonostante questo concetto sia alla base di una società sana e sostenibile, ulteriori sviluppi sono necessari. Nei prossimi anni, la scarsità d'acqua sarà una sfida sempre più grande per l'umanità, dovuta alla scarsa gestione delle risorse e alla crisi climatica. L'acqua ricopre il 70 % del nostro pianeta, ma solo il 3 % di questa è acqua dolce, e solo l'1 % è facilmente accessibile. Più di 2 miliardi di persone vivono già in paesi affetti da scarsa disponibilità idrica.

Inoltre, in una certa misura, questa tesi mostrerà come ci sia una sottile linea di separazione tra risorse e rifiuti, nutrienti e inquinanti, impurezza e valore aggiunto. Questa sottile linea è definita dalle nostre scelte quotidiane, dal nome che diamo alle cose e la loro relativa connotazione.

Il cibo è fondamentale per la vita, dagli umani ai batteri, dagli animali alle piante e funghi, anche se consumato in forme diverse. Questo perché il cibo contiene diverse sostanze, dette nutrienti, che sono necessari all'organismo per poter svolgere le funzioni vitali. Tra questi nutrienti, il fosforo è uno dei più importanti, ed è coinvolto in diverse funzioni vitali negli esseri viventi. Negli umani è presente ad esempio nel DNA, nelle ossa e nei denti e viene assunto attraverso il cibo sia di origine animale che vegetale, sottoforma di fosfato. Esso è una molecola contenente un atomo di fosforo (P) e quattro atomi di ossigeno (O). Il fosfato viene utilizzato in modalità diverse in varie industrie, farmaceutica, edile, elettronica, ma principalmente in quella agricola. In agricoltura, il fosfato costituisce una componente essenziale ed insostituibile dei fertilizzanti. È necessario per produrre frutta, verdura, cibo per gli animali, ed è quindi necessario per sostenere la popolazione mondiale e la sua crescita. Il fosfato viene ricavato da miniere di fosforite, che son presenti solo in pochi paesi, e la sua estrazione è causa di inquinamento (come ogni attività mineraria).

Una volta che espelliamo il cibo, questo finisce negli impianti di trattamento delle acque reflue. Qui, gli inquinanti vengono rimossi, mentre i nutrienti, come il fosfato, vengono parzialmente rimossi e (possibilmente) recuperati. Questo significa che una parte del fosfato finirà in acque di superficie (canali, fiumi, laghi).

Allo stesso tempo, l'abuso di fertilizzanti provoca accumuli di fosfato nei terrenti, che prima o poi verrà rilasciato in corsi e bacini d'acqua.

Il fosfato può accumularsi nelle acque di superficie fino a diventare un inquinante. Infatti, il fosfato funge da nutriente per gli organismi che vivono in acqua, come le alghe. Tuttavia, l'eccesso di nutrienti in acqua, detto eutrofizzazione, può comportare un'eccessiva crescita di alghe. Ciò porta alla formazione di quello strato sporco, verdastro e viscido che a volte ci capita di veder ricoprire canali, fiumi e laghi. La proliferazione di alghe può avere un impatto dannoso a più livelli. Dal punto di vista ambientale, può portare alla morte della vita acquatica di un bacino, mentre dal punto di vista della salute, certe alghe possono essere altamente tossiche. Dal punto di vista socioeconomico, la

proliferazione di alghe può colpire fortemente le industrie turistica, immobiliare e della pesca. È interessante vedere come, attraverso il suo consumo, il fosfato si è trasformato da risorsa a rifiuto, da nutriente ad inquinante.

Pertanto, è necessario eseguire in parallelo: la rimozione del fosfato dall'acqua, per evitare l'inquinamento, ed il recupero di tale risorsa, tanto importante quanto limitata, per poterla riutilizzare ad esempio come fertilizzante. Ciò risulterebbe in un utilizzo circolare del fosfato. Come detto precedentemente, ciò è già in atto negl'impianti di trattamento acque reflue, ma non al livello necessario per prevenire l'eutrofizzazione delle acque di superficie. A questo scopo, è necessario rimuovere il fosfato dall'acqua fino alle cosiddette concentrazioni bassissima (o ultra-basse), sotto i 0.01 mg/L o 10 ppb (parte per miliardo). Questa concentrazione equivale ad un cucchiaio di sale disciolto in una piscina olimpionica. O ancora, per chi preferisce i paragoni con le distanze, la distanza tra le orecchie rispetto al diametro della Terra, o la lunghezza di un'utilitaria (segmento B) rispetto alla distanza Terra-Luna.

Per raggiungere questo obiettivo, une delle tecnologie più promettenti è l'adsorbimento. Rispetto al meglio conosciuto absorbimento (o assorbimento), in cui una sostanza entra all'interno di un materiale più grande (per esempio quando asciughiamo l'acqua con lo scottex), durante l'adsorbimento una sostanza aderisce alla superficie di un altro materiale. Questo materiale è chiamato adsorbente. L'adsorbimento è potenzialmente in grado di raggiungere tali bassissime concentrazioni e una volta che l'adsorbente è completamente ricoperto di fosfato, questo può essere separato (desorbito) e recuperato. Per poter fare ciò, la superficie dell'adsorbente deve essere in grado di attrarre selettivamente il fosfato, anche quando ce n'è poco in acqua. Questa proprietà è chiamata affinità e ci dice quanto un adsorbente e il fosfato si piacciono (come per le relazioni tra persone). Allo stesso tempo, l'adsorbimento non deve essere troppo forte da prevenire il recupero del fosfato. In questo senso, una promettente categoria di adsorbenti sono gli ossidi di ferro, generalmente detti "ruggine".

Un ultimo importante punto per far sì che questa tecnologia sia economicamente a buon mercato è che l'adsorbente deve essere in grado di poter essere riutilizzato più volte. Ciò significa che deve essere in grado di sopportare multipli cicli di adsorbimento e desorbimento/recupero di fosfato. Questo è fondamentale per riuscire ad applicare nella realtà questa tecnologia. Sena poter rigenerare l'assorbente, questa tecnologia sarebbe troppo costosa o richiederebbe l'utilizzo eccessivo di materiali: non sarebbe conveniente.

Questa tesi si focalizza sul migliorare proprietà e prestazioni di adsorbenti a base di ossido di ferro per la rimozione e il recupero di fosfato dalle acque di superficie. L'obiettivo principale era di identificare strategie per aumentare l'affinità di tali adsorbenti per il fosfato, migliorandone al contempo stabilità e durevolezza.

La strategia adottata per manipolare gli ossidi di ferro e le loro proprietà di superficie è il drogaggio. Il drogaggio è una tecnica che consiste nell'aggiungere un'impurezza in

un materiale, per poterne cambiare le proprietà. Escludendo le infelici e disoneste (e illegali) pratiche sportive, il drogaggio è largamente impiegato in elettronica, per esempio nei circuiti dei nostri cellulari e computer. Così come si aggiungono gocce di cioccolato ai biscotti per renderli più appetibili, o si aggiunge sale nelle barrette di cioccolata per creare un drastico cambio di gusto, il drogaggio può migliorare gli ossidi di ferro, rendendoli più performanti, per esempio aumentando la loro affinità per il fosfato. Sorprendentemente, un'impurezza può dimostrarsi una preziosa ed un valore aggiunto per gli ossidi di ferro.

Questa ricerca è stata effettuata utilizzando nanoparticelle di ossidi di ferro (di circa 100 nm x 20 nm), che significa particelle decine o centinaia di migliaia di volte più piccole di un millimetro. Un nanometro è un miliardesimo di un metro, decine o centinaia di migliaia di volte più piccolo dello spessore di un capello, o dello spessore di un foglio di carta. Se una persona fosse alta un nanometro, un millimetro sarebbe più lungo dell'Italia intera, precisamente da Capo delle Correnti a Monaco di Baviera. Sarebbe più longo che guidare da Padova a Delft e poi fino a Leeuwarden. Questo salto a tali piccole dimensioni permette di studiare meglio l'interazione tra il fosfato e gli ossidi di ferro, concedendo flessibilità nella loro manipolazione attraverso il drogaggio.

Inoltre, in questo lavoro è stata utilizzata una particolare tecnica per studiare questi ossidi di ferro e l'effetto del drogaggio su di essi: la spettroscopia Mössbauer. La spettroscopia Mössbauer è una tecnica nucleare che sfrutta la radiazione gamma nucleare per studiare le proprietà delle sostanze a base di ferro. Può essere pensata come quando ci facciamo i raggi X all'ospedale. Lì, per esempio, irradiamo parte del nostro corpo per ottenere un'immagine delle nostre ossa e comparandola a come l'osso dovrebbe apparire, noi (o meglio, i dottori) possiamo trarre conclusioni. Con la spettroscopia Mössbauer possiamo fare delle sorta di "fotografie" (chiamate spettri) dei nostri ossidi di ferro. Comparando questi spettri tra loro e con spettri di riferimento possiamo osservare ad esempio gli effetti del drogaggio o dell'utilizzo prolungato sugli ossidi di ferro.

Questa tesi consiste in un viaggio attraverso lo sviluppo dell'assorbente, dal drogaggio di nanoparticelle di ossido di ferro fino alla loro implementazione in un analogo di un assorbente commerciale. Viene mostrato come il drogaggio possa essere una strategia promettente per migliorare le proprietà di superficie di un adsorbente, per poter recuperare efficacemente il fosfato dall'acqua. In questo senso, lo zinco pare essere un drogante promettente. Inoltre, questa tesi fornisce una maggior comprensione delle caratteristiche e del meccanismo di adsorbimento/desorbimento di fosfato per una particolare categoria di adsorbenti. Sono stati anche evidenziate le condizioni sperimentali che possono influenzare maggiormente i risultati e le interpretazioni. Infine, in base alle osservazioni sperimentali e all'esperienza acquisita, vengono fornite prospettive e raccomandazioni per la ricerca futura. Bisognerebbe prestare maggior attenzione all'affinità e alle proprietà di superficie, piuttosto che all'area superficiale, mentre i test dovrebbero esser condotti in condizioni quanto più possibile vicine a quelle dell'applicazione.

The answer to the ultimate question of
Life, the Universe and Everything is: **42**."

The Hitchhiker's Guide to the Galaxy,
Douglas Adams

Contents


1

1

Introduction

1.1 The Role of Phosphorus

Phosphorus (P) is one of the most important nutrients for living beings, together with carbon (C) and nitrogen (N). It is fundamental for carrying out vital processes. In humans it accounts for about 3 % in weight, and is present for instance in the DNA, RNA, ATP in organic form, and in bones, and teeth in the inorganic form [1,2]. In the inorganic form, as phosphate, PO_4^{3-}, it constitutes an irreplaceable part of fertilizers, fundamental for the world food production sustainability [3–5].

However, phosphorus can also become a pollutant. Fertilizers overuse can cause phosphorus accumulation in soil, which can leach out in water streams, known as agricultural runoff. Also, at the end of its usage cycle, through food excretion, domestic waste (e.g., detergents), industrial activities wastewater discharge, phosphorus ends up in wastewater treatment plants (1-15 mg L^{-1} [6]). Here, phosphorus is (usually) partially removed (and recovered), but the remaining fraction present in water will eventually end up in water bodies, where it can accumulate.

When phosphorus accumulates in freshwater bodies, it can result in nutrients overload, called eutrophication (well-nourished, from Greek "eu" = good; "trophè" = food / nourishment). Phosphorus was shown to be the cause of freshwater bodies eutrophication [7–11] (while for saline waters is nitrogen [12]). Eventually, eutrophication causes algae bloom, which is the rapid growth of microorganisms, called algae, present in surface waters. Freshwater bodies eutrophication and algae bloom may lead to several detrimental environmental, health and socio-economic issues. An algae bloom can cause the death of aquatic ecosystems. In fact, algae accumulation creates a thick layer covering the water body, reducing sunlight penetration necessary for photosynthesis, and

atmospheric oxygen exchange. The latter may lead to oxygen depletion, which can cause pollutants release from the sediments, such as heavy metals and micropollutants. Moreover, some cyanobacteria (algae) species are highly toxic to humans, posing health risks [13]. Such issues can end up in great economic losses, comprising water treatment and restoration, the impact on the fishing, tourism, and recreational activities industries, and property value losses [13–16]. Freshwater eutrophication was estimated to cost 100-200 million dollars in UK [14] up to 2.2 billion dollars in the US [15]. Eutrophication is mainly caused (or accelerated) by human activities [17].

Phosphorus concentrations in water are expressed in terms of total phosphorus, TP. This comprehends the particulate phosphorus, pP, consisting of small, suspended particles, and soluble phosphorus or orthophosphate, o-P, comprising phosphate ionic forms. The latter is also referred to as soluble reactive phosphorus, (SRP), being the only bioavailable form of P and direct cause of eutrophication [18]. Depending on water pH, o-P can be present as phosphoric acid, H_3PO_4 (pH $\lesssim$ 4); dihydrogen phosphate, $H_2PO_4^-$ (pH $\sim$ 0-9); hydrogen phosphate, HPO_4^{2-} (pH $\sim$ 5-14); and phosphate, PO_4^{3-} (pH $\gtrsim$ 10). Usually, wastewater treatment plant effluents and surface waters have a pH in the range 6-8, meaning that phosphate is present as a mixture of monovalent and divalent phosphate. Nevertheless, o-P can be released by pP in the sediments, depending on the different conditions, like pH, pP/o-P conditions, and so on [19].

According to the European Urban Water Treatment Directive, wastewater treatment plant discharge should be limited to 1-2 mg L^{-1} of TP [20]. The European Commission also provides some guidelines to assess the ecological quality of waters. Cut-off TP concentrations for lake at risk of eutrophication lie in a wide range of values, from below 0.01 to above 0.1 mg L^{-1}, while concentrations below 0.07 mg L^{-1} for rivers are considered as excellent waters [21,22].

Nevertheless, some of these concentrations are already ten to hundredfold the limit for eutrophication prevention of freshwater bodies, which is 10-15 μg L^{-1} [11], also defined as ultra-low P concentrations [23]. This means that phosphorus removal from contaminated waters is important, but that is not all.

Phosphate is also a finite resource, obtained from phosphate rock (phosphorite) mines. It is mainly used to produce fertilizers (80 %), followed by detergents (10 %), animal feeds (5 %) and other applications (softeners, steel-alloys, glass, etc.) [24]. In the past, its use has been mainly linear, and despite some improvements in managing phosphate, reducing the average phosphate rock consumption per person [25], a more circular approach is desirable [3,26]. In fact, phosphate availability is thought to last around two or three hundred years, although it is highly debated due to estimation difficulties [25–28]. Also, improving resource management to reduce mining activities would be environmentally beneficial, to reduce of soil, water, and air pollution [27,29,30]. Moreover, these phosphorite reserves are only present in a few countries, mainly Morocco (70 %), with the next country, China, having "only" 4 %. In Europe, phosphate rock mines are present in Finland and Russia, accounting for less than 2 % in total [31]. This makes Europe dependent on its import (above 90 %) [25,27,30]. For the above reasons, and to reduce the external dependency, the European Commission added phosphate to the Critical Raw Material list [32], establishing circular and sustainable guidelines for a better use and management of resources [32–34], complying with the United Nations Sustainable Development Goals [35].

For all the above reasons, phosphate removal is fundamental, and its recovery important.

1.2 Phosphorus Removal Techniques?

As previously said, human activities produce many P-rich streams. These are often seen as waste streams, but they can actually become secondary sources of phosphate. Many techniques for P removal are available and can be grouped in three main categories: Physical Phosphorus Removal (PPR), Biological Phosphorus Removal (BPR) and Chemical Phosphorus Removal (CPR). Each technology finds application depending on the water stream and characteristics, influent P concentration, and targeted effluent P concentration. Obviously, each one comes with limitations [23,36,45,46,37–44], depending on water volumes and flows to be treated, pH, competitive compounds, influent P concentrations and targeted effluent P concentrations. Hence, different technologies are often combined, according to the needs. Moreover, not all of these technologies allow to reach ultra-low P concentrations and not all of them have potential for P recovery.

For instance, PPR processes work mainly on the principle of size exclusion, like sand filters and membranes, and face difficulties in reaching concentrations low P concentration. They may require high water consumption for backwash regeneration, large area consumption, use of chemicals to adjust water conditions. Membranes which can work both on size and charge exclusion, can potentially reach ultra-low P concentrations. However, they are generally quite expensive systems, face high pressure drops over the membrane, produce significant volumes of concentrate, and display low throughput. Also, membrane scaling and fouling can highly impact their performances.

BPR removal techniques consists of bioreactors, like Enhanced Biological Phosphorus Removal (EBPR) or small ecosystems, like (constructed) wetlands. They both use microorganisms or plants to remove and accumulate P, like Polyphosphate Accumulating Organisms (PAO's). Such systems are highly

sensitive to environmental conditions (e.g., seasonality), and water conditions (e.g., temperature, pH) and composition (need of organic matter, affected by heavy metals and pollutants). Although complying with current regulations, the effluent P concentration from EBPR is generally as high as 0.5-2 mg L^{-1}. Wetlands are natural or engineered lands flooded or saturated with water, containing PAO's and/or adsorbing media, and constitute an option for reducing phosphate level in water to below 0.1 mg L^{-1}. However, they are also highly sensitive to water and environmental conditions, have a very high footprint and if saturated or overloaded, they can cause a decrease in biodiversity, greenhouse gas production and may become P hotspots for downstream waterbodies.

CPR consists of processes that remove P via chemical interactions, like charge, bonds, or chemical phase transformation. Precipitation and coagulation/flocculation are techniques which respectively promote formation or growth/agglomeration of P-based particles via metal salt dosing. However, these techniques face limitations when targeting low P concentrations, and produce high amount of sludge. Nevertheless, CPR is suited to target bulk P removal and recovery [23], although recovery of P is not always possible or easy, increasing sludge disposal costs. When applied to surface waters, caution is required, due to possible toxicity issues when using aluminium coagulants. Finally, the last CPR technique is adsorption, which will be discussed more in detail in the following section.

1.3 Phosphate Adsorption and Recovery

Adsorption [23,47–50] is a technique which mainly targets o-P, is able to reach the necessary ultra-low concentrations, and thus is mostly seen as a polishing step. It makes use of a solid medium, called adsorbent, to remove a compound, called adsorbate, via surface adhesion. This may happen either via

electrostatic forces, called physisorption (or outersphere complexation), or chemical bonds, called chemisorption (or innersphere complexation). Phosphate adsorption can either happen via ion exchange and hydrogen bond (physisorption), or ligand exchange, either monodentate or bidentate, mononuclear binuclear (chemisorption), as shown in Figure 1.1.

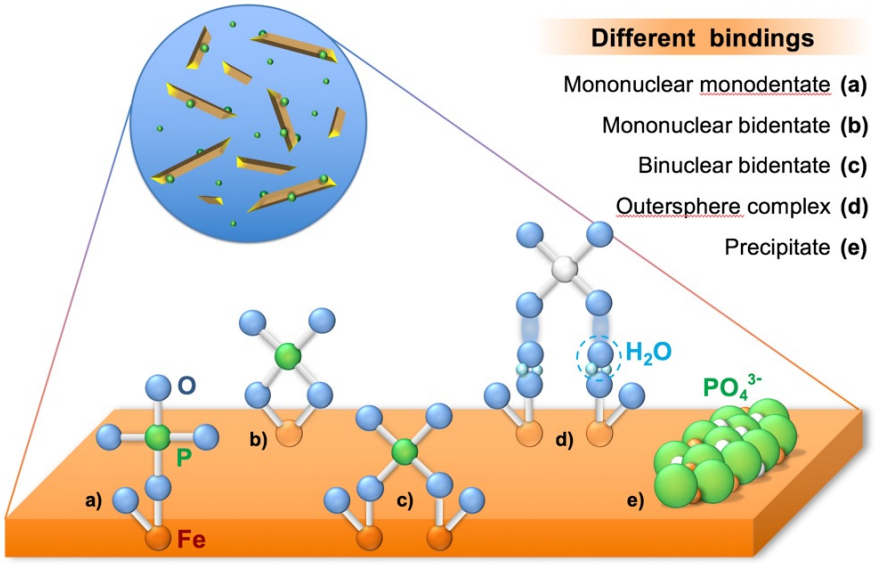

Figure 1.1: Scheme of binding mechanisms between iron oxide surface and phosphate, adapted from [51].

It is important to underline that physisorption, being a charge-based mechanism, entails a lower selectivity for P, while chemisorption entails a higher selectivity for P. Surface precipitation may also happen, which is not desirable, as it causes pore blockages and reduces accessibility to surface adsorption sites. This adsorption mechanism depends on the adsorbent and adsorbate chemistries and can also be influenced by environmental conditions (e.g., pH, P concentration, etc.). Moreover, adsorption can be (more or less easily) reversed, allowing P desorption and recovery. This procedure entails the regeneration of the adsorbent, which can also be reused for further adsorption cycles.

An adsorption system can be operated in batch or continuous column mode, with a fixed or fluidized bed. In general, these systems do not need pH adjustment before nor after the treatment, or any addition of chemicals to water. Adsorption systems are fairly flexible, as they can be designed and scaled depending on the volume of water and P concentrations to be treated. Moreover, the adsorbent medium can be conveniently chosen among a variety of adsorbents, according to the characteristics of the stream to be treated.

As previously mentioned, adsorbent characteristics can influence the adsorption mechanism and general functioning. An important characteristic is the point of zero charge (pzc) which is defined as the pH at which the overall surface charge is neutral. Below the pzc, an adsorbent is more positively charged, while above it is more negatively charged. Hence, pzc is fundamental to define the pH range of applicability of an adsorbent for phosphate removal and recovery. Another important characteristic is the adsorbent capacity, which tells how much P an adsorbent can host on its surface. Selectivity is another important characteristic, as it defines how well an adsorbent can target phosphate among other compounds present in water. It can determine the quality of the P-based recovered product. Finally, and probably the most important property for eutrophication prevention is the affinity of the adsorbent for P. This characteristic defines the extent of interaction between the adsorbent and the adsorbate. It tells how much an adsorbent is able to remove P, even when it is in low concentrations. This is thought to be a determining property to reach ultra-low P concentrations [23]. However, research has often been conducted only looking at high specific surface area (SSA) and adsorption capacities. High adsorption capacities are usually determined in experiments with high P concentrations, corresponding to high P equilibrium concentrations. To reach the ultra-low P concentrations for eutrophication prevention, the maximum adsorption capacity does not represent the suitability of an adsorbent, as it is unrelated to the adsorbent performances

for low effluent P concentrations [23]. Affinity, that can be thought of as the adsorbent capacity at the low equilibrium/effluent concentrations, is thus more relevant.

There are different types of phosphate adsorbents: they can be organic or inorganic, engineered or byproducts, one-type or composite/hybrid, one-time use or reusable. On the one hand, one-time use adsorbents (e.g., bio/organic waste, biochar) are generally cheaper than reusable adsorbents, especially compared to the engineered ones. On the other hand, one-time use adsorbents seem less economically convenient than reusable adsorbents in the long run [23].

Reusable adsorbents generally consist of polymeric media, porous metal (hydr)oxides, or a combination of both (composite/hybrid adsorbents). Some polymeric media, like macroporous resins, and metal hydroxides, like layered double hydroxides (LDH), belong to the category of anion exchangers. Although they display high capacities and fast kinetics, their selectivity (and in the case of LDH, their stability) is generally low, due to the nature of the interaction. For a more selective phosphate adsorption, porous metal hydroxides constitute a better option. These are porous oxides (henceforth referring to oxides, hydroxides and oxyhydroxides) of di-, tri-, and tetra-valent metals (Zn, Fe, Al, Mn, La, Ti, Zr, etc.), and can be either engineered or byproducts. Metal oxides adsorb phosphate via ligand exchange, making them less sensitive to the ionic strength of the water to be treated, and efficient even at low and ultra-low P concentrations. Alternatively, metal oxide can consist of nanoparticles, which can be fixed on a support, making a composite/hybrid adsorbent. An example of this are Hybrid Anion Exchange resins (HAIX), which consist of an anion exchange resin backbone (providing cations exclusion) impregnated with metal oxide nanoparticles (providing selectivity for P). HAIX displayed promising results, both in lab-scale tests and on-field application, both for P removal/recovery [49,52,61–66,53–60], and As removal [67–70] for safe drinking water production (as P and

As display similar chemistries). With metal oxide-based adsorbents, the process can be reversed using an alkaline wash, generally 0.1-1 M KOH or NaOH (pH 13-14), causing P desorption and allowing to reuse the adsorbent multiple times. If surface precipitation is taking places, causing pore blockage and reducing adsorption sites accessibility, an acid wash might be needed [71,72]. This can however deteriorate the adsorbent, reducing its lifespan. The regenerability and reusability (50-100 of times) of the adsorbent is fundamental for the economic viability of the process [23].

Among the different metal oxides, iron (Fe) oxides seem promising and will be presented in the following section.

1.4 Iron Oxide-based Adsorbents

Iron, Fe (from Latin "ferrum"), is the most abundant element on Earth by mass (32.1 %), followed by oxygen (30.1 %), and the fourth one on the Earth's crust (5.6 %), preceded by aluminium (8.3 %), silicon (28 %), and oxygen (46 %). Iron is also fundamental for life processes [73–77]. The human body contains about 4 g of Fe (0.005 % in weight), mostly in hemoglobin and myoglobin, for oxygen transport and storage, respectively. It has four stable isotopes: ^{54}Fe (5.8 % of natural Fe), ^{56}Fe (91.7 %), ^{57}Fe (2.1 %), and ^{58}Fe (0.3 %). Iron presents different possible states of oxidation, from -2 to +7, but Fe^{2+} and Fe^{3+} are the most common states. Iron easily interacts with oxygen and water, forming iron oxides, hydroxides and oxyhydroxides (henceforth referred to as oxides). Iron oxides usually contain divalent or trivalent iron, with electron configurations:

Fe^{2+}: $1s^2\ 2s^2\ 2p^6\ 3s^2\ 3p^6\ 3d^6$

Fe^{3+}: $1s^2\ 2s^2\ 2p^6\ 3s^2\ 3p^6\ 3d^5$

and there are 16 species in total [75,78]. Each species has different properties and features, from crystallinity, to thermodynamic stability, magnetic properties, and so on. In general, like other metal oxides, iron oxides display good properties for P adsorption. Due to their abundance, ease of synthesis and manipulation, iron oxide-based adsorbents have been widely investigated. Iron oxide-based adsorbents consist both of porous granules and nanoparticles, either commercial or synthesized in lab. Examples of commercial adsorbents are FerroSorp, GEH, Bayoxide E33, as porous granules [23,52,71,79–81], and Layne, ArsenX^{np}, FerriX A33E, as nanoparticle-based HAIX [62–65,68,80–84]. Among the different species, hematite and goethite (the two most thermodynamically stable oxides [78]), ferrihydrite (amorphous with SSA), akaganéite, and lepidocrocite are the most investigated species for P adsorption. Ferrihydrite has often been promoted, due to its high SSA and P capacity; however, its instability questions its durability [85]. Conversely, goethite, which displays lower SSA and P capacity, seems to display significantly higher affinity for P [85,86]. Together with its high thermodynamic stability, goethite seems a promising candidate for developing an efficient, stable, and regenerable adsorbent for P recovery.

To improve goethite performances, doping might constitute a valuable option. Doping is a popular technique in the electronics industry, for manipulating the properties of semiconductors, with important implications also in other fields, such as catalysis [87–93]. Doping consists of substituting an element, in this case Fe, with another element, to modify the overall properties of the crystal. For instance, Fe substitution can affect the crystallization process, crystal habit, particle size, SSA, the surface charge (i.e., the pzc), species stability, magnetic properties, and so on. The likelihood of M-for-Fe substitution depends mainly on three factors: 1) similarity in ionic radii; 2) similarity in ionic charge; 3) existence of isostructural compounds [78,94]. Many studies on natural and

synthetic impurities in goethite have been conducted, mainly on a crystallographic level [75,78,95–102].. Al has been by far the most investigated dopant [103,104,113–115,105–112], as it can substitute up to 1/3 of the Fe in goethite (similar levels can be also obtained for Mn and Ga) [75,78]. Few studies also investigated the effect of doping on goethite performances for P recovery. For instance, Li et al., 2015 [116], found that doping goethite with Al improved the P adsorption capacity with respect to pure goethite, but did not investigate P desorption and adsorbent stability. In general, not many studies in literature focus on adsorbent regeneration and reusability, but mostly on P removal. A systematic investigation on goethite doping could increase the understanding of the effect of dopants and their characteristics, improving the adsorption capacity, while preserving (or improving) its affinity for P and the stability of the adsorbent.

1.5 Mössbauer Spectroscopy

One of the most powerful techniques to investigate Fe-based materials is Mössbauer spectroscopy [75]. Mössbauer spectroscopy is a resonant nuclear gamma radiation-based technique, which works with few elements, of which iron (^{57}Fe) is the most convenient and investigated one. The reason why the number of Mössbauer sensitive elements is restricted is that these elements need to satisfy many conditions.

First of all, a resonance condition between gamma ray emission and adsorption needs to be satisfied, as is a condition necessary for spectroscopic systems. However, gamma rays or gamma photons generated from nuclear transitions are highly energetic. The high energy of this gamma ray, E_γ, causes the emitting nucleus (of mass M) to recoil, with an energy fraction loss equal to the recoil

energy, directly proportional to the squared gamma ray energy, and inversely proportional to M:

$$E_R = \frac{E_\gamma^2}{2Mc^2}$$

where c is the velocity of light. If E_R is smaller than the natural linewidth of the transition, Γ,the gamma ray can still be absorbed by a second atom (nucleus) of the same type, matching the resonance. The receiving nucleus will also experience a recoil ("forward"), which also needs to be small compared to the energy linewidth. For example, in the case of the 14.4 keV energy level of ^{57}Fe, E_R is five orders of magnitude larger than Γ ($\sim 10^{-3}$ eV vs $\sim 10^{-9}$ eV), times two, considering that of the receiving nucleus. This mismatch impeding the resonance condition, which is true for free atom nuclei, can be "compensated" for nuclei in a solid, as a fraction of the gamma rays will be emitted (or absorbed) without recoil (recoil-free). As a solid has a bigger mass than the nucleus alone (already $\sim 10^7$ times higher for powders), the recoil energy is highly reduced, being inversely proportional to the mass of the emitter. Also, nuclei recoil in solids is translated in quantized lattice vibrations (phonons). According to statistical quantum mechanics, there is a finite probability for a decay to occur without phonon emission, meaning that the recoil gets taken up by the solid as a whole. This means that there is a recoil-free fraction (Mössbauer-Lamb factor) of gamma ray emission (or adsorption), proportional to $\sim e^{\sim(-E_R^2)}$. Hence, Mössbauer spectroscopy can only work for gamma energies $E_\gamma \leq 100$ keV for transmission spectroscopy (our case), and $E_\gamma \leq 150$ keV for scattering spectroscopy. So, a first limitation is set by the gamma ray energy suited to fulfill the recoilless condition, as most of the gamma ray energies lies in the MeV region. Second, the recoilless fraction is temperature dependent, and only some materials are suited to work at room temperature, otherwise, low temperatures are necessary.

Third, the low-energy gamma ray emission must come from a transition from an excited state to a ground state, otherwise no absorption can happen. Fourth, gamma rays can investigate the hyperfine interactions, which are typically of the order of 10^{-9}-10^{-6} eV, which sets an upper value to the linewidth of the transition. This also requires nuclear transitions with a lifetime > 10^{-12} s. Finally, and obviously, the existence of a radioactive source is needed. It means that there has to be a parent nuclide able to match the above conditions and with a half-life long enough to conduct experiments. Lucky for us, ^{57}Co is a parent nuclide for ^{57}Fe, has a half-life of 270 days, and fulfils all the above requirements. Figure 1.2 shows the decay scheme of ^{57}Co to ^{57}Fe.

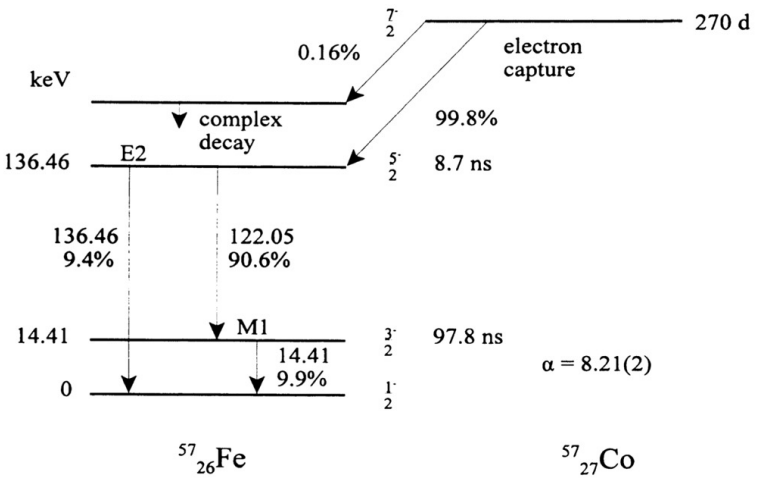

Figure 1.2: Transition scheme of the decay from ^{57}Co to ^{57}Fe (from [75]).

The transition from the 14.41 keV level is the one of interest for Mössbauer spectroscopy. This transition has a relatively low intensity (9.9 % of all decays), and the relative abundance of ^{57}Fe is only 2.14 % of all Fe. Nevertheless, all of the other characteristics are so favorable to make Fe suited for Mössbauer spectroscopy. If convenient, ^{57}Fe enrichment (e.g., ^{57}Fe impregnation) of samples

can be performed, to improve the signal. The only Mössbauer active nuclide lighter than ^{57}Fe is ^{40}K. The Mössbauer transitions that can be carried out at room temperature are only eight: ^{57}Fe (14.4 keV), ^{119}Sn (23.8 keV), ^{121}Sb (37.1 keV), ^{125}Te (35.5 keV), ^{129}I (27.7 keV), ^{151}Eu (21.6 keV), ^{155}Dy (25.6 keV), ^{169}Tm (8.4 keV), and ^{181}Ta (6.2 keV). All other possible transitions require the use of low temperature setups. In general, the most commonly used Mössbauer transitions are ^{57}Fe, ^{119}Sn, ^{121}Sb, ^{151} Eu, and ^{197}Au.

One last thing to mention is the impressive energy resolution of this technique, $\sim 10^{-12}$, which allowed to carry out the only experiments on Earth able to prove Einstein's special relativity theory [117–119].

Operationally speaking, the emitter is usually mounted on an oscillating driver, oscillating forth and back, to promote the Doppler shift, "broadening" the resonance window. This is done because the emitting atoms and the absorbing atoms are in two different lattice environments, which can slightly shift the resonance condition. Hence, slightly Doppler shifting the energies of the emitted gamma rays allows to match the resonance condition between the emitter and the adsorbent. The gamma rays are collected in intensity (count of gamma particles) as a function of the Doppler velocity. For this reason, the data are presented in Intensity (counts) vs Doppler velocity (mm s^{-1}) spectra.

As previously mentioned, Mössbauer spectroscopy relies on hyperfine interactions, which are interactions between electrons and nuclei promoting small shifts in the atomic energy levels. This is what is called the hyperfine structure ($\sim \mu$eV). These interactions are $\sim 10^{10}$ times smaller than the Coulombic interaction binding the electrons to the nucleus, and they are more important from the point of view of the nucleus. Moreover, Mössbauer spectroscopy has two characteristic times. The Larmor precession time, τ_L (~30 ns for ^{57}Fe) at which the nuclear magnetic moment precesses in the magnetic hyperfine field, at a

given temperature. If the transition time τ_t of a transition is $\tau_t \gg \tau_L$, the nucleus sees the electron cloud as static, experiencing its magnetic hyperfine field generated, becoming magnetically ordered. If $\tau_t \ll \tau_L$, the nucleus sees a dynamically changing electron distribution, not experiencing a hyperfine field, being paramagnetic. For $\tau_t \sim \tau_L$, the situation becomes complex, with mixed spectral features and line broadening. The second characteristic time is the mean life of the excited state, τ (for ^{57}Fe is 97.8 ns), which determines Mössbauer spectroscopy resolution. It has to be longer than τ_L to be able to resolve the existing structure. If the transition time is greater than τ, when the gamma ray is emitted, the system will be in either one state or the other, resulting in a spectral superposition of the two states. Conversely, if the transition is much faster, the system will be in both states at each τ, and the nucleus emitted gamma will be a result of an average state. If the two times are the same, then the lineshapes and the whole spectrum becomes complicated. These characteristic times are determining the so-called relaxation features in Mössbauer spectra (or relaxation effects in Fe), such as superparamagnetism (see below).

For Fe-based compounds, the Mössbauer spectra usually consist of a singlet, doublet, or sextuplet (i.e., one, two, or six spectral lines, respectively), or a combination of those. The three main hyperfine interactions are the isomer shift, the electric quadrupole splitting, and the magnetic dipole interaction.

The isomer shift is a correction to the Coulombic interaction, going from the nucleus point charge approximation, to the finite size of the nucleus. This is because the s-electrons have a small yet finite probability of being inside the nucleus of radius (for spherical approximation), $R \sim 10^{-15} Z^{1/3}$ m (with Z atomic number). This causes a shift of the energy levels. In the transition between the excited and ground states, the nucleus radius slightly changes. This implies a difference of a thin annular shell between the nuclear volumes of the two states,

and consequently, a change in the overlap region between the nuclear charge and the electron charge densities. Hence, the energy shifts of these two states are different, by an amount directly related to the electron charge density in the annular shell. This is represented by the isomer shift, δ, by:

$$\delta = \frac{4\pi}{5} Ze^2[|\Psi_a(0)|^2 - |\Psi_s(0)|^2]R\delta R$$

where e is the electric charge, Z is the atomic number, $|\Psi(0)|^2$ is the relativistic electron density inside the nucleus (R = 0) for the absorber, a, and the source, s, and δR is the thickness of the thin annular shell. Since the isomer shift is actually a potential energy, which zero levels are arbitrary, the usual and recommended reference value for ^{57}Fe is that of α-Fe at room temperature. For iron, an increase in isomer shift corresponds to a reduction in s-electron density, and for chemically bound Fe, where the s-electron density will change, the result is quite obvious. However, if a d-electron is involved, like in the transition Fe^{2+} → Fe^{3+}, the charge shielding effect on the nucleus will change, causing the electron cloud to slightly move inwards (this is why anions have bigger ionic radii than cations). Hence, the isomer shift is affected by the changes in oxidation state, coordination and type of ligands, and the changes in value are easier to discuss by comparison with different minerals (i.e., via fingerprint). In a Mössbauer spectrum, the isomer shift consists in a shift of the barycenter of the spectral lines from the zero of calibration (see Figure 1.5 and Figure 1.6).

The quadrupole splitting is related to the nuclear shape, which holds for nuclei with an angular momentum different or nuclear spin $I > \frac{1}{2}$. The deviation from a spherical shape is defined by the nuclear quadrupole moment, Q, via the integral over the nuclear volume:

$$Q = \frac{1}{e}\int \rho(r)(3z^2 - r^2)dV$$

where $\rho(r)$ is the nuclear charge density in r, which has ellipsoidal shape and z-axis of revolution. For $Q > 0$, the nucleus is prolate, for $Q < 0$, the nucleus is oblate. Since in solids Fe is surrounded by atoms, they are immersed in a charge distribution which can be described by an electric field gradient (EFG) of components V_{xx}, V_{yy}, and V_{zz}. The positively charged nuclear ellipsoid will have preferential orientations in this negatively charged electron ellipsoid, and this interaction leads to further energy splitting (see Figure 1.3).

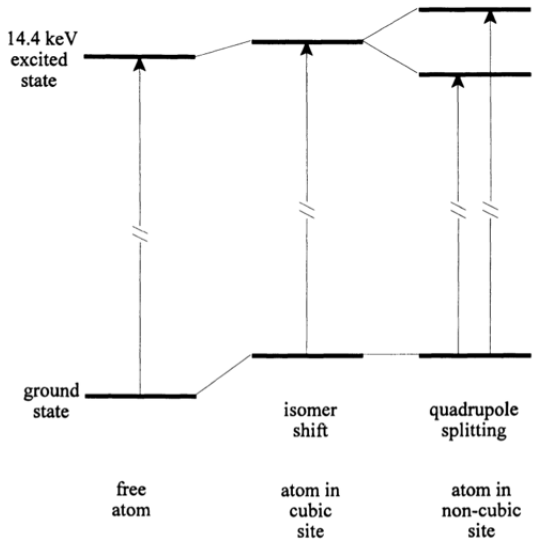

Figure 1.3: Representation of the nuclear energy levels and transitions in 57Fe, and the changes due to the isomer shift and quadrupole interaction (from [75]).

This quadrupole splitting, Δ, of the excited states of ^{57}Fe are given by:

$$\Delta = \frac{1}{2} eQV_{zz} \sqrt{\left(1 + \frac{\eta^2}{3}\right)}$$

where $\eta = (V_{xx} - V_{yy})/V_{zz}$ is the asymmetry factor of the EFG ellipsoid.

The EFG polarizes the closed shell electrons, affecting the nuclear energy levels and how the nucleus sees the lattice EFG itself. High-spin Fe^{3+} ions have

relatively small quadrupole splittings of 0.3-0.7 mm s^{-1} (small EFG contribution). High spin Fe^{2+} have larger quadrupole splittings, typically 1.5-3.0 mm s^{-1} (larger sixth d-electron contribution). Low-spin ions have even smaller quadrupole splitting, eventually equal to zero for perfectly symmetric (cubic) crystals. Hence, the quadrupole splitting provides information on the molecular (a)symmetry of a crystal, and further information on the oxidation sate and character of bonds. In a Mössbauer spectrum, the quadrupole splitting consists of a doublet with line positions given by $\delta \pm \frac{1}{2}\Delta$ (see Figure 1.5). In six-lines Mössbauer spectra, the quadrupole splitting is given by the relative position of the four central peaks, with respect to the two outer peaks (Figure 1.6).

Usually, an excited iron nucleus has a non-zero magnetic moment interacting which that of the (unpaired) electrons. This gives rise to the magnetic hyperfine interaction, in which the nucleus experiences an effective magnetic field generated by the electrons. This is a single-atom measurement providing information on the magnetic properties of the sample.

In paramagnets, the electron magnetic moments flip constantly, resulting in a zero-time average electron magnetic moment over the nuclear level lifetime. Hence, the nucleus does not experience any effective magnetic field.

In magnetically ordered materials, like ferromagnets, ferrimagnets and antiferromagnets, the electron magnetic moment time average is non-zero and the nucleus sees an effective static magnetic field. This causes a further nuclear level split into the $(2I + 1)$ components, $|m_I>$. The 14.4 keV ^{57}Fe ($I = 3/2$) will split in four non-degenerate levels (m_I = -3/2, -1/2, +1/2, +3/2). The ^{57}Fe ground level ($I = 1/2$) will split in two non-degenerate levels ($m_I = \pm$ 1/2). This results in a Mössbauer spectra with six lines (or sextuplet, as shown in Figure 1.5) arising from the different allowed transitions shown in Figure 1.4. The magnitude of the hyperfine field is given by the distance of the outer spectral lines.

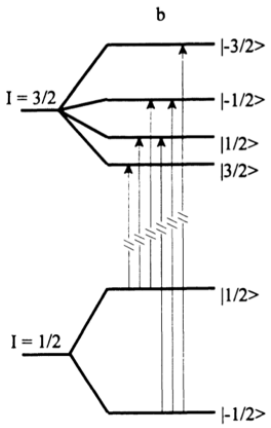

Figure 1.4: Conventional representation of the nuclear energy levels and transitions in magnetically ordered ^{57}Fe (from [75]).

A combination of a strong nuclear interaction and a smaller quadrupole interaction can be interpreted as a further perturbation on the former by the latter. In a Mössbauer spectrum, this appears as a shift of the four inner spectral lines with respect to the outer two (see Figure 1.6) to the left side or to the right side, depending on whether the quadrupole interaction is positive or negative, respectively. As an example, when hematite goes through the Morin transition, the quadrupole splitting changes from a negative to a positive value.

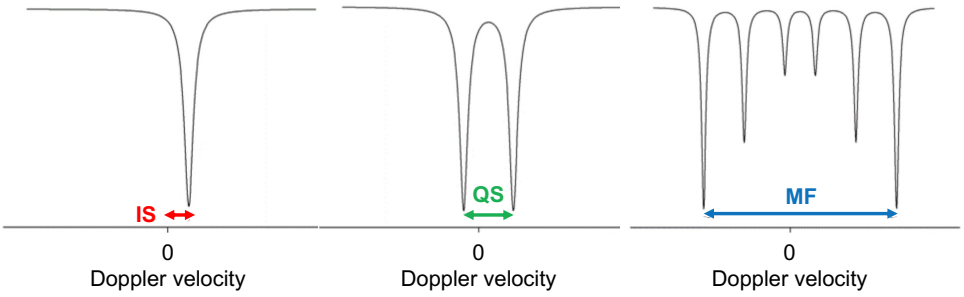

- **ISOMER SHIFT**: oxidation state, ligands electronegativity, character of bonds
- **QUADRUPOLE SPLITTING**: molecular symmetry, oxidation state, character of bonds
- **HYPERFINE MAGNETIC FIELD**: magnetic ordering of the sample *(ferromagnetic, antiferromagnetic, etc.)*

Figure 1.5: Representation of each spectral change related to each hyperfine transitions.

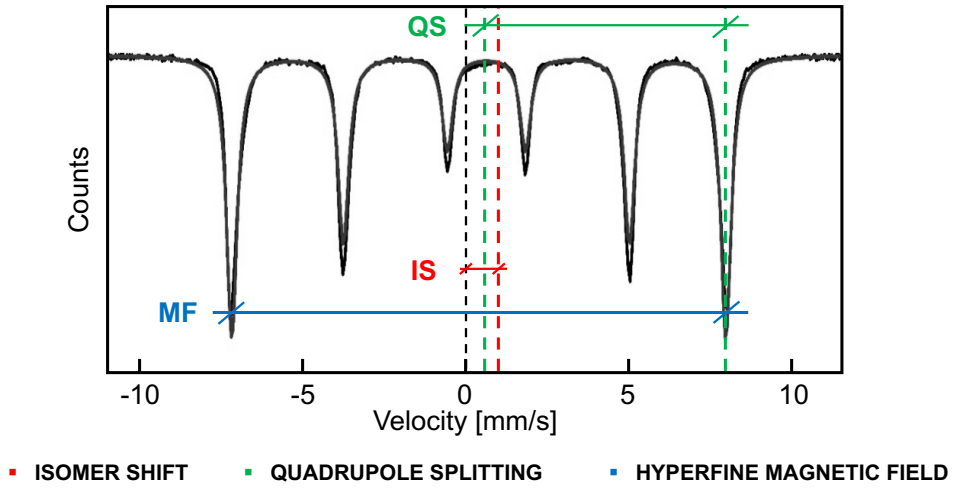

Figure 1.6: Representation of the overall spectral changes due to a combination of the different hyperfine transitions.

The size of the magnetic hyperfine field, B_{hf}, is given by four contributions:

$$\boldsymbol{B_{hf} = B_c + B_{sn} + B_{ln} + B_{ce}}$$

The first term is the Fermi contact term, accounting for the interaction between the electron and nuclear magnetic moments, and is ~ - 33 T. The next two terms are the dipole-dipole interactions terms of the nuclear magnetic moment with the spin and orbital parts of the electronic magnetic moments. For Fe^{3+}, the orbital contribution is ~ 0 T and the spin contribution can reach up to ~ - 11 T per spin. The last term is related to the conduction electrons and is generally negligible. Hence, the total maximum magnetic hyperfine field for a pure Fe^{3+} ion is - 55 T. The negative sign of the magnetic hyperfine field means that its direction is opposite to that of the electron magnetization causing it.

The relative line intensities linked to the different transitions in magnetically ordered iron oxides usually follows the ratio 3 : 2 : 1 : 1 : 2 : 3, according to:

$$I(|3/2> \rightarrow |1/2>) = 3 = I(|-3/2> \rightarrow |-1/2>)$$

$$I(|1/2> \rightarrow |1/2>) = 2 = I(|-1/2> \rightarrow |-1/2>)$$

$$I(|3/2> \rightarrow |-1/2>) = 1 = I(|-1/2> \rightarrow |1/2>)$$

For non-magnetically ordered material with quadrupole splitting, the first two transitions are combined in one line, and the other four in the other line, both of equal intensity. Line intensities can be affected by texture effects, i.e., preferential orientation of the crystals in the sample (e.g., nanorods orientating parallel to the holder bottom).

Line broadening can arise when heating a sample, dealing with significant vacancies, or dealing with small nanoparticles in soft materials (e.g., polymeric matrix). These are called diffusional broadening effects.

The area of the spectral lines is also very important, since it is proportional to the amount of iron present in that specific phase in the sample. Precise quantification becomes even more challenging when addressing non-magnetically ordered materials, even more when they might contain impurities (e.g., natural rocks or doped samples). It can also depend on the iron oxide species and/or particle size. In general, quantitative speciation works better for magnetically split materials, at low temperatures.

It is important to realize that the magnetic order definitions of Fe-based samples are temperature dependent. Magnetically ordered materials consist of smaller magnetic domains with different overall magnetic moments alignments which minimizes the internal energy of the material. Hence, these domains are characterized by magnetic anisotropy, and have preferred direction of magnetization called "easy" direction (which coincides with a crystallographic axis or set of axes). This entails the existence of an anisotropy energy barrier $E_{ani} = K_{ani}V$ (where K_{ani} is the anisotropy constant and V the domain or particle

volume) which needs to be overcome to be able to reverse the magnetization. Magnetization goes as $\sim\frac{H}{T}$, where T is the absolute temperature, meaning that increased magnetization can be obtained either by increasing the external field, H, or lowering the temperature. At high enough temperatures, the thermal vibrations of energy $E_T = k_B T$ (where k_B is the Boltzmann constant and T the absolute temperature) can be large enough to cause continuous spin flips of atoms (or domain). Below a certain temperature, the compound undergoes a transition to a magnetically ordered state, either ferromagnetic, ferrimagnetic, and antiferromagnetic. The characteristic temperatures of such transitions happen are the Curie temperature, T_C, for ferromagnetic and ferrimagnetic compounds, and the Néel temperature, T_N, for antiferromagnetic compounds.

Superparamagnetism is a fast relaxation process involving a group of spins (all moments in a magnetic domain or particle) which rotate together. This process is fast, causing the nucleus to see a zero time-averaged hyperfine field. However, magnetic ordere can be restored at low enough temperatures, below the so-called blocking temperature, T_B (smaller than T_C and T_N). This behavior is related to magnetic anisotropy spin-flips characteristic time, called relaxation time, τ_{rel}. This time is related to the previously introduced anisotropy barrier $K_{ani}V$, where V is the volume of the magnetic domain or particle, and the thermal agitation of energy $k_B T$, via the relation:

$$\tau_{rel} \propto exp\left(\frac{K_{ani}V}{k_B T}\right)$$

This means that ultrafine nanoparticles can go through spontaneous thermal spin reversal, resulting in reduced or absent magnetization. This effect is observed in iron oxide nanoparticles smaller than 10-15 nm (this is what sets the size limit computer disks).

Other relaxation effects cause asymmetrical spectral broadening arising from low crystallinity or impurities in the sample are part of these relaxation effect. For instance, impurities in antiferromagnetic particles will create an unbalance in the two oppositely directed magnetic domains, altering the resulting MS spectrum.

These temperature- and size-dependent effects can be used to estimate the particle size distribution in a sample.

Table 1.1 shows the main Mössbauer-related characteristics of iron oxides. Mössbauer spectroscopy has been used to characterize Fe-based adsorbents. This allowed for better iron oxide phase identification in GEH, showing it consisted of 90 % ferrihydrite and 10 % hematite, against a previous XRD-based characterization, suggesting it consisted of akaganéite [52]. It also allowed to monitor the fate of iron oxide nanoparticles in a type of HAIX, and their transformation from ferrihydrite to goethite after multiple adsorption-desorption cycles [52], partially explaining the decrease in adsorption performances.

Table 1.1: Mössbauer features of different iron oxide minerals (from [75]).

Mineral	T_N, T_C (K)	MAG [a]	B_{hf} (Room Temperature)	δ/Fe (Room Temperature)	Δ (Room Temperature)	B_{hf} (4.2 K)	Δ (4.2 K)
Hematite	955	wfm	51.8	0.37	-0.20	53.5 *or* 54.2 [b]	-0.20 0.41
Magnetite	850	fim	49.2 46.1	0.26 0.67	≤|0.02| ≤|0.02|	50.6 36 - 52 [c]	0.00 1.18-(-0.79)
Maghemite	~ 950	fim	50.0 50.0	0.23 0.35	≤|0.02| ≤|0.02|	52.0 53.0	≤|0.02| ≤|0.02|
Goethite	400	afm	38.0	0.37	-0.26	50.6	-0.25
Akaganéite	299	afm	–	0.38 0.37	0.55 0.95	47.3 47.8 48.9	-0.81 -0.24 -0.02
Lepidocrocite	77	afm	–	0.37	0.53	45.8	0.02
Feroxyhite	450	fim	41	0.37	-0.06	53 52	~0.0 ~0.0
Ferrihydrite	115 [d] 25 [d]	spm	– –	0.35 0.35	0.62 [e] 0.78 [e]	50 [e] 47 [e]	-0.07 -0.02
Bernalite	427	wfm	41.5	0.38	≤|0.01|	56.2	≤|0.01|

Data from Murad and Johnston (1988) and Murad (1996) and references therein. B_{hf} in T, δ and Δ in mm/s.

[a] Magnetic character: fim = ferrimagnetic, afm = antiferromagnetic, wfm = weakly ferromagnetic, spm = speromagnetic.

[b] For afm hematites (that have passed through a Morin transition).

[c] Several magnetic B-site subspectra below the Verwey transition at ~ 120 K.

[d] Range of superparamagnetic blocking temperatures, which vary as a function of crystallinity.

[e] Maximum probabilities of quadrupole-splitting and hyperfine-field distributions.

1.6 Thesis Structure and Outline

1

In the previous sections it was shown how adsorption is a technology that provides enough versatility for P recovery. It has a low footprint, is easily scalable, resilient to a relatively broad range of conditions (temperature, pH, flows, etc.), flexible in operational conditions, and requires minimum operation and maintenance effort. Most importantly, it allows to reach ultra-low P concentrations and to recover P, the latter being highly desirable in the circularity and sustainability framework. The target streams are wastewater treatment plants effluents and surface waters (pH 6-8). In this sense, iron oxides constitute a valuable option as an adsorbent, for the many reasons previously introduced.

This work focuses on manipulating iron oxide-based adsorbents to improve their performances. The starting point was the work of Prashanth Suresh Kumar (my predecessor at Wetsus/TU Delft) finished. The main messages of his work were:

1. To reach ultra-low P concentrations, research should look more into affinity than capacity, with the latter parameter being often misleading.
2. The stability, regenerability, and lifespan of the adsorbent are crucial for the process economic viability.
3. The adsorbent porous structure is critical for the adsorption kinetics.

Hence, the goal of this thesis was to develop a stable and regenerable phosphate adsorbent, with high affinity for P, able to reach the ultra-low P concentrations.

First, goethite was identified as the starting iron oxide. A "nanoparticle approach" was preferred, to better investigate the goethite-phosphate interaction and surface properties, without the influence of pore diffusion. Doping was identified as the right strategy to manipulate goethite properties, mainly the surface properties (e.g., pzc), improving its weaker points (e.g., capacity), while

preserving (or improving) its stronger points (e.g., high affinity, high thermodynamic stability). Different doping strategies were applied, i.e., doping with elements of different oxidation state and increasing doping percentages. The effects of goethite doping on P adsorption was investigated at conditions closer to real life conditions, compared to previous works. These nanoparticles were then fixed on a support, to move towards application. The selected support were anion exchange resins, providing developed HAIX adsorbents, which were tested in solutions with different compositions and conditions. Alternative approaches to improve the lifespan of the adsorbent have been investigated, applying polyelectrolytes multilayers to HAIX, to improve size and charge selectivities, with the final goal to ease the regeneration procedure and increase the durability of the adsorbent.

Throughout these investigations, Mössbauer spectroscopy was applied to finely characterize and monitor the stability of the synthesized nanoparticles. It provided a thorough phase speciation, revealing the successful doping and its effect on goethite properties and speciation.

Chapter 2 investigates and interprets the effect of preferential oxidation states of different dopants on goethite properties.

Chapter 3 follows the results of the previous chapter and investigates the effect of increasing Zn^{2+}-doping of goethite on the adsorption performances, identifying the optimal doping percentage for improved P recovery.

Chapter 4 provides a link between the fundamental nanoparticle studies and their real-life application, by means of HAIX. This work provides many insights on P recovery with HAIX: the dependency of adsorption performances on the choice of experimental conditions; the competition between chemisorption and physisorption, and related implications; the role of the resin backbone; the

speciation and transformation of the nanoparticles; and reveals the complex OH-adsorbed P interaction within the resin during regeneration.

Chapter 5 investigates the effect of multilayer polyelectrolyte coatings of HAIX on adsorption performances and selectivity. This project highlights some limitations of experimental design choices, especially when investigating dynamic processes like selectivity.

Chapter 6 collects and discusses the main findings of this thesis, putting them in perspective for applied P recovery. It also highlights the limitations of experimental conditions and approaches for P recovery studies, together with recommendations on better practices, and little researched or unexplored areas to focus the research on.

1


2

2

Effect of goethite doping using elements with different preferential oxidation states for improved reversible phosphate adsorption

A modified version of this chapter has been submitted as: **Belloni, C.**, Korving, L., Witkamp, G.J., Brück, E., Dugulan, A.I., 2023, *Effect of goethite doping using elements with different preferential oxidation states for improved reversible phosphate adsorption*, Journal of Environmental Chemical Engineering.

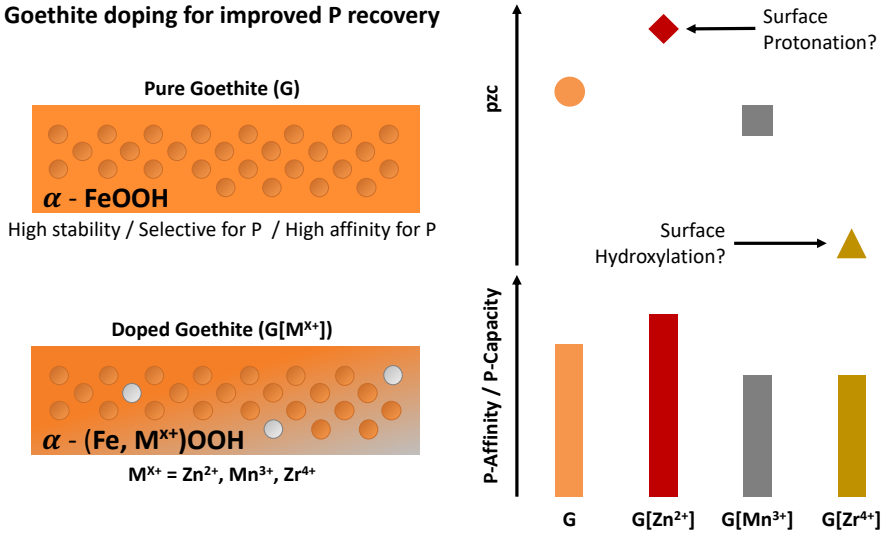

Highlights

- Three different elements with different oxidation states were used as dopants for goethite: Zn^{2+}, Mn^{3+}, Zr^{4+}.
- Zn-doped goethite showed the highest point of zero charge and P adsorption.
- Zr doping of goethite, which has never been attempted before, was successful.
- Mn- and Zr-doped goethite displayed a decrease in P adsorption performances.
- Charge compensation mechanism during doping interesting for adsorbent development.

Keywords:
phosphate recovery, adsorption, regeneration, iron oxide, goethite doping, oxidation state

2

Abstract

Phosphorus (P) removal from freshwater bodies to ultra-low concentrations is fundamental to prevent eutrophication, while its recovery is necessary to close the P usage cycle. Iron oxide-based adsorbents seem promising candidates, being abundant, cheap, and easy to synthesize compounds, with good affinity for P. Affinity is the key parameter when targeting ultra-low concentrations. Also, adsorbent regeneration and re-use is fundamental for the economic viability, hence the adsorbent stability is important. Goethite, (α-FeOOH), is one of the most stable iron (Fe^{3+}) (hydr)oxide species, with higher affinity, but lower adsorption capacity (per kg) compared to other species. Doping could change goethite surface properties, to boost the adsorption capacity, while preserving the high stability and affinity for P. In this work, pure goethite was compared to goethite doped (5 %at.) with different elements of different preferential oxidation states: Zn^{2+}, Mn^{3+}, and Zr^{4+}. Doping was successfully achieved for all elements, albeit Zr showed a lower Fe substitution than targeted. Zn doping increased the goethite point of zero charge and adsorption capacity (per mass and per surface area), preserving the high affinity, while Mn- and Zr- doping displayed a decrease in all the parameters. These could be explained with surface protonation as a charge compensation mechanism in Zn^{2+}-for-Fe^{3+} substitution. The regeneration test showed improved P recovery for Zr- and Zn-doped goethite. All samples remained stable throughout the whole process. This work provides promising insights on doping as a strategy to manipulate iron oxides surface properties and for developing a highly performing and long-lasting goethite-based adsorbent.

2.1 Introduction

Freshwater bodies eutrophication is mainly caused by excess phosphorus (P) [120,121], eventually leading to algae blooms, causing several harmful environmental and socio-economic issues [122–124]. P ends up in water bodies via municipal wastewater and agricultural run-off, being a vital and irreplaceable nutrient, which is (over)used as a fertilizer. Moreover, P is a scarce and non-renewable resource extracted from phosphate rock mines present in a few countries, and its usage is mainly linear. As Europe almost completely relies on its import [32,125,126], the European Commission listed phosphate as a Critical Raw Material, asking for cyclic usage and better management [32,33,127]. In this perspective, P removal and recovery technologies have been developed, especially for wastewater treatment plants (WWTP). However, WWTP effluents P concentration requirements (< 1 - 2 mg L^{-1}) [20] are hundred times higher than the threshold of eutrophication, as algae bloom in freshwater bodies can take place at concentrations above 10 - 20 µg L^{-1} [121]. This is mainly due to the soluble P fraction, phosphate (henceforth also referred to as P for simplicity), which is the bioavailable form of P and the most challenging fraction to remove. For instance, P removal via chemical precipitation in WWTP faces technical and economical limitations to reach such low concentrations [23]. Therefore, a polishing step to remove P down the so-called ultra-low concentrations (< 20 µg L^{-1}) is necessary.

Adsorption with iron oxide-based adsorbents looks promising for reaching ultra-low P concentrations, while allowing for P recovery. Iron oxides (including hydroxides and oxyhydroxides) are abundant, cheap, and easy to synthesize compounds, which display good affinity and selectivity for P. This is because the adsorption mechanism is based on chemisorption, meaning that a chemical bond is formed between the iron oxide surface and phosphate [78]. The process

can be reversed via an alkaline wash, allowing to recover P and regenerate the adsorbent, that can be reused for further adsorption cycles[49]. Many studies have been performed under laboratory conditions, favouring the development of adsorbents with high specific surface area (SSA), and thereby potentially increasing adsorption capacities. An example of that is the work performed by Wang et al., 2013 [85]. In their work, it is shown how ferrihydrite, an amorphous iron oxide species with very high SSA, offers high P-capacity and has often been preferred to other crystalline species such as goethite (α-FeOOH). However, goethite displays higher affinity for P compared to ferrihydrite [85,86]. Affinity is a parameter that provides information on the extent of interaction between the adsorbent and the adsorbate and has also been interpreted as the adsorbent capacity at low adsorbate concentrations [128]. This means that affinity provides an indication on how well an adsorbent is able to adsorb P, even at the low concentrations, making it a crucial parameter when targeting ultra-low concentrations. In this perspective, goethite is an interesting candidate for developing an adsorbent for eutrophication prevention. Moreover, P adsorption studies spent little attention to P recovery and adsorbent regeneration. Kumar et al, 2019 [23], highlighted that reusing an adsorbent for 50 - 100 times would make the process economically viable. Therefore, goethite, being one of the most stable iron oxide species, is promising in regard to reuse than the highly unstable ferrihydrite.

Doping could help manipulating goethite surface properties, increasing adsorption capacity while preserving its affinity and stability. Doping is a key technique in the semiconductor [87–89] and catalysis fields [90–93]. It consists in introducing an elemental impurity, for instance a metal (M), either via inclusion (in interstices) or through substitution, in a host material to alter its properties. The resulting effects depend on the properties of M, such as ionic radius, electronegativity, and oxidation state, and so on [78,94]. Natural and synthetic

goethite, both pure and M-substituted goethite, have been widely investigated from a crystallographic point of view, as well as for their adsorption properties [75,78,95–97,105,129,130]. Often, these studies have been focusing on a single doped goethite sample, and different syntheses procedures were adopted. Among the different M-substituted goethite, several studies have been performed on Al^{3+}-doped goethite [103,104,114,115,105–110,112,113], mainly from a crystallographic point of view, with a few focusing also on P adsorption but not on P-desorption and adsorbent regeneration. Also, a few studies on Mn^{3+}- and Zn^{2+}-doped goethite [97–102,131] crystallographic properties are present in literature, though without addressing P-adsorption. To our knowledge, no mineral study nor attempt of synthesis has yet been conducted on Zr^{4+}-substituted goethite.

In this work, the effect of M-for-Fe substitution in goethite nanoparticles with elements of different preferential oxidation state, i.e., Zn^{2+}, Mn^{3+}, and Zr^{4+}, on its properties and the regenerative P adsorption behaviour has been investigated and compared in a systematic way. In particular, the effect of these dopants on the surface charge and the consequent P-adsorption/desorption performances have been evaluated, and a regeneration of the nanoparticles has been performed. The aim of this study is to provide a coherent investigation and insights on doping as a strategy to effectively manipulate goethite properties to develop an efficient, regenerable and long-lasting adsorbent for P-recovery.

2.2 Materials and Methods

2.2.1 Chemicals

Potassium dihydrogen phosphate (KH2PO4), sodium chloride (NaCl), 1 M sodium hydroxide (NaOH), 1 M hydrochloric acid, 37 % hydrochloric acid

(HCl) and manganese nitrate hexahydrate ($Mn(NO_3)_2 \cdot 6H_2O$) were purchased at VWR (The Netherlands). 3-(N-morpholino) propane sulfonic acid (MOPS) and iron nitrate nonahydrate ($Fe(NO_3)_3 \cdot 9H_2O$) were obtained from Sigma-Aldrich (The Netherlands), and zinc nitrate hexahydrate ($Zn(NO_3)_2 \cdot 6H_2O$) and zirconyl nitrate ($ZrO(NO_3)_2 \cdot xH2O$) from Alfa Aesar (Germany).

2.2.2 Nanoparticles Synthesis

The goethite NPs synthesis was adapted from Villacís-García et al., 2015 [132] and presented here in short. 200 ml of 2.5 M NaOH CO_2-free solution was added to an Fe solution of 50 g of $Fe(NO_3)_3 \cdot 9H_2O$ in 825 g of the CO_2-free MQ at 1 mL min^{-1} with a peristaltic pump (Cole-Palmer, Masterflex L/S), under N_2 bubbling and 250 rpm stirring. After NaOH addition the solution was let stirring for additional 30 min. The suspension, consisting of ferrihydrite, was aged to goethite in an oven at 60 °C for 48 h, occasionally shaking it for better homogeneity. The transformation from ferrihydrite to goethite caused the suspension to turn from dark brown to ochre.

The doped nanoparticles were synthesized following the same procedure, with the only difference of having a mixture of Fe and 5 %at. M/Fe solution, for which the Zn, Mn and Zr salts were weighed accordingly. The color change in this process was from dark brown to orange/purple for Zn, to black/olive green for Mn and to a different shade of ochre for Zr.

The NPs were then separated via Buchner filtration, thoroughly rinsed with MQ water, resuspended in Demineralized Water (DW), thoroughly shaking and sonicating for 10 min at 40 kHz (Bandelin, Sonorex RM16UH). The pH was adjusted to around 7 with HCl and NaOH. The NPs were let to settle while the supernatant replaced with DW and adjusted to pH 7, until its conductivity was below 0.1 µS cm^{-1}.

The synthesized samples are referred to as G for the pure goethite, and G[Zn5], G[Mn5] and G[Zr5], based on the nominal doping.

2.2.3 Nanoparticles Characterization

The NPs were characterized with several techniques, to retrieve as many information as possible.

The pH and conductivity of the suspensions were measured with a SevenExcellence pH/Cond meter S470, Mettler-Toledo.

The NPs mass concentration of each suspension was assessed by dry weight, drying NPs suspension aliquots in the oven at 60 °C.

The M-for-Fe %at. was verified by dissolving the NPs (upon centrifugation) in HCl 37 % acid solution and analyzing the elemental composition with a Perkin Elmer Optima 5300 DV Inductively Coupled Plasma Optical Emission Spectroscopy (henceforth referred to as ICP).

The size and shape of the pure and doped NPs were retrieved with a JOEL JEM1400-plus Transmission Electron Microscopy (TEM) with a TVIPS F416 camera operating at 120 kV. Over 200 NPs per sample were analyzed with ImageJ software to estimate the NPs size distribution. The NPs crystallinity was also qualitatively investigated with Selected Area Electron Diffraction (SAED).

Qualitative crystallinity and crystallite size estimation, and precise phase identification were obtained with X-Ray Diffraction (XRD) measurements. The diffractometer was a PANalytical X'Pert pro X-Ray mounted in the Bragg-Brentano configuration with a Cu anode (0.4 mm x 12 mm line focus, 45 KV, 40 mA). X-Ray scattered intensities were measured with a real-time multi strip (RTMS) detector (X'Celerator). The sample holder was a spinner, and the angle range for data collection was $10° < 2\theta < 100°$ with a step size of 0.008° (2θ) and

measuring time of 1 h. XRD patterns were analyzed in fingerprinting mode using the PANalytical X'Pert software.

Mössbauer spectroscopy (MS) was employed to thoroughly identify the iron oxide phases of the pure and doped samples, investigating the effect of the dopants on the goethite properties. MS was also used to assess the sample stability after regeneration. Measurements were performed at three different temperatures, 300 K, 120 K (set-up thermalization with liquid N_2) and 4.2 K (liquid He temperature), as the low temperatures promote the Zeeman splitting, helping to better identify the different species. Transmission ^{57}Fe MS spectra were collected with conventional constant acceleration or sinusoidal velocity spectrometers using a ^{57}Co (Rh) source and calibrated to α-Fe. The MS spectra were analyzed with MossWinn 4.0 software [133] to obtain some fundamental parameters for the phase identification: the isomer shift (IS) [mm s^{-1}], the quadrupole splitting (QS) [mm s^{-1}], the hyperfine magnetic field (H_f) [mm s^{-1}], as well as the peaks line-width (Γ) [mm s^{-1}] and the spectral phase contribution [%].

The surface charge of the pure and doped NPs was estimated in terms of point of zero charge (pzc), i.e., the pH at which the net surface charge of the adsorbent is neutral. The pzc was estimated adapting the salt addition method from Mahmood et al., 2011 [134], and Tan et al., 2008 [135]. The whole procedure was performed in a glovebox, with all solutions being bubbled with N_2 gas to prevent pH fluctuations, and all NPs suspensions were sonicated for 10 min before use. Shortly, 50 mL centrifuge tubes with 10 mL of 5 g L^{-1} NPs suspensions were prepared (in duplicates) with different initial pH between 5 - 10 using HCl and NaOH. The samples were placed in a shaking incubator at 150 rpm and 25 °C for 5 days, to let the solution equilibrate. The initial pH, pH_{in}, were then measured, and 0.526 of 2 M NaCl solution was consequently added to the samples, obtaining a final NaCl concentration of 0.1 M. The samples were placed in the shaking incubator for at least a week for equilibration. The final pH, pH_{fin},

was then measured and recorded for each NP sample, the pH differences, ΔpH = pH_{fin} - pH_{in}, were plotted against the pH_{in} values. The data were then interpolated with two approaches: a polynomial curve applied to the whole data range; a linear function applied to the data for which ΔpH approaches zero. The pzc is the pH value at which ΔpH = 0, which is the value at which the plotted curve crosses the x axis (pH_{in}). The error assigned to the pzc was ± 0.15, which is an excess approximation of the root mean squared sum of the single contributions being: ± 0.10 for pH_{in}, ± 0.05 for pH_{fin}, and ± 0.02 of the pH meter (handheld PH 20, VWR, with GE 114 WD electrode).

The specific surface area (SSA) of the NPs was estimate using Micromeritics Tristar 3000 via Brunauer-Emmett-Teller analysis. Samples of 100 mg of dried NPs were degassed overnight under N_2 atmosphere, followed by N_2 adsorption-desorption cycles for SSA estimation. The data were analyzed with the non-local density functional theory model in the built-in software.

The NPs samples for MB, XRD and SSA measurements were centrifuged, oven-dried at 40-60 °C and grinded before being placed in the respective sample holders.

2.2.4 Phosphate Adsorption Experiments

For the P adsorption experiments, a stock solution of 500 mg L^{-1} of P in DW was prepared from KH_2PO_4 salt. Different dilutions were prepared, to obtain P concentrations of 0.1, 0.5, 0.75, 1, 2.5, 5, 7.5 and 10 mg L^{-1}, each with 20 mM MOPS as a pH buffer, and pH adjusted to around 7.2 with NaOH/HCl. The NPs suspensions of 1 g L^{-1} were prepared and sonicated for 10 min before addition. The addition consisted of 100 mL of P diluted solutions, from which 10 mL were removed for ICP analysis, and 10 mL of NPs suspensions, for the adsorption duplicates (adsorbent concentration of 0.1 g L^{-1}), or 10 mL of DW, for the blanks, were added. The samples were then placed in a shaking incubator at 25

°C and 150 rpm for 2 days, as previous tests showed this time was more than enough to reach the adsorption equilibrium. Nevertheless, a few samples were kept running for one more week and then analyzed for control, without showing any relevant difference.

2.2.5 Desorption/Regeneration Experiments

The regeneration test was performed following an adsorption experiment similar to that performed for the adsorption equilibrium experiment. In this case, after equilibrium was reached, the pH was increased in the same solution via NaOH addition. This procedure was chosen to avoid NPs separation via centrifugation, which can cause irreversible NPs agglomeration, and long sonication to redisperse them, which can structurally affect the NPs. For these reasons it was opted for a single regeneration run and not multiple adsorption-desorption cycles. Moreover, the idea of this test is to verify whether regeneration would require more effort with doped goethite in case doping would promote a stronger NPs-to-P bond or other P removal mechanism such as surface precipitation.

The adsorption experiment preceding the regeneration step was performed preparing 100 mL solutions with P concentrations of 25 mg L^{-1} and 20 mM MOPS at pH 7.2, from which 10 mL were removed for ICP analysis, replaced by 10 mL of 3 g L^{-1} NPs suspension for the adsorption duplicates, and 10 mL of DW for the blanks. The samples were placed in a shaking incubator at 25 °C and 150 rpm for 5 days. Then, 5 mL were collected for ICP analysis while 5 mL of 1 M NaOH solution was added, increasing the pH to about 12.6. The samples were shaken at 25 °C and 150 rpm for 1 day. The solution was then analyzed with ICP and the NPs with MS. The regeneration pH was deliberately at a lower value compared to the usual pH 13 - 14 (0.1 - 1 M NaOH) to enhance the desorption differences. In fact, the main goal is to investigate whether a different P uptake mechanism (e.g., surface precipitation, stronger bond, etc.) due to

doping would require higher effort for desorption. Moreover, for a single run, desorbing at pH 13-14, where usually all the P is desorbed, would not highlight any difference, and would not show any relevant information on possible NPs (synthesized at pH > 12) deterioration.

2.2.6 Samples Analysis

All the P-based solutions were analyzed with ICP, to determine the initial concentrations, C_0 [mg L^{-1}] of the blanks and the equilibrium concentrations, C_{eq} [mg L^{-1}] of the adsorption samples. The latter were always filtered with a 25 nm pore size filter (MF-Millipore Membrane Filter, 0.025 μm pore size, Merck), with the help of a six channel NE-1600 syringe pump (New Era Pump Systems, Inc.) prior ICP samples preparation. No appreciable difference in P concentrations was observed between the filtered and unfiltered blank samples, assuming filtration to have a negligible influence on the P concentrations at these ranges. The amount of P adsorbed per mass of adsorbent, q [mg g^{-1}], was calculated with:

$$q = \frac{C_0 - C_{eq}}{m_{NPs}} V$$

where m_{NPs} [g] is the mass of adsorbent and V [L] is the volume of the sample.

2.2.7 Data Analysis

The adsorption isotherms were obtained by plotting q against C_{eq} (with duplicate data) and fitting them with two adsorption isotherm models, the Langmuir [136] and the Freundlich [137] isotherm models.

The Langmuir isotherm assumes a monolayer-like adsorption with homogeneous adsorption sites and without interaction between the adsorbed adsorbate molecules. Hence, this is an ideal model, and it was developed for gas adsorption on solid phase. The Langmuir isotherm equation is:

$$q = \frac{q_{max} K_L C_{eq}}{1 + K_L C_{eq}}$$

where q_{max} [mg g^{-1}], is the capacity, identified by the height of the isotherm plateau, and K_L [L mg^{-1}] is the Langmuir constant which is related to the affinity between the adsorbate and the adsorbent binding sites, identified by the steepness of the ascending part of the isotherm.

The Freundlich isotherm is an empirical model, i.e., its constants do not have a physical meaning, and it assumes adsorption to happen on a heterogeneity of sites. The Freundlich isotherm equation is:

$$q = K_F {C_{eq}}^n$$

where K_F [(mg g^{-1})(mg L^{-1})$^{-n}$] is the Freundlich constant, also called adsorption strength, which is related to the capacity of the adsorbent, and n is a dimensionless constant related to the surface sites' heterogeneity.

Given the strong limitation of the two models, the fitting parameters were evaluated carefully, as a mere mean of comparison, meaning that results were interpreted in relative terms between the different samples, rather than in absolute terms or with too much physical interpretation.

Similarly, data were also analyzed in terms of P adsorption per SSA of the NPs.

The fittings were performed using Microsoft Excel Solver, minimizing the RMSPE (Root Mean Square Percentage Error), which values were reported as a measure of the goodness of the fit.

For the regeneration tests, the adsorbed P per mass and per SSA and the percentage of P desorbed have been reported in histogram plots, together with the duplicate values.

Finally, the P surface coverage percentage after adsorption and the un-desorbed P fraction after regeneration have been calculated considering a phosphate ionic radius of 238 pm [138].

2.3 Results and Discussion

2.3.1 Characterization

The synthesized NPs suspensions display different colors, as visible in Figure 2.1. G and G[Zr5] display different shades of ochre, G[Zn5] an orange/purple color while G[Mn5] a black/olive green color. In particular, the latter appears to be slightly attracted to strong magnets (not shown here).

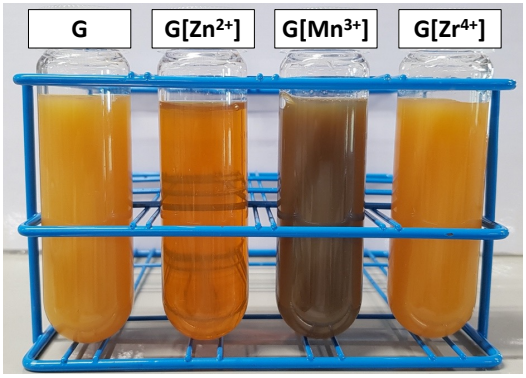

Figure 2.1: The synthesized NPs suspensions (1 g L-1, pH ~ 7), G, G[Zn5], G[Mn5], G[Zr5] (left to right), showing the different colors of the suspensions.

2.3.1.1 Elemental Composition and SSA Measurements

The ICP elemental analysis performed on the doped samples after NPs dissolution, values are reported in Table 2.1, confirmed the desired 5 %at. M-for-Fe substitution for Zn and Mn, while a lower Zr-for-Fe substitution ((3.9 ± 0.2) %at.) was observed. Zr has an ionic radius of 72 pm [139], about 12 % larger than that of Fe^{3+} (65 pm, for high-spin Fe^{3+} in sixfold coordination, as is in goethite [139]), which falls within the ionic radius difference range for successful

isomorphous substitution in goethite (< 18 %, [78]). Nevertheless a different Zr-for-Fe substitution can be expected since the ionic charge of Zr (+4) is higher than that of Fe in goethite (+3) [78]. A reason for that could be a combination of the higher charge and bigger size compared to Fe^{3+} [78], since other higher oxidation state elements like Ti^{4+}, which has a smaller radius (61 pm, [139]) than that of Fe^{3+}, was shown to successfully substitute for Fe in goethite [130].

Table 2.1: Theoretical and experimental doping %at. from ICP analysis after NPs acid dissolution, and SSA values from BET analysis of the different synthesized NPs.

Sample	*Theoretical Zn/Fe %at.*	*Experimental Zn/Fe %at.*	*SSA [m^2 g^{-1}]*
G	0	0	84.7 ± 0.9
G[Zn5]	5	5.1 ± 0.3	76.0 ± 0.8
G[Mn5]	5	5.1 ± 0.3	74.2 ± 0.3
G[Zr5]	5	3.9 ± 0.2	69.4 ± 0.2

The BET analyses show all the samples to have SSA values of the same order of magnitude, following the trend: G > G[Zn5] > G[Mn5] > G[Zr5]. SSA values are reported in Table 2.1.

2.3.1.2 TEM and SAED

The NPs morphology analysis performed with TEM, shown in Figure 2.2, reveals that all the samples consist of rods, typical of goethite[78], with aspect ratio changing with doping, as expected [78]. G[Zn5] displays elongated and narrower rods, compared to G, as observed also by Krehula et al., 2006 [131]. Similarly, G[Mn5] displays elongated and narrower rods, with also the presence

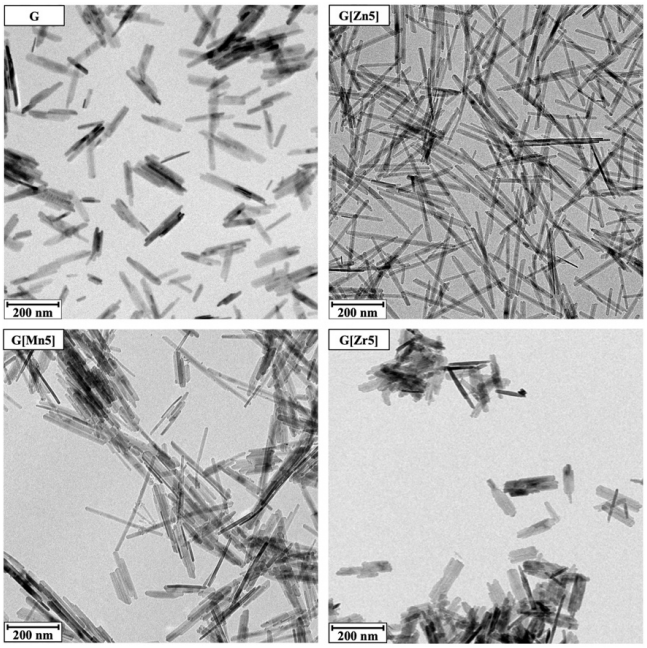

Figure 2.2: TEM images of the synthesized NPs.

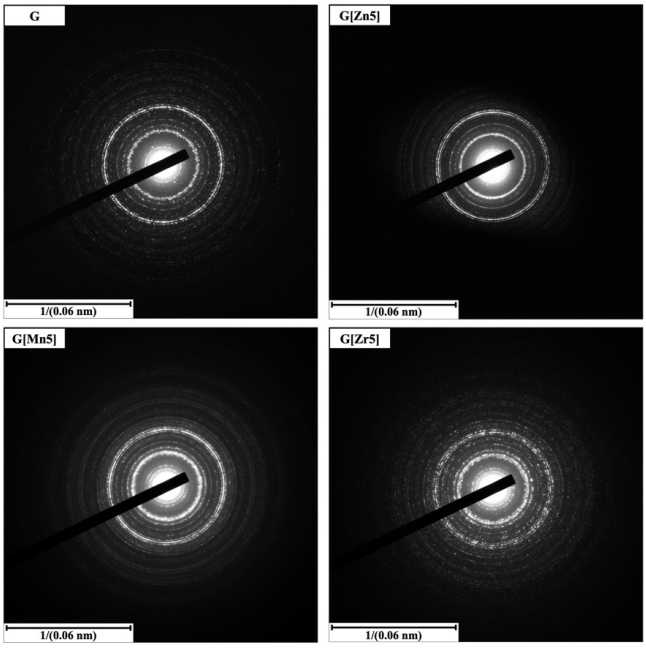

Figure 2.3: SAED patterns of the synthesized NPs.X-Ray Diffraction

of filament like rods, in agreement with observations by Rout et al., 2014 [100]. Conversely, G[Zr5] NPs displayed a shortening and widening of the rods with irregular shape and a rougher surface compared to the other samples. The different habit could be explained with the different mechanism of Zr substitution in goethite, causing retardation in the growth of different crystal facets compared to the other dopants. This could perhaps be related as well to the lower Zr %at. observed, suggesting that Zr is over all less prone to substitute Fe in goethite.

A precise size estimation was not possible given the agglomeration of the NPs during TEM sample preparation. Thus, a more qualitative size estimation was performed with ImageJ, supporting what was previously discussed on the different aspect ratios, and the corresponding values are reported in Table 2.2.

Table 2.2: Particle size estimation of the synthesized NPs from TEM images using ImageJ software.

Sample	Length [nm]			Width [nm]		
	Min	Max	Mean	Min	Max	Mean
G	11	305	102 ± 46	3	23	11 ± 3
G[Zn5]	12	330	115 ± 55	3	20	9 ± 3
G[Mn5]	13	417	133 ± 61	1	33	11 ± 5
G[Zr5]	16	196	98 ± 35	2	30	15 ± 6

SAED images, shown in Figure 2.3, reveal that all the samples consist of polycrystalline NPs of goethite, as inferable from the well-defined ring patterns with intense spots.

2.3.1.3 X-Ray Diffraction

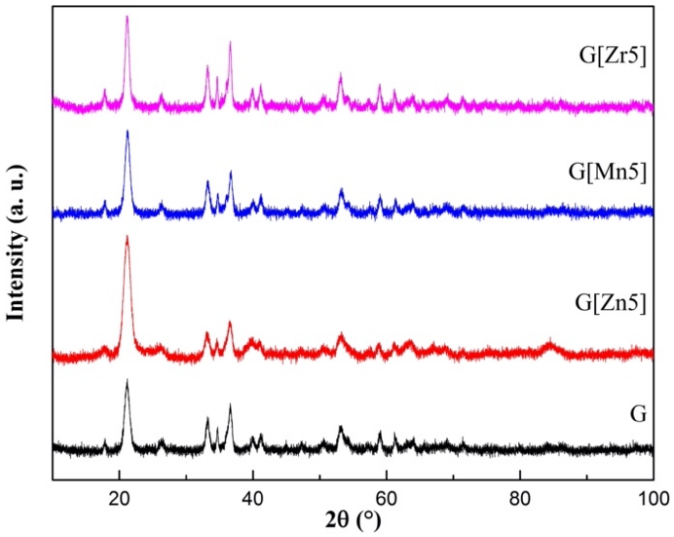

Figure 2.4: XRD patterns of the synthesized NPs.

The analysis of the XRD patterns, shown in Figure 2.4, displayed good agreement with the goethite phase for all samples, meaning that doping did not promote the formation of other iron oxide species. Differences in the peak intensity and broadening can be ascribed to different causes, such as preferential orientation, different aspect ratio, and different crystallinities of the NPs rods. These results are in agreement with SAED observations. A qualitative crystallite size estimation for each sample has been obtained with the PANalytical X'Pert software, and the values are reported in Table 2.3.

Table 2.3: Indicative estimation of the crystallite sizes from XRD patterns of the synthesized NPs.

Sample	*α-FeOOH*
G	120 Å
G[Zn5]	70 Å
G[Mn5]	105 Å
G[Zr5]	140 Å

2.3.1.4 Mössbauer Spectroscopy

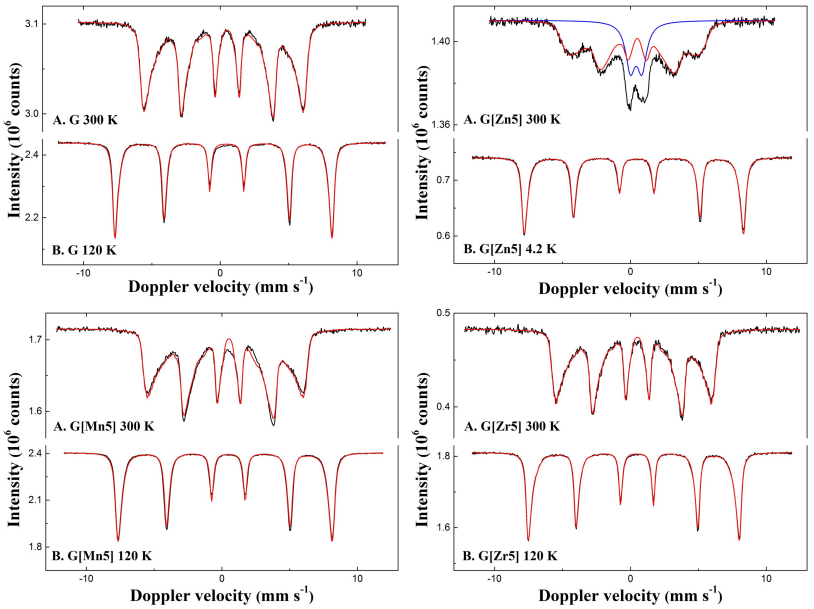

Figure 2.5: MS spectra of the synthesized NPs measured at different temperatures (300, 120 and 4.2 K). Black lines represent the measured spectra, colored lines represent the fitted spectral contributions.

MS spectra are reported in Figure 2.5, while Table 2.4 reports the fitting parameters values, together with the hyperfine parameters of bulk goethite [140]. The analyses support what was already observed with TEM-SAED and XRD, namely, the sample consist of goethite-like phases. The 300 K spectra of all samples provided IS and QS values typical of high-spin Fe^{3+} in octahedral coordination. The peaks asymmetrical broadening at 300 K is typical of the goethite phase with a distribution in particle sizes, hence a magnetic distribution fit was applied. The observed H_f values are lower compared to the 38.0 T typical of bulk goethite, and this is indeed related to the nanosized nature of the samples. Moreover, a further reduction in the H_f value was registered for the doped samples, suggesting a successful M-for-Fe substitution, as impurities are known

Table 2.4: MS reference values and fitting parameters of G, G[Zn5], G[Mn5] and G[Zr5] at 300 K, 120 K and 4.2 K.

Sample	*T (K)*	*IS (mm·s^{-1})*	*QS (mm·s^{-1})*	*H_f (T)*	*Γ (mm·s^{-1})*	*Phase*	*Spectral contribution (%)*
Bulk goethite reference values [140]	300	0.37	-0.26	38.0	-	-	-
	4.2	0.37	-0.25	50.6	-	-	-
G	300	0.38	-0.26	32.4*	0.28	α-FeOOH	100
	120	0.36	-0.24	48.9*	0.26	α-FeOOH	100
G[Zn5]	300	0.38	-0.24	24.6*	0.53	α-(Zn,Fe)OOH	77
		0.42	0.85^	-	0.85	Fe^{3+}	23
	4.2	0.35	-0.21	49.6*	0.32	α-(Zn,Fe)OOH	100
G[Mn5]	300	0.38	-0.27	29.8*	0.25	α-(Mn,Fe)OOH	100
	120	0.36	-0.25	48.4	0.29	α-(Mn,Fe)OOH	100
G[Zr5]	300	0.38	-0.27	30.9	0.26	α-(Zr,Fe)OOH	100
	120	0.36	-0.24	46.9	0.23	α-(Zr,Fe)OOH	100

Experimental uncertainties: I.S. ± 0.01 mm s^{-1}; Q.S. ± 0.01 mm s^{-1}; Γ ± 0.01 mm s^{-1}; H_f ± 0.1 T; Spectral contribution: ± 3 %.
**Average magnetic field. ^Fixed value.*

to reduce the magnetic coupling between the Fe atoms in the crystals. Sample G[Zn5] 300 K spectrum appears different from the others, as its spectrum consists of a broad sextet ($\Gamma = 0.53$ mm s^{-1} compared to $\Gamma \sim 0.3$ mm s^{-1} of the other samples) and a doublet. This latter contribution represents a paramagnetic-like behavior, suggesting that either two different phases are coexisting, or the magnetic coupling was more reduced for Zn substitution compared to Mn and Zr. Thus, a measurement at 4.2 K was performed on G[Zn5], which proved the sample to consist of one unique phase of homogeneously Zn-doped goethite, as inferable from the unique sharp sextet and the retrieved fitting parameters. For the other samples, measurements at 120 K were enough to confirm that G consisted of pure goethite, while G[Mn5] and G[Zr5] consisted of unique Mn-doped and Zr-doped goethite phases, respectively.

2.3.1.5 Point of Zero Charge

The pzc of the different samples estimated with both the polynomial (degree 4) and linear interpolations, see Figure 2.6, are reported in Table 2.5 and Figure 2.7. Both approaches show agreement in the pzc determination, except for G[Zr5] with a deviation within the errors and thus does not affecting the overall trend, which is G[Zn5] > G > G[Mn5] > G[Zr5]. This is contrary to what was hypothesized, a higher oxidation state to favor a more positive surface charge (higher pzc) in goethite, since Zn, Mn and Zr Pauling's electronegativity values are similar, (1.5 - 1.6 [141]), and lower than that of Fe (1.8). However, a similar result was obtained by Mohapatra et al., 2006 [129], which observed an increase in the pzc of goethite when doping with Cu^{2+}, while the opposite was observed when doping with Ni^{2+}. This effect could be explained by hypothesizing a higher surface protonation in G[Zn5], due to a charge compensation mechanism in Zn^{2+}-for-Fe^{3+} substitution, as proposed by Giovanoli et al., 1992 [97].

These results suggest G[Zn5] having a "more positive" surface charge in the pH range 6 - 8 of interest for freshwater bodies and WWTP effluents, while the opposite holds for G[Zr5], which would transition from weakly positive to weakly negative. This could be due to the opposite trend, in which Zr^{4+}-doped goethite might retain more OH^- surface groups, as a charge compensation mechanism or others, as a similar result was observed for Al^{3+}-doped goethite [116].

Table 2.5: pzc values of the synthesized NPs obtained from the polynomial and the linear data interpolation approaches.

Sample	*pzc (polynomial)*	*pzc (linear)*
G	8.42	8.42
G[Zn5]	8.81	8.81
G[Mn5]	8.24	8.24
G[Zr5]	7.50	7.40

An excess error of ± 0.15 is assigned to all the pzc values.

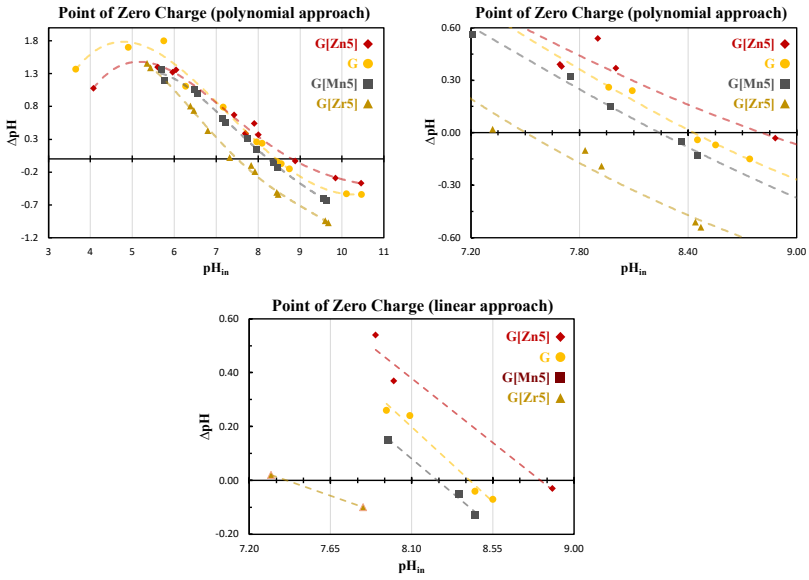

Figure 2.6: graphs of the pzc values estimated with the polynomial (whole range and zoom on the axis) and linear data interpolation.

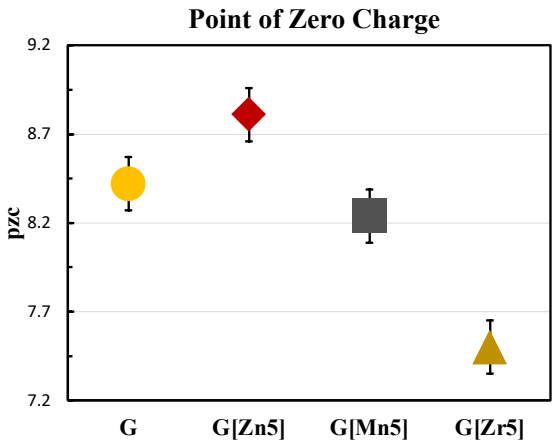

Figure 2.7: pzc values estimated from the polynomial data interpolation.

2.3.1.6 Adsorption Experiments

Figure 2.8 shows the adsorption isotherms per unit mass for all the NPs samples, with the fitted Langmuir and Freundlich curves, fitting parameter values are reported in Table 2.6. Both models seem to describe the adsorption trends well, probably due to the low adsorbent concentrations involved in the experiments (maximum SSA P coverages between 20-30 %) and relative homogeneity of the different NPs surface morphologies. Nevertheless, it is important to remind that the two models face several limitations, and their application and fitting parameter values are meant just to help with the comparison and should be interpreted in relative rather than absolute terms. The adsorption trend is the same as that observed for the pzc: G[Zn5] > G > G[Mn5] > G[Zr5], as reflected by the fitting parameters: q_{max}, K_L, K_F and n^{-1}. Focusing on the affinity constant K_L, it is visible that goethite affinity for P has not been compromised by Zn-doping (actually slightly improved), while a reduction to a less than a third was observed with both Mn and Zr. This might be related to the higher pzc of G[Zn5], meaning that the more positive surface charge is able to attract more P. Figure 2.9 shows the adsorption isotherms per SSA, and the fitting parameters

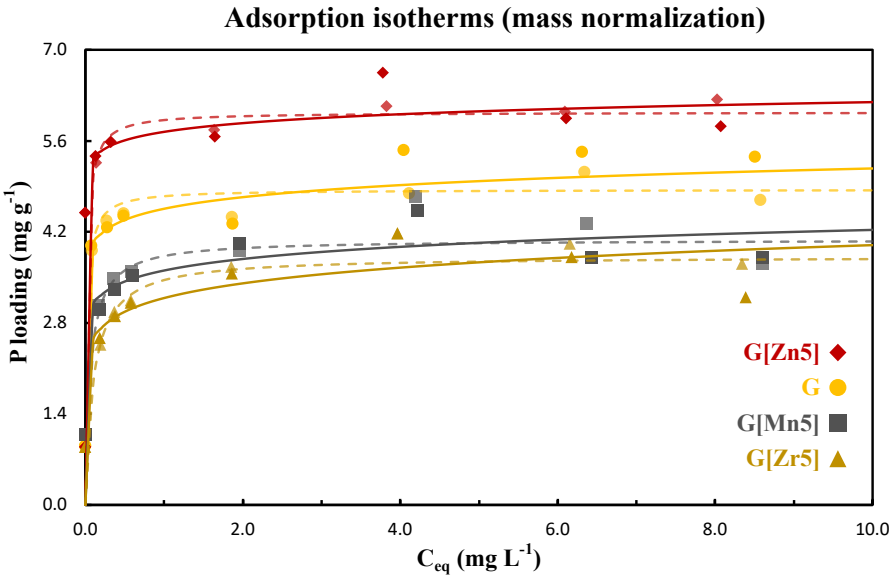

Figure 2.8: Freundlich (solid line) and Langmuir (dashed line) adsorption isotherms with the duplicates data of the different synthesized NPs. Results are normalized with respect to the mass of adsorbent.

Table 2.6: Langmuir and Freundlich fitting parameter of G, G[Zn5], G[Mn5] and G[Zr5] adsorption isotherms normalized to the mass of the adsorbent, with the relative RMSPE.

Sample	*Langmuir*			*Freundlich*		
	q_{max} *[mg g^{-1}]*	K_L *[L mg^{-1}]*	*RMSPE*	n	K_F [(mg g^{-1})(mg L^{-1})$^{-n}$]	RMSPE
G	5	47	0.34	0.06	5	0.34
G[Zn5]	6	49	0.47	0.03	6	0.47
G[Mn5]	4	15	0.34	0.07	4	0.34
G[Zr5]	4	10	0.34	0.10	3	0.34

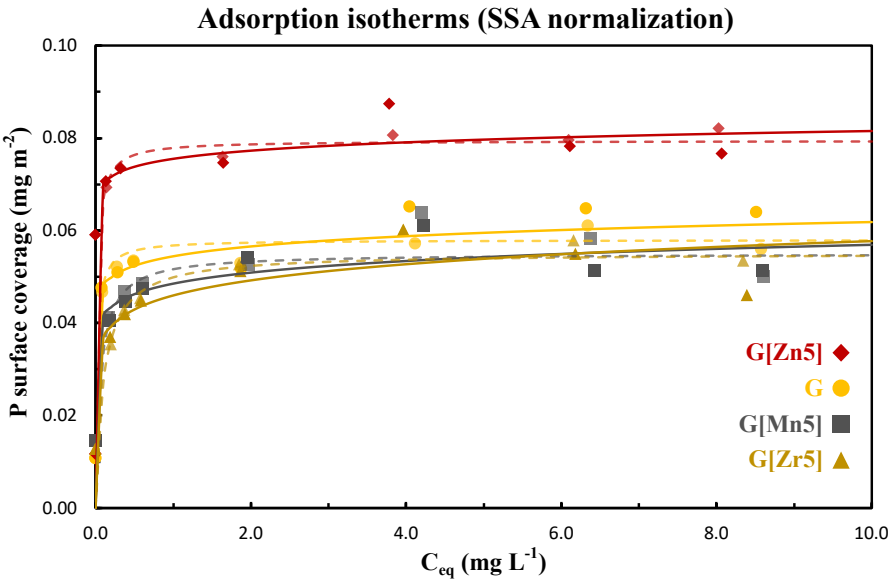

Figure 2.9: Freundlich (solid line) and Langmuir (dashed line) adsorption isotherms with the duplicates data of the different synthesized NPs. Results are normalized with respect to the SSA of the adsorbent.

Table 2.7: Langmuir and Freundlich fitting parameter of G, G[Zn5], G[Mn5] and G[Zr5] adsorption isotherms normalized to the SSA of the adsorbent, with the relative RMSPE.

Sample	*Langmuir*			*Freundlich*		
	q_{max} $[mg\ m^{-2}]$	K_L $[L\ mg^{-1}]$	*RMSPE*	n	K_F $[(mg\ m^{-2})(mg\ L^{-1})^{-n}]$	RMSPE
G	0.06	47	0.34	0.06	0.05	0.34
G[Zn5]	0.08	49	0.47	0.03	0.08	0.47
G[Mn5]	0.06	15	0.34	0.07	0.05	0.34
G[Zr5]	0.06	10	0.34	0.10	0.05	0.34

are reported in Table 2.7. Also in this case, G[Zn5] shows the highest P adsorbed, about 50 % higher (both per mass and SSA) compared to the others. This suggests G[Zn5] to have a more efficient surface for P adsorption, with the more positive charge able to attract more P, and possibly a higher site density or wider functional crystal faces for P adsorption. Further, this shows that SSA is not directly related to the adsorption performances, hence not being a determining factor for the adsorption capacity.

2.3.1.7 Regeneration Experiments

The regeneration tests followed an adsorption experiment that consistently reproduced the trends observed in the isotherm experiments, both per mass and per SSA, as visible in Figure 2.10 and Table 2.8.

These results translate in a higher P surface coverage of about 33 % for G[Zn5], while a similar coverage between 22 - 24 % were observed for the other samples, further corroborating the higher adsorption sites density of G[Zn5].

The regeneration tests, desorption percentages reported in Table 2.9 and Figure 2.11, show the following trend: G[Zr5] > G[Zn5] ≳ G > G[Mn5]. This means that samples G[Zn5] and G[Zr5] did not require more effort for the regeneration compared to G, suggesting that no different P removal mechanism, such as precipitation, was promoted by the dopant. Sample G[Mn5], however, displayed the lowest desorption potential, and it is not to be excluded that a stronger bond or other mechanisms like surface precipitation might have happened. We conclude from these results that that Zn- and Zr- doping did not affect the P bonding mechanism to the extent of requiring more or less effort for desorption.

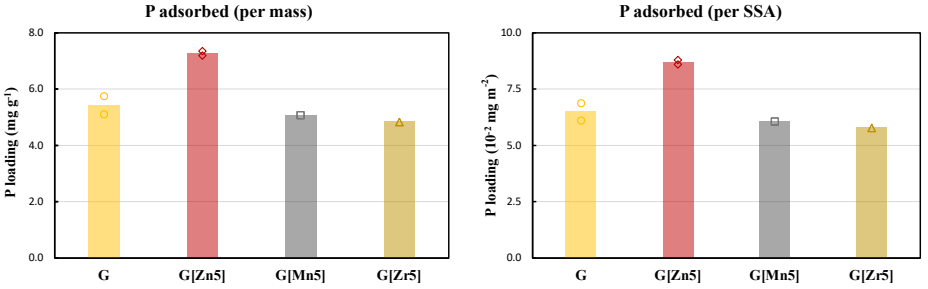

Figure 2.10: P adsorbed normalized to the mass (left) and SSA (right) of adsorbent per each sample.

Table 2.8: Amount of adsorbed P per mass and SSA of adsorbent and relative surface coverage of samples G, G[Zn5], G[Mn5] and G[Zr5].

Sample	*P adsorbed [mg g^{-1}]*	*P adsorbed [10^{-2} mg m^{-2}]*	*% SSA coverage*
G	5.4 ± 0.3	6.5 ± 0.4	22 ± 1
G[Zn5]	7.27 ± 0.08	8.7 ± 0.1	33.1 ± 0.4
G[Mn5]	5.06 ± 0.05	6.05 ± 0.06	23.6 ± 0.2
G[Zr5]	4.84 ± 0.05	5.78 ± 0.06	24.1 ± 0.2

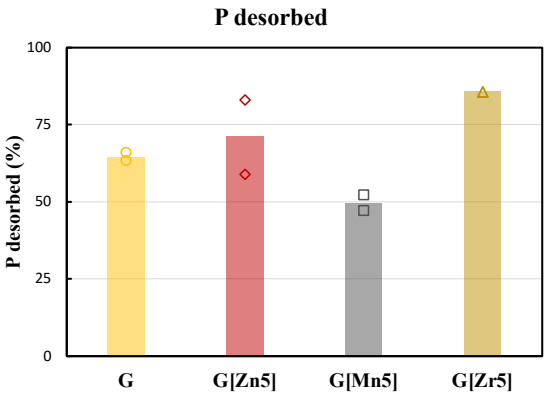

Figure 2.11: Desorbed P and relative surface hindrance of undesorbed P of samples G, G[Zn5], G[Mn5] and G[Zr5].

Table 2.9: Desorbed P and relative surface hindrance of undesorbed P of samples G, G[Zn5], G[Mn5] and G[Zr5].

Sample	P desorbed % w/w	% SSA still covered
G	65 ± 1	6.8 ± 0.7
G[Zn5]	71 ± 12	8 ± 4
G[Mn5]	50 ± 4	10.7 ± 0.6
G[Zr5]	86 ± 8	2.2 ± 1

2.4 Mössbauer Spectroscopy on the Regenerated Samples

The MS measurements of the regenerated samples were performed only at 300 K, as this was sufficient to draw conclusions, with the exception of sample G[Zn5], for similar reasons as explained in section 3.4. The spectra are shown in Figure 2.12 while the fitting parameters from data analysis are reported in Table 2.10. G, G[Mn5], and G[Zr5] appeared to still consist of goethite-like phase, with slight differences ascribable to increased NPs size, probably due to sintering during centrifugation and oven drying of the samples. Conversely, G[Zn5] shows a slightly different spectrum compared to that of the virgin sample, with a significantly reduced intensity of the double contribution. Hence, a further measurement at 120 K was performed to exclude the possibility that the sample consists now of two different goethite-like phases, a pure one, and a Zn-doped one, or of another iron oxide phase. However, G[Zn5] displays a lower mean $H_f = 46.5$ T value compared to that of G, $H_f = 48.9$ T, at 120 K, and since no Fe and Zn dissolution was observed throughout the whole process, it was considered to have remained stable. Also in this case, NPs sintering might have taken place, as well as improved crystallinity, due to the observed reduction of

Γ. From MS analysis it could be concluded that all the samples remain in the goethite-like phase, possibly preserving the level of doping, as no Zn, Mn or Zr was detected by the ICP in any solution. Further investigation at higher desorption pH values and multiple regeneration is needed, to obtain a rough estimation of the lifespan of the adsorbent. Finally, further consistent comparative studies on goethite doping, both using different elements and doping percentages, are recommended to better understand the effect of the different dopant features on the overall goethite properties. Also, providing a support, such as ion exchange resins, would allow to perform multiple adsorption/desorption tests, better estimating the reusability and life span of the adsorbent, while providing application to such nanoparticles in real-life systems.

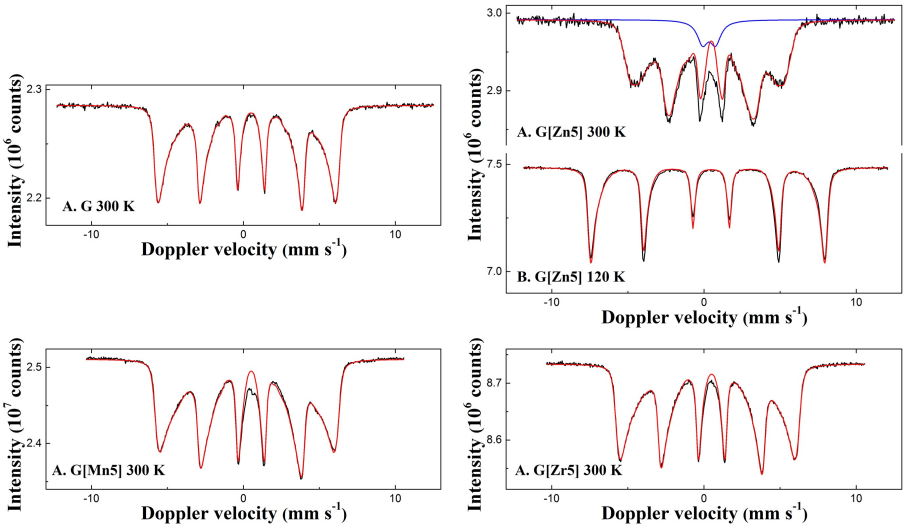

Figure 2.12: MS spectra of the regenerated NPs measured at different temperatures (300 and 120 K). Black lines represent the measured spectra, colored lines represent the fitted spectral contributions.

Table 2.10: Mössbauer fitting parameters of the regenerated G, G[Zn5], G[Mn5] and G[Zr5] at 300 K and 120 K.

Sample	*T (K)*	*IS (mm·s^{-1})*	*QS (mm·s^{-1})*	*H_f (T)*	*Γ (mm·s^{-1})*	*Phase*	*Spectral contribution (%)*
G	300	0.37	-0.27	32.6*	0.26	α-FeOOH	100
G[Zn5]	300	0.36	-0.26	25.6*	0.35	α-(Zn,Fe)OOH	92
		0.33	0.85^	-	0.85^	Fe^{3+}	8
	120	0.36	-0.22	46.5*	0.26	Fe^{3+}	100
G[Mn5]	300	0.38	-0.28	30.2*	0.25	α-(Mn,Fe)OOH	100
G[Zr5]	300	0.38	-0.26	30.1*	0.26	α-(Zr,Fe)OOH	100

Experimental uncertainties: I.S. ± 0.01 mm s^{-1}; Q.S. ± 0.01 mm s^{-1}; Γ ± 0.01 mm s^{-1}; H_f ± 0.1 T; Spectral contribution: ± 3 %.
**Average magnetic field. ^Fixed value.*

2.5 Conclusions

The characteristics and adsorption properties of pure and doped goethite NPs using elements of different preferential oxidation states were investigated. A successful M-for-Fe substitution was obtained for all the elements, i.e., Zn^{2+}, Mn^{3+} and Zr^{4+}, although Zr displayed a lower substitution than targeted. This latter observation was ascribed to a combination of substitution mechanism and size and charge differences between Zr^{4+} and Fe^{3+}. It was observed that Zn^{2+}-doping increased the pzc of goethite, probably as a combination of protonation, as a charge compensation mechanism, and preferential growth of goethite crystal faces with high functional site density. This effect resulted in improved adsorption performances in terms of capacity, both per mass and per SSA, and affinity. It was also highlighted that SSA is not a determining factor for the adsorption capacity. Conversely, Mn^{3+} and Zr^{4+} doping caused a decrease in pzc and P-adsorption performance. The desorption test showed on average improved P-desorption for Zn^{2+}- and Zr^{4+}-doped goethite, while a decrease in desorption was observed for Mn^{3+}. This consistent comparative study shows the promising effects of Zn-doping for developing an effective and stable goethite-based adsorbent and provides insights on how to employ doping as a strategy to manipulate iron oxide surface properties.

Acknowledgements

This work was performed in the cooperation framework of Wetsus, European Centre of Ex-cellence for Sustainable Water Technology (www.wetsus.nl). Wetsus is co-funded by the Dutch Ministry of Economic Affairs and Ministry of Infrastructure and Environment, the Euro-pean Union Regional Development Fund, the Province of Fryslân and the Northern Nether-lands Provinces. This research received funding from the Netherlands Organization for Scientific Research (NWO) in the framework of the Innovation Fund for Chemistry, and from the Ministry of Economic Affairs and Climate Policy in the framework of the TKI/PPS-Toeslagregeling. The authors thank the participants of the research theme "Phosphate recovery" for the interest, fruitful discussions, and financial support. A special thanks goes to Pim de Jager and Raimonda Buliauskaitė (Aquacare) for the frequent knowledge exchange and interest in the research, Harm van der Kooi for the technical support, Michel Steenvoorden and Maxim Ariens for the support with Mössbauer spectroscopy related matters, Kees Goubitz (TU Delft) for the support on XRD, Wiel Evers (TU Delft) for the TEM measurements, Jouk Jansen (TU Delft) for the sup-port with SAED analysis, Renata van der Weijden (WUR) for the fruitful discussions, Prashanth Suresh Kumar (Plaksha University) and Terica Sinclair for the support and guidance, Amandine Dronne, Varad Kapur, Maddalena Tigli for the work done together.


3

3

Zn induced surface modification of stable goethite nanoparticles for improved regenerative phosphate adsorption

A modified version of this chapter has been submitted as: **Belloni, C.**, Korving, L., Witkamp, G.J., Brück, E., Dugulan, A.I., 2023, *Zn induced surface modification of stable goe-thite nanoparticles for improved regenerative phosphate adsorption*, Journal of Colloid and Interface Science.

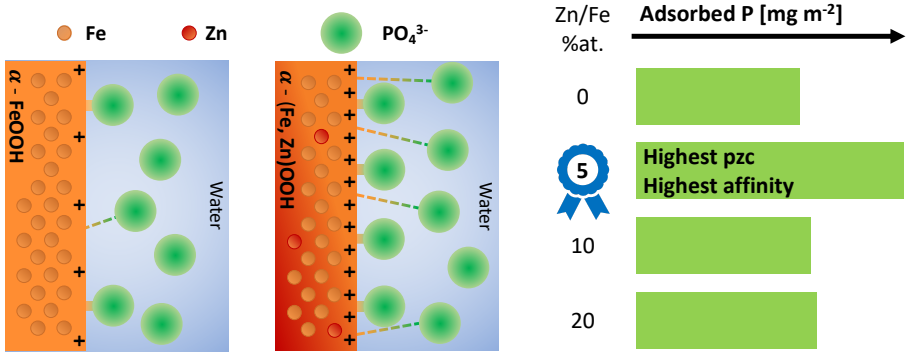

Highlights

- Zn-doping of goethite improved P removal at low P concentrations (0.1 - 10 mg L^{-1}).
- 5 %at. Zn-doped goethite showed the highest surface charge.
- 5 %at. Zn-doped goethite showed the highest P removal per surface area.
- Zn-doped goethite showed improved P desorption, without phase changes.

Keywords:

phosphate recovery, adsorption, regeneration, iron oxide, goethite, zinc doping

3

Abstract

Iron oxide-based phosphate (P) adsorbents showed potential to reach ultra-low P concentrations to prevent eutrophication, while allowing P recovery for recycling. A high affinity and capacity at low P concentrations (< 1 mg L^{-1}), as well as good stability and reusability of the adsorbent are key factors for economic viability. In this study, nanoparticles of goethite (α-FeOOH), a highly stable phase, have been synthesized with increasing Zn^{2+}-doping, from 0 to 20 %at. Zn/Fe, as a strategy to manipulate the surface charge and area to improve its performance. Mössbauer spectroscopy showed that at low doping percentages the Zn was incorporated into the goethite structure, while at higher % (> 5 %) co-existing phases formed. The doping impacted the specific surface area (SSA) and point of zero charge (pzc). Batch adsorption tests, performed at low P concentrations, 0.1 to 10 mg L^{-1}, showed increased P removal per mass of adsorbent with increasing doping (and SSA). However, the highest affinity and P removal per SSA were observed for the 5 %at. doped sample, which together with the pzc show that this do-pant concentration provides the most effective surface. A regeneration test, performed at a low-er pH than usual, showed that P desorption on average improved with nanoparticles doping. Mössbauer spectroscopy showed that the nanoparticle phase and composition, up to 5 %at. doping, did not change during regeneration. These results are promising to develop a stable high performing Zn-doped goethite-based adsorbent for P recovery at ultra-low concentrations.

3.1 Introduction

Phosphorus (P) recovery is fundamental for three main reasons. First, it is an irreplaceable and vital nutrient, essential to the world food production sustainability [26], and its demand will further increase due to population growth [126]. Second, P is a finite and non-renewable resource which comes from phosphate rock mines, with reserves available in only a few countries, making Europe almost completely dependent on its import [32,125,126]. This led the European Commission to include P in the Critical Raw Materials list [32], asking for a more circular nutrients and resources management [33,127]. Third, through agricultural runoff and wastewater treatment-plant (WWTP) effluents, P reaches surface water-bodies where it accumulates, becoming a pollutant [8,10,120,142,143]. P in water can be found both in particulate and solute state (i.e., phosphate), the latter being the bioavailable P fraction causing eutrophication and promoting algae bloom, which entails severe environmental, health and socio-economic damages [122–124]. To prevent eutrophication, P concentrations in freshwater bodies need to be limited to ultra-low concentrations, below 0.02 mg L^{-1} [121], which is hundred times lower than current regulations for WWTP effluents (< 1 - 2 mg L^{-1}) [20]. Therefore, it is important to remove P from water, as well as to recover it to be reused, following a circular approach. Physical, biological and chemical methods have been widely investigated for P removal, but few of them display potential for P recovery, even less when targeting ultra-low P concentrations [23].

Among the chemical methods, adsorption showed promising results at concentrations below 1 mg L^{-1}, especially to target the ultra-low P concentrations and to recover P, since the process can be reversed [23,49,72]. A lot of work has been done on adsorption, often under laboratory conditions and either with single use or with expensive and sophisticated adsorbents [144–147]. However,

little efforts have been spent on P-recovery and adsorbent regeneration, the latter being a key factor to make the P-removal process economically viable. In fact, studies showed that reusing the adsorbent 50 to 100 times, would make the process economically convenient [23,54].

In this regard, iron oxide-based adsorbents constitute a promising option, being cheap due to their high abundance, and showing good properties for P removal, such as good affinity and selectivity. Also, by means of an alkaline wash they allow the recovery of P and the regeneration of the adsorbent, which can be further reused [49,60,72,148]. There are several commercially available iron oxide-based adsorbents but the mainly employed ones are porous granular adsorbents and hybrid anion exchange adsorbents (HAIX) [23,72]. The former type, usually industrial by-products, is cheaper, relatively stable, and good performing thanks to their high specific surface area (SSA). However, this high SSA mainly comes from micropores, in which diffusion is very slow, resulting in slow kinetics [23]. The latter type is a more expensive engineered adsorbent, consisting of iron oxide nanoparticles (NPs) embedded in macroporous resin beads, and showed good P removal performances and faster kinetics [23]. However, Kumar et al., 2018 [72], observed a consistent phase transformation of the iron oxide NPs already after few P adsorption/desorption cycles, which highly lowered the performances. In fact, these NPs mainly consist of ferrihydrite, an amorphous and highly reactive species, which offers high SSA and hence high capacity. Nevertheless, ferrihydrite is also the most unstable iron oxide species, likely to transform over a wide pH range [78] into more stable and less reactive phases, such as hematite (the most stable species) and goethite.

Goethite (α-FeOOH) is one of the most abundant and most stable phases, which showed good affinity for phosphate [132,149–155]. On the one hand, the stability of goethite makes it an interesting candidate from the regeneration point of view, implying a longer lifespan of the adsorbent. On the other hand, it might

limit its reactivity, and thus its P adsorption potential. Many studies suggested ferrihydrite as a promising adsorbent for P recovery, due to its high capacity. Nevertheless, these studies were often performed at P concentrations 50 to 100 times higher than those of WWTP effluents and surface water bodies, giving little insight into the potential for application, and often neglecting ferrihydrite affinity for P. In this regard, Wang et al., 2013 [85], in their comparison study between ferrihydrite, goethite and hematite P removal performances, suggested ferrihydrite to be the most promising species, mainly based on its high capacity. In fact, they showed that ferrihydrite had the highest P removal per mass capacity, more than 10 and 20 times higher than that of goethite and hematite, respectively. However, at P equilibrium concentrations below ~ 77 mg L^{-1}, goethite showed significantly higher P removal compared to the others. This is also supported by its higher estimated affinity, about 10 and 20 times higher than that of hematite and ferrihydrite, respectively. Moreover, ferrihydrite dissolution was observed throughout the experiments. These results support the ideas that goethite is the most promising species for targeting the ultra-low P concentrations of interest, and that using adsorption capacity at high P concentrations is a misleading parameter, as previously pointed out by Kumar et al., 2019 [23].

In the current work the goal was to develop an efficient goethite-based adsorbent. To exploit goethite stability while increasing its P recovery performances, doping constitutes a promising option. Doping is a technique widely employed in semiconductors [87–89] and catalysis [90–93], in which an elemental metal (M) impurity, i.e., the dopant, is introduced in a hosting material to alter its properties. Doping has often been erroneously referred to when dealing with coating, assembling, loading or impregnation of metal and/or NPs in composite materials [60,156–160]. Pure and M-substituted goethite has been widely investigated, both as naturally occurring goethite rock or as synthetic goethite [75,78,95–97]. The effects of impurities in goethite, mainly Al

[103,104,113–115,105–112] and Mn [98–102], have been investigated for many different applications, some including phosphate, arsenate, and divalent cations adsorption. Zn-for-Fe substitution in goethite has been investigated mainly from the crystallization point of view [97,131], and it has been proposed to promote goethite protonation as a charge compensation mechanism [97]. However, its effect on the surface charge and P adsorption were not investigated. So far, no study on Zn-doped goethite for P recovery has been previously conducted.

Finally, Mössbauer spectroscopy (MS) has been employed in this study as the main characterization technique for the synthesized (doped) goethite samples. MS is a high-resolution nuclear gamma-ray based technique mainly used to investigate Fe-based materials, providing information on the sample properties from the "Fe-nuclei point of view". Employed as a fingerprint technique, it is possible to retrieve mainly three parameters from the spectral analysis: the isomer shift (IS), which provides information such as the oxidation state and character of ligands of Fe atoms; the quadrupole splitting (QS), which provides further information on the oxidation state as well as the charge distribution asymmetry around the Fe nuclei; and the hyperfine magnetic field (H_f), which provides information on the magnetic ordering of the sample. MS offers very high-resolution spectral features, and compared to other techniques, such as XRD, it has the advantage to be sensitive even to very fine and amorphous NPs and to be more specific in Fe phase identification and quantitative speciation. Especially when performing measurements at different temperatures, since low temperatures are necessary to obtain the Zeeman split in the Mössbauer spectra, allowing the identification of (super)paramagnetic phases [75]. Moreover, MS can help in confirming a successful and homogeneous M-for-Fe substitution in doped samples, while providing information on the effect of the dopants on the structural, chemical and magnetic properties [99,105,106].

This study presents an investigation on the effect of increasing Zn-for-Fe substitution in goethite NPs, and its influence on the surface charge and the P adsorption/desorption performances, enabling the development of a stable and high performing Zn-doped goethite-based adsorbent for P recovery.

3.2 Materials and Methods

3.2.1 Chemicals

Potassium dihydrogen phosphate (KH2PO4), sodium chloride (NaCl), 1 M sodium hydroxide (NaOH), 1 M hydrochloric acid and 37 % hydrochloric acid (HCl) were purchased at VWR (The Netherlands). 3-(N-morpholino) propane sulfonic acid (MOPS) and iron nitrate nonahydrate ($Fe(NO_3)_3 \cdot 9H_2O$) were obtained from Sigma-Aldrich (The Netherlands), and zinc nitrate hexahydrate ($Zn(NO_3)_2 \cdot 6H_2O$) from Alfa Aesar (Germany).

3.2.2 Nanoparticles Synthesis

The goethite NPs were synthesized adapting the procedure of Villacís-García et al., 2015 [132]. In short: CO_2-free Milli-Q (MQ) water was prepared by overnight N_2-bubbling, to eliminate CO_2. Then, 50 g of $Fe(NO_3)_3 \cdot 9H_2O$ was added to 825 g of the CO_2-free MQ. Meanwhile, 200 ml of 2.5 M NaOH CO_2-free solution was prepared. The NaOH solution was then injected in the Fe solution at a controlled flow of 1 mL min^{-1} through a peristaltic pump (Cole-Palmer, Masterflex L/S), to obtain consistent results, under N_2 bubbling and 250 rpm stirring. Once NaOH addition was completed, the solution, now at pH > 12, was let stirring for further 30 min. The solution was then placed in an oven at 60 °C for 48 h, occasionally shook for homogeneity, to age the ferrihydrite-based suspension into goethite. The phase transformation was visually confirmed by the suspension color change, from a dark brown to ochre.

For the doped goethite NPs, the same procedure was applied, with the difference of the Fe solution consisting of a mixture of Fe and Zn salts in the 5, 10 and 20 %at. Zn/Fe ratio, for which the salts were weighed accordingly. In this case, after the aging, the color changed from dark brown to orange/dark red/purple, depending on the amount of Zn added.

Each synthesis provided around 8 g of NPs suspension. The NPs suspensions were then filtered via Buchner filtration, obtaining the so-called NPs cake, which was first thoroughly rinsed with MQ water, and then recovered, resuspended in Demineralized Water (DW) through thorough shaking and 10 min sonication at 40 kHz (Bandelin, Sonorex RM16UH). Then, the pH was adjusted to around 7 (pH of interest for the adsorption experiments) using HCl and NaOH. The NPs were let to settle, and the supernatant was removed and replaced by DW adjusted to pH 7, until the supernatant reached a conductivity below 0.1 µS cm^{-1}.

The synthesized samples are referred to as G for the pure goethite, and G[Zn5], G[Zn10] and G[Zn20] for the 5, 10, and 20 %at. Zn/Fe doped goethite NPs.

3.2.3 Nanoparticles Characterization

The NPs were characterized combining several methods, to obtain a complete description of their features and properties.

The NPs suspensions pH and conductivity were measured with a SevenExcellence pH/Cond meter S470, Mettler-Toledo.

The NPs mass concentration in solution was estimated by weighing oven-dried (60 °C) fixed volumes of the suspensions.

To confirm the Zn/Fe %at. in the doped goethite NPs samples, an aliquot of the suspension was centrifuged, to remove the supernatant, dissolved in HCl 37

% acid solutions, and analyzed with a Perkin Elmer Optima 5300 DV Inductively Coupled Plasma Optical Emission Spectroscopy (referred to as ICP).

The morphology of the synthesized NPs was observed using a JOEL JEM1400-plus Transmission Electron Microscopy (TEM) with a TVIPS F416 camera operating at 120 kV. The images were analyzed with ImageJ software to estimate the size of the NPs. Selected Area Electron Diffraction (SAED) was also employed to qualitatively investigate the NPs crystallinity.

X-Ray Diffraction (XRD) measurements provided information on the speciation of the NPs, as well as their crystalline structure and crystallite size. XRD measurements were performed with a PANalytical X'Pert pro X-Ray diffractometer mounted in the Bragg-Brentano configuration with a Cu anode (0.4 mm x 12 mm line focus, 45 KV, 40 mA). X-Ray scattered intensities were measured with a real-time multi strip (RTMS) detector (X'Celerator). The data were collected in the angle range $10° < 2\theta < 100°$ with a step size of 0.008° (2θ); total measuring times were 1 h for G and G[Zn5], 1.5 h for G[Zn10] and 2 h for G[Zn20]. A spinner was used as a sample holder, to homogenize the results and minimize artifacts, such as increased intensity due to NPs preferential orientation during sample preparation. XRD patterns were analyzed in fingerprinting mode using the PANalytical X'Pert software.

MS measurements provided the speciation of the NPs, identifying and quantifying the different phases, assessing the successful and homogeneous Zn-for-Fe substitution and its effects on the intrinsic properties of the NPs, and investigating the NPs stability after regeneration. Measurements were performed at three different temperatures, 300 K (room temperature, RT), 120 K (set-up thermalization with liquid N_2) and 4.2 K (liquid He temperature). Transmission ^{57}Fe MS spectra were collected with conventional constant acceleration or sinusoidal velocity spectrometers using a ^{57}Co (Rh) source and calibrated to α-Fe. The MS

spectra were analyzed with Mosswin 4.0 software [133], to retrieve the different parameters, i.e., IS, QS and H_f, the line-width (Γ) [mm s^{-1}] and the spectral contribution [%].

The point of zero charge (pzc), defined as the pH at which the net surface charge of the adsorbent is neutral, is an indirect measurement of the surface charge of the adsorbent. The pzc was estimated using the salt addition method, adapted from Mahmood et al., 2011 [134], and Tan et al., 2008 [135]. In short, multiple 50 mL centrifuge tubes were prepared with 10 mL of 5 g L^{-1} NPs suspension adjusted at different initial pH in the range 5-10, using NaOH and HCl. The samples were let to equilibrate in a shaking incubator (150 rpm, 25 °C) for at least 5 days. Then, the initial pH values, pH_{in}, were recorded, followed by addition of 0.526 mL 2 M NaCl solution (final NaCl concentration of 0.1 M). The samples were again let to equilibrate in a shaking incubator for at least a week. The final pH values, pH_{fin}, were recorded and the $\Delta pH = pH_{fin} - pH_{in}$ calculated. Experiments were run in duplicates. Sample preparation and measurements took place in a glovebox with N_2 atmosphere, and all solutions and NPs suspension where N_2-bubbled for several hours prior use, to prevent pH fluctuations due to CO_2 exchange with the solutions. The NPs suspensions were also sonicated for 10 min before use. The pzc corresponds to the pH value at which $\Delta pH = 0$, i.e., the pH value at which the plot ΔpH vs pH_{in} crosses the x axis (pH_{in}). The pzc was determined with two different approaches. The first, by interpolating the whole data sets with a polynomial curve that could better represent the trend over a wide range of data. The second, by identifying the closest data at the opposite sides to the x axis and interpolating them with a linear function. pH measurements provided maximum pH fluctuations around ± 0.10 after pH adjustment (pH_{in}), and within ± 0.05 after pH equilibrations (pH_{fin}), while the pH meter (handheld PH 20, VWR, with GE 114 WD electrode) had an accuracy of ± 0.02. The root squared sum combinations of these contributions

provided an uncertainty of ± 0.11, which has been rounded up to ± 0.15, to provide a larger range of confidence. The results have been discussed in relative terms, i.e., by comparing the results obtained for the different samples, rather than in absolute terms.

Micromeritics Tristar 3000 was used to estimate the specific surface area (SSA) of the NPs via Brunauer-Emmett-Teller analysis. The measurement was carried out by degassing about 100 mg of dried NPs overnight under N_2 atmosphere, followed by N_2 adsorption-desorption cycles, which can be related to the surface area of the material. The retrieved data were analyzed through non-local density functional theory model in the built-in software.

Note that for MB, XRD and SSA measurements, the sample preparation consisted of NPs centrifugation to remove the supernatant from the so-called NPs cake; oven-drying at 40-60 °C of the NPs cake; grinding the recovered NPs powder to be then placed in the respective sample holders.

3.2.4 Phosphate Adsorption Experiments

To perform P adsorption experiments, KH_2PO_4 salt was used as a source of phosphate and all concentrations are reported in terms of phosphorus concentrations. A 500 mg L^{-1} P stock solution in DW was prepared, from which different dilutions were obtained, with P concentrations of 0.1, 0.5, 0.75, 1, 2.5, 5, 7.5 and 10 mg L^{-1} as starting concentrations (C_{dil} [mg L^{-1}]). Adsorption experiments were performed in duplicates plus blank, i. e., P solution without adsorbent as a control. To keep the pH constant during the adsorption experiments, 20 mM of MOPS was added as a pH buffer, and the pH value adjusted to around 7.2 using NaOH and/or HCl. Meanwhile, a NPs suspension of 1 g L^{-1} was prepared and sonicated for 10 min to promote NPs dispersion, and the concentration verified by weighing oven-dried volumes. Then, 10 mL of the P dilutions samples were removed (and analyzed with ICP) and replaced with 10 mL of the NPs

suspension for the adsorption samples (final adsorbent concentration of 0.1 g L^{-1}), and with 10 mL DW for the blank samples. This procedure was chosen for practical reasons. The samples were then placed in a shaking incubator at 25 °C, 150 rpm. It was observed that the adsorption experiments reached equilibrium within two days. Nevertheless, some samples were further analyzed after one week, as a further control, without showing any appreciable difference.

3.2.5 Desorption/Regeneration Experiments

A regeneration experiment was run with the aim of assessing the influence of doping on the ease of P desorption and NPs regeneration, and NPs stability. It is well known that metal oxide-based adsorbents can be easily regenerated via an alkaline wash, often using 0.1 to 1 M NaOH, i.e., pH 13 - 14 [23,49,60,72,148,156,161]. Usually, in studies with NPs, the adsorption samples are centrifuged to separate the NPs from the adsorption solution, and then redispersed and regenerated. However, centrifugation is known to promote irreversible agglomeration of the NPs, which might cause phosphate blocking, while redispersion of NPs can require long sonication which might alter the NPs. In this study, the desorption was therefore performed by increasing the pH directly in the P solution after the adsorption equilibrium was reached, with the following procedure. First, an adsorption experiment was run similarly to the isotherm experiments, again in duplicates plus blank. Samples of 100 mL P solution at 25 mg L^{-1}, with 20 mM MOPS and pH 7.2 were prepared. Meanwhile, a 3 g L^{-1} NPs suspension was prepared and sonicated for 10 min. Then, 10 mL of the P solutions were removed and analyzed with ICP and replaced by 10 mL of the NPs suspension solution for the adsorption samples (adsorbent concentration of 0.3 g L^{-1}), and by 10 mL of DW for the blanks. The samples were then placed in a shaking incubator at 25 °C, 150 rpm. After five days, to be sure equilibrium was reached, 5 mL of the solution was collected and filtered for

analysis and replaced with 5 mL of 1 M NaOH solution, which increased the pH to around 12.6. The regeneration pH was deliberately chosen to be low compared to the usual pH, to enhance the differences in desorption.

The samples were placed in a shaking incubator at 25 °C, 150 rpm, for one day. Then, the solutions were filtered and analyzed with the ICP. The adsorption/desorption samples were then centrifuged to recover the NPs, which were then oven dried and analyzed with Mössbauer spectroscopy.

3.2.6 Samples Analysis

The elemental composition of the P-based solutions was analyzed with ICP. The initial concentrations, C_0 [mg L^{-1}], were obtained both from the ICP analysis of the blanks at the start and end of the experiments, and from calculations from the C_{dil} analysis, and always displayed a good agreement, well within the 3 % error. The equilibrium concentrations, C_{eq} [mg L^{-1}], were obtained from the ICP analysis of the adsorption samples. Prior to analysis, the samples were filtered with a 25 nm pore size filters (MF-Millipore Membrane Filter, 0.025 μm pore size, Merck), with the help of a six channel NE-1600 syringe pump (New Era Pump Systems, Inc.). Since no appreciable difference in the ICP results was observed between filtered and unfiltered blank samples, it was assumed that filtration had a negligible influence on the samples' elemental concentrations at these ranges. The amount of P adsorbed normalized to the mass of adsorbent, q [mg g^{-1}], was calculated through the equation:

$$q = \frac{C_0 - C_{eq}}{m_{NPs}} V$$

where m_{NPs} [g] is the mass of adsorbent and V [L] is the volume of the sample.

3.2.7 Data Analysis

For the adsorption isotherm analysis, the data were analyzed by plotting q against C_{eq}, and fitting them with two adsorption isotherm models, the Langmuir [136] and the Freundlich [137] isotherm models.

The Langmuir isotherm is an ideal adsorption model developed for gas adsorption on solid phase. The model is based on monolayer adsorption on homogeneous adsorption sites without interaction between adsorbate molecules. The Langmuir isotherm equation is given by:

$$q = \frac{q_{max} K_L C_{eq}}{1 + K_L C_{eq}}$$

where q_{max} [mg g^{-1}], is the capacity, which is represented by the height of the plateau of the curve, and K_L [L mg^{-1}] is the Langmuir constant which is related to the affinity between the adsorbate and the adsorbent binding sites, represented by the steepness of the ascending portion of the curve.

The Freundlich isotherm, suited to describe adsorption on heterogeneous adsorption sites, is an empirical model, meaning that its constants do not have a physical meaning. The Freundlich isotherm equation is given by:

$$q = K_F {C_{eq}}^n$$

where K_F [(mg g^{-1})(mg L^{-1})$^{-n}$] is the Freundlich constant (or adsorption strength), which is related to the capacity of the adsorbent, and n is a dimensionless constant representing the adsorption intensity, related to the surface sites' heterogeneity.

The fitting results were interpreted in relative terms, rather than absolute terms, purely as a matter of comparison. In fact, given the two models' limitations, the fitting parameters values should be evaluated with care.

Finally, the data were normalized not only to the mass of adsorbent, but also to its SSA, to provide further information from two different criteria of comparison, and again fit with the Langmuir and Freundlich models.

The fitting was performed using Microsoft Excel Solver, minimizing the RMSPE (Root Mean Square Percentage Error) and the goodness provided the reported RMSPE.

For the desorption analysis, the mass of P adsorbed, $m_{P,ads}$ [mg], was calculated using:

$$m_{P,ads} = (C_0 - C_{eq})V$$

and the mass of P desorbed, $m_{P,des}$ [mg], using:

$$m_{P,des} = (C_{des} - C_{eq}')V$$

where V [L] is the volume of sample, C_{des} [mg L^{-1}] represents the P concentration after desorption, and C_{eq}' represents the equilibrium concentration after adsorption, corrected for the dilution due to sampling and NaOH addition. Then, the mass percentages of desorbed P have been calculated via:

$$\%\ mg\ P\ desorbed = \frac{m_{P,des}}{m_{P,ads}}\%$$

These results have been reported in histogram plots.

Finally, the P surface coverage percentage in the adsorption/desorption experiments (both of the adsorbed P after adsorption and the undesorbed P after regeneration) were calculated, considering a phosphate ionic radium of 238 pm [138].

3.3 Results and Discussion

3.3.1 Characterization

3.3.1.1 Observations

The different synthesized NPs suspensions show different colors and settling behaviors after pH adjustment, already suggesting that the dopants caused changes in the structure and properties of the NPs (Figure 3.1).

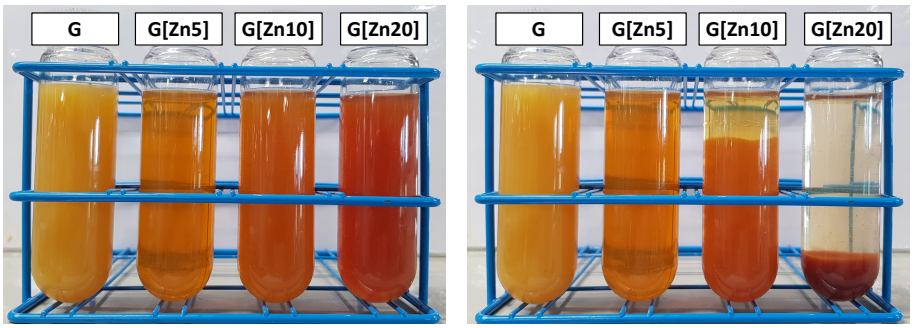

Figure 3.1: Picture of the synthesized NPs suspensions (1 g L^{-1}, pH ~ 7), G, G[Zn5], G[Zn10], G[Zn20] (left to right), showing the different colors of the suspensions (left picture) and the different settling of the NPs (after 10 min) (right picture).

3.3.1.2 Elemental Analysis

ICP measurements of dissolved NPs (in HCl 37%) confirmed the nominal Zn/Fe %at. for all samples, as reported in the Table 3.1. The average error from the replicates' measurements was smaller than 1 % and was considered under-estimated. Hence, an excess error of 5 % was assigned to all the resulting values, to have a wider range of confidence.

3.3.1.3 Specific Surface Area

From the BET analysis of the SSA measurements the following SSA trend was observed: G[Zn20] > G[Zn10] > G ≳ G[Zn5], as visible in Table 3.1, with

G[Zn10] and G[Zn20] having SSA respectively two and three times higher than G and G[Zn5].

Table 3.1: Theoretical and experimental doping %at. from ICP analysis after NPs acid dissolution, and SSA values from BET analysis of the different synthesized NPs.

Sample	*Theoretical Zn/Fe %at.*	*Experimental Zn/Fe %at.*	*SSA [m^2 g^{-1}]*
G	0	0	84.7 ± 0.9
G[Zn5]	5	5.1 ± 0.3	76.0 ± 0.8
G[Zn10]	10	10.2 ± 0.5	165 ± 1
G[Zn20]	20	21 ± 1	231 ± 2

3.3.1.4 TEM

TEM imaging (Figure 3.2) showed that the NPs in sample G have a rod-like shape, as expected [78], with a certain degree of size distribution. For the doped samples, it is visible that the length of these rods increases with increasing doping, while the opposite trend is observed for the width, insofar they look like filaments in the G[Zn20] images. While G[Zn5] appear to display one unique phase of elongated rod-shaped NPs, G[Zn10] and G[Zn20] display a coexistence of multiple phases, with the former presenting a moderate amorphous/fine NPs fraction, while the latter presenting a consistent amorphous/fine NPs fraction and few small spherical/cubic NPs. A clear particle size estimation from TEM images was not possible since the NPs clustered together during sample preparation. However, a rough estimation was obtained analyzing the images with ImageJ, by mean of a gaussian distribution of the measured values of more than 200 NPs per sample, and the values are reported in Table 3.2. For the rod-shaped NPs it is visible how, with increasing doping, the average length

increased from 102 nm up to 185 nm for G[Zn10] (164 nm for G[Zn20]), while the average width decreased from 11 nm down to 6 nm. For the spherical/cubic NPs in sample G[Zn20], an average diameter of 13 nm was estimated.

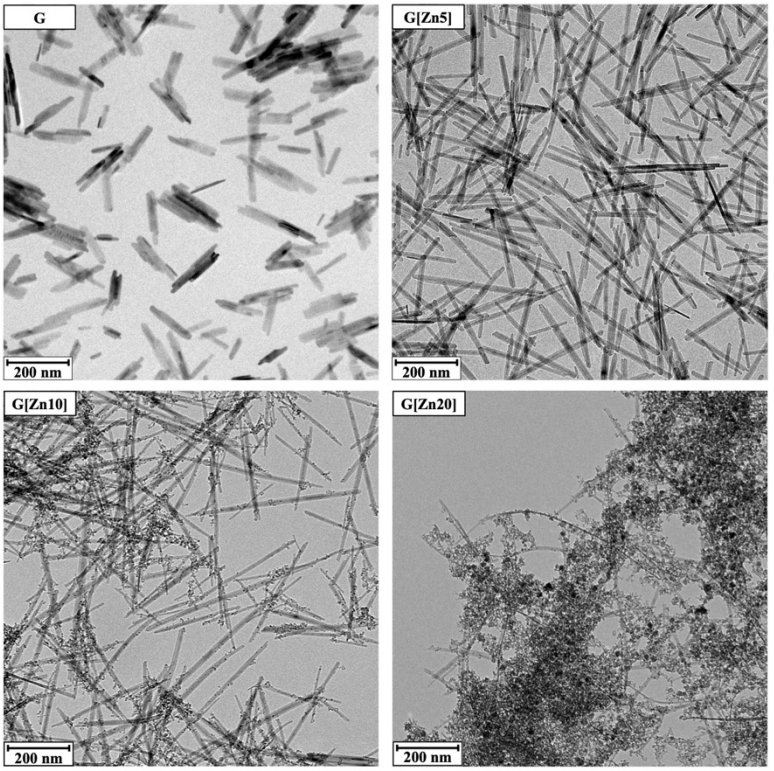

Figure 3.2: TEM images of the synthesized NPs.

Table 3.2: Particle size estimation of the synthesized NPs from TEM images using ImageJ software.

Sample	*Rod-shaped NPs*						*Spherical/cubic NPs*			*Amorphous NPs*
	Length [nm]			*Width [nm]*			*Diameter/Side [nm]*			
	Min	*Max*	*Mean*	*Min*	*Max*	*Mean*	*Min*	*Max*	*Mean*	
G	11	305	102 ± 46	3	23	11 ± 3	-	-	-	-
G[Zn5]	12	330	115 ± 55	3	20	9 ± 3	-	-	-	-
G[Zn10]	25	468	185 ± 88	2	13	6 ± 2	-	-	-	Small amount
G[Zn20]	24	462	164 ± 77	1	13	6 ± 2	5	24	13 ± 4	Significant amount

3.3.1.5 X-Ray Diffraction

XRD patterns (Figure 3.3) analyzed with PANalytical X'Pert software showed a good match of samples G, G[Zn5] and G[Zn10] with the goethite phase. Differences in peak intensities could be related to the preferential orientation of the rods, and difference in aspect ratio and crystallinity of the NPs, the latter also influencing the peak broadening. Sample G[Zn20] showed a good agreement with both the goethite and the zinc ferrite ($ZnFe_2O_4$) phases, with a semiquantitative estimation of 44 % and 56 %, respectively. This estimation provides an order of magnitude, rather than an absolute value. The increased peak broadening and noise in G[Zn10] and G[Zn20] can be attributed to reduced crystallinity of the NPs (as confirmed by SAED, Figure 3.10). It is challenging to confirm whether the amorphous/fine NPs observed with TEM contributed to the XRD signal, and thus to the phase identification. In this sense, MS becomes essential. Finally, an indicative estimation of the crystallite sizes from the XRD patterns analysis is reported in Table 3.3.

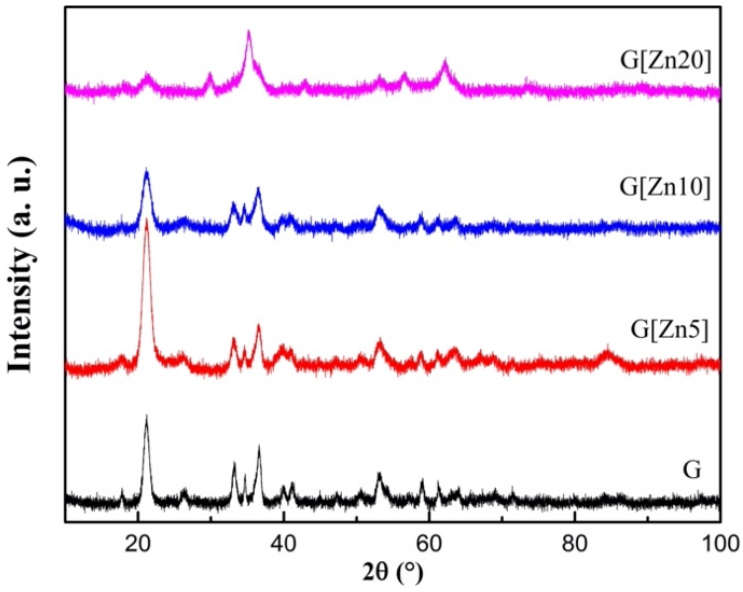

Figure 3.3: XRD patterns of the synthesized NPs.

Table 3.3: Indicative estimation of the crystallite sizes from the measured XRD patterns of the synthesized NPs.

Sample	*α-FeOOH*	*$ZnFe_2O_4$*
G	120 Å	-
G[Zn5]	70 Å	-
G[Zn10]	60 Å	-
G[Zn20]	60 Å	170 Å

3.3.1.6 Mössbauer Spectroscopy

Mössbauer spectra are presented in Figure 3.4 and the fitting parameters of interests, IS, QS, and H_f, together with Γ and the spectral contribution are reported in Table 3.4, where also the reference hyperfine values of bulk goethite [140] are reported.

MS measurements of sample G were performed at RT and 120 K. The RT spectrum of G displays a sextet with asymmetrically broadened peaks typical of non-bulk goethite with particle size distribution and non-perfect crystallinity. The 120 K shows a sextet with sharper and more symmetrical lines, as expected since the internal magnetic field increases with decreasing temperature, as a consequence of reduced thermal excitations, which causes the magnetic spins to flip [140]. The spectral analysis provided IS and QS values typical of high-spin Fe^{3+} in octahedral coordination. The RT mean H_f = 32.4 T is close but smaller than that of bulk goethite (38.0 T), due to the nano-sized dimension of the particles, for which surface boundary effects attain higher importance, the particle size distribution in the sample and the non-perfect crystallinity. The 120 K mean

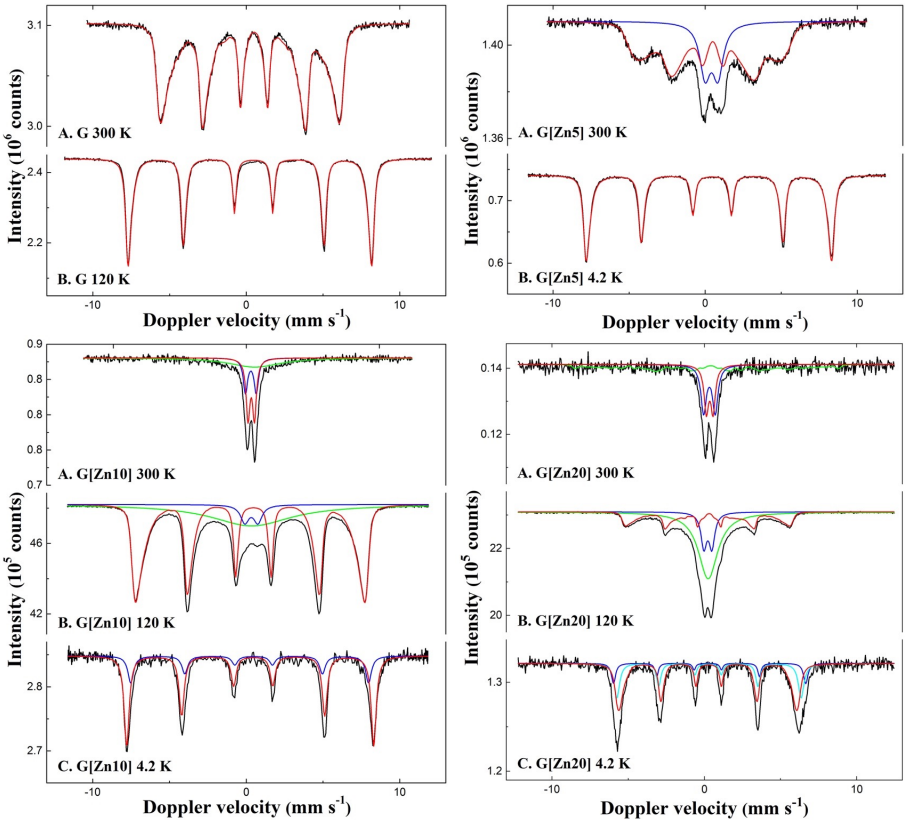

Figure 3.4: MS spectra of the synthesized NPs measured at different temperatures (300, 120 and 4.2 K). Black lines represent the measured spectra, colored lines represent the fitted spectral contributions.

H_f = 48.9 T is closer to the saturation value of bulk goethite (50.6 T), following the expected behavior of the hyperfine magnetic field with temperature [75]. Since no other spectral contributions are visible at this temperature, the spectrum was unambiguously attributed to pure polycrystalline goethite.

Sample G[Zn5] was analyzed at RT and 4.2 K, the latter temperature to investigate whether the Zn-for-Fe substitution was homogeneous or promoted multiple phases formation. Again, both spectra provided IS and QS values in agreement with high-spin Fe^{3+} in octahedral coordination and with those of G.

The peak broadening in the RT spectrum of G[Zn5] are again related to the particle size distribution and non-perfect crystallinity. As expected from the diamagnetic Zn-for-Fe substitution (similarly to Al-doping [104–106]), there is a reduced magnetic coupling between the different Fe sites in the crystal, which entails mainly two effects. First, the decrease of the magnetic interaction between Fe sites, reducing the magnetic ordering temperature or Néel temperature (T_N), which for pure goethite is ~ 400 K. This is represented by the doublet feature, accounting for paramagnetic-like behavior. Second, the reduced magnetic hyperfine field supertransfer, which reduces the H_f value [140], now equal to 24.6 T, against 38.0 T of bulk goethite and 32.4 T of G. Considerations on particle size distribution and surface effects still hold. The 4.2 K spectrum displays one unique sextet with sharper peaks, proving the uniqueness of the phase and the successful and homogeneous Zn-for-Fe substitution. The mean H_f = 49.6 T is lower than the saturation value of bulk goethite (50.6 T), due to the presence of Zn (as previously discussed), in agreement with what was observed by Krehula et al., 2006 [131], and for Al-substitution by Murad et al. 1987 [105].

For the G[Zn10] sample, measurements at RT, 120 K and 4.2 K were carried out. It is possible to see that the increasing Zn-for-Fe substitution and the formation of an amorphous/fine NPs fraction increased the relaxation effects (see section 3.5.2 in S. I.), causing the RT spectrum to collapse into a broad doublet. As temperature decreases, magnetic ordering takes place, until complete magnetic ordering is restored at 4.2 K, as visible by the sextet. The green spectral features present at RT and 120 K account for relaxation effects. For all the spectra, the IS and QS values fall within the high-spin Fe^{3+} in octahedral coordination range. In particular, the QS = 0.48 mm s^{-1} of the red doublet in the RT spectrum is in good agreement with that expected for paramagnetic goethite (0.48 mm s^{-1} [162–164]), while that of the blue doublet at RT and 120 K, 0.81

Table 3.4: MS reference values and fitting parameters of G, G[Zn5], G[Zn10] and G[Zn20] at 300 K, 120 K and 4.2 K.

Sample	T (K)	IS ($mm \cdot s^{-1}$)	QS ($mm \cdot s^{-1}$)	H_f (T)	Γ ($mm \cdot s^{-1}$)	Phase	Spectral contribution (%)
Bulk goethite reference values [140]	300	0.37	-0.26	38.0	-	-	-
	4.2	0.37	-0.25	50.6	-	-	-
G	300	0.38	-0.26	32.4*	0.28	α-FeOOH	100
	120	0.36	-0.24	48.9*	0.26	α-FeOOH	100
G[Zn5]	300	0.38	-0.24	24.6*	0.53	α-(Zn,Fe)OOH	77
		0.42	0.85^	-	0.85	Fe^{3+}	23
	4.2	0.35	-0.21	49.6*	0.32	α-(Zn,Fe)OOH	100
G[Zn10]	300	0.35	0.81	-	0.40	Fe^{3+}	24
		0.38	0.48	-	0.34	Fe^{3+}	37
		0.65	-	-	4.67	Fe^{3+}	39

G[Zn10]	120	0.33	0.85	-	0.65	Fe^{3+}	5
		0.36	-0.21	44.5*	0.28	α-(Zn,Fe)OOH	64
		0.35	-	-	6.32	Fe^{3+}	31
	4.2	0.35	-0.20	50.0	0.39	α-(Zn,Fe)OOH	75
		0.35	-0.26	48.2	0.44	α-(Zn,Fe)OOH	25
G[Zn20]	300	0.33	0.76	-	0.43	Fe^{3+}	35
		0.35	0.44	-	0.36	Fe^{3+}	28
		0.28	-0.26	36.1*	0.30	Fe^{3+}	37
	120	0.32	0.79	-	0.67	Fe^{3+}	16
		0.36	-0.19	36.5*	0.26	α-(Zn,Fe)OOH	29
		0.35	-	-	2.29	Fe^{3+}	55
	4.2	0.34	0.06	52.3	0.34	γ-Fe_2O_3	13
		0.34	0.00	50.6	0.47	ZnFe2O4	31
		0.33	-0.14	48.7*	0.41	α-(Zn,Fe)OOH	56

Experimental uncertainties: I.S. ± 0.01 mm s^{-1}; Q.S. ± 0.01 mm s^{-1}; Γ ± 0.01 mm s^{-1}; H_f ± 0.1 T; Spectral contribution: ± 3 %.
**Average magnetic field. ^Fixed value.*

and 0.85 mm s^{-1} respectively, are close to that of the doublet contribution of G[Zn5] at RT spectrum (0.85 mm s^{-1}). These results suggest the presence of two species differing in Zn-for-Fe substitution, one still superparamagnetic (the fine NPs fraction) and one already magnetically ordered (the elongated rods) at 120 K. At 4.2 K the spectrum consists of a broadened sextet, which was analyzed with two contributions. A main spectral contribution (75 %) was assigned to the magnetically ordered goethite-like phase observed at 120 K. The H_f = 50.0 T is smaller than that of bulk goethite (50.6 T). The smaller contribution (25 %) has the QS = - 0.26 mm s^{-1} in good agreement with that of bulk goethite (similarly to what observed at RT), and the H_f = 48.2 T, also smaller than that of bulk goethite. This contribution was assigned to the fine NPs fraction observed with TEM, identified as a low-to-null Zn-doped goethite phase (see Section 3.5.3 in S. I.).

The G[Zn20] spectra, obtained at RT, 120 K and 4.2 K, display similar features to that of G[Zn10], passing from a (super)paramagnetic state at RT, to a magnetically ordered state at 4.2 K, with similar hyperfine parameters for the spectral contributions at RT and 120 K. At 120 K, a smaller and less intense sextet is visible, with a mean H_f = 36.5 T lower than that of G[Zn10] (H_f = 44.5 T). The 4.2 K spectrum displays a sextet with broad peaks, especially for line 6 (far right peak), which suggests the presence of at least two different phases, and has been fit with three spectral contributions. The red sextet (65 %), with an IS = 0.33 mm s^{-1} and a QS = -0.14 mm s^{-1}, and a mean H_f = 48.7 T, suggests the presence of a Zn-doped goethite-like phase. The significant spectral contributions of the goethite phase most likely accounts for both the elongated fine rods and a consistent (if not the whole) fraction of fine NPs observed with TEM, similarly to what was observed for G[Zn10]. The intermediate cyan sextet (31 %) has QS = 0.00 mm s^{-1}, typical of spinel-like structures, and H_f = 50.6 T. These suggest the presence of a non-stoichiometric zinc ferrite phase (known

for having T_N < 10 K), in agreement with the XRD results and literature [165–171]. This phase could belong to a fraction of the fine and/or small spherical NPs observed with TEM, in agreement with the FE-SEM observations by Krehula et al., 2006 [131]. Finally, the blue sextet (13 %) has QS = 0.06 mm s^{-1}, again close to zero, with a high H_f = 52.3 T, suggesting the presence of a low-to-null Zn-substituted maghemite phase. This probably belongs to a fraction of the fine NPs observed with TEM, as no contribution from this phase was observed at higher temperatures (superparamagnetism) and with XRD.

To summarize TEM, SAED, XRD and MS results: G consisted of rod-shaped NPs of pure polycrystalline goethite dispersed in size; G[Zn5] consisted of elongated rod-shaped NPS of homogeneously 5 %at. Zn-doped polycrystalline goethite dispersed in size; G[Zn10] consisted of two goethite-like phases, one of fine elongated rods with a certain degree of Zn-for-Fe substitution (75 %), and one of fine NPs with low-to-null Zn-for-Fe substitution (25 %); G[Zn20] consisted of two Zn-doped goethite-like structures, consisting of a few extremely fine elongated rods and a consistent amount of fine NPs (56 %), a relatively consistent fraction of non-stoichiometric zinc ferrite NPs (31 %), and a small fraction of fine maghemite NPs (13 %).

3.3.1.7 Point of Zero Charge

The polynomial and linear interpolations of the calculated ΔpH against pH_{in} for all samples are shown in Figure 3.11.

Both methods provided similar pzc estimations for each sample (Table 3.5), with the only exception of G[Zn10], which slight deviation was anyway within the assigned error, and displayed the following overall trend: G[Zn5] > G[Zn10] ~ G > G[Zn20]. Nevertheless, the polynomial approach was considered the best method, as it appears to better describe the data trend (Figure 3.12), and results are shown in Figure 3.5. The fact that G[Zn5] displays the highest point of zero

charge implies that its surface is "more positive" in the pH range of interest, i.e., pH 6 - 8. This should translate in a surface with higher surface sites density and hence higher adsorption performances (surface-wise) compared to the other samples. It seems surprising that substituting Fe^{3+} in goethite with Zn^{2+}, which has a lower preferential oxidation state and a lower Pauling's electronegativity (1.5) compared to Fe (1.8) [141], promotes an overall higher surface charge. Two possible effects might explain this unexpected observation. The first is based on Giovanoli et al., 1992 [97], who proposed that the charge imbalance due to Zn-for-Fe substitution in goethite is compensated by protonation of the Zn site. This might result in an overall higher protonation of the goethite NPs surface in water. The second is based on the observed elongation of the NPs, which might have promoted the growth of crystal faces with higher active adsorption sites density, and thus more effective surface. A combination of the two effects is not to be excluded.

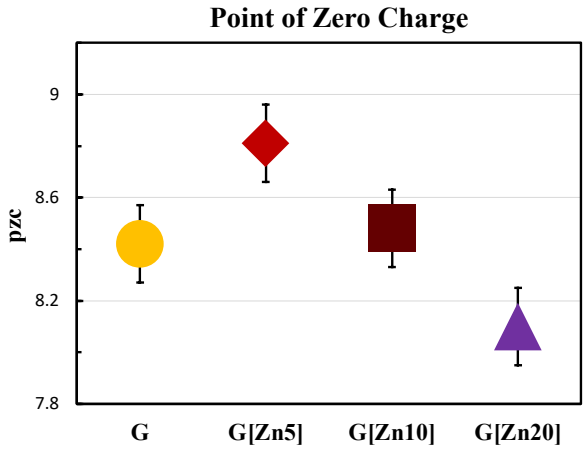

Figure 3.5: pzc values estimated from the polynomial data interpolation.

Table 3.5: pzc values of the synthesized NPs obtained from the polynomial and the linear data interpolation approaches.

Sample	*pzc (polynomial)*	*pzc (linear)*
G	8.42	8.42
G[Zn5]	8.81	8.81
G[Zn10]	8.48	8.56
G[Zn20]	8.10	8.12

An excess error of ± 0.15 is assigned to all the pzc values.

3.3.2 Adsorption Equilibrium

As previously mentioned, the adsorption results have been analyzed with both the Langmuir and Freundlich isotherm models. Before diving into the discussion, it is important to remind that the Langmuir model is based on unrealistic assumptions when applied to adsorption in water, meaning that even if the agreement with the data is good, one cannot assume a homogeneous monolayer-like adsorption is happening; while the Freundlich isotherm is purely empirical, meaning that its parameters do not have a physical meaning. However, while these considerations prevent retrieving information on the nature of the adsorption mechanism, both models can provide a simplistic indication of the trend, and a benchmark for comparison. Finally, it is important to stress that the results interpretation is focused on the relative comparison between the different samples, rather than on the absolute values obtained.

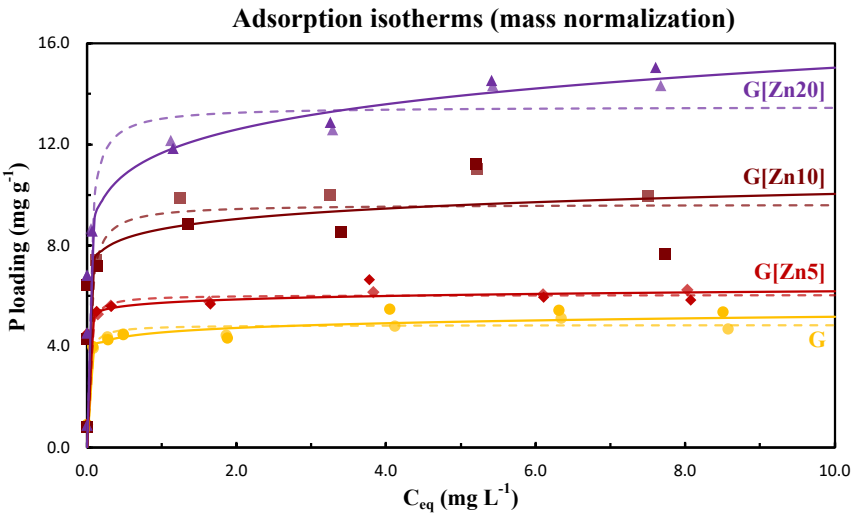

Figure 3.6: Freundlich (solid line) and Langmuir (dashed line) adsorption isotherms with the duplicates data of the different synthesized NPs. Results are normalized with respect to the mass of adsorbent.

Table 3.6: Langmuir and Freundlich fitting parameter of G, G[Zn5], G[Zn10] and G[Zn20] adsorption isotherms normalized to the mass of the adsorbent, with the relative RMSPE.

Sample	*Langmuir*			*Freundlich*		
	q_{max} [mg g^{-1}]	K_L [L mg^{-1}]	*RMSPE*	n	K_F [(mg g^{-1})(mg L^{-1})$^{-n}$]	RMSPE
G	5	47	0.34	0.06	5	0.34
G[Zn5]	6	49	0.47	0.03	6	0.47
G[Zn10]	10	25	0.58	0.07	9	0.58
G[Zn20]	14	27	0.58	0.10	12	0.58

Figure 3.6 shows the mass normalized adsorption isotherms, which fitting parameters values are reported in Table 3.6. For both G and G[Zn5], both models seem to describe the adsorption trend well, and in the case of the Langmuir model, this could be explained with the more homogeneous particles' shape of

the two samples, as well as a general low initial P concentration at which the experiments have been run. For G[Zn10] it is not clear whether a multistep adsorption mechanism is taking place, given the two different NPs phases in G[Zn10], and both isotherms appear to reasonably describe the adsorption trend. For G[Zn20], either a multistep adsorption or a Freundlich-like adsorption trend is visible, as expected by the presence of multiple NPs phases, and the Langmuir model is clearly inadequate to describe the data. P adsorption is increasing with increased doping, and the respective q_{max} and K_F values confirm this trend. In the case of G[Zn10] and G[Zn20], this is explained by the higher SSA available, due to the fine NPs fraction. The affinities, K_L, follow the trend: G[Zn5] > G >> G[Zn20] > G[Zn10] (Figure 3.7) which suggests G[Zn5] being more efficient in adsorbing P even at low concentrations, compared to the other samples. As previously stated, affinity is a key factor when targeting removal at ultra-low concentrations [23]. The high affinity of G[Zn5] might be due to the presence of Zn itself, as well as of the protonation and/or specific crystal faces growth mentioned for the pzc.

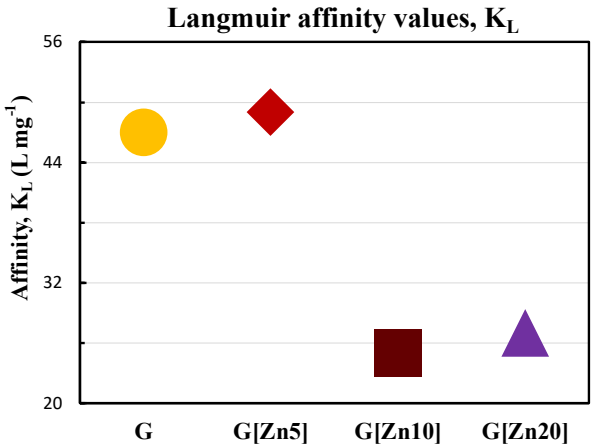

Figure 3.7: Affinity values, KL, retrieved from the adsorption isotherm analysis for each sample.

No clear trend could be identified from the Freundlich parameter n. These results suggest that the higher P removal performances of G[Zn10] and G[Zn20] are due to the higher SSA, which offer higher capacity, while G and G[Zn5] showed higher affinity for P, but lower capacity.

The adsorption isotherm results have also been normalized per SSA, to identify the sample with the "most effective" surface for P adsorption. Figure 3.8 shows the resulting graph and the fitting parameters values are reported in Table 3.7. All the isotherms collapsed within the same range of G, except for G[Zn5], which appeared to outperform the others. This further suggest that its surface is more effective in P adsorption, supporting the hypotheses about protonation and functional crystal faces growth. Namely, the surface protonation might exert an additional driving force on phosphate, attracting more of it to the NPs surface (higher affinity). Then, phosphate is adsorbed to the crystal faces with high adsorption sites density promoted by the increased NPs aspect ratio (higher capacity per SSA).

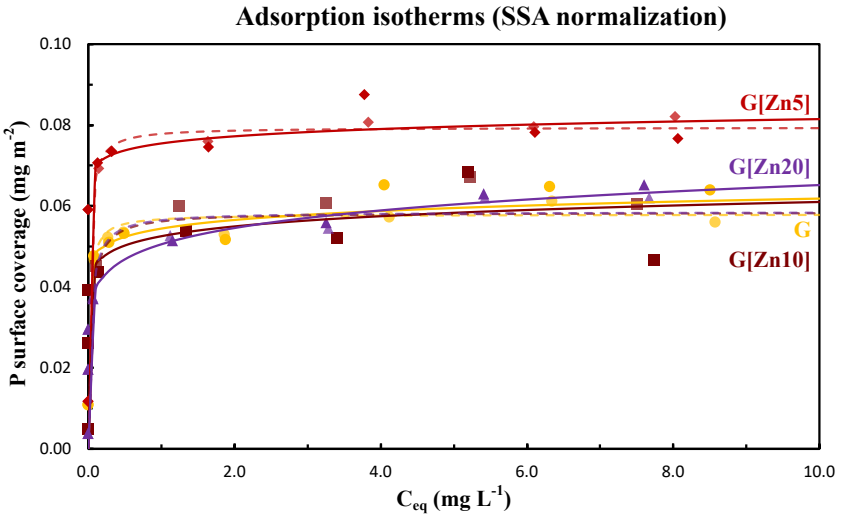

Figure 3.8: Freundlich (solid line) and Langmuir (dashed line) adsorption isotherms with the duplicate data of the different synthesized NPs. Results are normalized with respect to the SSA of adsorbent.

Table 3.7: Langmuir and Freundlich fitting parameter of G, G[Zn5], G[Zn10] and G[Zn20] adsorption isotherms normalized to the SSA of the adsorbent, with the relative RMSPE.

Sample	*Langmuir*			*Freundlich*		
	q_{max} *[mg m^{-2}]*	K_L *[L mg^{-1}]*	*RMSPE*	n	K_F [(mg m^{-2})(mg L^{-1})$^{-n}$]	RMSPE
G	0.06	47	0.34	0.06	0.05	0.34
G[Zn5]	0.08	49	0.47	0.03	0.07	0.47
G[Zn10]	0.06	25	0.58	0.07	0.05	0.58
G[Zn20]	0.06	27	0.58	0.11	0.05	0.58

3.3.3 Regeneration Test

The adsorption experiment performed prior the regeneration test showed the same trend observed for the adsorption isotherms experiments in Figure 3.6 and Figure 3.8, and the results are reported in Figure 3.13 and Table 3.9.

Note that the desorption experiments were performed at a much lower pH (12.6), compared to the usual pH of 13 - 14 found in literature [23,49,60,72,148,156,161]. This was deliberately done to enhance any observable differences in the desorption behaviors. Figure 3.9 reports the desorbed P percentages for each sample, calculated as the mg P desorbed over the mg P adsorbed. Table 3.8 reports these values, with the SSA coverage percentage of the undesorbed P. The desorption results show that, on average, P desorption increased with increasing doping, or at least it was in the same order of magnitude of that of pure G, following a trend: G[Zn20] ≳ G[Zn10] > G[Zn5] ≳ G. The undesorbed fraction caused a surface coverage from a minimum of 3.7(9) % for G[Zn10], to a maximum value of 8(4) % for G[Zn5]. These results show the high recovery potential of P for the doped samples, already at a pH of 12.6,

which means that Zn-doping did not affect the P binding mechanism, such as creating stronger bonds, other complexes or phases (surface precipitates), which would require more effort to be desorbed. Further investigation on the P recovery potential and long term regenerability of the NPs, especially at higher pH, is needed.

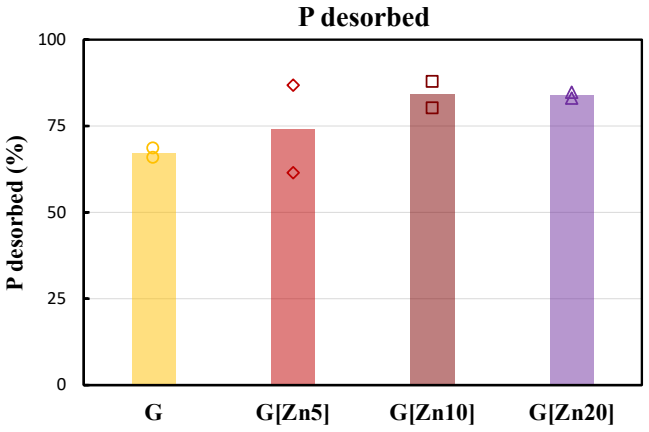

Figure 3.9: Percentage of P desorbed after pH increase.

Table 3.8: Desorbed P and relative surface hindrance of undesorbed P of samples G, G[Zn5], G[Zn10] and G[Zn20].

Sample	P desorbed % w/w	% SSA still covered
G	65 ± 1	6.8 ± 0.7
G[Zn5]	71 ± 12	8 ± 4
G[Zn10]	80 ± 4	3.7 ± 0.9
G[Zn20]	80 ± 1	4.0 ± 0.2

3.3.3.1 Mössbauer Analysis of the Regenerated Samples

After the adsorption-desorption cycle, all samples have been analyzed with Mössbauer spectroscopy, to inspect the stability and any possible change in the structure and phase of the NPs, related to the whole process. However, spectral changes are expected as a result of crystallite growth, fine NPs loss, improved crystallinity (NaOH exposure) and statistical thermal transformation during sample preparation. All graphs are shown in Figure 3.14 and the fitting parameters' values are reported in Table 3.10.

Sample G did not show any appreciable difference from that of the fresh sample, and the analysis confirmed that the sample remained stable.

Conversely, the spectrum of G[Zn5] at RT does display some differences, showing a better definition of the sextet with a slight increase in the mean H_f = 25.6 T (24.6 T in the fresh sample). However, the spectrum at 120 K is in good agreement to that of the fresh sample, suggesting that the differences observed at RT are probably related to the sample preparation effects, such as crystallite growth. An effect linked to the undesorbed P could be excluded, as the residual fraction on the surface is negligible, and it anyway should further reduce the H_f [172], rather than increase it. No dissolved Zn and Fe was observed with ICP analysis, suggesting that G[Zn5] remained stable throughout the process.

The MS spectra of G[Zn10] display similar features to that of the fresh sample, also with better defined peaks, and differences in the spectral contributions. This suggests that some of the fine NPs contributing to the significant superparamagnetic relaxation features observed in the fresh samples went through crystallite growth and/or went lost during sample manipulation.

Finally, the MS spectra of G[Zn20], similarly to G[Zn10], displays better defined peaks and differences in spectral contributions. In particular, the 4.2 K measurement still consists of three contributions, but the observed differences

suggest that recrystallization might have happened throughout the process. In fact, the maghemite-like phase, shows an increase in H_f value from 52.3 T to 52.9 T, as a result of improved crystallinity. Similarly, the zinc ferrite phase displayed improved crystallinity as the H_f increased from 50. 6 T to 51.5 T, as well as the Zn-doped goethite, which mean H_f increased from 48.7 T to 49.3 T. However, a consistent relative reduction in the maghemite-like and zinc ferrite phases, and a consequent increase in that of Zn-doped goethite, suggests that either a fraction of the maghemite and zinc ferrite NPs recrystallized into goethite or went lost during sample manipulation.

To summarize, throughout the adsorption-desorption cycle, G and G[Zn5] appeared to remain stable, as no significant phase changes have been observed in the Mössbauer analysis of the regenerated samples. G[Zn10] displayed slight changes, due to improved crystallinity or fine NPs loss. Differently, G[Zn20] displayed consistent differences, due to either consistent dissolution/recrystallization of zinc ferrite NPs and/or fine NPs loss.

3.3.3.2 Towards an Effective, Stable, and Regenerable P Adsorbent

The experimental results show that 5 %at. was the best Zn-doping percentage for goethite to boost its P recovery performances. First, the NPs phase and morphology were preserved up to 5 %at. doping, as TEM, XRD and MS measurements proved them to consist of Zn-doped goethite rods, with increased aspect ratio. This Zn-doping percentage lead to an increase in the (positive) surface charge, testified by the highest pzc. Regarding P adsorption, sample G[Zn5] was able to remove about 25 % more P per mass of adsorbent compared to the pure goethite phase. Even though G[Zn10] and G[Zn20] had SSA two and three times higher than that of G[Zn5], respectively, the P removal performances for them did not increase accordingly (50 % and 100 % more, respectively). Moreover, the G[Zn5] also displayed the highest affinity for P, and the highest P removal

per SSA. These results support the idea of the higher surface protonation and growth of crystal faces with higher active sites density in Zn-doped goethite. Furthermore, P desorption was not compromised but on average improved with Zn-doping, meaning that the P binding mechanism was not affected, and suggesting an improved P recovery potential. In addition, G and G[Zn5] appeared to remain stable throughout the whole adsorption/desorption process, better sustaining the different environmental conditions compared to G[Zn10] and G[Zn20]. Further research is needed to identify the optimum Zn-doping percentage, and to fully assess the adsorption performances in a real water matrix and the stability of the adsorbent in the long term, after multiple adsorption/desorption studies, with regenerations performed at higher pH.

3.4 Conclusions

This study showed that Zn-doping of goethite NPs improves the P recovery potential of goethite, while preserving its stability. The higher P adsorption was linked to the higher pzc and the higher affinity of Zn-doped goethite for P, the latter being a key factor when targeting the ultra-low P concentrations. This highlights the importance of developing adsorbents with more effective and functional surfaces for P adsorption, rather than adsorbents with only higher SSA. These results set the basis for developing a regenerable and stable, thus long lasting, goethite-based adsorbent with enhanced P recovery potential. Embedding such developed NPs on a support (e.g., HAIX), would bring them to real-life application, improve the adsorbent reusability and make the process economically viable. Further research on adsorbent Zn-doping optimization, NPs support and long-term reusability with real-life conditions would be highly recommended.

Acknowledgements

This work was performed in the cooperation framework of Wetsus, European Centre of Ex-cellence for Sustainable Water Technology (www.wetsus.nl). Wetsus is co-funded by the Dutch Ministry of Economic Affairs and Ministry of Infrastructure and Environment, the Euro-pean Union Regional Development Fund, the Province of Fryslân and the Northern Nether-lands Provinces. This research received funding from the Netherlands Organization for Scientific Research (NWO) in the framework of the Innovation Fund for Chemistry, and from the Ministry of Economic Affairs and Climate Policy in the framework of the TKI/PPS-Toeslagregeling. The authors thank the participants of the research theme "Phosphate recovery" for the interest, fruitful discussions, and financial support. A special thanks goes to Pim de Jager and Raimonda Buliauskaitė (Aquacare) for the frequent knowledge exchange and interest in the research, Harm van der Kooi for the technical support, Michel Steenvoorden and Maxim Ariens for the support with Mössbauer spectroscopy related matters, Kees Goubitz (TU Delft) for the support on XRD, Wiel Evers (TU Delft) for the TEM measurements, Jouk Jansen (TU Delft) for the sup-port with SAED analysis, Renata van der Weijden (WUR) for the fruitful discussions, Prashanth Suresh Kumar (Plaksha University) and Terica Sinclair for the support and guidance, Amandine Dronne, Varad Kapur, Maddalena Tigli for the work done together.

3.5 Supplementary Information

3.5.1 SAED

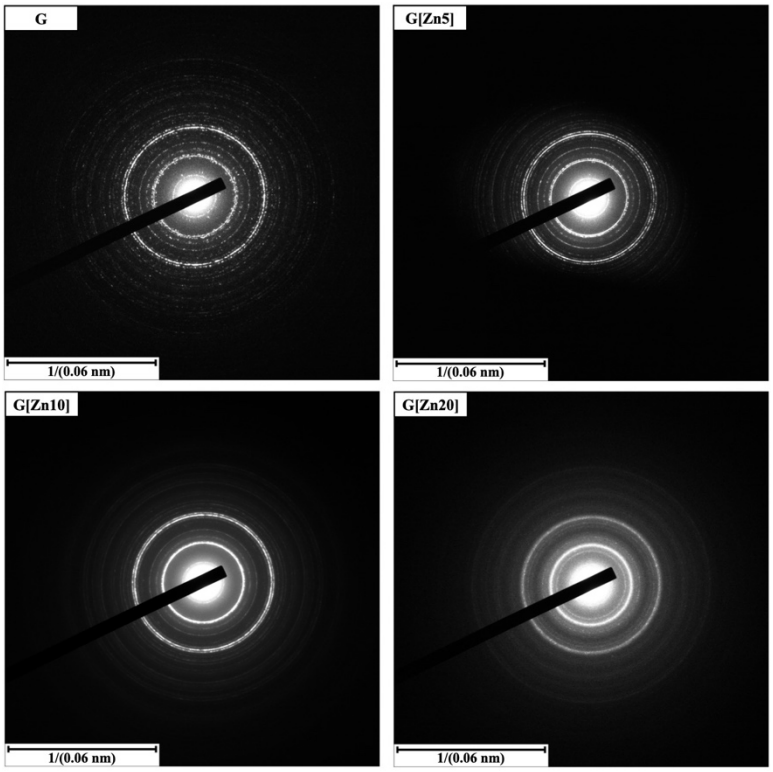

Figure 3.10: SAED patterns of the synthesized NPs.

The SAED diffraction patterns are all reported in Figure 3.10, and have been analyzed qualitatively, in support of XRD observations. The ring patterns show the polycrystalline nature of the NPs for G and G[Zn5], meaning they consist of agglomerated crystalline grains, as inferable from the well-defined ring with very intense spots. This is in agreement with the proposed precipitation mechanism in the synthesis proposed by Villacís-García et al., 2015 [132]. For sample G[Zn10] the SAED pattern still highlights the presence of polycrystalline NPs, as rings with intense spot are still visible, with the broadening of the rings and

the decreased intensity due to the smaller size of the rods and the presence of amorphous NPs. For sample G[Zn20], the SAED pattern with blurry rings surrounded by halos testifies the consistent presence of small amorphous NPs. However, relatively defined rings and intense spots are still visible, most likely due to the presence of the polycrystalline rods and the spherical/cubic NPs.

3.5.2 Superparamagnetism

The relaxation features addressed in sample G[Zn10] and G[Zn20] refer to deviations from the ideal magnetic ordering behavior typical of small NPs (< 15 nm). These deviations arise when the so-called anisotropy energy, KV (K is the anisotropy constant and V is the NPs volume), required to flip the magnetic spins, is of the same order of magnitude of the thermal energy, K_BT (K_B is the Boltzman constant and T the temperature), which cause the magnetic spins to flip due to the thermal excitation in the NPs. If the system is in the low relaxation limit ($KV >> K_BT$), the nuclei will feel an effective magnetic field (thus, are magnetized) and a well-developed sextet will be visible. If the system is in the fast relaxation limit ($KV << K_BT$), then the nuclei experience a vanishing magnetic field, providing a paramagnetic-like feature (doublet), even below the ordering temperature, T_N, and this phenomenon is called superparamagnetism. In the intermediate range, a transition from a paramagnetic-like state to a magnetically ordered state takes place, resulting in complicated spectral features, like the green spectral contribution observed for G[Zn10] and G[Zn20] at 120 K. However, also for the superparamagnetic NPs, the magnetic order can be restored at a sufficient low temperature. The blocking temperature, T_B, is defined as the temperature at which the relaxation time (describing how fast the spin flip) is equal to the characteristic time of the measurement. This latter characteristic time, for Mössbauer spectroscopy, coincides with the Larmor precession time ($\sim 10^{-8}$-10^{-9} s for ^{57}Fe). Thus, below the blocking temperature, magnetic

order can be restored, as observed in the 4.2 K spectra of G[Zn10] and G[Zn20] [173][140].

3.5.3 Collective Magnetic Excitation

The smaller spectral contribution (25 %) of sample G[Zn10] measured at 4.2 K was assigned to the fine NPs fraction with low-to-null Zn substitution. This sextet showed IS = 0.35 mm s^{-1} and QS = -0.26 mm s^{-1}, in agreement with that of bulk goethite, while the H_f = 48.2 T results smaller. However, the H_f value is about 5 % lower than that of bulk goethite, suggesting that either some Zn managed to enter in the structure, or a phenomenon called "collective magnetic excitation" is taking place. The latter is characteristic of very small nanoparticles (below 10 nm), and it is caused by fluctuations of the magnetization vector around an easy direction of magnetization, reducing the observed H_f (up to 15 %) value even below the blocking temperature [140,173]. For this reason, this contribution of the G[Zn10] Mössbauer spectrum at 4.2 K has been assigned to the amorphous/fine fraction of NPs with a low-to-null Zn-doped goethite.

3.5.4 Point of Zero Charge with Polynomial and Linear Interpolation

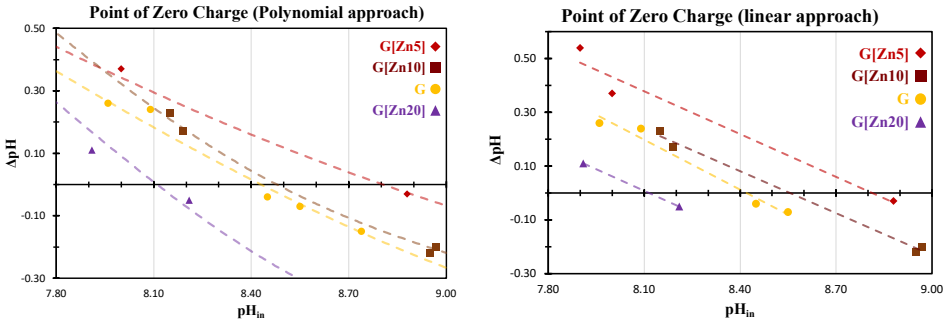

Figure 3.11: Polynomial (left) and linear (right) interpolation of the pzc measurement data for each sample.

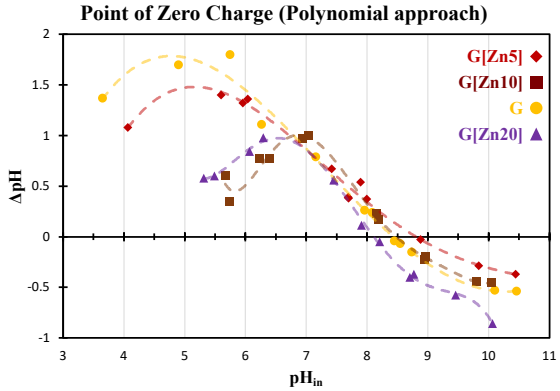

Figure 3.12: Polynomial interpolation of the pzc data over the whole data sets.

3.5.5 Adsorption/Desorption Test

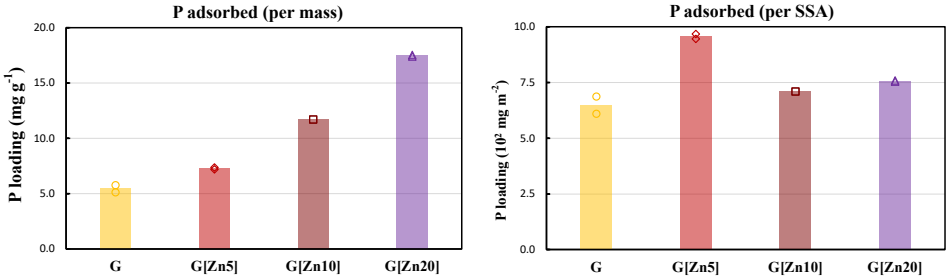

Figure 3.13: P adsorbed normalized to the mass of adsorbent per each sample.

Table 3.9: Amount of adsorbed P per mass of adsorbent and relative surface coverage of samples G, G[Zn5], G[Zn10] and G[Zn20].

Sample	*P adsorbed [mg g^{-1}]*	*% SSA coverage*
G	5.4 ± 0.3	22 ± 1
G[Zn5]	7.27 ± 0.08	33.1 ± 0.4
G[Zn10]	11.7 ± 0.1	24.6 ± 0.2
G[Zn20]	17.5 ± 0.2	26..2 ± 0.3

Figure 3.13 show the P removed per mass and per SSA, and Table 3.9 reports the respective P loading and % SSA coverage. The observed P loadings and surface coverages followed the same trend as for the adsorption isotherm experiments, with the highest surface coverage observed for G[Zn5], up to 33.1(4) %. This further supports the idea of a more effective SSA of G[Zn5] compared to the other samples.

3.5.6 Mössbauer Spectroscopy Analysis of the Regenerated Samples

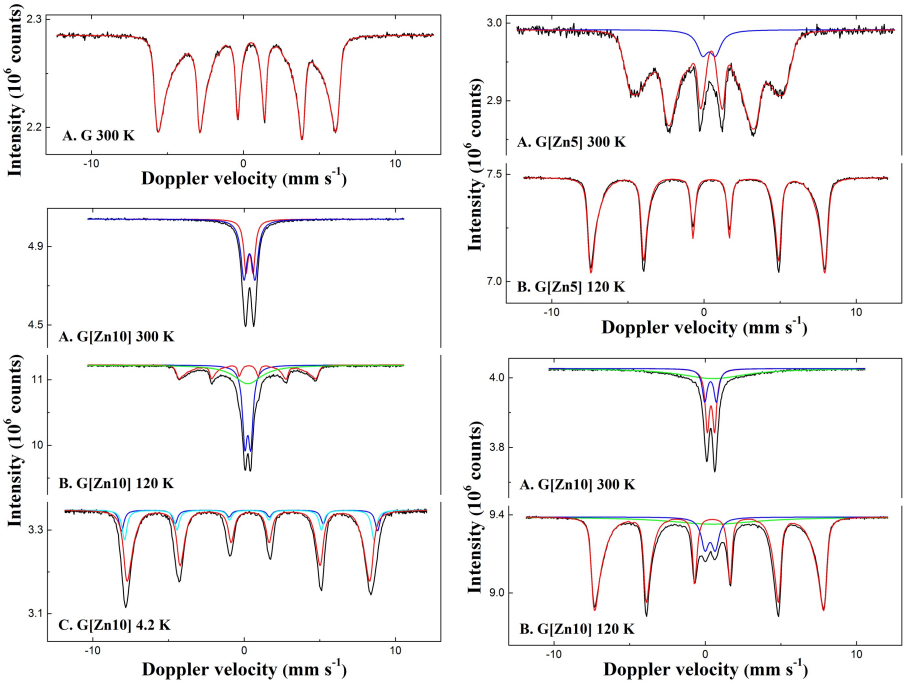

Figure 3.14: MS spectra of the regenerated NPs measured at different temperatures (300, 120 and 4.2 K). Black lines represent the measured spectra, colored lines represent the fitted spectral contributions.

Table 3.10: Mössbauer fitting parameters of the regenerated G, G[Zn5], G[Zn10] and G[Zn20] at 300 K, 120 K and 4.2 K.

Sample	*T (K)*	*IS (mm·s^{-1})*	*QS (mm·s^{-1})*	*H_f (T)*	*Γ (mm·s^{-1})*	*Phase*	*Spectral contribution (%)*
G *Pure goethite*	300	0.37	-0.27	32.6*	0.26	α-FeOOH	100
G[Zn5] 5 %at. Zn/Fe doped goethite	300	0.36	-0.26	25.6*	0.35	α-(Zn,Fe)OOH	92
		0.33	0.85^	-	0.85^	Fe^{3+}	8
	120	0.36	-0.22	46.5*	0.26	Fe^{3+}	100
G[Zn10] 10% at. Zn/Fe doped goethite	300	0.35	0.77	-	0.39	Fe^{3+}	22
		0.38	0.48	-	0.33	Fe^{3+}	33
		0.55	-	-	5.25	Fe^{3+}	45
	120	0.32	0.68	-	0.58	Fe^{3+}	10
		0.36	-0.21	45.1*	0.25	α-(Zn,Fe)OOH	75
		0.53	-	-	7.03	Fe^{3+}	15

G[Zn20] 20% at. Zn/Fe doped goethite	300	0.35	0.76	-	0.43	Fe^{3+}	61
		0.36	0.44	-	0.36	Fe^{3+}	39
	120	0.34	0.69	-	0.67	Fe^{3+}	42
		0.36	-0.20	42.0*	0.32	α-(Zn,Fe)OOH	25
		0.35	-	-	3.96	Fe^{3+}	32
	4.2	0.35	0.03	52.9	0.31	γ-Fe_2O_3	7
		0.34	0.01	51.5	0.38	$ZnFe_2O_4$	20
		0.34	-0.11	49.3*	0.45	α-(Zn,Fe)OOH	73

*Experimental uncertainties: I.S. ± 0.01 mm s^{-1}; Q.S. ± 0.01 mm s^{-1}; Γ ± 0.01 mm s^{-1}; H_f ± 0.1 T; Spectral contribution: ± 3 %. *Average magnetic field. ^Fixed value.*


4

4

FeOOH- and (Fe,Zn)OOH-based hybrid anion exchange adsorbents for phosphate recovery: a thorough determination of Fe-phases and adsorption-desorption mechanisms

A modified version of this chapter has been submitted as: **Belloni, C.**, de Jager, P., Korving, L., Witkamp, G.J., Brück, E., Dugulan, A.I., 2023, *FeOOH- and (Fe,Zn)OOH-based hybrid anion exchange adsorbents for phosphate recovery: a thorough determination of Fe-phases and adsorption-desorption mechanisms,* Chemical Engineering Journal.

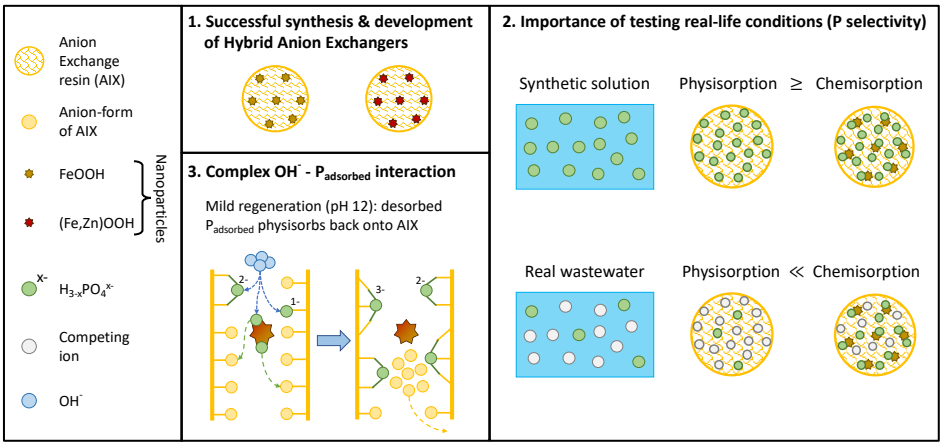

Highlights

- Successful immobilization and performance of Zn-doped iron (hydr)oxide nanoparticles (NPs) in anion exchange resins (AIX).
- Mössbauer spectroscopy revealed the goethite nature of the NPs in HAIX, against "amorphous hydrous ferric oxides" reported in literature.
- In experiments with pure phosphate synthetic solutions, physisorption hides the advantages of chemisorption, even more at high P concentrations.
- The P selectivity provided by the NPs in HAIX is crucial for real life applications.
- During HAIX regeneration, the resin backbone hampers P desorption, and more OH^- is required to fully desorb P.
- Mössbauer spectroscopy revealed consistent NPs growth throughout the adsorption-desorption cycles, questioning the robustness of AIX as a support for NPs

Keywords:
phosphate recovery, adsorption, regeneration, iron oxide, HAIX

Abstract

Hybrid anion exchange adsorbents (HAIX) seem promising to prevent eutrophication and recover phosphate (P). HAIX consist of an anion exchange resin (AIX) backbone, promoting anion physisorption, impregnated with iron (hydr)oxide nanoparticles (NPs), for selective P chemisorption. In this work, for the first time, Zn-doped iron (hydr)oxide NPs were embedded in AIX, and the performances compared with conventional HAIX, both commercial and synthesized. Zn-doped HAIX displayed improved P adsorption performances. A thorough HAIX characterization with Mössbauer spectroscopy (MS) revealed the goethite nature of the NPs, against the "amorphous hydrous ferric oxide" claimed in literature. The P adsorption comparisons, made in synthetic solution and real wastewater, underlined the crucial role of the NPs for selective P adsorption, while improving the understanding on the competition between physisorption and chemisorption. In pure P synthetic solutions, especially at high P concentrations, physisorption can "hide" chemisorption. This depends also on the anionic form of the AIX, due to their higher affinity for multivalent anions, which affects HAIX adsorption selectivity and P desorption. In fact, a mild alkaline regeneration over three adsorption-desorption cycles revealed a complex interaction between the regenerant OH^- and the adsorbed P. OH^- molecules are consumed to transform phosphate speciation, causing (stronger) P re-adsorption and preventing desorption. Finally, MS revealed NPs sintering after the three cycles, questioning the suitability of AIX as backbone. This study provides further understanding on the P adsorption-desorption mechanism in HAIX, drawing attention on the choice of experimental conditions for reliable performance assessment, and questioning HAIX efficacy and efficiency for P recovery.

4.1 Introduction

Hybrid anion exchanger adsorbents (HAIX), widely applied for arsenic (As) removal [84,174–177], also showed promising results for phosphate (P) recovery [60,62,64,65]. Moreover, HAIX displayed the possibility to reach ultra-low P concentrations [23,178], necessary to prevent eutrophication [121]. HAIX consist of an anion exchange resin (AIX) backbone impregnated with metal (hydr)oxide nanoparticles (NPs). The adsorption mechanism for HAIX is thus twofold. Firstly, the resin backbone, which provides the Donnan exclusion effect [179–181], promotes anion physisorption, which is charge driven and hence non-selective for ion species. The anion interaction and adsorption mechanism depend on the backbone material, adsorption sites and their ionic form, i.e., the counterion compensating for the charge (e.g., sulfate or chloride) [182–185]. Secondly, the NPs, which provide higher selectivity, remove phosphate via chemisorption [52,65,70,84,181], i.e., forming a chemical bond. The NPs role is fundamental for treating complex water matrices for phosphate (henceforth referred to as P) recovery, and they often consist of iron oxides (comprising hydroxide and oxyhydroxides) species [62,64,65,185]. In fact, iron oxides show good affinity for P, are abundant and relatively cheap compounds, and have been widely investigated [23,51,52,60,71,78,128]. Different HAIX synthesis methods are available in literature [68,82,177,186] and commercial adsorbents, like Layne^{RT}, have been widely investigated [62,64,65,82–84,185]. These are usually claimed to contain amorphous/non-crystalline iron oxide nanoparticles, defined with the general and vague term "hydrous ferric oxide", HFO, mostly ascribed to ferrihydrite [56,57,75,81,84,176,178,187,58,60–65,68].

For the economic viability of adsorption technology for P recovery, it is necessary to be able to regenerate and reuse the adsorbent for multiple adsorption cycles [23]. Desorption of P and regeneration of Fe-based adsorbents is typically performed with an alkaline wash, e.g., 0.1-1 M NaOH (pH 13-14) [49] ,

sometimes also with the addition of NaCl. Little focus has been spent on the adsorbent regeneration, with only a few studies investigating mechanism and strategies [52,71], even less analyzing in depth the desorption mechanism with HAIX [49]. Especially for the HAIX, no clear explanation has been provided on the role and desorption mechanism of NaOH and NaCl during the regeneration procedure. Some authors claimed that a mixture of NaOH and NaCl is needed to regenerate the AIX sites and the NPs, respectively [64,185]; others claimed that NaCl is needed to remove the organics [62] and to replace the OH^- in the AIX sites with Cl^- [62,66]; other authors suggested the use of NaOH alone would suffice [54,65]. Kumar et al, 2018 [52], pointed out that regeneration of HAIX may affect the NPs speciation and performance, causing a decrease in adsorption performances already after a few adsorption cycles. Anyway, no solid theoretical basis on the desorption mechanism with HAIX is provided.

Finally, iron oxide doping could help improving the performances and stability of HAIX. Doping is a technique popular in the semiconductor and catalysis fields [88–91,93], which consists in adding one or more impurities (via inclusion or substitution) into the structure of a material. This allows to manipulate the material properties, like oxidation, magnetic properties, surface properties, conductivity, and so on [188–193]. Two recent studies from our group on goethite (a highly stable iron oxide) NPs doping showed Zn-doped goethite to be promising for P recovery (see Chapters 2 and 3). These studies suggest Zn to increase the affinity and adsorption site density for P, with goethite providing the intrinsic phase stability. However, these NP's have never been tested in an AIX resin.

In this study, two different syntheses procedures for HAIX with strong base AIX have been compared, and a successful impregnation of Zn-doped iron oxide was achieved. HAIX characterization with Mössbauer spectroscopy revealed that the iron oxide NPs in HAIX generally consist of goethite, in contrast

to reports in literature. These HAIX were tested and compared to a commercial HAIX and a commercial anion exchange resin, both in synthetic P solution and P-spiked wastewater. These tests highlight the importance of the selectivity for P of the HAIX over the AIX, provided by the NPs, and showed promising results for the Zn-doped HAIX. Also, the effect of the AIX backbone form and the interaction with anions were investigated, further supporting the higher affinity of strong base AIX for multivalent ions over the monovalent ones. Moreover, an unexpected behavior in multiple adsorption-desorption cycles in synthetic solutions provided insights in the complex interaction between OH^- and the adsorbed P, which prevented P desorption but displayed a beneficial effect on the successive adsorption cycles.

This study shows the performances of an improved Zn-doped iron oxide-based HAIX, while improving the understanding on the adsorption mechanism, selectivity for P and the P-desorption mechanism when using AIX-based adsorbents.

Crystallization of lactose is an interplay of three processes: mutarotation between α- and β-lactose, initial creation of nuclei (nucleation), and growth of the crystals (Mimouni et al., 2009). Each of these steps can influence the rate of the process and the final morphology and size of the crystals. Furthermore, they are affected by the operating conditions (temperature, concentration, impurities, and agitation rate). Impurities can catalyse or slow down the crystallization process. DLP has a high content of minerals, acids, and organics, which can be expected to have an impact on the process and the final crystals. The effect of different additives on the growth of lactose crystals has been studied by different authors, and an overview was given by Wong and Hartel (2014). However, in these studies, only the effect of one individual compound was investigated rather than a mixture as present in DLP.

This study investigates the further recovery of lactose from DLP using a sub-zero crystallization process. Furthermore, a population balance model is used to analyse the kinetics of mutarotation, nucleation, and crystal growth. The yield, final crystal size distribution, and crystallization rate of a pure lactose solution (Halfwerk et al., 2023a) and DLP are compared.

4.2 Materials and methods

4.2.1 Chemicals

Iron sulphate ($Fe(SO_4)\cdot 6H_2O$) and 3-(N-morpholino)-propane sulfonic acid (MOPS) were purchased from Sigma-Aldrich (The Netherlands). Potassium di-hydrogen phosphate (KH_2PO_4), potassium permanganate ($KMnO_4$), sodium chloride (NaCl), sodium hydroxide (NaOH), hydrochloric acid (HCl) and nitric acid (HNO_3) were purchased from VWR (The Netherlands). Iron chloride ($FeCl_3\cdot 6H_2O$) and zinc chloride ($ZnCl_2\cdot H_2O$) were purchased from Alfa Aesar (Germany).

4.2.2 Adsorbents

4.2.2.1 Commercial Adsorbents

The anion exchange resin A500Plus (A500+) was obtained by Purolite GmbH (Germany). It consists of 300-1200µm beads of a light-yellow color and was chosen as it is a macroporous polystyrene cross-linked with divinylbenzene resin with quaternary ammonium functional groups in chloride form, which often constitutes the backbone of HAIX adsorbents [62,64,65,68,83,185,194].

The commercial HAIX adsorbent selected as a reference was LayneRT™ (Layne) [62,64,65,82,83,185], of Layne Christensen Co (United States), which

was obtained via Aquacare (’s-Hertogenbosch, The Netherlands). Table 4.1 shows the main characteristics of the commercial adsorbents.

Table 4.1: Characteristics of A500Plus and LayneRT.

Name	A500Plus	LayneRT™
Producer	Purolite®	Layne Christensen Co.
General	Strong base anion exchange resin	Hybrid strong base anion exchange resin
Structure	Macroporous polystyrene cross-linked with divinylbenzene	Macroporous polystyrene cross-linked with divinylbenzene impregnated with iron hydroxide nanoparticles
Appearence	Light yellow beads	Brown spherical beads
Particle size (μm)	300-1200	300-1200
Specific gravity	1.08	1.25-1.30
Functional groups	Type 1* quaternary ammonium in chloride form	(Type 1)** Quaternary ammonium in chloride form (resin) Hydroxide (nanoparticles)
Fe content	-	9.5 wt.%

*Methyl group as radical (CH_3)

**Unsure radical type, most likely type 1 (see [194])

4.2.2.2 Synthesized Adsorbents

The synthesis procedure consisted of impregnating pure and doped iron hydroxide nanoparticles in the A500+ resin following two different procedures.

The first procedure was adapted from the patent of SenGupta et al., 2007 [194], which is the basis of HAIX used for As removal from drinking water [68][175]. In short, about 15 g of A500+ was weighed and thoroughly washed in Deionized Water (DW), and a 2 L solution of 500 mg/L $KMnO_4$ concentration and a 0.5 L CO_2-free solution 5 %w/v $FeSO_4$ were prepared. The resins were first immersed in the $KMnO_4$ solution and let to shake for 30 min, then removed and thoroughly washed in DW. The $KMnO_4$ impregnated resins (now of a violet color) were then immersed in the $FeSO_4$ solution and let to shake for 4 h. The resins (now of a dark brown color) were then separated from the solution and thoroughly washed in DW. The whole procedure was performed for a total of 3 impregnation cycles, to increase the Fe loading. The so-synthesized adsorbent is referred to as R_{Mn}[Fe]. An attempt to embed 5 %at. Zn/(Zn+Fe) doped iron hydroxide NPs via this procedure was performed without success, hence no follow-up experiments were performed with this type of adsorbent.

The second synthesis procedure was adapted from Kociołek-Balawejder et al., 2017 [194]. In short, about 10 g of A500+ was weighed and thoroughly washed in DW. The resins were then immersed for 24 h in 100 mL of 0.5 M $FeCl_3$ in 5 M HCl solution. Then, the resins were filtered out via Büchner filtration and immersed in 50 mL of 1 M NaCl in 1 M NaOH solution for 24 h to promote the iron hydroxide precipitation within the resin. The resins (now of a brownish color) were separated and thoroughly washed in DW. The so-synthesized adsorbent is referred to as R_{HCl}[Fe]. Similarly, this procedure allowed for Zn-doped iron hydroxide precipitation within the resin, by adding $ZnCl_2$ to the $FeCl_3$ solution, in this case to obtain a doping percentage of 5 %at. Zn/(Fe+Zn). This sample is referred to as R_{HCl}[Fe+Zn].

4.2.2.3 Adsorbent Characterization

The commercial and synthesized HAIX elemental composition, mainly focusing on the Fe and Zn wt.% content, was investigated with two methods. Firstly, via HNO_3 (69 %) microwave digestion (MWD) with a Milestone Ethos Easy digester with a SK-15 High-Pressure rotor, followed by an elemental analysis with a Perkin Elmer Optima 5300 DV Inductively Coupled Plasma Optical Emission Spectroscopy (ICP). Secondly, with a JEOL JSM-6480 LV Scanning Electron Microscope (SEM) equipped with an Oxford Instruments x-act SDD Energy Dispersive X-ray (EDX) spectrometer. Samples were coated with < 10 nm of gold to make them conductive. The SEM images were analyzed with the JEOL SEM Control User Interface software and while the EDX data were processed with the Oxford Instruments Aztec software.

The commercial and synthesized HAIX Fe speciation was investigated using Mössbauer spectroscopy (MS). Transmission ^{57}Fe MS spectra were measured at 300 K (room temperature), 120 K (set-up thermalization with liquid nitrogen) and 4.2 K (liquid helium). The lower temperatures are needed as they promote the Zeeman splitting of Mössbauer spectral lines, allowing for better identification of (super)paramagnetic phases [75]. The MS spectra were collected with conventional constant acceleration or sinusoidal velocity spectrometers using a ^{57}Co (Rh) source. The MS spectra, calibrated to α-Fe, were analyzed with MossWinn 4.0 software [133], to retrieve the different relevant parameters, here explained. The isomer shift, IS, related to the oxidation state of the Fe atoms; the quadrupole splitting, QS, mainly related to the asymmetry of the charge distribution around the Fe nuclei; the magnetic hyperfine field, H_f, related to the magnetic ordering within the sample; the line-width (Γ), which can provide information on the crystallinity of the sample; and the spectral contribution [%], for Fe species quantification.

4.2.3 P Solutions

The adsorption experiments consist of adsorption kinetics experiments and adsorption-desorption experiments. For both types of experiments, all adsorbents (A500+, Layne, R_{Mn}[Fe], R_{HCl}[Fe] and R_{HCl}[Fe+Zn]) were tested at an adsorbent concentration of 2 g L^{-1} in two water scenarios: in P synthetic solution and in P-spiked wastewater (ww).

First, a 500 mg L^{-1} P stock solution was prepared by dissolving KH_2PO_4 in Demineralized Water (DW), adjusting the pH to around 7 using NaOH/HCl. For the experiments in synthetic solution, a proper dilution was performed adding 20 mM MOPS as a pH buffer, and the pH further adjusted to around 7.2 using NaOH/HCl. For the experiment with P-spiked ww, the wastewater was collected from the sewage effluent of the WWTP in Leeuwarden, and Table 4.2 reports its main characteristics, with the composition expressed in terms of total concentrations. The wastewater was filtered via Büchner filtration and spiked by slowly adding a proper aliquot of the P stock solution while stirring. The wastewater pH after P-spiking remained between 7.4 and 7.6, and it was measured after adsorption, with final pH values between 8.00 and 8.5.

The solutions for the adsorption tests were analyzed before and after adsorption with the ICP for the elemental composition, a Metrohm Compact IC Flex 930 ion Chromatograph (IC) for the ionic composition (in both cases, IC and ICP samples were filtered with a 0.45 µm hydrophilic filter) and a Shimadzu TOC-L CPH (CHECK) to assess the total organic carbon (TOC), total inorganic carbon (TIC) and hence the total carbon (TC) content. All data were then analyzed using Microsoft Excel.

Table 4.2: Characteristics of the wastewater collected from the WWTP in Leeuwarden.

Parameters	**Values**
Temperature (during adsorption)	25°C
pH	7.4 -7.6
Conductivity	1.2 ± 0.2 mS cm^{-1}
Phosphorus	0.100 ± 0.01 mg L^{-1}
Calcium (Ca)	60 ± 1 mg L^{-1}
Magnesium (Mg)	20.0 ± 0.2 mg L^{-1}
Sulphur (S)	9.2 ± 0.2 mg L^{-1}
Nitrate (NO_3^-)	2.3 ± 0.1 mg L^{-1}
TOC	12 ± 1 mg L^{-1}
TIC	73 ± 1 mg L^{-1}
Silicon (Si)	12.0 ± 0.1 mg L^{-1}
Zinc (Zn)	0.072 ± 0.007 mg L^{-1}
Iron (Fe)	0.064 ± 0.008 mg L^{-1}

4.2.3.1 Adsorption Kinetics

The adsorption kinetics experiments were performed in batch mode, with both water scenarios (demi water and wastewater) for two main reasons. Firstly, to assess the time required for the adsorbent to reach equilibrium, to design the adsorption-desorption experiments. Secondly, to monitor over time the different

adsorbent behavior in the two different scenarios. For both scenarios, the initial P concentration was of 25 mg L^{-1}, which was chosen to allow for relatively frequent sampling with small volumes of solution, to minimize perturbations to the system. The experiments were performed in duplicates plus blank (or control), and water samples were collected after 15, 30 min, 1, 2, 4, 22, 24, 28, 48, 52, 71 h, 1, 2, 3, 4 weeks and the P content analyzed with ICP. The amount of P adsorbed per mass of adsorbent was calculated via:

$$q_i(t_i) = \frac{c_0(t_0) - c_i(t_i)}{m} V$$

where q_i [mg g^{-1}] is the adsorbent loading at the time t_i, c_0 [mg L^{-1}] is the initial P concentration, c_i [mg L^{-1}] is the P concentration at time t_i, m [g] is the adsorbent mass and V [L] is the solution volume. For each q_i, the change in volumes due to sampling were taken into account.

The results were analyzed with two models, the Pseudo-First Order (PFO) [195,196] and Pseudo-Second Order (PSO) [197] kinetics, to investigate the behavior of the different adsorbent and to estimate the equilibration time, t_{eq}, and t_{95}, at which 95 % of equilibrium is reached.

The PFO kinetic model, based on the assumption that the adsorption mechanism limiting factor is the concentration of the adsorbate, usually describes better physisorption. The PSO kinetic model, based on the assumption that the adsorption mechanism limiting factor is the adsorbent capacity, usually describes better chemisorption (in which a chemical bond forms between the adsorbent and the adsorbate). The two models are respectively described by the equations:

$$q(t) = q_{eq}(1 - e^{-k_1 t})$$

$$q(t) = \frac{k_2 q_{eq}^2 t}{1 + k_2 q_{eq} t}$$

where t [h] is the time, $q(t)$ [mg g^{-1}] is the adsorbent loading at time t, k_1 [g mg^{-1} min^{-1}] is the kinetic rate constant of the PFO kinetic model, k_2 [g mg^{-1} min^{-1}] is the kinetic rate constant of the PSO kinetic model, and q_{eq} [mg g^{-1}] is the adsorbent loading at equilibrium. The fittings were performed using the Microsoft Excel Solver add-in, and the goodness of the fit assessed both evaluating the Root Mean Squared Percentage Error (RMSPE) and the Chi-squared (χ^2).

4.2.3.2 Adsorption-Desorption Tests

The adsorption-desorption experiments were performed for 3 cycles in batch mode with both water scenarios, at an initial P concentration of 5 mg L^{-1} for both scenarios, and in triplicates plus blank (or control).

The equilibration time was 5 days and the amount of P adsorbed was estimated after each cycle using equation (1) and plotted in histograms. After adsorption, the solution was removed, the adsorbent washed with DW (3 x 50 mL, shaken for couple of minutes), and exposed for one day to a 0.01 M NaOH solution (pH 12), which was reused over the 3 cycles. The low pH, compared to the higher pH 13-14 usually employed [49,62,65,194], was chosen to enhance any difference in the desorption behavior. After desorption, the NaOH solution was analyzed and the adsorbents were washed with DW several times (3 x 50 mL, shaken for couple of minutes each time), until the pH dropped to around 7, to then start a new adsorption cycle. Also, the concentration of P in the DW washings was measured.

After the last regeneration cycle, the adsorbent was regenerated with 1 M NaOH solution (pH 13.7) to fully regenerate the adsorbent and estimate the residual P adsorbed.

4.3 Results

4.3.1 Adsorbent Characterization

4.3.1.1 Microwave Digestion

The results of the ICP analysis of the MWD samples are shown in Table 4.3 and Figure 4.1. LayneRT and R_{Mn}[Fe] display similar Fe content, together with Mn and S content. R_{HCl}[Fe] and R_{HCl}[Fe+Zn] adsorbents also display similar Fe content, lower compared to Layne and R_{Mn}[Fe]. For R_{HCl}[Fe+Zn], the Zn content was the 5 %at. targeted.

Table 4.3.: Elemental composition of the adsorbents, after MWD and ICP analysis.

Sample	Fe [% w/w]	Mn [% w/w]	S [% w/w]	Zn [% w/w]	Zn-doping [%at. Zn/(Fe+Zn)]
A500+	-	-	-	-	-
Layne	9.5 ± 0.2	< 0.1	0.95 ± 0.02	-	-
R_{Mn}[Fe]	8.9 ± 0.3	< 0.01	3.2 ± 0.1	-	-
R_{HCl}[Fe]	6.2 ± 0.2	-		-	-
R_{HCl}[Fe+Zn]	6.2 ± 0.2	-		0.38 ± 0.01	5

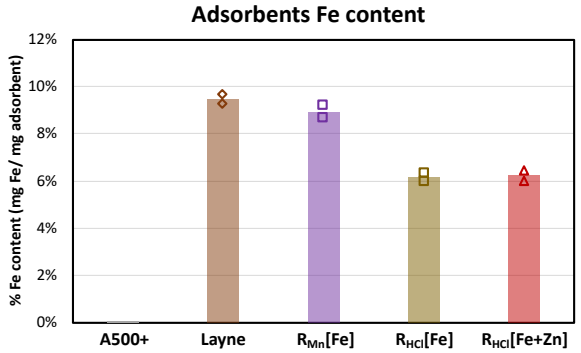

Figure 4.1:Fe content of the different adsorbents, as determined by ICP analysis of the MWD samples.

4.3.1.2 SEM-EDX

SEM-EDX analysis (see S.I.) shows for all HAIX a significant and homogeneous Fe distribution. Sample R_{HCl}[Fe+Zn] shows also a homogeneous distribution of Zn, close to 5 %at. compared to the Fe. Samples A500+, R_{HCl}[Fe] and R_{HCl}[Fe+Zn] displayed a significant presence of homogeneously distributed Chlorine, while Layne and R_{Mn}[Fe] showed the same for Sulfur with also traces of Chlorine.

4.3.1.3 Mössbauer Spectroscopy Characterization

Figure 4.2 shows the Mössbauer spectra of the HAIX, and Table 4.4 reports the related fitting parameters. Layne and R_{Mn}[Fe] display a unspecific (super)paramagnetic Fe^{3+} species doublet at 300 K, and a well-defined sextuplet at low temperatures, identifying the goethite phase. R_{HCl}[Fe] and R_{HCl}[Fe+Zn] display coexisting doublet and sextuplet at both 300 K and 120 K, describing unspecific (super)paramagnetic Fe^{3+} species and goethite, respectively.The effect of parameters and their interaction is complex and can be optimized by response surface methodology.

4.3.2 Adsorption Kinetics

4.3.2.1 P Synthetic Solution

The long-term (4 weeks) adsorption kinetics graphs in P synthetic solution are showed in S.I., and the fitting results are reported in Table 4.5. Figure 4.3 shows the kinetics results within the first 24 h and 10 h, since all samples reached equilibrium well within 24 h. The fitting was performed over the entire time range (4 weeks), providing more data points and higher confidence on the maximum loading at equilibrium. The PFO model showed slightly lower RMSPE than the PSO and was used to estimate t_{95}, as the PSO seemed to largely overestimate q_{eq} and t_{eq}. The faster sample to reach equilibrium was

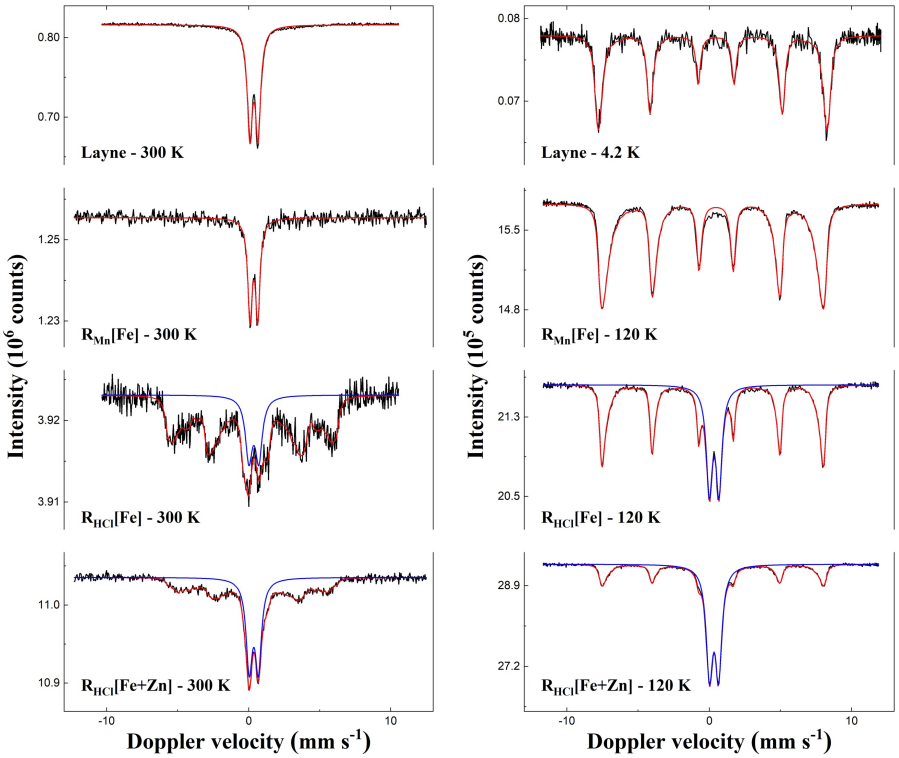

Figure 4.2: 300 K MS spectra (left) and low temperature MS spectra (right) of the HAIX.

Table 4.4: MS parameters of the HAIX and reference values for goethite and ferrihydrite.

Sample	*T (K)*	*IS (mm·s^{-1})*	*QS (mm·s^{-1})*	*H_f (T)*	*Γ (mm·s^{-1})*	*Phase*	*Spectral contribution (%)*
Bulk goethite reference values [75]	300	0.37	-0.26	38.0	-	α-FeOOH	-
	4.2	0.37	-0.25	50.6	-	α-FeOOH	-
Ferrihydrite reference values** [75]	300	0.35	[0.62-0.78]	-	-	$Fe_5HO_8 \cdot 4H_2O$	-
	4.2	0.35	-[0.2-0.7]	[50-47]	-	$Fe_5HO_8 \cdot 4H_2O$	-
Layne	300	0.37	0.58	-	0.44	Fe^{3+}	100
	4.2	0.36	-0.24	49.5*	0.35	α-FeOOH	100
R_{Mn}[Fe]	300	0.36	0.55	-	0.37	Fe^{3+}	100
	120	0.36	-0.24	44.4*	0.35	α-FeOOH	100

R_{HCl}[Fe]	300	0.36	0.69	-	0.58	Fe^{3+}	20
		0.37	-0.26	29.2*	0.35	α-FeOOH	80
	120	0.34	0.69	-	0.50	Fe^{3+}	39
		0.36	-0.23	46.9*	0.25	α-FeOOH	61
R_{HCl}[Fe+Zn]	300	0.36	0.65	-	0.53	Fe^{3+}	47
		0.40	-0.26	26.6*	0.30	α-FeOOH	53
	120	0.33	0.65	-	0.54	Fe^{3+}	69
		0.36	-0.21	46.7*	0.31	α-FeOOH	31

Experimental uncertainties: I.S. ± 0.01 mm s^{-1}; Q.S. ± 0.01 mm s^{-1}; Γ ± 0.01 mm s^{-1}; H_f ± 0.1 T; Spectral contribution: ± 3 %.
**Average magnetic field.*
***The value ranges for ferrihydrite QS and H_f are related to the different crystallinities and forms of ferrihydrite, i.e., 2-line and 6-line ferrihydrites.*

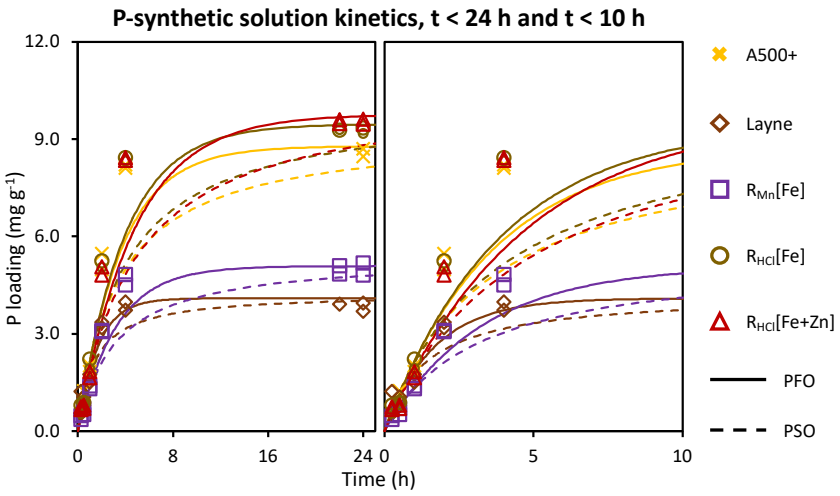

Figure 4.3: Adsorption kinetics of all samples in P synthetic solution, within 24 h and 10 h. The solid and the dashed lines represent the PFO and the PSO fitting curves, respectively.

Layne, which reached 95 % of equilibrium within 5 h, followed by R_{Mn}[Fe], A500+, R_{HCl}[Fe], between 10 and 11 h, and lastly R_{HCl}[Fe+Zn], around 14 h. Samples A500+, R_{HCl}[Fe] and R_{HCl}[Fe+Zn] show higher P capacities (8.3, 9.0 and 9.3 mg g^{-1}, respectively), about double that of Layne and R_{Mn}[Fe] (4.1 and 5.1 mg g^{-1}, respectively).

4.3.2.2 P-Spiked Wastwater

The long-term (4 weeks) adsorption kinetics graphs in P-spiked wastewater are shown in S.I. and display a multistep trend. Figure 4.4 shows the kinetics within the first 24 h, which is closer to the timescale of interest, also according to the kinetics results in P synthetic solution. Within 24 h, all the adsorption curves saturate around the same P loading range. The P loading follows the trend: R_{HCl}[Fe+Zn] > R_{HCl}[Fe] > R_{Mn}[Fe] > A500+, Layne.

Figure 4.5 shows the comparison between the adsorption kinetics in P synthetic solution and in P-spiked wastewater.

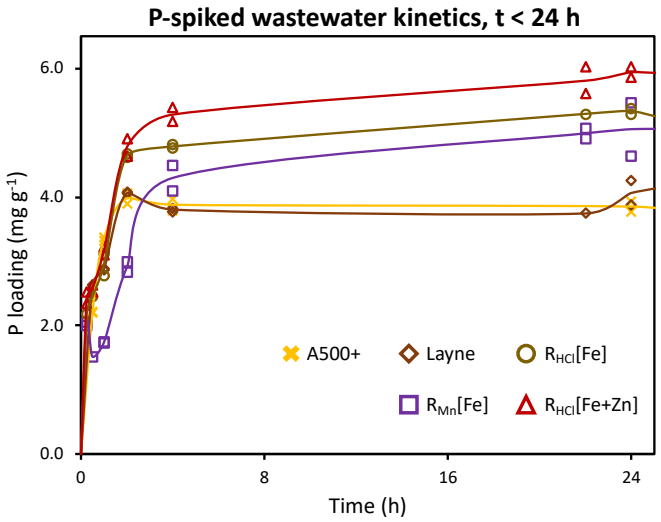

Figure 4.4: Adsorption kinetics of all samples in P-spiked wastewater, within 24 h. The duplicate data are superimposed to the solid line representing the average trend.

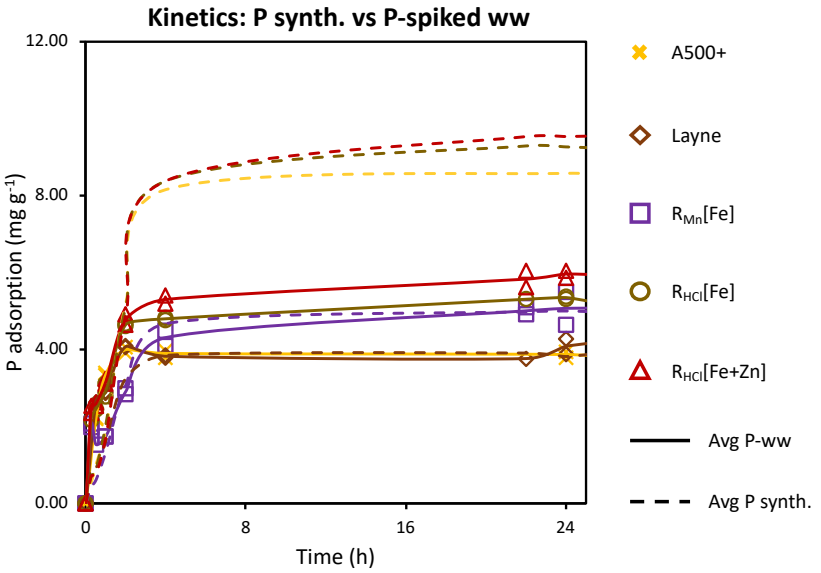

Figure 4.5: Comparison between the kinetics in P synthetic solution and P-spiked wastewater, within the first 24 h. The markers and solid lines represent the duplicate data and average trend in P-spiked wastewater, respectively. The dashed lines represent the average trend in P synthetic solution.

Table 4.5: Adsorption kinetics fitting results.

Sample	PFO			PSO			t_{95} [h] *(based on PFO)*
	k_1 [g mg^{-1} min^{-1}]	q_1 [mg g^{-1}]	RMSPE	k_2 [g mg^{-1} min^{-1}]	q_2 [mg g^{-1}]	RMSPE	
A500+	0.005	8.8	0.112	0.0005	9.3	0.158	11
Layne	0.010	4.1	0.116	0.003	4.2	0.123	5
R_{Mn}[Fe]	0.005	5.1	0.106	0.001	5.4	0.143	10
R_{HCl}[Fe]	0.004	9.5	0.126	0.0004	10.1	0.159	12
R_{HCl}[Fe+Zn]	0.004	9.8	0.165	0.0003	10.5	0.190	14

4.3.3 Adsorption-Desorption Tests

4.3.3.1 P synthetic Solution

The averaged results of the three adsorption-desorption cycles in P synthetic solution are shown in Figure 4.6 for adsorption, and Figure 4.7 for desorption. All samples showed similar P loadings in the first cycle, around 2 mg g^{-1}. The adsorbents behaved differently from the second cycle. A500+, R_{HCl}[Fe] and R_{HCl}[Fe+Zn] maintained almost the same adsorption performances throughout the three cycles (deviation within 6 %), while Layne and R_{Mn}[Fe] faced a decrease of about 50 % and 38 %, respectively, in the second cycle, and up to 61 % and 41 %, respectively (compared to the first cycle), in the third cycle.

Figure 4.7-left shows the averaged percentages of desorbed P compared to the total P loading after each adsorption cycle. The desorbed P takes into account the P detected in the regeneration solution and in the DW washings, and is cumulative, as the regeneration solution was reused. No desorbed P was detected for A500+, R_{HCl}[Fe] and R_{HCl}[Fe+Zn] until the third desorption cycle, which accounted for less than 4 % of the total P adsorbed. Layne also did not show any desorbed P after the first cycle, while in the second and third desorption cycles, P was detected up to 12 % and 20 %, respectively. Conversely, R_{Mn}[Fe] desorbed P in all cycles, from 10 % to 34 %.

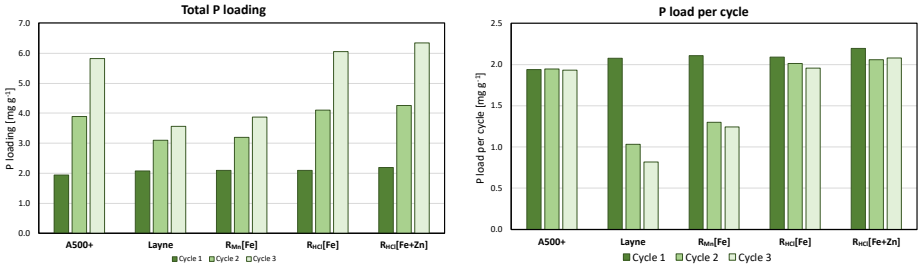

Figure 4.6: Adsorption results in P synthetic solution for all adsorbents. Results are shown in terms of cumulative P loading cycle after cycle (left) and P loading per cycle (right).

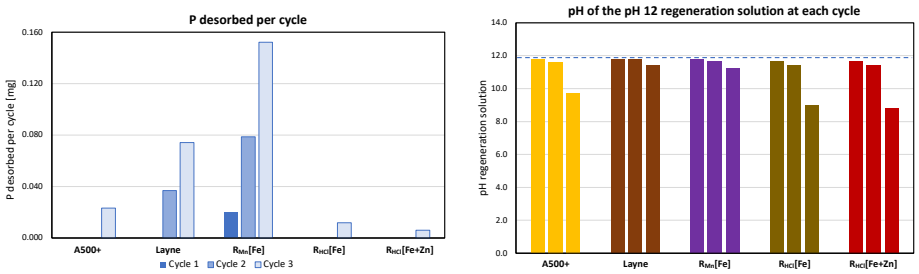

Figure 4.7: Percentage of P desorbed after each adsorption cycle in P synthetic solution, with respect to the total cumulative P loading (left); and pH value of the regeneration solution after each desorption cycle (right), with the dashed line representing the initial pH.

Figure 4.7-right shows the pH values of the regeneration solution after each desorption cycle. The initial pH value was 11.9. All samples show similar pH drops in the first two desorption cycles, with pH drops of 0.2-0.5. In the third cycle, A500+, R_{HCl}[Fe] and R_{HCl}[Fe+Zn] showed a pH drop down to pH 9.0-9.7, while Layne and R_{Mn}[Fe] reached pH 11.2-11.4.

Regeneration at pH 14 returned all the P retained during the regenerations at pH 12 for all samples.

4.3.3.2 P-Spiked Wastewater

The averaged results of the three adsorption-desorption cycles in P-spiked ww are shown in Figure 4.8 for the adsorption, and Figure 4.9 for the desorption. In the first adsorption cycle, all HAIX showed similar P adsorption performances, with P loading between 1.5-2.1 mg g^{-1}, which is about double the P loading of A500+ of 0.8 mg g^{-1}. The second cycle showed a drop in P loading for all samples: 40 % for A500+; around 70 % for Layne and R_{Mn}[Fe]; around 50 % for R_{HCl}[Fe] and R_{HCl}[Fe+Zn]. Finally, in the third cycle, this continues with a reduction in P loadings compared to the first cycle of: 65 % for A500+; about 80 % for Layne and R_{Mn}[Fe]; about 70 % for R_{HCl}[Fe] and R_{HCl}[Fe+Zn].

It is interesting to notice that the Zn-doped HAIX managed to adsorb on average more P than Layne and R_{Mn}[Fe], despite these having higher Fe content.

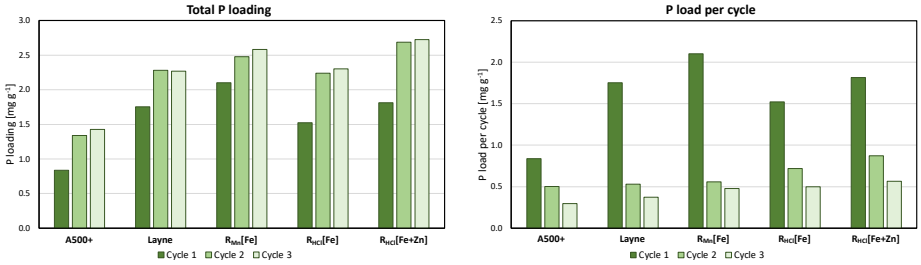

Figure 4.8: Adsorption results in P-spiked wastewater for all adsorbents. Results are shown in terms of cumulative P loading cycle after cycle (left) and P loading per cycle (right).

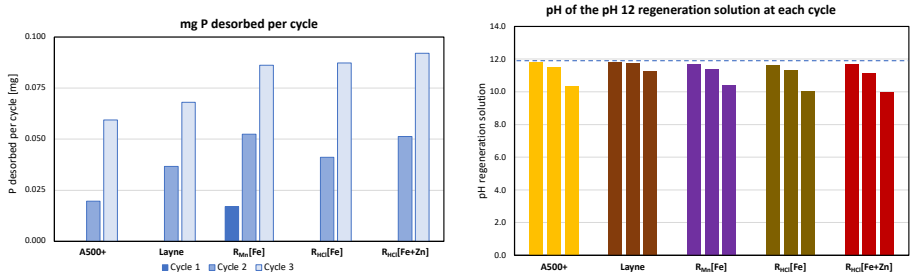

Figure 4.9: P desorbed after each adsorption cycle in P-spiked wastewater, with respect to the total cumulative P loading (left); and pH value of the regeneration solution after each desorption (right), with the dashed line representing the initial pH.

The results on competitive ions, TOC and inorganic carbon removal are reported in S.I.

Figure 4.9-left shows the averaged percentages of desorbed P compared to the total P loading after each adsorption cycle. The amount of desorbed P is calculated as in section 3.3.1. Also in this case, no desorbed P was detected in the first cycle for all samples except for R_{Mn}[Fe] (around 8 %). However, this time all samples desorbed between 16-20 % of the adsorbed P after the second regeneration cycle, and up to 26-38 % after the third regeneration cycle.

Figure 4.9-right shows the pH values of the regeneration solution after each desorption cycle. Also in this case, the initial pH was 11.9, and showed minor decreases for all samples after the first two desorption cycles, 11.7-11.8 after the first and 11.2-11.7 after the second. However, after the third cycle, the desorption solution reached pH values between 10.0-10.4 for all samples, except Layne, which displayed a value of 11.2.

Regeneration at pH 14 returned all the P retained during the regenerations at pH 12 for all samples.

4.3.3.3 Mössbauer Analysis of the Regenerated Samples

Table 4.6 reports the fitting parameters of the MS spectra showed in Figure 4.10 of the fully regenerated (pH 14) HAIX after the three adsorption-desorption cycles in synthetic P solution. All samples display coexisting doublets and sextuplets at 300 K, assigned to generic Fe^{3+} species and goethite, while the low temperature spectra fittings show that all samples contain goethite-based NPs.

Table 4.7 reports the fitting parameters of the MS spectra showed in Figure 4.11 of the fully regenerated (pH 14) HAIX after the three adsorption-desorption cycles in P-spiked wastewater. All samples display coexisting doublets and sextuplets at 300 K, assigned to generic Fe^{3+} species and goethite, while the low temperature spectra fittings show that Layne, R_{Mn}[Fe] and R_{HCl}[Fe+Zn] contain goethite-based NPs, while R_{HCl}[Fe] still displays a generic Fe^{3+} doublet and a sextuplet ascribed to the goethite phase.

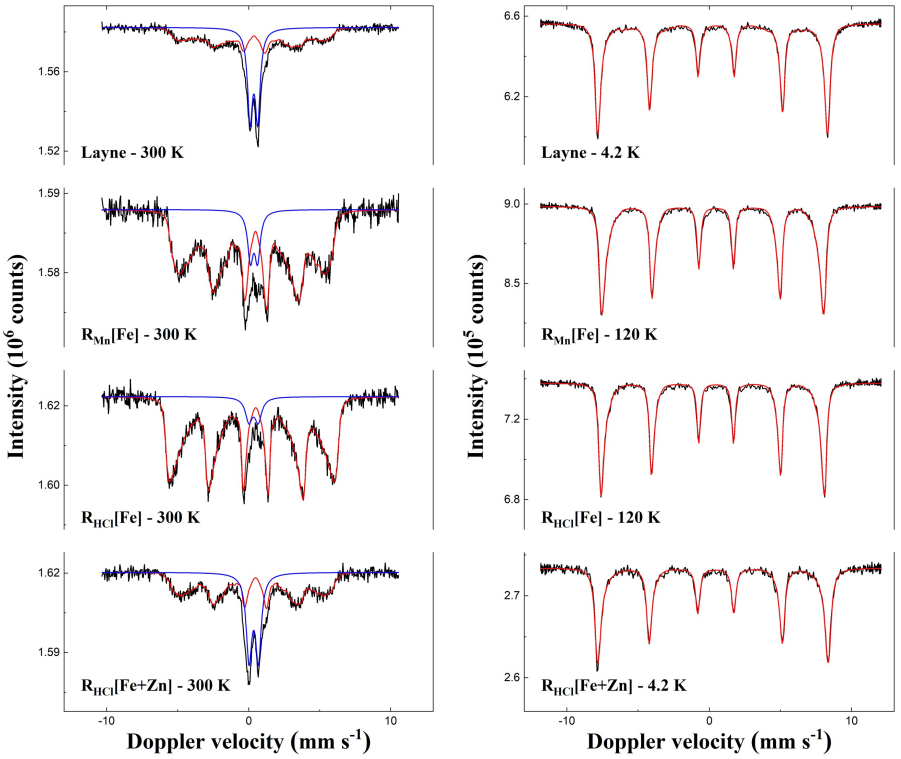

Figure 4.10: 300 K MS spectra (left) and low temperature MS spectra (right) of the HAIX after the three adsorption-desorption cycles in synthetic P solution and the final pH 14 regeneration.

Table 4.6: MS parameters of the HAIX regenerated after the adsorption-desorption cycles in synthetic P solution.

Synthetic P solution							
Sample	*T (K)*	*IS (mm·s^{-1})*	*QS (mm·s^{-1})*	*H_f (T)*	*Γ (mm·s^{-1})*	*Phase*	*Spectral contribution (%)*
Layne	300	0.36	0.54	-	0.42	Fe^{3+}	40
		0.30	-0.14	23.9*	0.33	α-FeOOH	60
	4.2	0.36	-0.24	48.8*	0.31	α-FeOOH	100
R_{Mn}[Fe]	300	0.37	0.50	-	0.46^	Fe^{3+}	9
		0.36	-0.24	26.0*	0.28	α-FeOOH	91
	120	0.36	-0.24	47.5*	0.27	α-FeOOH	100
R_{HCl}[Fe]	300	0.34	0.66	-	0.58	Fe^{3+}	6
		0.37	-0.26	30.3*	0.23	α-FeOOH	94
	120	0.36	-0.23	48.0*	0.26	α-FeOOH	100
R_{HCl}[Fe+Zn]	300	0.35	0.66	-	0.48	Fe^{3+}	34
		0.37	-0.23	26.7*	0.22	α-FeOOH	66
	4.2	0.35	-0.19	49.7*	0.34	α-FeOOH	100

Experimental uncertainties: I.S. ± 0.01 mm s^{-1}; Q.S. ± 0.01 mm s^{-1}; Γ ± 0.01 mm s^{-1}; H_f ± 0.1 T; Spectral contribution: ± 3 %.
**Average magnetic field ^ Fixed value.*

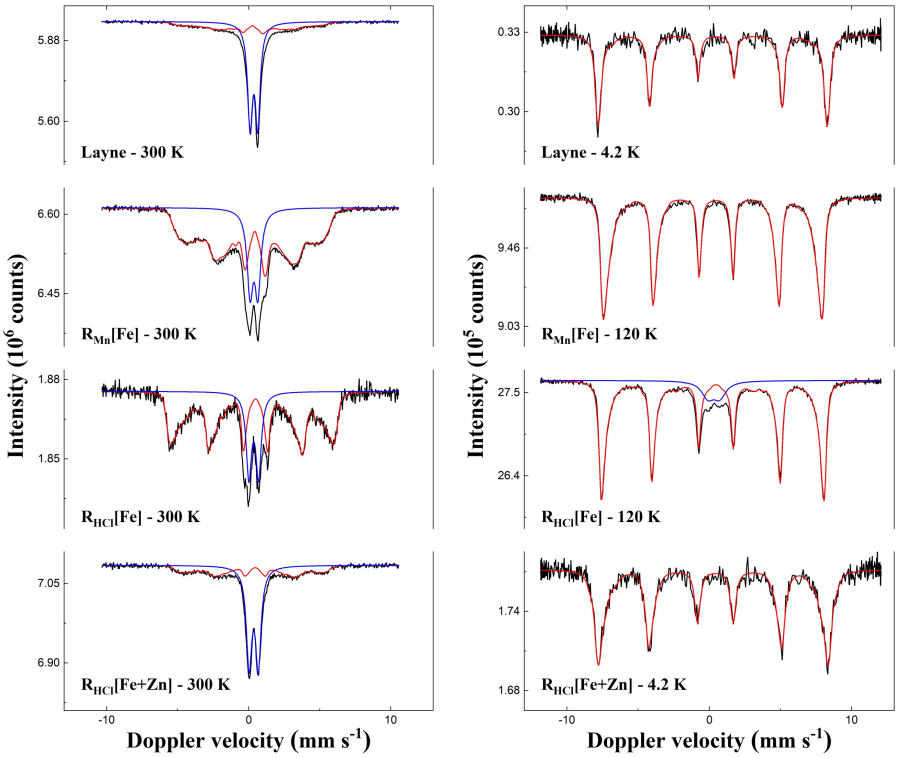

Figure 4.11: 300 K MS spectra (left) and low temperature MS spectra (right) of the HAIX after the three adsorption-desorption cycles in P-spiked wastewater and the final pH 14 regeneration.

Table 4.7: MS parameters of the HAIX regenerated after the adsorption-desorption cycles in P-spiked wastewater.

P-spiked wastewater							
Sample	*T (K)*	*IS (mm·s^{-1})*	*QS (mm·s^{-1})*	*H_f (T)*	*Γ (mm·s^{-1})*	*Phase*	*Spectral contribution (%)*
Layne	300	0.37	0.54	-	0.41	Fe^{3+}	64
		0.18	-0.18	20.9*	0.27^	α-FeOOH	36
	4.2	0.36	-0.23	49.4*	0.33	α-FeOOH	100
R_{Mn}[Fe]	300	0.37	0.55	-	0.51	Fe^{3+}	21
		0.32	-0.22	23.0*	0.25	α-FeOOH	79
	120	0.36	-0.24	46.1*	0.28	α-FeOOH	100
R_{HCl}[Fe]	300	0.35	0.68	-	0.45	Fe^{3+}	23
		0.36	-0.25	30.0*	0.25	α-FeOOH	77
	120	0.31	0.82	-	1.05	Fe^{3+}	10
		0.36	-0.23	44.6*	0.29	α-FeOOH	90
R_{HCl}[Fe+Zn]	300	0.35	0.65	-	0.46	Fe^{3+}	63
		0.35	-0.20	24.8*	0.27^	α-FeOOH	37
	4.2	0.35	-0.14	49.2*	0.43	α-FeOOH	100

Experimental uncertainties: I.S. ± 0.01 mm s^{-1}; Q.S. ± 0.01 mm s^{-1}; Γ ± 0.01 mm s^{-1}; H_f ± 0.1 T; Spectral contribution: ± 3 %.
**Average magnetic field ^ Fixed value.*

4.4 Discussion

4.4.1 Samples Characterization

The results from MWD+ICP and SEM-EDX reported in section 4.3.1.1 and 4.3.1.2 show that the two synthesis procedures were both successful, and that it was also possible to obtain HAIX with Zn-doped iron oxide NPs. R_{Mn}[Fe] achieved Fe loadings around 9 %w/w, similar to Layne and higher than R_{HCl}[Fe] and R_{HCl}[Fe+Zn], for which it was around 6 %w/w. This is most likely due to the fact that the first synthesis allows for three consecutive impregnation cycles, while the second allows only for a single impregnation cycle. Nevertheless, the second synthesis could be tuned to obtain Fe loadings similar to the first one (out from the scopes of this research). It is important to note that the Fe content does not provide a direct indication on the adsorption performances, as was observed by Zhang et al., 2008 [198]. Moreover, the fact that Layne and R_{Mn}[Fe], other than having similar Fe loadings, display also Mn and S content, suggests that both HAIX are synthesized with the same (or similar) synthesis procedure. The results from SEM-EDX show a uniform distribution of S for Layne and R_{Mn}[Fe], suggesting that for both resins the adsorption sites are in sulfate form ([185]). Conversely, A500+, R_{HCl}[Fe] and R_{HCl}[Fe+Zn] show a uniform distribution of Cl, meaning that the adsorption sites of these adsorbents are in chloride form. Hence, the adsorbents can be divided in two groups: S-based adsorbents and Cl-based adsorbents.

Interestingly, only the hydrochloric acid synthesis allowed to embed Zn-doped Fe oxide NPs within the anion exchange resin, with a Zn content equal to 5 %at. as targeted. Hence, the goal of immobilizing Zn-doped iron (hydr)oxide NPs on a support, i.e., the anion exchange resin, was successfully achieved.

MS results, shown in section 4.3.1.3, show that all samples contained goethite NPs, with Layne and R_{Mn}[Fe] having NPs of smaller size compared to

R_{HCl}[Fe] and R_{HCl}[Fe+Zn], and with the latter HAIXs containing other superparamagnetic iron oxide phases.

Layne shows the highest dispersion of "ultrafine" NPs of goethite. The goethite phase is recognizable by the MS parameters of the sextuplet in the 4.2 K spectrum, with the IS and QS values typical of high-spin Fe^{3+} in octahedral coordination and the H_f average value of 49.5 T, close to that of bulk goethite 50.6 T. This is in contrast to literature, where HAIX like Layne are claimed to consist of "non-crystalline iron oxides", "amorphous iron hydroxide", "hydrous ferric oxide" (or HFO) [56,57,81,84,176,178,187,58,60–65,68], or other similar inaccurate and generic terms [75], most likely referring to ferrihydrite. These interpretations arose from X-ray diffraction (XRD) measurements, due to the limitations faced by XRD when dealing with ultrafine (< 10-15 nm) and/or amorphous NPs. Only Sylvester et al., 2007 [56], hypothesized the possibility of the presence of the goethite phase in such adsorbents. The "ultrafine" size of the NPs is suggested by the need of ultra-low temperatures (i.e., 4.2 K) to observe a full splitting, and the need of a magnetic distribution fit even at 4.2 K, which provided an H_f average value smaller than that of bulk goethite. The latter is most likely related to the collective magnetic excitation phenomenon, characteristic of ultrafine NPs (< 10-15 nm) [140,173].

Similarly, R_{Mn}[Fe] also consists of fine goethite NPs of slightly bigger size compared to those of Layne, as the full splitting was already visible at 120 K.

Differently, R_{HCl}[Fe] and R_{HCl}[Fe+Zn] seem to consist of a mixture of goethite phases and/or ferrihydrite or other superparamagnetic phases. Both samples display a broad doublet and a sextuplet at 300 K and 120 K. For the doublets, the IS values, the relatively high QS values, and their presence still at 120 K agree with the reference values for ferrihydrite, with superparamagnetic blocking temperatures lying in the range 25-115 K (depending on the

crystallinity). Nevertheless, due to the nonspecific nature of Fe^{3+} doublets, it cannot be excluded whether these contributions arise from ultrafine superparamagnetic goethite (or other oxide phases) or ferrihydrite. The magnetically ordered goethite phase is already recognizable at 300 K, from IS and QS values consistent with the high-spin Fe^{3+} in octahedral coordination, and the relatively low H_f average value obtained from a magnetic distribution fit. At 120 K, the H_f average values are close to the saturation value of bulk goethite, as expected. The lower H_f average values of R_{HCl}[Fe+Zn] compared to those of R_{HCl}[Fe], both at 300 K and 120 K, suggest that the NPs in R_{HCl}[Fe+Zn] consist of a Zn-doped goethite phase. This is further supported by the differences in IS and QS values, and relative abundance of goethite and superparamagnetic phases/ferrihydrite between the two samples. In fact, Zn is known to retard the transformation of ferrihydrite to goethite [97]. On the one hand, the presence of magnetically ordered goethite already at 300 K entails that both samples contain goethite NPs of bigger sizes compared to Layne and R_{Mn}[Fe]. On the other hand, the doublet contribution follows the order: R_{Mn}[Fe] < R_{HCl}[Fe] < R_{HCl}[Fe+Zn], meaning that the NPs size dispersion increases also in the same order.

These results suggest that the MnO_4-based synthesis is more successful for embedding goethite NPs in AIX, while the HCl-based synthesis might need an additional aging step to transform all the ferrihydrite "precursor" into goethite, especially when doped with Zn. However, the HCl-based synthesis was successful for embedding Zn-doped iron hydroxides NPs within the AIX. These observations suggest that a different strategy should be followed to successfully embed specific iron oxide NPs, e.g., Zn-doped goethite NPs, onto a support, in a controlled way. Such strategy should consist of a first NPs synthesis step, which would provide iron oxide NPs of controlled specie and properties, and a second step in which either these NPs are blocked on a support, or the support is "built around" such NPs.

4.4.2 Adsorption Kinetics

The fit results from the adsorption kinetics in P-synthetic solution, reported in section 4.3.2.1, show for all samples a (slightly) better agreement with the PFO kinetic model compared to the PSO kinetic model, both in terms of RMSPE and agreement between the curve and the data trend. This is most likely due to the relatively high initial P concentration [199,200]. The (slight) better agreement with the PFO model does not necessarily mean that physisorption is the only adsorption mechanism taking place for all samples, but rather that the limiting factor during adsorption was the P concentration. Surely, physisorption takes place, as all samples have an anion exchange resin as a backbone. What needs to be determined is to what extent also chemisorption takes place on the iron oxide NPs, in particular for the HAIX. Hence, it is important to remind that the kinetic model fitting does not tell anything on the adsorption pathway or mechanism, which can only be determined with direct measurements.

Despite the similarities in removal behavior, there is a significant difference in the P adsorption performances. The faster sample to reach 95 % of C_{eq} (t_{95}) was Layne, which reached 95 % of equilibrium within 5 h, followed by R_{Mn}[Fe], A500+, R_{HCl}[Fe], between 10 and 11 h, and lastly R_{HCl}[Fe+Zn], around 14 h. A500+, R_{HCl}[Fe] and R_{HCl}[Fe+Zn] show higher P adsorption capacities of 8.3, 9.0 and 9.3 mg g^{-1}, respectively, about double the capacities of Layne and R_{Mn}[Fe], of 4.1 and 5.1 mg g^{-1}, respectively. On the one hand, it looks striking that A500+ performed similarly to or even better than the other HAIX, despite the absence of iron hydroxide NPs. On the other hand, the role of iron hydroxide NPs is to improve adsorption selectivity, not the capacity. Hence A500+, being an anion exchange resin, is expected to physisorb anions, as is phosphate, and to perform well especially when phosphate is the only anion in solution. One further minor consideration is that A500+ has a lower density compared to the

other HAIX. This implies that, at equal adsorbent masses, A500+ sample contains more resin beads, and hence more adsorption sites available to exchange with phosphate. This questions whether adsorption experiments preparation and results discussion should be referred only to the mass of adsorbent (as usually done), or rather per surface area or per volume. This point was not the focus of this research, but further investigation in this sense could be beneficial to identify and define consistent comparison criteria.

The difference in adsorption capacities between the S-based and the Cl-based adsorbents is related to the counterion form in the resin. Before diving into this discussion point, a premise on anion exchange resins first, and pH conditions next, are necessary. First, Anion exchange resins with type I quaternary ammonium sites are known to have a higher selectivity for (hydrophilic) divalent anions over monovalent anions, if there are closely spaced anion-exchange sites [182,183,201,202]. It was shown that type I quaternary ammonium anion exchange resins have higher selectivity for SO_4^{2-} over Cl^- [182,183,203]. Concerning NO_3^-, the selectivity depends on the hydrophobicity of the resin, which is mostly determined by the length of the quaternary ammonium radicals. In this case, type I (trimethyl) is the shortest, making the resin less hydrophobic, hence more selective for SO_4^{2-} than for NO_3^-, according to [182,183,185,201], and opposed to [65]. Second, adsorption is performed at pH 7.2, which is equal to the second pK_a of phosphate [204], meaning that its speciation is dynamically evenly distributed as the monovalent and divalent phosphate, $H_2PO_4^-$ and HPO_4^{2-}, respectively.

These considerations help understanding the differences in adsorption mechanism between the S-based and the Cl-based adsorbents. In fact, in the case of the Cl-based ones, phosphate may adsorb both in the monovalent and divalent state, either via physisorption by the resin, exchanging with Cl^-, or via chemisorption by the NPs. In the case of the S-based adsorbents, both forms can

chemisorb onto the NPs, while only the divalent phosphate can compete for physisorption with the SO_4^{2-}, depending on its concentration. For the Cl-based resins, it could be that only the divalent P is adsorb on the backbone, with MOPS restoring the speciation in solution. For the S-based resins, Martin et al, 2018 [185], suggested that P adsorption in Layne is due 90 % to the NPs and 10 % to the resin backbone. Thus, Layne and R_{Mn}[Fe] get quickly saturated (as supported by the t_{95} values) and hence cease adsorbing P at a capacity about 50 % that of the Cl-based adsorbents. It could be concluded that for the Cl-based adsorbents, physisorption is the dominant process, while for the S-based adsorbents, either chemisorption is the dominant process, or a combination of chemisorption and physisorption.

This is further corroborated by the results obtained in P-spiked wastewater. It is important to underline that the data of interest are those within the first 24 h. The reasons for that are the following. First, adsorption with AIX/HAIX is a fast process, usually happening within few hours (< 14 h in synthetic solution). Second, the timescale of interest for adsorption systems, like continuous columns, is much shorter (tens of minutes). Third, the experiments in P-spiked wastewater display multistep P removal, which might be due to other phenomena (see S.I.).

Looking at the results in wastewater (see section 4.3.2.2), it is evident that all the adsorption curves collapsed around the same range of values. This is due to the higher ion competition taking place in the more complex water matrix. R_{HCl}[Fe+Zn] shows still the highest P adsorption capacity, followed by R_{HCl}[Fe] and R_{Mn}[Fe], while A500+ and Layne showed the lowest. Nevertheless, R_{Mn}[Fe] and Layne kept a similar adsorption capacity as observed in the P-synthetic solution. As the selectivity for P is determined by the presence of the NPs, this further supports the hypothesis that chemisorption was the dominant adsorption mechanism in the P-synthetic solution for these samples, in agreement with

[185]. Conversely, the performance drop observed for the Cl-based adsorbents further support the idea that physisorption was the dominant adsorption mechanism in P-synthetic solution for these samples. Moreover, the higher performances of R_{HCl}[Fe+Zn] and R_{HCl}[Fe] compared to A500+ can be ascribed to the NPs, which provided higher selectivity for P.

4.4.3 Adsorption-Desorption Results

The results from the adsorption-desorption experiments in section 4.3.3 show different adsorbent behaviors. First, looking at the results in P-synthetic solution, section 4.3.3.1, it appears somewhat surprising that in the first adsorption cycle all adsorbents showed similar performances, with P loadings around 2 mg g^{-1}, with the HAIX generally performing better than A500+. This behavior goes against what was observed in the kinetic experiments. This is due to the lower P starting concentration, and this further highlights the importance of the choice of the initial conditions when performing adsorption experiments. Looking at the P loading per cycle (Figure 4.6-right) and comparing these results with those of desorption (Figure 4.7), one notices an unexpected behavior of the Cl-based adsorbents. First, in the first two desorption cycles no P was released by the adsorbent, while in the third regeneration only a minor fraction of the total P (< 4 %) was desorbed. Previous studies with iron oxide NPs (see Chapters 2 and 3) showed that already at pH 12.6, desorption reached values above 65 %, up to 80 %. The fact that completely no desorption is observed for all HAIX suggests that it has to do with the resin backbone. Second, despite no desorption was observed in-between the three adsorption cycles, the adsorbent managed to maintain the same P loading at each cycle. An experimental or measurement error could be excluded, since the regeneration at pH 14 returned all the (accumulated) adsorbed P, proving indeed that these adsorbents kept performing as shown in Figure 4.6. This behavior goes against what usually is observed in

adsorption experiments. In fact, neglecting the desorption and washing steps, this experiment could be thought of as an equivalent of an adsorption isotherm experiment, in which the equilibrium concentration is repeatedly perturbed. This perturbation, consisting in an increase of P concentration back to the initial one, leads to a continuation of the adsorption process to a new equilibrium. Based on the obtained adsorption data, this would translate in a convex adsorption isotherm following an exponential- or sigmoidal-like trend. This goes against any previous P adsorption observation and model, for which concave adsorption isotherms where obtained. The reasoning is represented in Figure 4.12 for the A500+ case.

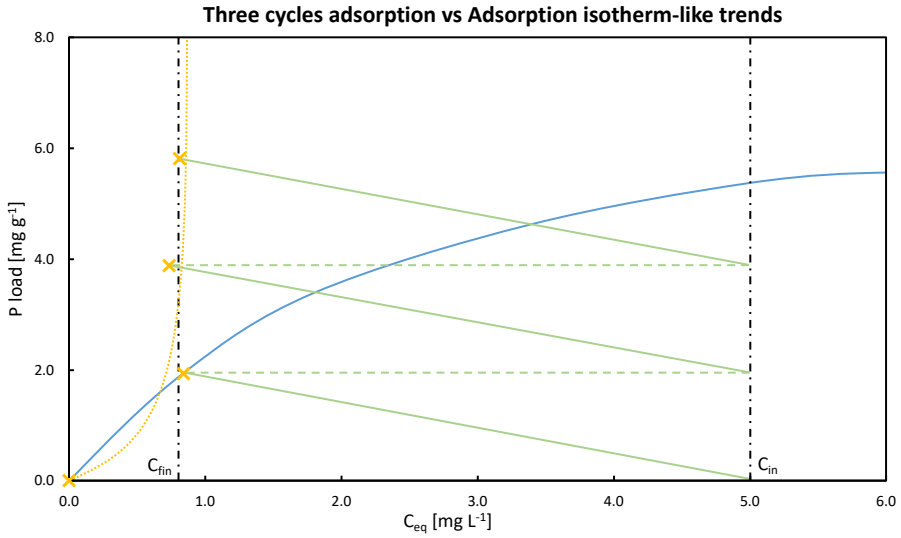

Figure 4.12: Representation of the equivalence between the three cycles adsorption experiment and an adsorption isotherm experiment. The yellow X icons represent A500+ adsorption data. The yellow exponential-like dotted line serves to lead the eye through the data trend. The blue solid line represents an isotherm-like trend. The black dashed-dotted lines identify the initial (C_{in}) and equilibrium (C_{fin}) concentrations in the adsorption experiment. The green solid lines represent the change in P concentration in solution during adsorption, while the green dashed lines the increase of the equilibrium concentration, back to the initial one.

Hence, something is happening when exposing the adsorbents to the regeneration solution. The reasoning will be first provided for the A500+ case and

extended to the HAIX afterwards. In the adsorption experiment the pH of the solution is around 7.2, which is equal to the second pK_a of phosphate [204] at which its speciation is dynamically evenly distributed as $H_2PO_4^-$ and HPO_4^{2-}. Either both fractions get adsorbed by the resin, through ion exchange with Cl^-, or only the divalent fraction, with MOPS restoring the speciation in liquid, favoring adsorption continuation. The adsorbent gets then exposed to the 0.01 NaOH regeneration solution at pH 12, which is evidently not enough concentrated in OH^- to promote P desorption. However, during this step the resin pH environment is changing from 7.2 to 12, which is close to the third pK_a (12.3 [204]) of phosphate, at which the speciation is (almost) evenly distributed as HPO_4^{2-} and PO_4^{3-}. Therefore, the OH^- molecules in the regeneration solution are not consumed for P desorption but rather for the speciation shift from $H_2PO_4^-$ /HPO_4^{2-} to HPO_4^{2-}/PO_4^{3-}. This can be thought as a "net transformation" in which all the adsorbed $H_2PO_4^-$ transforms into PO_4^{3-}, meaning that 1 mole of OH^- is consumed for each mole of P adsorbed. This was compared with the ratio between the moles of consumed OH^-, calculated from the pH drop, and those of adsorbed P. In the first cycle, the ratio was equal to 3, meaning that one mole of OH^- was consumed to transform $H_2PO_4^-$ into PO_4^{3-}, while the other 2 were probably retained by the resin or exchanged with Cl^-. By doing so, PO_4^{3-} occupies two further adsorption sites within the resin, exchanging with two further Cl^-. This reasoning is in agreement with previous observations on multivalent anion adsorption behavior for strong base quaternary anion exchange resins [178,184]. When the adsorbent is exposed again to pH 7.2 in the following adsorption experiment, the P speciation follows the opposite transformation path, freeing the two adsorption sites occupied in the regeneration step. Most likely, these adsorption sites get charge compensated by OH^- molecules coming from water. It has been observed that OH^- has lower affinity than Cl^- for the resin adsorption sites [185,202], meaning that the incoming P (especially the divalent one) would

basically "see" free adsorption sites. In these sites no Cl^- gets exchanged, while the exchanged OH^- molecules are "taken up" by the MOPS pH buffer, leading to a lower anion (hence negative charge) build up in solution. The combination of these conditions probably caused the system to behave in this unusual manner, reaching the same adsorption equilibrium observed in the preceding cycle. After the third cycle, a significant drop in pH was observed, as a consequence of the accumulation of P inside the resin, which caused a significant OH^- consumption. Also, the buildup of negative charge inside the resin and most likely the running out of available adsorption sites to compensate for the transformation to PO_4^{3-} resulted in a small P desorption. It is important to mention that only the divalent form might have been adsorbed by the resin, according to the resin affinity series [184] (even though it depends on both the concentrations and magnitude of affinity difference between the different anions in the series). Nevertheless, a similar reasoning can still be applied.

A similar phenomenon might have happened also for R_{HCl}[Fe] and R_{HCl}[Fe+Zn], with the difference that some phosphate might have desorbed from the NPs, getting then physisorbed by the resin (and perhaps adsorbed back onto the NPs). In fact, in the first two regeneration cycles, higher OH^- consumption was observed for each mole of adsorbed P compared to A500+. In the first cycle, the estimated OH^-/P molar ratio returned a value of 4, where the "extra" mole of OH^- was probably consumed to regenerate the NPs.

In the case of Layne and R_{Mn}[Fe], a slightly different phenomenon might have taken place. The discussion will be discussed for the case of Layne, and can easily be transferred to that of R_{Mn}[Fe]. During adsorption, Layne should physisorb P onto the resin backbone in a limited manner [185], due to the higher affinity for sulfate than for mono- and divalent phosphate [184]. In the first regeneration cycle, the regeneration solution probably desorbed the chemisorbed P transforming its speciation and favoring re-adsorption onto the resin, similarly

to what was previously discussed for the Cl-based adsorbents. However, in the second regeneration cycle, the desorbed P fraction only partially re-adsorbs onto the resin backbone, i.e., only (mainly) $PO4^{3-}$, since sulfate outcompetes divalent phosphate. Hence, this desorbed P can leave the adsorbent and start accumulating in the regeneration solution. This is supported by the fact that the OH^- moles consumed during regeneration was slightly lower than 3 in the first cycle (in the same order of that of A500+), and lower than 1 in the second cycle (lower than A500+). Nevertheless, Layne still managed to adsorb P in the second and third cycles, since these starting P concentrations (5 mg L^{-1}) where not high enough to saturate the adsorbent. In fact, its adsorption capacity estimated in the kinetic experiments was around 4 mg g^{-1}. The P loading registered after the first adsorption cycle was around 2 mg g^{-1}, that of the second cycle around 1 mg g^{-1}, and that of the third cycle lower than 1 mg g^{-1}. Thus, the total sum of the three P loadings throughout the whole experiment is below 4 mg g^{-1}. This is shown in Figure 4.8-left, in which is also evident how Layne and R_{Mn}[Fe] seem to be close to saturation.

Surely, these results highlight that there was a flaw in the experimental design, as the pH 12 regeneration did not manage to (efficiently) desorb P. Nevertheless, it provided insights for a better understanding of the interaction between and alkaline regeneration solution and a P-loaded anion exchange resin-based adsorbent. First, it is important to consider that not fully saturated adsorbents can still show high or even constant adsorption performances, irrespective of a successful regeneration. Second, while lower pH values during regeneration can still lead to P desorption for iron hydroxide NPs (see Chapters 2 and 3), this does not apply to HAIX adsorbents. Third, even though OH^- has a low affinity for the resin adsorption sites, it is not true that a highly concentrated alkaline solution cannot be used to regenerate HAIX adsorbents, as previously suggested [185]. In fact, in our case, the regeneration at pH 14 managed to fully desorb all

the P accumulated from all adsorbents, A500+ included, in agreement with what reported by others [52,62,64,65]. Although challenging, tuning the regeneration procedure to only desorb the chemisorbed P would lead to a purer recovered P-based product.

Figure 4.13 shows a simplistic scheme of the reactions for the different adsorbents.

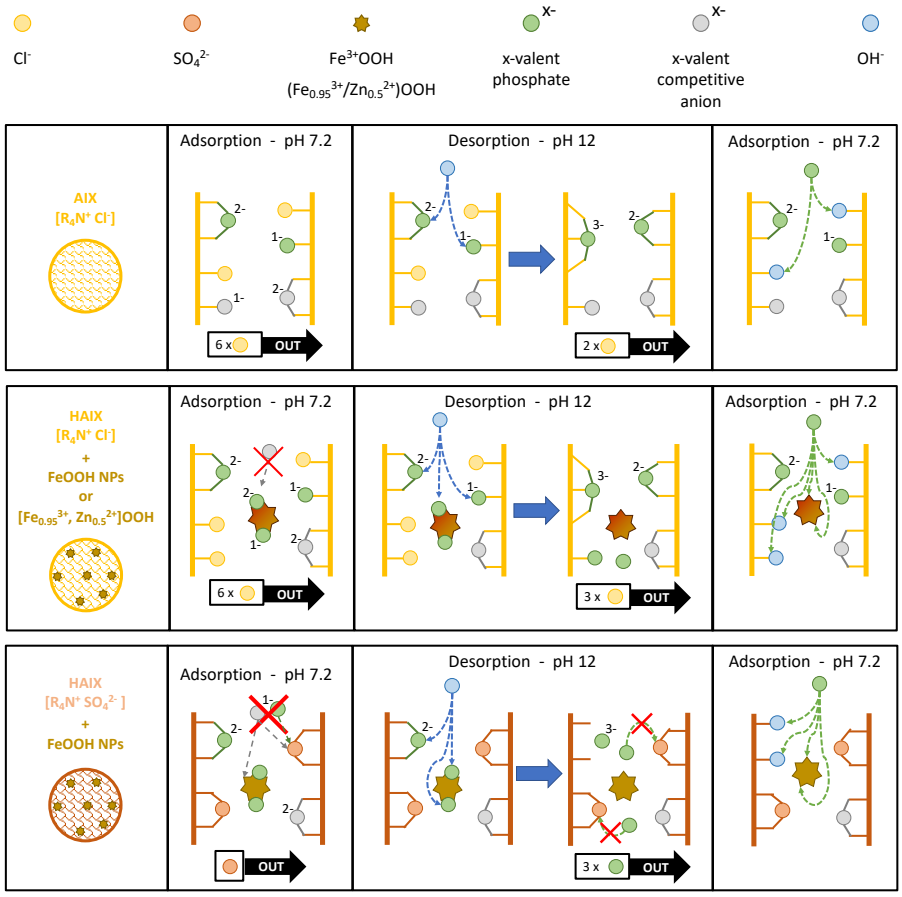

Figure 4.13: Simplistic representation and reaction scheme of the P adsorption-desorption-adsorption process for the different adsorbents.

Moving to the results in P-spiked ww, in section 4.3.3.2, the fundamental role of the NPs for P selectivity becomes more evident. In fact, in the first cycle,

all HAIX maintained adsorption performances close to those observed with synthetic solution. The average decrease in P adsorption for Layne and R_{Mn}[Fe] were 15 % and 0 %, respectively, while for R_{HCl}[Fe] and R_{HCl}[Fe+Zn] were 27 % and 18 %, respectively. Conversely, A500+ faced an average decrease in P adsorption of 57 %. A comparison between the results in P synthetic solution and P-spiked wastewater are shown in Figure 4.14. These results further prove that the iron oxide NPs provide higher selectivity.

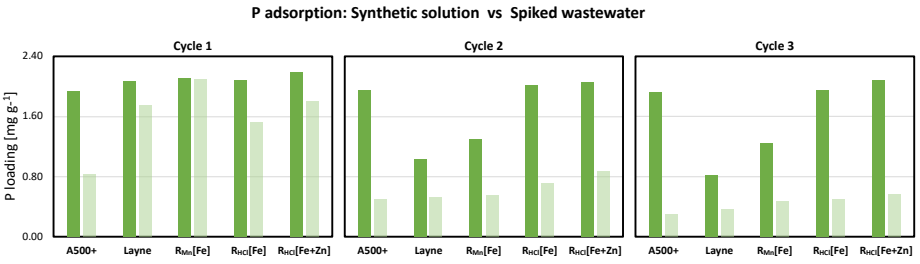

Figure 4.14: Comparison between the P removal in P synthetic solution (full green) and P-spiked wastewater (shaded green), per cycle, for the different adsorbents.

Moreover, the results for Layne and R_{Mn}[Fe] support what was hypothesized in the kinetic study, that the dominant adsorption mechanism for them was chemisorption. This is partially in agreement with what was observed for Layne by Martin et al., 2017 [185]. From the second cycle, all samples show a decrease in performances, caused by the combination of inefficient desorption during regeneration and competitive species. Interestingly, while in the first cycle no P desorption was observed (again with the exception of R_{Mn}[Fe]), 16-20 % of desorbed P was detected for all samples already from the second desorption cycle, up to 26-38 % in the third cycle. Two main reasons could explain this different behavior for the Cl-based adsorbents. First, the competitive ionic species are saturating the adsorption sites, not allowing the P speciation shift and further exchange with Cl^- to the extent observed in the P synthetic solution experiment, causing P to get desorbed earlier. Second, TOC removal was observed (see S.I.), most likely consisting in adsorption of humic substances, known to interact with

IEX and iron (hydr)oxides, and to actively adsorb P [86,205–208]. Most likely, during regeneration, a fraction of this bound P might have desorbed from or together with the humics. It is also interesting to notice that after the third regeneration, the alkaline solution remained at pH > 10 for all samples, without any abrupt drop.

Unfortunately, no measurements on Cl^- or SO_4^{2-} are available for the synthetic solutions, due to the presence of MOPS. This limits the possibility of making a complete mass balance and definitively prove the mechanism suggested in this discussion.

The results on competitive adsorption in ww are reported in S.I. and are briefly discussed here. Anions adsorption was in general greater for the adsorbent in chloride form, compared to that in sulfate form, and decreased throughout the three cycles, probably as a consequence of the unsuccessful desorption. Sulphate adsorption was observed in the Cl-based adsorbents, supporting the higher affinity of these resins for sulfate, compared to chloride. Sulphate desorption was observed for Layne and R_{Mn}[Fe], instead, probably coming from retained sulfate after the synthesis procedure, or exchange with other species. Nitrates were removed by Cl-based adsorbents to a higher extent compared to the SO_4-form ones. Inorganic carbon, mostly carbonate, was also significantly adsorbed by all samples. Silicates, which can cause surface precipitation on iron oxides, were removed only by the HAIX, not by the AIX, with R_{HCl}[Fe+Zn] displaying the highest Si removal.

Cations should be repelled by the adsorbents due to the Donnan exclusion effect. Nevertheless, cations retention or removal can happen due to the accumulation of negative charges, OH^- retention after desorption causing precipitation and presence of iron (hydr)oxides, which can remove anions as well as some divalent cations. First of all, calcium, present as Ca^{2+}, which can have both

a favourable effect on adsorption, increasing the adsorbent positive surface charge and attracting more P [52,56], and a negative effect, causing carbonate and phosphate precipitation, obstructing pores and adsorption surface sites. It was observed to accumulate in the adsorbents, following the trend A500+ > Layne > R_{Mn}[Fe] > R_{HCl}[Fe] > R_{HCl}[Fe+Zn]. This suggests the occurrence of precipitation within the adsorbents, requiring a further acid regeneration step [52,71]. Similar reasoning applies to magnesium, Mg^{2+}, however with lower removal. Iron, Fe^{3+}, and zinc, Zn^{2+}, were both removed, even though they were present in small concentrations, and zinc removal was lower for A500+ and R_{HCl}[Fe+Zn]. This suggests that zinc was mainly removed by the iron oxide NPs, as expected [209]. However, in the case of R_{HCl}[Fe+Zn], it needs to be investigated whether the Zn-doped NPs had lower affinity for Zn^{2+}, or whether the low uptakes comes from a balance between the Zn adsorbed by and that dissolved from the NPs.

Finally, for the organic carbon species, mainly consisting of humic substances, a considerable loading on the adsorbent was observed during the first cycle, which consistently reduced in the second and third cycles.

The MS analysis results of the regenerated HAIX showed in section 3.3.3 provide as main message that throughout the adsorption-desorption cycles, NPs crystal growth is taking place. This could have happened either via dissolution and reprecipitation of NPs within the resin bead or via oriented attachment (or oriented agglomeration), which can cause crystal growth and is a size-dependent mechanism [210–214], and is suggested to be promoted by water [212,215], even more at alkaline conditions [214] and by phosphate adsorption for goethite [213]. For Layne and R_{Mn}[Fe], this is evident from the magnetic splitting already present at 300 K in the regenerated samples, which can only be explained with the growth of the particle size. However, with increasing particle sizes, also an increase of the H_f at 4.2 K should be expected, but this was not the case for

Layne. This is probably due to non-perfect crystallinity during NPs growth and/or adsorbed species on NPs surface (both supporting oriented attachment), which can lower the H_f value. Moreover, looking at the H_f values and spectral contributions, the adsorption-desorption cycles in synthetic solution seem to have promoted more NPs growth than those in ww. This suggests that in the second case, some competing compounds like organics might have caused a sort of "surface passivation", inhibiting or reducing the growth. In the case of R_{Mn}[Fe], the same phenomena could have taken place, but the change in spectral contributions and H_f values is more straightforward compared to Layne.

Regenerated R_{HCl}[Fe] also shows both an increase of the goethite phase spectral contribution and related H_f value. Compared to the virgin sample characterization, the spectrum at 120 K of the regenerated sample used in synthetic solution provides a well split sextet, which suggests the presence of only goethite. This means that the doublet contribution observed at 300 K belongs to superparamagnetic goethite, suggesting that the virgin sample consisted of size distributed (superparamagnetic) goethite NPs. The 120 K spectrum of the sample used in ww still displays doublet and sextuplet contributions, suggesting that some compounds in ww (e.g., silicates, organics) might have slowed down the NPs growth process.

MS spectra of the regenerated R_{HCl}[Fe+Zn] also suggest an increase in particle sizes, with similar differences between the effect of synthetic and ww solutions as discussed for R_{HCl}[Fe]. The relatively high H_f values observed at 4.2 K, compared to those of Layne, can be explained in two different ways. Either the Zn-doped NPs are partially dissolving, releasing Zn, and recrystallizing (via oriented agglomeration) as purer goethite, or the nanoparticles grew via oriented attachment to bigger sizes compared to those in Layne. However, the first idea is supported by the competing species adsorption results, which suggests that Zn might have been released throughout the experiments, and the fact that in

MS, particle size-related effects are expected to vanish at 4.2 K. However, it was observed that the magnetic distributions of the 4.2 K sextuplets (not shown here) reached a maximum H_f values around 52 T, which suggest the presence of ultrafine maghemite or hematite NPs. Hematite (trans)formation in HAIX was also observed by Kumar et al., 2018 [52], and this might cause an overestimation of the goethite average H_f value. Hence, further experiments are needed to verify the stability of such synthesized Zn-doped goethite nanoparticles in HAIX.

Overall, the MS results highlight that NPs crystal growth is taking place in HAIX throughout the adsorption-desorption cycles. This suggests that AIX resins do not provide a solid support to NPs.

4.4.4 Challenges and Limitations of HAIX Adsorbents

Further work on tailoring of the two synthesis procedures is needed to achieve similar Fe loadings in the resins, obtaining a fairer P adsorption performances comparison. Also, all HAIX should be converted to either the chloride form or the sulphate form. This would provide further insights on the different synthesized NPs properties and P adsorption performances, leveling the influence of the resin counter-ion on adsorption selectivity. Mössbauer spectroscopy revealed that the synthesized adsorbents, including the commercial HAIX Layne, consisted of goethite NPs, against what is claimed in previous studies, which reported generic amorphous HFO species. This was because of XRD limitation to characterize NPs below 15 nm in HAIX. This stresses the importance of utilizing the proper tool to properly characterize samples. MS also revealed the NPs growth taking place in HAIX, suggesting that AIX resins do not provide a solid enough support to the NPs and/or such ultrafine NPs are not stable enough to sustain multiple adsorption-desorption cycles, with consequent dissolution and reprecipitation. Furthermore, the desorption experiments highlighted the complex interaction between the OH^- regenerant molecules and the

adsorbed P within the resin bead, and in particular the inefficient OH consumption resulting in inefficient desorption. Hence, long term experiments with real ww and regeneration performed at pH 13-14 are needed, coupled with MS monitoring of the NPs, to fully assess the stability of such adsorbents, and in particular the potential of the Zn-doped iron oxide NPs. Nevertheless, these results strongly question the use of AIX resins as a backbone for iron oxide NPs for P recovery.

4.5 Conclusions

In this work, Zn-doped iron (hydr)oxides NPs, which previous studies showed to be promising for improved P recovery, were successfully immobilized in an anion exchange resin, and compared to conventional Fe-based hybrid anion exchange adsorbents. The Zn-doped hybrid anion exchange adsorbents displayed on average similar to better P adsorption performances compared to the others. Mössbauer spectroscopy revealed that both commercial and synthesized HAIX consist of goethite and not of amorphous hydrous ferric oxides as previously claimed.

The adsorption tests revealed the different contributions of physisorption and chemisorption mechanisms, underlining the importance of the latter for selective and efficient P removal. Moreover, the importance of testing adsorbents at realistic water conditions was highlighted.

The regeneration procedure adopted in this study made use of an alkaline solution with a relatively low pH 12 (0.01 M NaOH). This was deliberately chosen to enhance differences in desorption/saturation behaviors between the different adsorbents. This low strength procedure revealed a complex interaction between OH^- and P adsorbed molecules within the resin backbone. In fact, OH^- is consumed to transform the speciation (i.e., increased valency) of the adsorbed P, resulting in P re-adsorption onto the AIX backbone and ineffective

desorption. This effect is more evident for HAIX in chloride form than in sulfate form. Desorption at pH 14 (1 M NaOH) was effective to fully desorb P, without the need of NaCl, as claimed in literature. Mössbauer spectroscopy performed on the regenerated HAIX revealed particle growth in the samples, questioning the robustness of the AIX as a support for NPs.

These findings will serve as a warning when interpreting adsorption and desorption mechanisms with HAIX, highlighting the importance of thoroughly understanding both mechanisms, and questioning the efficacy of AIX-based adsorbents for regenerative P adsorption at ultra-low concentrations.

Acknowledgments

This work was performed in the cooperation framework of Wetsus, European Centre of Excellence for Sustainable Water Technology (www.wetsus.nl). Wetsus is co-funded by the Dutch Ministry of Economic Affairs and Ministry of Infrastructure and Environment, the European Union Regional Development Fund, the Province of Fryslân and the Northern Netherlands Provinces. This research received funding from the Netherlands Organization for Scientific Research (NWO) in the framework of the Innovation Fund for Chemistry, and from the Ministry of Economic Affairs and Climate Policy in the framework of the TKI/PPS-Toeslagregeling. The authors thank the participants of the research theme "Phosphate recovery" for the interest, fruitful discussions, and financial support. A special thanks goes to Pim de Jager and Raimonda Buliauskaitė (Aquacare) for the frequent knowledge exchange and interest in the research, my colleagues Chris Schott, Antony Cyril Arulrajan, Wokke Wijdeveld, Thomas Prot, Amanda Larasati, Sam Rutten, Daniele Chinello, Qingdian Shu, for the brainstorming sessions and scientific discussions, Guendolina van der Linden for the work done together.

4.6 Supplementary Information

4.6.1 SEM-EDX Characterization

SEM-EDX results are evaluated from a qualitatively, rather than quantitatively.

Layne

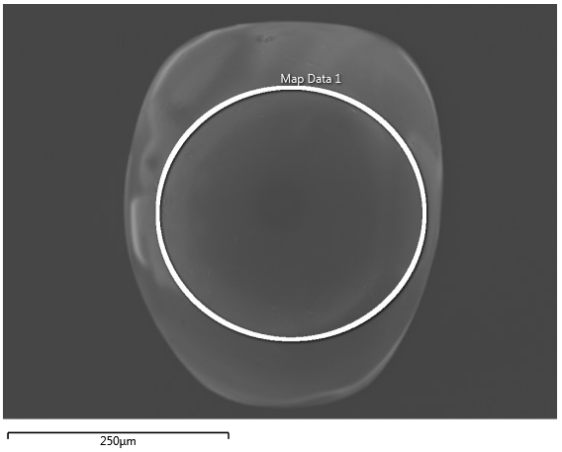

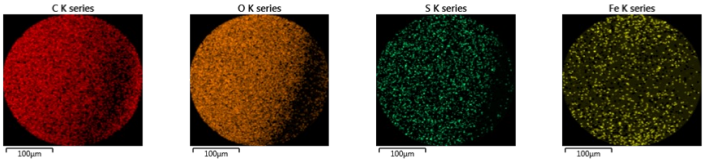

Element	Wt%	Wt% Sigma	Atomic %
C	39.5	0.6	47.51
O	53.8	0.7	48.51
Fe	3.0	0.1	0.78
S	0.76	0.06	0.34
Cl	0.22	0.04	0.09
Total:	100.00		100.00

R_{Mn}[Fe]

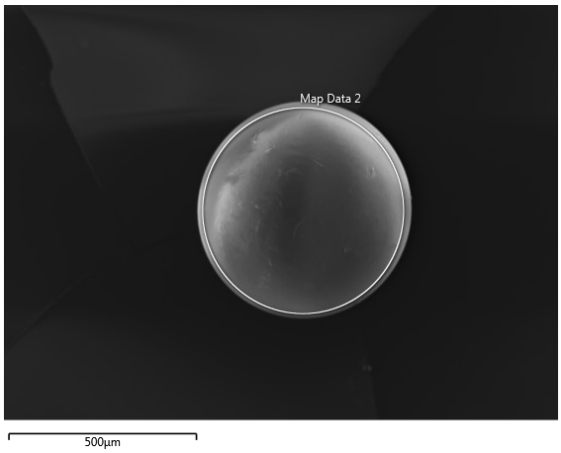

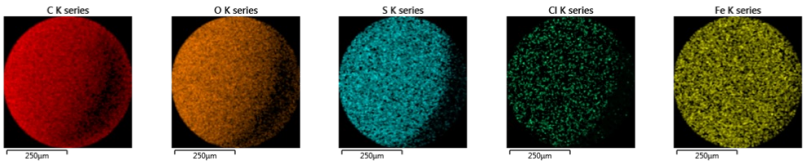

Element	Wt%	Wt% Sigma	Atomic %
C	52.9	0.3	64.85
O	33.6	0.2	30.93
Fe	10.3	0.1	2.70
S	3.19	0.05	1.47
Cl	0.10	0.02	0.04
Total:	100.00		100.00

R_{HCl}[Fe]

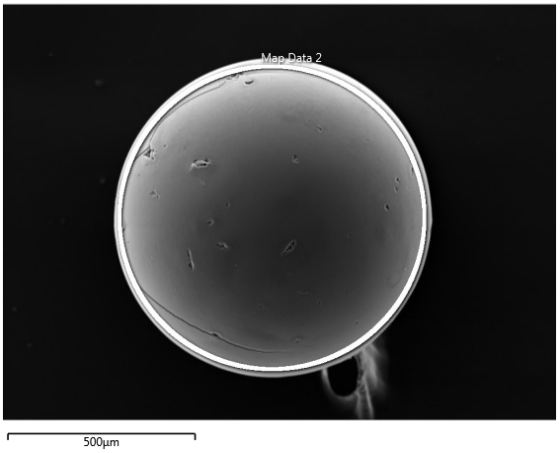

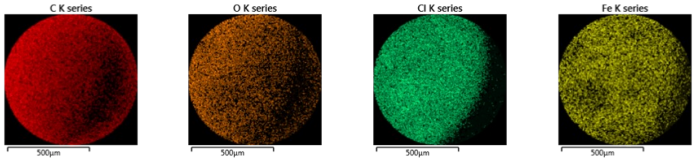

Element	Wt%	Wt% Sigma	Atomic %
C	66.9	0.3	78.94
O	18.6	0.3	16.48
Fe	8.0	0.1	2.04
Cl	6.25	0.06	2.50
Total:	100.00		100.00

R_{HCl}[Fe+Zn]

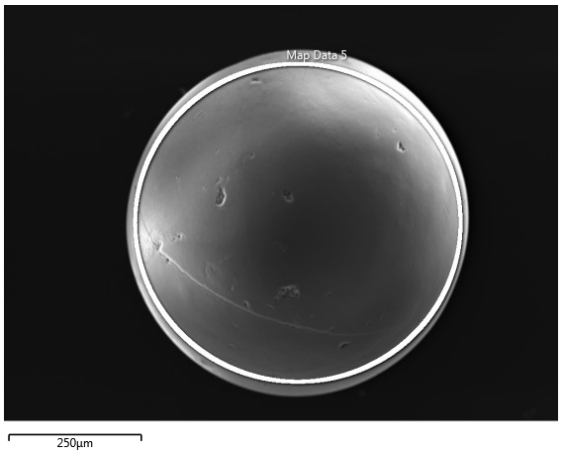

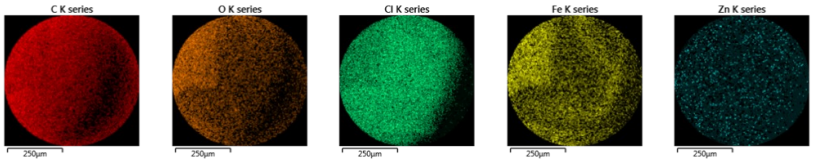

Element	Wt%	Wt% Sigma	Atomic %
C	66.5	0.3	78.09
O	19.8	0.3	17.46
Fe	6.27	0.07	1.58
Zn	0.44	0.05	0.10
Cl	6.86	0.06	2.73
Total:	100.00		100.00

4.6.2 Adsorption Kinetics (Long-Term)

4.6.2.1 P Synthetic Solution

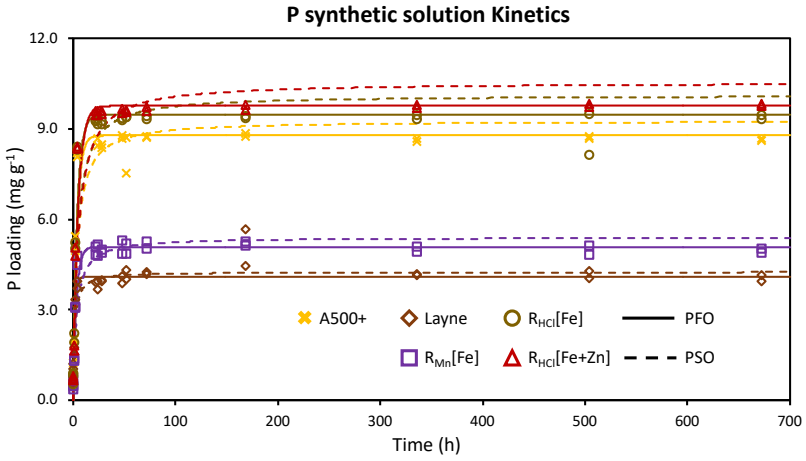

Figure 4.15: Long-term (4 weeks) adsorption kinetics in P synthetic solution for all HAIX. The duplicate data are superimposed to the related PFO (solid lines) and PSO (dashed lines) models fitting.

4.6.2.2 P-Spiked Wastewater

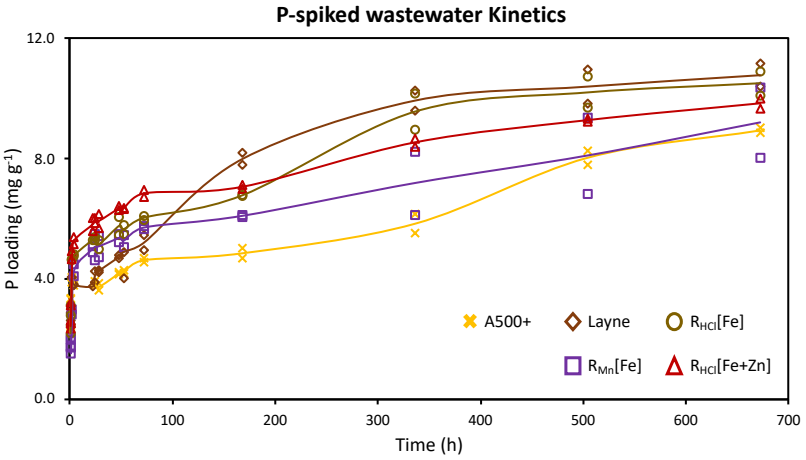

Figure 4.16: Long-term (4 weeks) adsorption kinetics in P-spiked wastewater for all HAIX. The duplicate data are superimposed to the solid lines representing the average trend.

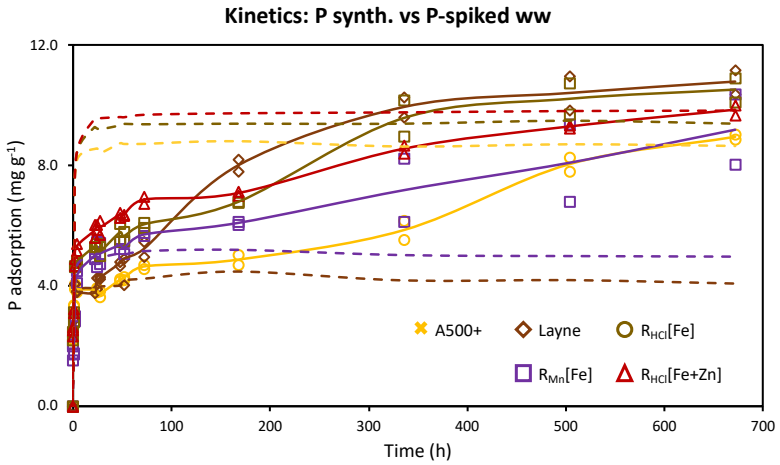

Figure 4.17: Comparison between the long-term (4 weeks) adsorption kinetics in P-spiked wastewater and P synthetic solution for all HAIX. The duplicate data from the P-spiked wastewater kinetics are superimposed to the solid line representing their average trend. The dashed lines represent the average trend in P synthetic solution.

Figure 4.16 shows the long-term kinetics in P-spiked wastewater. After more than a week, the solutions started to display some precipitate (white fine suspended particles), and after few weeks, the formation of biofouling. Probably, the longer a complex system is let running, the likelier some slower phenomena can take place, such as precipitation, adsorption by other species like humics, etc., developing of microorganisms that can uptake P. These considerations make the long-term data unreliable, or at least not ascribable to adsorption alone. Nevertheless, these data were collected in the long term for monitoring purposes.

4.6.3 Competitive Species

4.6.3.1 Competitive Anions

Figure 4.18 shows the competitive anion removal per cycle in the adsorption-desorption experiment in P-spiked wastewater. Sulphate was significantly removed by the Cl-based adsorbents, to a higher extent compared to P. In the first

cycle, 2.9-3.6 mg g^{-1} of S (vs 0.8-1.8 mg g^{-1} of P) were removed, with the removal being still around 1.6-1.9 mg g^{-1} (vs 0.3-0.6 mg g^{-1} of P) in the third cycle. This supports the higher affinity of SO_4^{2-} for the resin adsorption sites, and the hypothesis that for these adsorbents, physisorption is the dominant removal mechanism. Conversely, the S-based adsorbents displayed desorption of SO_4^{2-}, as expected. For Layne, it went from -3.5 mg g^{-1} in the first cycle, to -0.35 mg g^{-1} in the second cycle, ending up adsorbing a minor fraction of SO_4^{2-} in the third one. For R_{Mn}[Fe] the desorption was significant, with -11.6 mg g^{-1}, which means that probably some SO_4^{2-} remained confined within the resin after the synthesis and was not efficiently washed out. Then, SO_4^{2-} desorption decreased to -1.8 mg g^{-1} in the second cycle, and -0.6 mg g^{-1} in the third one.

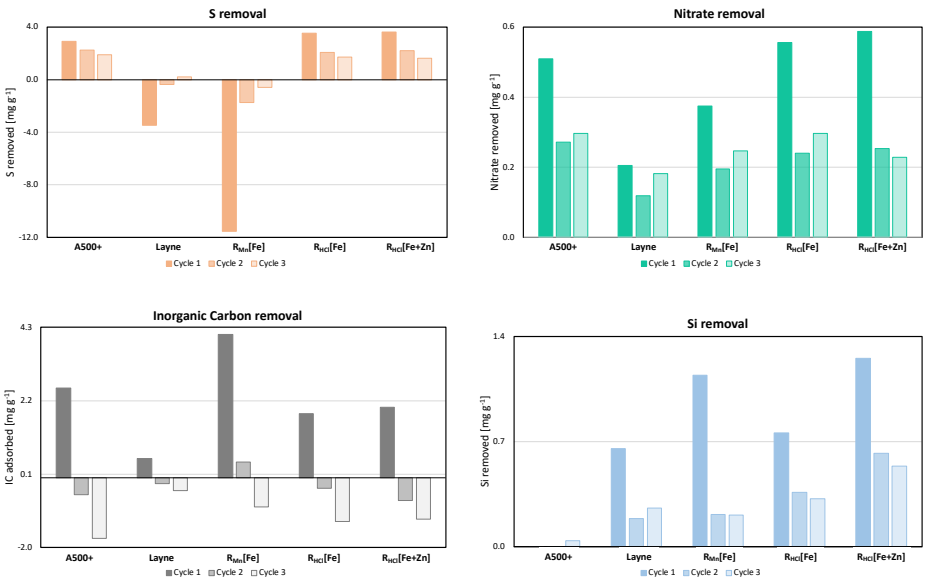

Figure 4.18: Sulphate, nitrate, inorganic carbon and silicates removal per cycle during adsorption-desorption experiments in P-spiked wastewater.

Nitrate was adsorbed by the Cl-based resins, with initial NO_3^- loadings of 0.5-0.6 mg g^{-1} (~ 0.1 mg g^{-1} of N) in the first cycle, and half of this loading in the second and third cycles. Lower NO_3^- loadings were observed for the S-based

adsorbents, again, due to the higher selectivity of these resins for divalent anions, compared to the monovalent ones.

Inorganic carbon, mostly carbonate, HCO_3^-, appeared to have been significantly removed during the first cycle (2-4 mg g^{-1}) to then be desorbed in the following ones. However, these results could have been affected by CO_2 exchange during sample preparation, also considering that the relative change after adsorption compared to the initial value was always below 7 % (12 % only for R_{Mn}[Fe]).

Although not an anion, silicates, predominantly occurring as H_4SiO_4 at pH 7.2, can adsorb onto iron (hydr)oxides as an anion, and it can cause surface precipitation as well. In fact, silicates were removed only by the HAIX, with Si loadings of 0.6-1.2 mg g^{-1} in the first cycle, which reduced to 30-50 % in the second and third cycles. R_{HCl}[Fe+Zn] showed on average the highest Si removal.

4.6.3.2 Competitive Cations

Figure 4.19 shows the competitive cation removal per cycle in the adsorption-desorption experiment in P-spiked wastewater. In theory, cations should be repelled due to the Donnan exclusion effect provided by the anion exchange resin structure. However, cations retention or removal can happen due to the accumulation of negative charges, OH^- retention after desorption causing precipitation and presence of iron (hydr)oxides, which can remove anions as well as some divalent cations.

Calcium, present as Ca^{2+}, can precipitate mainly with carbonate and phosphate. It is known to cause a favorable effect on P adsorption, as Ca^{2+} increases the positive charge to attract P, and an unfavorable effect, as it causes surface precipitation on the adsorbent, blocking pores and adsorption sites. It was observed on average increasing Ca^{2+} removal over the three cycles, which followed the trend: A500+ > Layne > R_{Mn}[Fe] > R_{HCl}[Fe] > R_{HCl}[Fe+Zn]. This

might suggest that some precipitation might have taken place within the adsorbents, with R_{HCl}[Fe+Zn] being the most affected one.

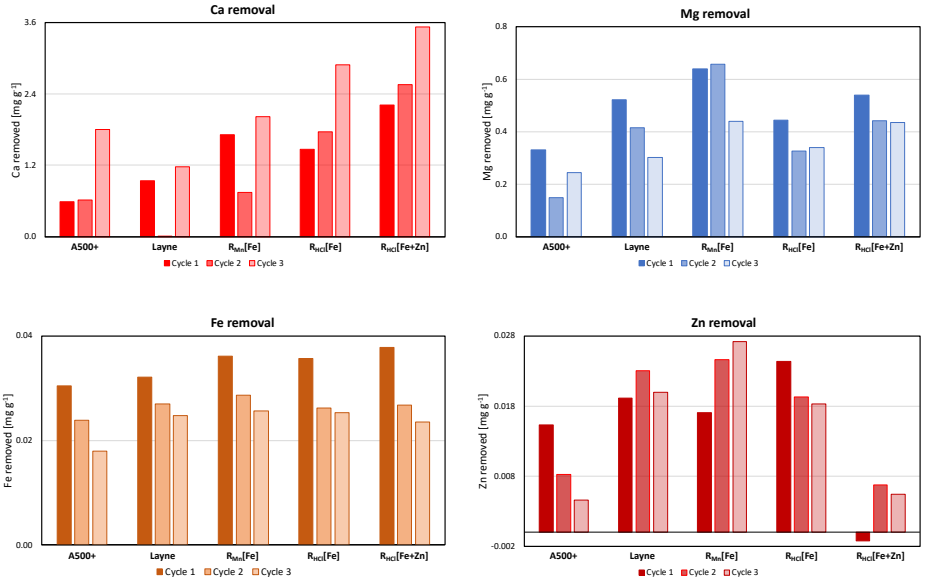

Figure 4.19: Calcium, magnesium, iron and zinc removal per cycle during adsorption-desorption experiments in P-spiked wastewater.

Magnesium, also present as a divalent cation Mg^{2+}, displayed lower removal (< 0.7 mg g^{-1}) and it appeared on average to have better affinity for the S-based adsorbents, rather than the Cl-based ones.

Iron, present mainly as Fe^{3+}, was uptake similarly by all adsorbents, although at negligible levels (< 0.04 mg g^{-1}).

Similar reasoning applies to zinc, Zn^{2+}, which was uptake at similar magnitudes to Fe, although showing lower uptakes for A500+ and R_{HCl}[Fe+Zn]. For A500+ it might suggest a lower affinity for the resin itself. However, in the case of R_{HCl}[Fe+Zn] it needs to be investigated whether the Zn-doped NPs had lower affinity for Zn^{2+}, or whether the low uptakes comes from a balance between the Zn adsorbed by and that dissolved from the NPs.

4.6.3.3 Total Organic Carbon

Figure 4.20 shows the total organic carbon removal per cycle in the adsorption-desorption experiment in P-spiked wastewater. Organic carbon, mostly present as humic substances, was significantly removed by all adsorbents during the first cycle (6.2-6.6 mg g^{-1}), with a 58-70 % reduction in the second cycle (except Layne, 38 %) and > 80 % in the third one. This agrees with what discussed in section 4.3.

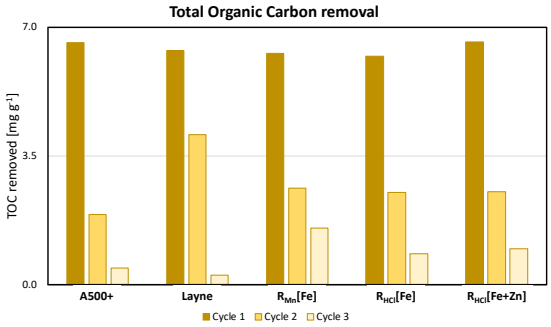

Figure 4.20: Total organic carbon removal per cycle during adsorption-desorption experiments in P-spiked wastewater.


5

5

Polyelectrolyte multilayer coating of hybrid anion exchange adsorbents: potential for improved selectivity?

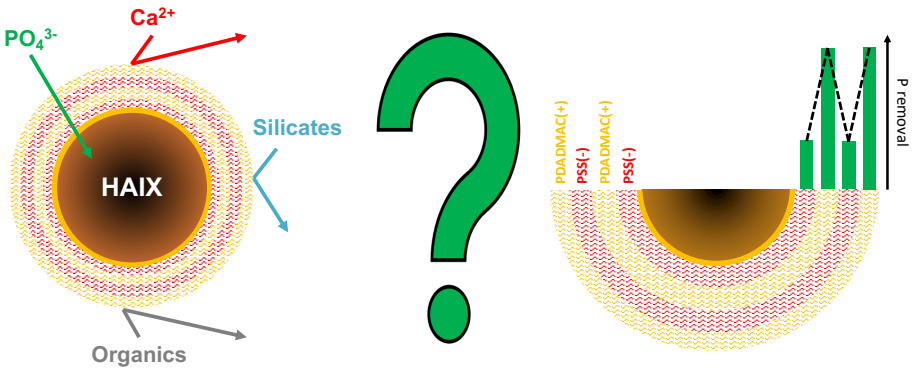
PO_4^{3-}
Ca^{2+}
Silicates
HAIX
Organics
PDADMAC(+)
PSS(-)
PDADMAC(+)
PSS(-)
P removal

Abstract

Polyelectrolyte multilayer coating of hybrid anion exchange adsorbents (HAIX) was investigated with the goal to improve the size/charge selectivity of the adsorbent for phosphate (P) and increase its durability. The investigated polyelectrolytes were the widely investigated pair: polystyrene sulfonic acid (PSS, negative) and poly-(diallyl-dimethylammonium chloride) (PDADMAC, positive). The coating procedure consisted in the layer-by-layer coating procedure, popular in membrane science, with three different scenarios: 1) five thick low-density bilayers; 2) five thin high-density bilayers; and 3) three thick low-density bilayers topped by two thin high-density bilayers. The coated adsorbents were tested for P adsorption in batch mode in different modalities. The effect of the terminating layer charge on adsorption was investigated with synthetic solutions of P and/or Ca. The expected zig-zag trend on P and/or Ca removal was not clearly observed, due to significant experimental uncertainties. Similarly, adsorption kinetics experiments did not show any effect on ion transport and adsorption. Adsorption tests in P spiked wastewater effluent did not show any improved selectivity for P. Surprisingly, no effect on organics rejections was observed, not even when the terminating layer was negative. In general, no effect on P loading was observed throughout the experiments. This works highlights experimental challenges related to HAIX and batch mode experiments. Particularly, batch mode experiments might not be suited for investigating dynamic processes like selectivity. Suggestions on alternative polyelectrolyte pairs, coating procedures and experimental designs are provided, to unequivocally determine whether multilayer polyelectrolyte coatings can improve the selectivity and durability of HAIX.

5.1 Introduction

Hybrid anion exchange adsorbents (HAIX) have shown great potential for phosphorus (P) recovery from water. HAIX have been developed and patented by Cumball & SenGupta in the early 2000s [194] and have been widely applied to arsenic (As) removal for safe drinking water production in areas affected by As pollution and water scarcity [68,84,175]. Due to the similar chemistry of As and P, they have also been tested for P removal and recovery from water, with promising results [52,53,216,59,61–65,83,185].

HAIX consist of an anion exchange resin impregnated with metal (hydr)oxides nanoparticles (NPs), in particular iron (hydr)oxides (iron oxides for simplicity). The anion exchange resin can either be a weak or strong base, gel or a macroporous resin, and indeed HAIX backbones often consist in a strong base macroporous polystyrene cross-linked with divinylbenzene anion exchanger, with type I (trimethyl) quaternary ammonium active groups in chloride (Cl^-) form [62,65,185,194]. In this sense, in the last years, a commercial adsorbent, Layne^{RT} (Layne Christensen Co., United States), has drawn attention and has been investigated for P recovery, displaying great potential [62,64,65,82–84,185]. For Layne^{RT} (Layne henceforth), the resin ionic form, or counterion on the adsorption sites, is sulfate, SO_4^{2-}, which has higher affinity than Cl^- for the adsorption sites [178,182–184], and its presence is due to the patented production process [185]. This system provides selectivity for phosphates, as a combination of the Donnan exclusion effect provided by the resin, favoring anion physisorption, and the intrinsic selectivity of the iron oxides, favoring phosphate chemisorption [181]. Moreover, HAIX show higher intraparticle diffusion compared to granular media, thanks to their swelling capabilities, compared to the rigid (micro)porous structure of the granules [72,128]. Lastly, adsorption is one of the few technologies able to reach the ultra-low concentrations of P for eutrophication prevention, i.e., below 10 µg L^{-1} [23]. P adsorption can be reversed

via an alkaline wash, which allows to recover P, while regenerating the adsorbent. It has been observed that an adsorbent needs to be able to sustain tens to hundreds of regenerations (i.e., adsorption desorption cycles) to make adsorption an economically viable process [23]. Adsorbent selectivity is crucial for obtaining a purer P-based recovered product, while maintaining high performances in the long term, easing the regeneration procedure [23,217].

Regeneration is usually performed with 0.1-1 M NaOH at pH 13-14 [23,52,62,64,65]. Concentrated NaOH (pH 13-14) was observed to be able to regenerate both the NPs and the resin [53,64,65], hence targeting both the chemisorbed and physisorbed P, contrary to what reported by others [185]. Also, it can desorb organics, like humics, as well [72], which is fundamental since the steric hindrance of humics obstructs pores and reduces accessibility to the P adsorption sites. However, the high solution retention displayed by HAIX could cause OH^- retention within the resins, which might cause precipitation within the resin in the following adsorption cycles, impacting the adsorbent capacity. Some of the species causing scaling surface precipitation are calcium, Ca^{2+}, and magnesium, Mg^{2+} [56,72,151,217]. With accumulating precipitates over time, an acid wash would be needed to restore the original adsorbent capacity [23,52,217]. However, this procedure was shown to affect the NPs, leading to a significant decrease in performances already after few regeneration cycles [52]. Also, all these competing species and mechanisms contaminate the regeneration solution, decreasing the purity of the potential P-based recovered product. Hence, further increasing the selectivity of HAIX against cations, but also against some anions, neutral molecules, or organics, would reduce competing mechanisms, perhaps easing the regeneration procedure, and providing a purer recyclable P-based product.

A way to improve the selectivity is by applying polymeric coatings to the adsorbents. Polymeric coatings can increase selectivity via charge exclusion

and/or size exclusion, and have been widely investigated, especially in the membrane field [218–220]. A similar approach has been also applied to membranes and anion exchange resins to reduce the biofouling [221,222]. Among the different coating strategies, layer-by-layer (LbL) coating using polyelectrolytes (PE) showed promising results [219]. This coating technique consists in alternating positively and negatively charged layers, so-called bilayers, which allow to control different properties of the final product [223]. Namely, LbL-PE coatings allow to control the membrane surface charge, mostly determined by the last applied layer, influencing charge selectivity, and reducing biofouling; pore size, dependent on the thickness of the coating, influencing size selectivity; water permeability, determined on the thickness and intrinsic properties of the PE (hydrophilicity vs hydrophobicity), influencing ion transport/mass transfer; and so on. The characteristics of the coating layers are determined by several factors, and one of the most important is the ionic strength (i.e., salinity) of the PE coating solution. In fact, at higher ionic strengths, the PE layers tend to grow thicker and less dense, compared to lower ionic strengths, which generate thinner and denser layers. This is a consequence of the charge compensation mechanism during the coating procedure, which at high ionic strength is driven by the solution counterions, while at low ionic strength is driven by surface charges (i.e., by the PE themselves). For high ionic strength coatings this translates in higher excess surface charge throughout the whole multilayer. Conversely, for low ionic strength coatings the net charge throughout the multilayer will be almost neutral, with a weaker external surface charge determined by the last applied layer. Also, the different densities and swelling properties of the different layers (the latter depending also on the type for PE) will also determine the permeability and transport features of the final product. Overall, the properties of the final applied PE layer, or terminating layer, determine the surface charge, even though it is not always the case [219]. When dealing with LbL coatings, it is

possible to investigate the properties and performances of the terminating layer after each layer deposition, known as the odd-even effect. In membrane science, this also provides an indirect proof of the successful multi-layer deposition. In our case, for phosphate adsorption, being phosphate a negative ion, an odd-even effect (i.e., zig-zag trend) in the adsorption behavior would be expected depending on whether the terminating layer is positive or negative. Namely, a lower P uptake after the first negative layer deposition, then a higher P uptake after the first positive layer deposition, then lower again, and so on. The opposite is expected for cations, like Ca^{2+}. Despite all these versatile features provided by the PE coating layers, it is important to bear in mind the possible limitations which could be encountered. For example, when dealing with gel-based and resin-based materials, which display swelling properties depending on the type of solution and salinity they are exposed to. This swelling and shrinking behavior might cause a mechanical stress on the coating layer, resulting in defects formation and coating deterioration, affecting the overall properties and performances.

Previous research showed promising results investigating a popular PE pair for membranes: polystyrene sulfonic acid (PSS) and poly-(diallyl-dimethylammonium chloride) (PDADMAC) [219,220,224]. PSS has a negatively charged sulfonic group, and is more hydrophilic, while PDADMAC has a positive dimethylamine group, and is more hydrophobic. De Grooth et al., 2015 [219], provided a thorough investigation on the role of ionic strength and odd-even effects of this PE pair on membrane performances. A higher mass deposition of PE was observed at higher ionic strength (0.5 M NaCl), resulting in a non-linear layer growth, compared to what observed at lower ionic strengths (≤ 0.05 M NaCl, threshold ~ 0.3 M NaCl). Consequently, the membrane resistance to water flux observed increased after each layer deposition, displaying a higher effect at higher ionic strengths. Nevertheless, at equal mass deposition, higher

permeability was observed for the coatings at higher ionic strengths. This is due to the higher hydration power and swelling capability of such thicker and less dense layers, favoring water transport through the membrane. Also, flips in the zig-zag trend of water resistance and permeability were observed at high ionic strength, after a certain number of layers. This is due to a combination of hydrophilicity, hydration and water mobility of the terminating layer. Moreover, when measuring the zeta potential of the membrane, it was observed that at high salinity the odd-even effect ceased after the 5th bilayer, and no zeta potential reversal was observed thereafter. This means that PSS is not able to compensate and overtake the positive charge of PDADMAC. These latter results highlight the complexities that can arise when performing PE multilayer coatings. Furthermore, this PE pair displayed also high resistance to extreme pH conditions, as a previous study showed their stability in the whole pH range 1-14 [220]. This is promising in view of performing frequent regeneration with HAIX, suggesting that such coatings could be resistant and perhaps improve the resistance of the whole adsorbent to alkaline (and acid) washes.

In this work, PE LbL coating of Layne was performed with the PSS/PDADMAC pair, with the goal to enhance the charge and size selectivity of the HAIX, and to reduce the organics adsorption. This would minimize surface precipitation and in the long term, easing the regeneration procedure. Moreover, in view of regeneration, the high resistance to harsh pH conditions makes this PE pair makes them promising for improving the adsorbent durability. The coatings were performed up to 5 bilayers, and in three different scenarios: at high ionic strength, low ionic strength, and in a mixed mode, with 3 high and 2 low ionic strength bilayers. The P adsorption kinetics of the system were investigated, as well as the effect of the terminating layer (charge) on P and Ca^{2+} adsorption in single- and double-solute synthetic solutions. An adsorption test

in P-spiked wastewater effluent (ww) was performed for the thick and mixed scenarios, with both the 5th negative and 5th positive terminating bilayers.

5.2 Materials and methods

5.2.1 Chemicals

Poly-(diallyl-dimethylammonium chloride) (PDADMAC, Mw = 200 - 350 kDa, 20 wt% in water) and polystyrene sulfonic acid (PSS, Mw = 200 kDa, 30 wt% in water) and 3-(N-morpholino)-propane sulfonic acid (MOPS) were purchased from Sigma-Aldrich (The Netherlands). Potassium dihydrogen phosphate (KH_2PO_4), sodium chloride (NaCl), sodium hydroxide (NaOH), hydrochloric acid (HCl) and nitric acid (HNO_3) were purchased from VWR (The Netherlands). Calcium nitrate tetrahydrate ($Ca(NO_3)_2{\cdot}4H_2O$) was purchased from Merck KGaA (Germany).

The commercial HAIX adsorbent selected as a reference was Layne^{RT} [62,64,65,82,83,185], of Layne Christensen Co (United States), which was obtained via Aquacare (’s-Hertogenbosch, The Netherlands).

5.2.2 Adsorbents

As previously stated, the adsorbent selected for tests was the commercial HAIX, Layne. Table 5.1 displays the properties of the adsorbent, as from the provider.

Layne Fe wt.% content was verified via HNO_3 (69 %) microwave digestion (MWD) with a Milestone Ethos Easy digester with a SK-15 High-Pressure rotor. The elemental composition of the digestate was analyzed with a Perkin Elmer Optima 5300 DV Inductively Coupled Plasma Optical Emission Spectroscopy (referred to as ICP).

Table 5.1: Properties of Layne^{RT}.

Name	LayneRT^{TM}
Producer	Layne Christensen Co.
General	Hybrid strong base anion exchange resin
Structure	Macroporous polystyrene cross-linked with divinylbenzene impregnated with iron hydroxide nanoparticles
Appearence	Brown spherical beads
Particle size (μm)	300-1200
Specific gravity	1.25-1.30
Functional groups	(Type 1)* Quaternary ammonium in chloride form (resin) Hydroxide (nanoparticles)
Fe content	17 wt.%

**Unsure radical type, most likely type 1, methyl group as radical (CH_3) (see* [194]*)*

The Layne Fe speciation was investigated using Mössbauer spectroscopy (MS). Transmission ^{57}Fe MS spectra were measured at 300 K and 120 K and collected with conventional constant acceleration or sinusoidal velocity spectrometers using a ^{57}Co (Rh) source. The MS spectra, calibrated to α-Fe, were analyzed with MossWinn 4.0 software [133], to retrieve the different relevant parameters, here explained. The isomer shift, IS, related to the oxidation state of the Fe atoms; the quadrupole splitting, QS, mainly related to the asymmetry of the charge distribution around the Fe nuclei; the magnetic hyperfine field, H_f, related to the magnetic ordering within the sample; the line-width (Γ), which can provide information on the crystallinity of the sample; and the spectral

contribution [%], for Fe species quantification. The characterization results are shown in Chapter 4 sections 4.3.1.3 and 4.4.1. In short, the nanoparticles in HAIX consist of superparamagnetic goethite.

5.2.3 V-Vis Measurements of PE Deposition

UV-Vis spectrophotometry was used to monitor PE deposition on Layne by measuring the change in PE concentration in solution. This method was chosen as the PE coatings are challenging to visualize and characterize, as the thickness of such layers reaches maximum few tens of nm [224]. Even more when dealing with size distributed resin beads. Moreover, since the resin backbone of Layne consists of quaternary ammonium active groups in sulfate form, it is challenging to confirm the successful coating of PSS and PDADMAC based on the elemental analysis, i.e., by measuring S and N. Hence, UV-Vis measurements were performed with a Shimadzu 1800 240 V UV-Vis spectrophotometer, adapting the procedure from Ghoussoub et al., 2018 [221], to monitor the PE deposition onto Layne as follows. PSS absorbs light in the UV-Vis range at a wavelength of 261 nm (absorption peak maximum), and the measured absorbance is directly proportional to the PSS concentration in solution via the Beer-Lambert law (BL law):

$$A = \varepsilon c l$$

where A is the light absorbance, ε is the PSS mass absorption coefficient, c is the PSS mass concentration and l is the optical path length (here, l = 1 cm of the 1 x 1 cm^2 of the quartz cuvette). First, a calibration curve relating A to c was determined. To do so, 2 g L^{-1} PSS stock solution was prepared and diluted to 0.01, 0.05, 0.1, 0.5, 1 g L^{-1}. Then, 3 mL of these dilutions were measured with the UV-Vis spectrophotometer, recording the maximum of absorbance of the PSS characteristic absorbance peak. The recorded absorbance data, A^i, were

plotted against the initial concentrations, c^i, and interpolated with the BL law to retrieve the proportionality constant ε.

Then, a PSS deposition kinetics experiment was performed to determine the deposition equilibrium time. First, the UV-Vis absorbance spectrum of 3 mL of PSS solution with an initial concentration $c_0(t_0)$ = 1 g L^{-1} was measured. Then, 300 mg of Layne were transferred to the cuvette, and the sample was shaken and measured every 30 s for 6 min, and then after 30 min and 1 h. The time-dependent PSS solution molar concentrations, $c_i(t_i)$, were estimated from the measured absorbance, $A_i(t_i)$, using the calibration curve. Then, the PSS loading (deposited PSS per Layne unit mass), $q_i(t_i)$, was calculated via:

$$q_i(t_i) = \frac{c_0(t_0) - c_i(t_i)}{m_R} V$$

The equilibrium time, t_{eq}, was estimated by plotting $q_i(t_i)$ against $c_i(t_i)$, and fitting the data with two common kinetic models, the Pseudo-First Order (PFO) [195,196] and the Pseudo-Second Order (PSO) [197] kinetic models. The two models are respectively described by the equations:

$$q(t) = q_{eq}(1 - e^{-k_1 t})$$

$$q(t) = \frac{k_2 q_{eq}^2 t}{1 + k_2 q_{eq} t}$$

where t [h] is the time, q(t) [mg g^{-1}] the adsorbent loading at time t, k_1 [g mg^{-1} min^{-1}] the kinetic rate constant of the PFO kinetic model, k_2 [g mg^{-1} min^{-1}] the kinetic rate constant of the PSO kinetic model, and q_{eq} [mg g^{-1}] the adsorbent loading at equilibrium. The fittings were performed using the Microsoft Excel Solver add-in, and the goodness of the fit assessed based on the Root Mean Squared Percentage Error (RMSPE). The goal of this analysis was not to

understand the mechanism, but to better design the coating procedure of the adsorbent.

Unfortunately, PDADMAC is not UV-Vis sensitive [225,226], meaning that the same kinetics measurements were not possible. Hence, an indirect proof of the PDADMAC deposition onto Layne was performed by investigating its effect on PSS depositions. The procedure is briefly described. First, 300 mg Layne were placed in a cuvette and exposed to 3 mL of 1 g L^{-1} PSS solution and shaken for 6 min, after which the supernatant absorbance was measured. Then, the PSS solution was removed and saved, the beads were rinsed 3 times in DW, and exposed to 3 mL of 1 g L^{-1} PDADMAC solution and shaken for 6 min. Then, the PDADMAC solution was removed and saved, the beads rinsed 3 times in DW, and exposed again to the previously saved PSS solution, shaken for further 6 min, and measured. In parallel, the same procedure was performed, without the intermediate PDADMAC deposition step. The difference in PSS loading with and without PDADMAC deposition was then estimated, assessing the effect of the latter.

5.2.4 PE LbL coating

The PE coating procedure was adapted from de Grooth et al., 2015 [219]. As previously explained, it consists in immerging Layne in PSS(-) and PDADMAC(+) alternately, growing the coatings one layer at the time (hence, layer-by-layer), and the combination of a PSS and PDADMAC layers is called bilayer. As a reminder, higher ionic strength produces thicker and lower density layers, able to swell in water; a lower ionic strength produces thinner and denser layers, with lower swelling capabilities. In this work, the coatings reached up to 10 alternating PSS and PDADMAC layers, hence 5 bilayers, starting with PSS, as Layne are originally positively charged. Moreover, the coatings were investigated in three different background ionic strength scenarios, as shown in

Figure 5.1: 1) 0.5 M NaCl, R_{Thick}(#+/-); 2) 0.005 M NaCl, R_{thin}(#+/-); 3) three bilayers at 0.5 M NaCl, followed by 2 bilayers at 0.005 M NaCl, R_{MIX}(#+/-). The letter R stands for 'Resin', while the symbols #± represents the bi-layer number and the charge of the final applied layer (e.g, 3- represents the third bi-layer up to the PSS coating; 3+ represents the third bi-layer up to the PDADMAC coating).

The procedure steps are shown in Figure 5.2 and briefly described hereafter. First, about 20 g of Layne were washed several times in Deionized Water (DW). Meanwhile, 1 g L^{-1} PE solutions, one with PSS and one with PDADMAC, were prepared in NaCl background, together with three washing solutions (i.e., DW + NaCl). All solutions had the same NaCl concentration, according to the respective coating scenario. Then, Layne beads were immersed for 15 min in the PSS solution, followed by 15 min washing procedure (i.e., 5 min immersion in each washing solution), then immersed for 15 min in the PDADMAC solution, followed by other 15 min of washing, and so on, up to 5 bilayers. After the washing procedure of each layer deposition, part of the coated Layne was saved for testing (terminating layer effect).

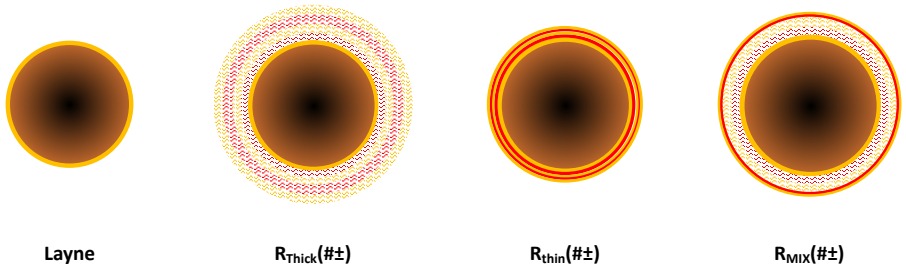

Figure 5.1: Fresh and PE coated Layne representation.

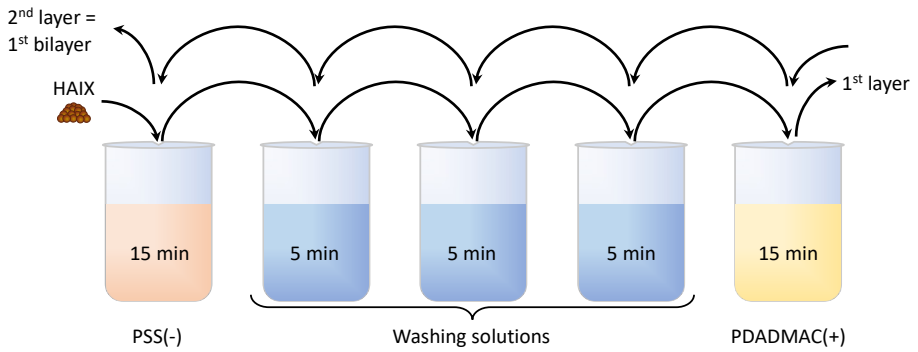

Figure 5.2: Scheme of the layer-by-layer.

5.2.5 Adsorption Solutions

The P adsorption kinetics and the terminating layer effect on adsorption experiments were performed in batch mode, placing the samples in a shaking incubator at 25 °C and 150 rpm, using a single-solute P synthetic solution and a double-solute (P+Ca) synthetic solution. As a reminder, the reason for Ca is that it is a highly abundant cation in wastewater effluents causing precipitation (e.f., with carbonate or phosphate). A 500 mg L^{-1} P and a 500 mg L^{-1} Ca stock solutions were prepared by dissolving KH_2PO_4 and $Ca(NO_3)_2 \cdot 4H_2O$ in DW and used for the adsorption sample preparation. From these stock solutions, proper dilutions were performed, depending on the type of experiments, and the pH adjusted to 7.2 with NaOH/HCl addition. Moreover, all solutions were buffered with 20 mM MOPS [79], to maintain the pH constant throughout the whole adsorption process.

For the experiment with P-spiked ww, the ww was collected from the sewage effluent of the wastewater treatment plant (WWTP) in Leeuwarden, and Table 5.2 reports its main characteristics, with the composition expressed in terms of total concentrations. The collected ww was let to settle overnight, to separate the particulates, followed by P measurements using the Hack Lange kits

LCK349. This provided a total P concentration of 0.112 mg L^{-1} and a soluble P concentration of 0.035 mg L^{-1}.

Table 5.2: Characteristics of the wastewater collected from the WWTP in Leeuwarden. Concentrations are reported in terms of total elemental/compound concentrations.

Parameters	**Values**
Temperature (during adsorption)	25°C
pH	7.4
Conductivity	1.0 ± 0.1 mS cm^{-1}
Phosphorus (P)	0.22 ± 0.01 mg L^{-1}
Calcium (Ca)	52.9 ± 0.8 mg L^{-1}
Magnesium (Mg)	8.9 ± 0.2 mg L^{-1}
Sulphur (S)	8.8 ± 0.1 mg L^{-1}
Nitrate (NO_3^-)	10.2 ± 0.1 mg L^{-1}
TOC	9.3 ± 0.5 mg L^{-1}
Silicon (Si)	8.5 ± 0.1 mg L^{-1}

All tests were run in duplicates plus blank (or control), which is just a solution without adsorbent, to monitor if any change happens during the experiment time. The solutions were analyzed before and after adsorption with ICP for the elemental composition, a Metrohm Compact IC Flex 930 ion Chromatograph (IC) for the ionic composition (in both cases, IC and ICP samples were filtered with a 0.45 µm hydrophilic filter) and a Shimadzu TOC-L CPH (CHECK) to assess the total organic carbon (TOC), total inorganic carbon (TIC) and hence

the total carbon (TC) content. All data were then analyzed using Microsoft Excel.

5.2.6 Adsorption Experiments

For practical reasons, the adsorption experiments preparation, results, and discussion will be merged and presented together in the following Experimental section. This will allow to follow the "chronological" course of events which will motivate the reasoning behind experimental design choices, linked to some non-optimal (in the sense of not evident or manifest) results.

It is important to highlight the challenges on the adsorbent weighing for the batch tests. In fact, resin-based adsorbents are known to retain water, up to 50-70% w/w, which makes it tricky when measuring their mass. When working with HAIX, drying the adsorbent is not an option, as it would cause a structural collapse. Hence, the adsorbent was transferred to the adsorption tubes with water, by means of a plastic pipette. Then, the water was removed with the same pipette, by creating vacuum at the tube bottom, and the adsorbent mass determined. The measurement error associated with this method was assessed in duplicate by repeatedly measuring a certain amount of adsorbent multiple times (> 10), by adding and removing the water. The resulting average error was equal to $\pm$ 5 %, with (rare) maximum absolute deviations of 15 %. It is important to keep this in mind when interpreting the adsorption results. The adsorbent dosage was 2 g L^{-1} in all the adsorption experiments.

5.3 Results

5.3.1 UV-Vis Measurements

Figure 5.3 shows the PSS deposition data over time, together with the PFO and PSO kinetic models fit, reported in Table 5.3. Also, Table 5.3 reports t_{eq}

together with t_{95} and t_{99}, which are the time required to reach 95 % and 99 % of q_{eq}. Both models describe the deposition trend fairly well. However, the PFO model seems to better estimate t_{eq}, t_{95}, and t_{99}, while the PSO model seems to overestimate them, especially considering what observed after 30 min and 1 h of PSS deposition. The t_{eq} estimated from the PFO model equals 6 min, in agreement with what found by [221]. Hence, for the synthesis procedure, 15 min of exposition time to the coating solutions was established, as it was considered close to equilibrium for both models (compared to both t_{95} values) and a good compromise for the coating procedures.

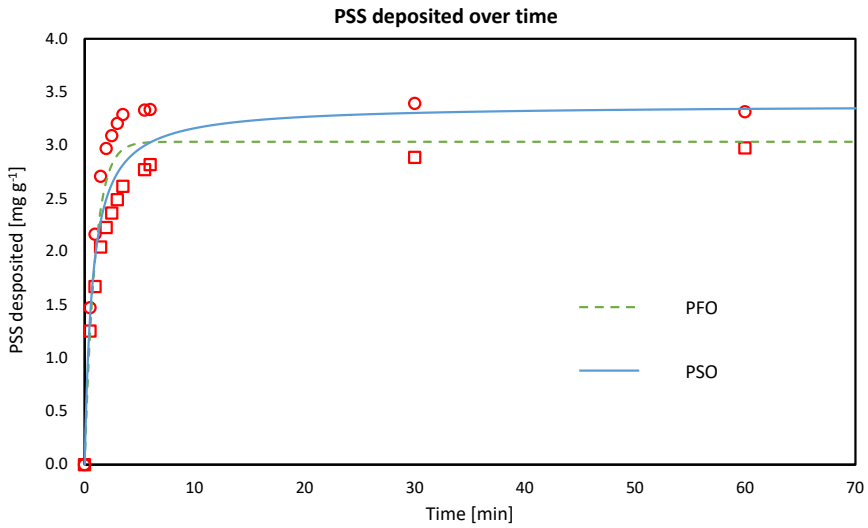

Figure 5.3: PSS deposition kinetics. The graph shows the data points from the duplicate runs and the PFO and PSO kinetic models fittings performed over the data average.

Table 5.3: PFO and PSO kinetic models fitting results for PSS deposition.

	k_1, k_2 [g mg^{-1} h^{-1}]	q_{eq} [mg g^{-1}]	RMSPE	t_{eq} [min]	t_{95} [min]	t_{99} [min]
PFO	1.07	3.03	0.034	6	3	4
PSO	0.42	3.38	0.037	334	13	63

Figure 5.4 shows the amount of PSS deposited during the second coating procedure with and without an intermediate PDADMAC coating. It seems that PDADMAC promoted slightly higher PSS deposition. However, the deviation between the replicates is significant, while the difference between the amount of PSS deposited with and without PDADMAC is rather small. These results might provide an indirect indication of occurred PDADMAC deposition, although not unequivocally proving it.

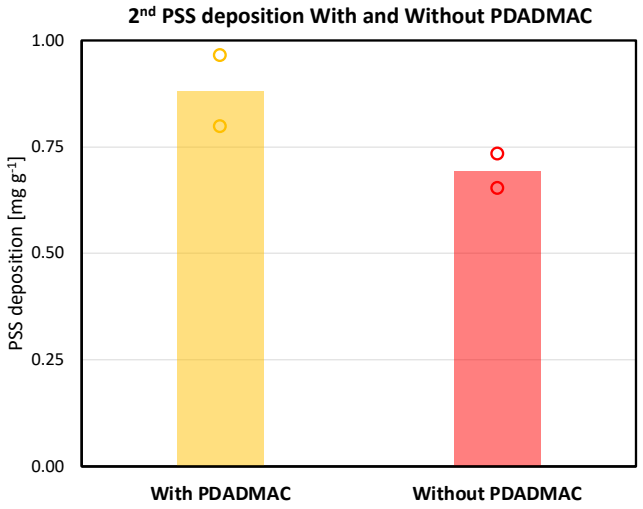

Figure 5.4: Amount of PSS deposited on Layne with and without intermediate PDADMAC deposition.

5.3.2 Adsorption Kinetics

The P adsorption kinetics experiments were performed in single-solute solution, prepared as explained in section 5.2.6. These experiments were performed only with Layne^{RT}, just to estimate the time, t_{eq}, needed to reach equilibrium and to design the other adsorption experiments. The adsorbate starting concentrations was 25 mg L^{-1} for P. The relatively high concentration of P was chosen to

minimize system perturbation when sampling for ICP analysis. The dilutions were prepared starting from the stock solutions as explained in section 5.2.5.

Concentrations of P and Fe (to ensure no adsorbent dissolution was happening) were monitored with ICP measurements, performed at different time intervals: 15, 30 min, 1, 2, 3 h, 1, 4, 5, 7, 11, 14, 21, 28 and 35 d. The results were analyzed using the PFO and PSO kinetic models, as reported in section 5.2.3, for a better t_{eq} estimation. The results (not shown here) displayed relatively high deviations, probably due to the difficulties in weighing the adsorbent. However, it was observed the solution concentrations (hence the adsorption process) to remain stable after 5 days, which was chosen as t_{eq} for the following adsorption experiments.

5.3.3 Effect of the Terminating Layer on Adsorption

The tests on the effect of the terminating layer on adsorption are expected to provide indirect confirmation of the successful coating, similarly to what is usually done in membrane science (see Introduction). In fact, the adsorption performances for P and Ca should be affected by the charge of the terminating layer, resulting in a sort of zig-zag trend (odd-even-like effect), as schematically showed in Figure 5.5. This means that for P, being negative, lower adsorption can be expected when PSS(-) is the terminating layer, while higher P adsorption when PDADMAC(+) is the terminating one, and vice versa for the Ca. Moreover, these tests should provide insights on the effect of the coating thickness and density on adsorption (e.g., ion transport, size exclusion, etc.).

In these adsorption experiments, the starting P concentration was 5 mg L^{-1}, while the starting Ca concentration was 60 mg L^{-1} and prepared as explained in section 5.2.5.

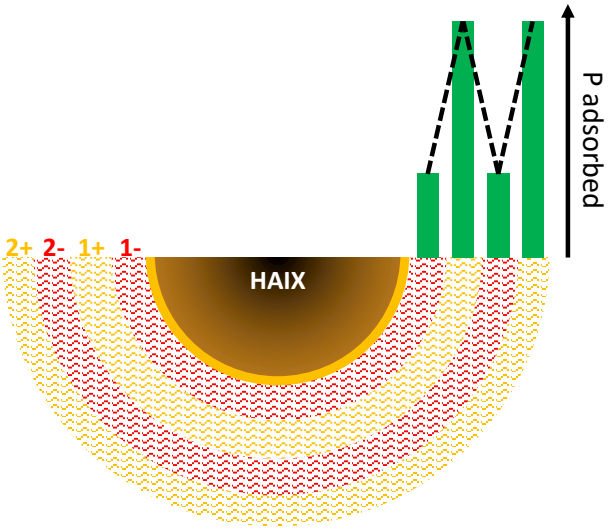

Figure 5.5: Schematic rapresentation of the expected zig-zag trend of P adsorption due to the terminating layer effect.

A first terminating layer effect on P adsorption test was performed with R_{Thick}, as a proof of principle, and the results are shown in Figure 5.6. The solid line represents the average trend of the duplicate data and seems to follow the zig-zag trend, but only from the 3- layer on. This "delayed" behavior could be expected, as it usually takes few layers before having a steady coating growth and could be related to the transition from a pore-dominated regime to a layer-dominated regime. Nevertheless, when looking at the duplicate data, a significant deviation between the data can be noticed (e.g., see R_{Thick}(5-)). Hence, a further LbL PE coating at 0.5 M NaCl was performed, when synthesizing also R_{thin} and R_{MIX}, and further tested.

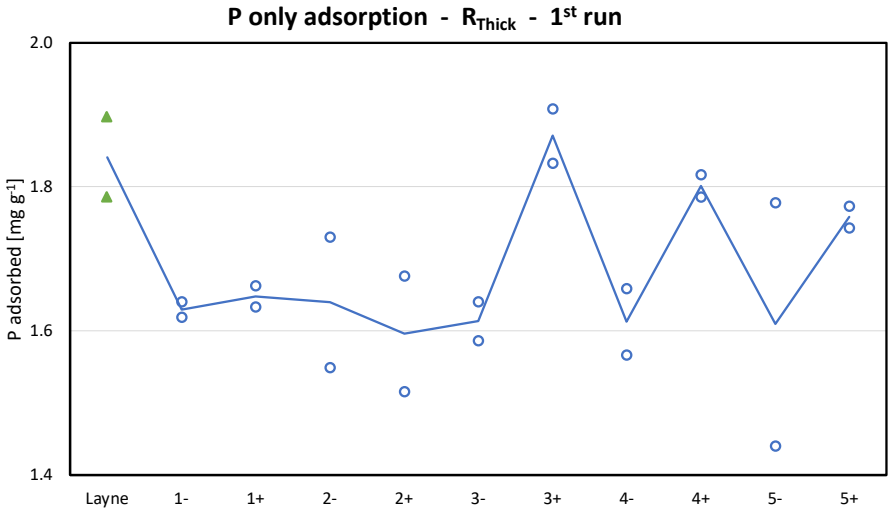

Figure 5.6: Results of the first run on the zig-zag effect on P adsorption due to the terminating layer in synthetic single-solute solution, reported with the duplicate (empty dots) data and average trends (lines), for Layne coated with thick low-density PE layers.

Figure 5.7 shows the results of the second adsorption test in single-solute P solution, for all the adsorbent (also the results of the first run are reported for comparison). No clear trend is visible for any of the adsorbents, this time not even for R_{Thick}.

Figure 5.8 shows the adsorption results of P adsorption in double-solute P+Ca solution, for all adsorbents. In this case, on average, the zig-zag trend seems to be followed by for all of them, but again the difference between the duplicate data points is too large to draw clear conclusions.

A clear trend was not visible also for Ca adsorption in the double-solute P+Ca solution. The results are clearly distributed within the experimental error, see Figure 5.9.

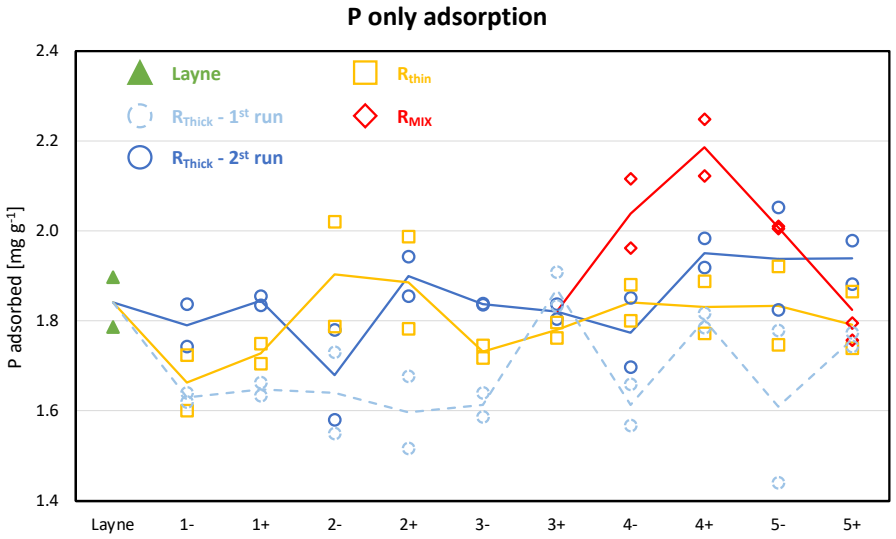

Figure 5.7: Results of the first run on the zig-zag effect on P adsorption due to the terminating layer in synthetic single-solute solution, reported with the duplicate (empty dots) data and average trends (lines), for all coating scenarios.

These results do not show a significant nor clear effect of the coatings on the adsorption performances. This means that either the coatings do not cause any evident change on P and Ca adsorption, or that the experimental error (associated to the adsorbent weight) is too big to observe any change, or even that the experimental design was not suited for this purpose. In fact, the hypothesis is that the screening provided by the PE coatings is not enough to show relevant differences in simple single- or double-solute synthetics solutions. The only conclusion which can be drawn from these experiments is that the PE coatings did not affect (neither positively or negatively) the ability to adsorb P, which remained of the same order for all adsorbents. It could be that by testing the coated adsorbents in a more complex matrix, with competing ions of different valency, and in particular with organics, the effect of the PE coating could become evident.

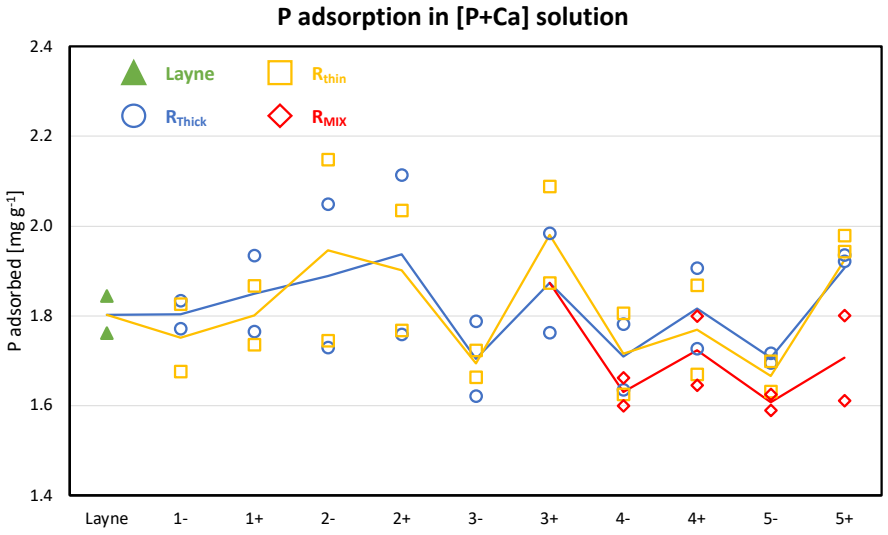

Figure 5.8: Results of the first run on the zig-zag effect on P adsorption due to the terminating layer in synthetic double-solute (P+Ca) solution, reported with the duplicate data (empty dots) data and average trends (lines), for all coating scenarios.

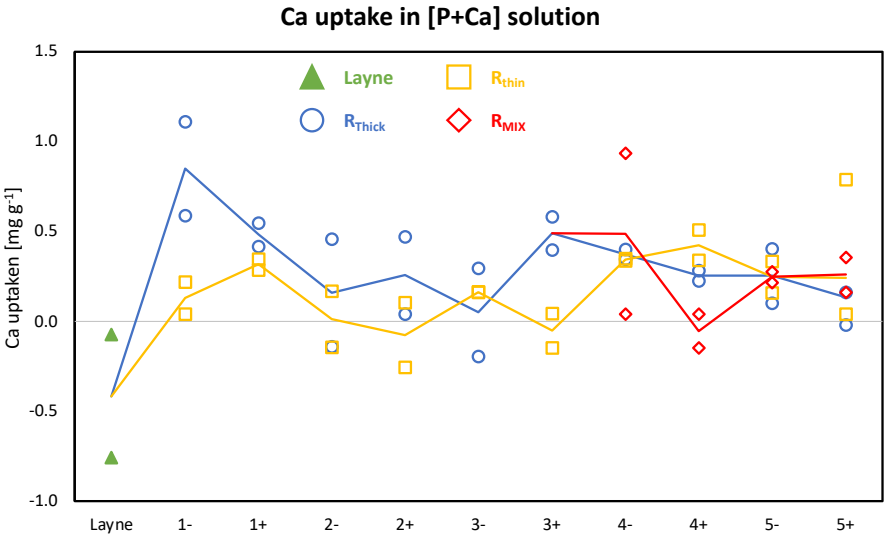

Figure 5.9: Results of the first run on the zig-zag effect on Ca adsorption due to the terminating layer in synthetic double-solute (P+Ca) solution, reported with the duplicate (empty dots) data and average trends (lines), for all coating scenarios.

These results do not show a significant nor clear effect of the coatings on the adsorption performances. This means that either the coatings do not cause any evident change on P and Ca adsorption, or that the experimental error (associated to the adsorbent weight) is too big to observe any change, or even that the experimental design was not suited for this purpose. In fact, the hypothesis is that the screening provided by the PE coatings is not enough to show relevant differences in simple single- or double-solute synthetics solutions. The only conclusion which can be drawn from these experiments is that the PE coatings did not affect (neither positively or negatively) the ability to adsorb P, which remained of the same order for all adsorbents. It could be that by testing the coated adsorbents in a more complex matrix, with competing ions of different valency, and in particular with organics, the effect of the PE coating could become evident.

5.3.4 Adsorption in P-Spiked Wastewater

The adsorption tests in P-spiked wastewater were performed with Layne, as a reference, R_{Thick}(5-), R_{Thick}(5+), R_{MIX}(5-) and R_{MIX}(5+). R_{thin} was not considered as a sample of interest for these tests due to the features of thin multilayer coatings, and hence excluded. In fact, thin dense coatings are basically neutral throughout the whole coating layer, with an overall weak effective surface charge dependent on the terminating layer. For R_{Thick} and R_{MIX}, both the 5- and 5+ layers were tested to investigate any effect ascribable to the terminating layer. For instance, negative terminating layer are known to favor biofouling prevention, especially in the presence of humic substances [221,227–233].

Figure 5.10 reports the P adsorption results for all adsorbents. Once again, no evident difference caused by the coatings is visible, and it can be observed that also in this case, the coatings did not impact the P adsorption capability of Layne.

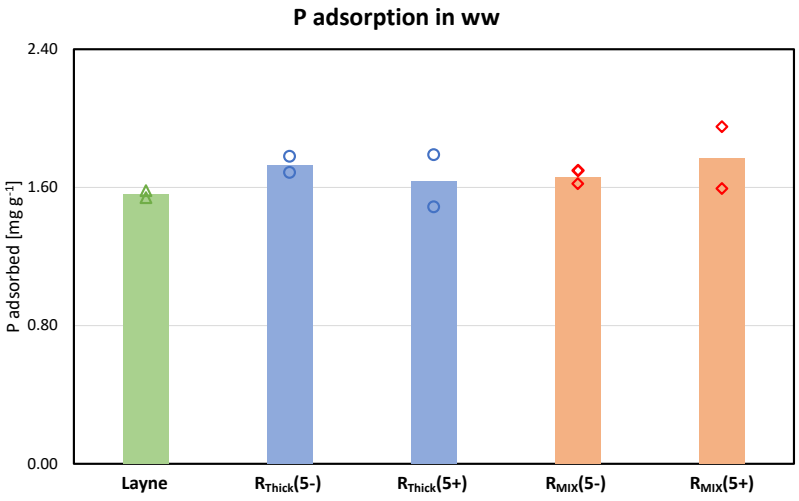

Figure 5.10: P adsorption in P-spiked ww for Layne, $R_{Thick}(5\pm)$ and $R_{MIX}(5\pm)$.

Figure 5.11 shows the results for the competing ions. No clear trend can be observed for nitrate. It seems to be absorbed to a greater extent by $R_{Thick}(5-)$, and completely repelled by $R_{Thick}(5+)$, $R_{MIX}(5-)$ and $R_{MIX}(5+)$. These results go against what expected. In fact, nitrate is known to be more hydrophobic ion, and a higher removal would be expected when PDADMAC is the terminating layer [182,183]. Also, PE coatings usually increase selectivity against multivalent ions, thus, nitrate diffusion through the layers should not be hindered. Hence, the apparent selectivity against nitrate observed for $R_{Thick}(5+)$, $R_{MIX}(5-)$ and $R_{MIX}(5+)$ should be further investigated. Similarly, when looking at silicates, $R_{MIX}(5-)$ and $R_{MIX}(5+)$ seem to display slightly higher selectivity against them. Silicates are difficult to speciate in ww, making it complicated to understand which phases are rejected (ICP measurements provide elemental Si results). Looking at sulfate results, the results can be explained as follows. First, sulfate desorption from Layne is due to the fact that Layne is in sulfate form, and it can be exchanged with other anions. Second, the reason why the PE coated Layne adsorb sulfate instead is probably due to the coating procedure, in which the

sulfate present in Layne might have exchanged with the highly concentrated chloride, and/or with the deposited PSS. Moreover, since PDADMAC comes in chloride form, it is expected to be able to adsorb sulfate.

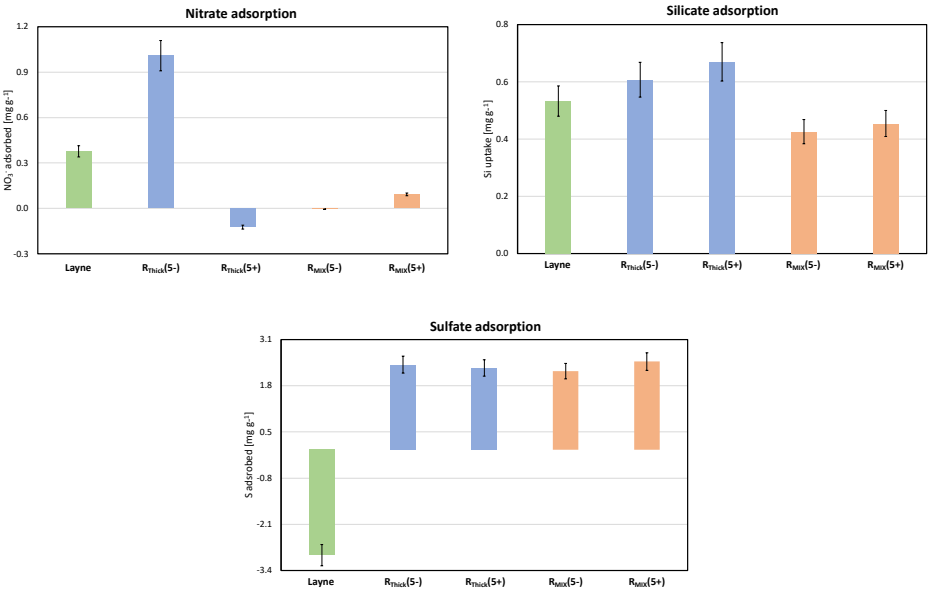

Figure 5.11: Competing ions removal in P-spiked ww for Layne, $R_{Thick}(5\pm)$ and $R_{MIX}(5\pm)$.

Figure 5.12 shows the results for total carbon, inorganic and organic carbon removal. The results are also in this case not conclusive. It seems that the thicker coating promotes higher TC removal compared to the mixed coating or the pure Layne. For TIC measurements, mostly related to carbonate, bicarbonate, and dissolved CO_2, it is important to consider the fact that the measurements are significantly affected by the preparation and handling of the adsorption samples and TOC measurement samples. This is mostly due to the CO_2 exchange with the atmosphere. For R_{Thick}, higher TIC removal is observed with a negative terminating layer, compared to the positive one, while the opposite is observed for R_{MIX}. This may be due to the different permeability and water mobility of the two coatings. For the TOC results, higher removal is observed for the coated

adsorbents compared to Layne. This is surprising, as PE coatings are expected to reduce biofouling in membranes, by reducing humics and other organics uptake, especially for the thicker coatings. In fact, in a thick layer, the higher contributions of negative charges should prevent the adsorption of organics, even more when the terminating layer is negative [227–233]. This could be due to the fact that at the 5th PE bilayer, the charge contribution of the underlying PDADMAC layers is not compensated by the PSS [219].

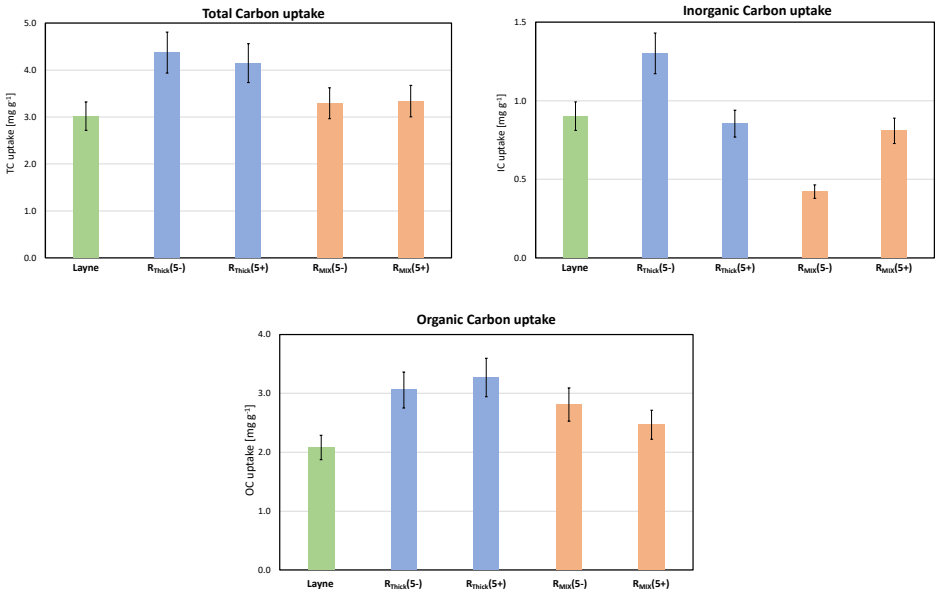

Figure 5.12: Total carbon, total inorganic carbon and total organic carbon removal in P-spiked ww for Layne, $R_{Thick}(5\pm)$ and $R_{MIX}(5\pm)$.

To conclude, also these experiments in ww did not provide any evidence of the favorable role of PE coatings onto HAIX. Four reasons could explain these observations. First, the overall results might be due to intrinsic reasons, meaning that LbL PE coatings of HAIX might not be an effective strategy to improve the adsorbent selectivity. Second, the couple PSS/PDADMAC, due to the difficulties in tuning the properties of the coating (charge imbalances, switches in

behaviors, etc.), might not be the optimal PE couple for this purpose. Third, the large experimental errors associated to the sample preparation, in particular the weighing of the adsorbent, might explain the differences in behavior. Fourth, the experimental design was not appropriate. In fact, PE coatings play an important role on selectivity by affecting the mass transfer at the boundary layer, when this is the diffusion rate-limiting step. However, in batch experiments, the boundary layer thickness is affected by the stirring/agitation speed, and it often becomes negligible in the diffusion process. Moreover, experiments with membranes are performed in continuous mode, where the results are dependent on the contact time between the membrane and the solution and present compounds. Therefore, concentration gradients remain constant during the experiment and kinetic differences can lead to selectivity. This is clearly not satisfied in batch mode equilibrium experiments where concentration gradients will eventually reduce. This means that the choice of performing experiments in batch mode (chosen due to the relatively high number of samples to be tested) was not optimal to highlight differences in selectivity. To validate this last hypothesis a short kinetic experiment was performed.

5.3.5 Adsorption Kinetics (Second Experiment)

This second kinetic experiment was performed in a binary solution of P and Ca, this time both at a starting concentration of 5 mg L^{-1}, in 20 mM MOPS, and at an adsorbent concentration of 2 g L^{-1}. All scenarios were tested with the following adsorbents: Layne, R_{Thick}(5-), R_{Thick}(5+), R_{thin}(5-), R_{thin}(5+), R_{MIX}(5-) and R_{MIX}(5+). The experiments were run in duplicates plus blank, with ICP samples collected after 5, 10, 15, 30 min, 1, 2, 3, 4, 24 h, and the last one after two days. First, the error associated with P and Ca concentration measurements due to samples preparation and handling was investigated by repeatedly measuring the blanks. An average deviation of 1 % was estimated, with maximum deviations

of 5 % for P and 6 % for Ca. Then, the kinetic results were fitted with both the PFO and PSO kinetic models and evaluated. The fitting results are reported in Table 5.4 and Table 5.5, respectively. In general, it was observed that the PFO fitting line was better describing the data trend, as shown in Figure 5.13, also considering that q_{eq} and t_{eq} were significantly overestimated with the PSO model. For the latter reason, Table 5.5 reports two t_{95} for the PSO model, one estimated from the q_{eq} fitting results and one directly from maximum q of the data set.

Figure 5.14 shows all the PFO (left) and PSO (right) curves superimposed to the data, up to 25 h, to highlight the differences in the first minutes. On average, for each adsorbent coating scenario, the 5- samples showed slower adsorption rates and lower q_{eq} compared to the 5+ samples. Nevertheless, the results do not seem to show evident changes, especially given the associated experimental errors, thus no clear kinetic effect of the coatings on the uptake of phosphate from a double solute solution was evident.

The results for Ca adsorption are not shown here, as all adsorbents displayed a slight Ca removal increase with time, reaching a maximum Ca removal up to 5 % of the starting concentration, and in line with what observed for Layne. Thus, no significant Ca adsorption was happening, meaning that the influence of the negative layers, if any, was negligible.

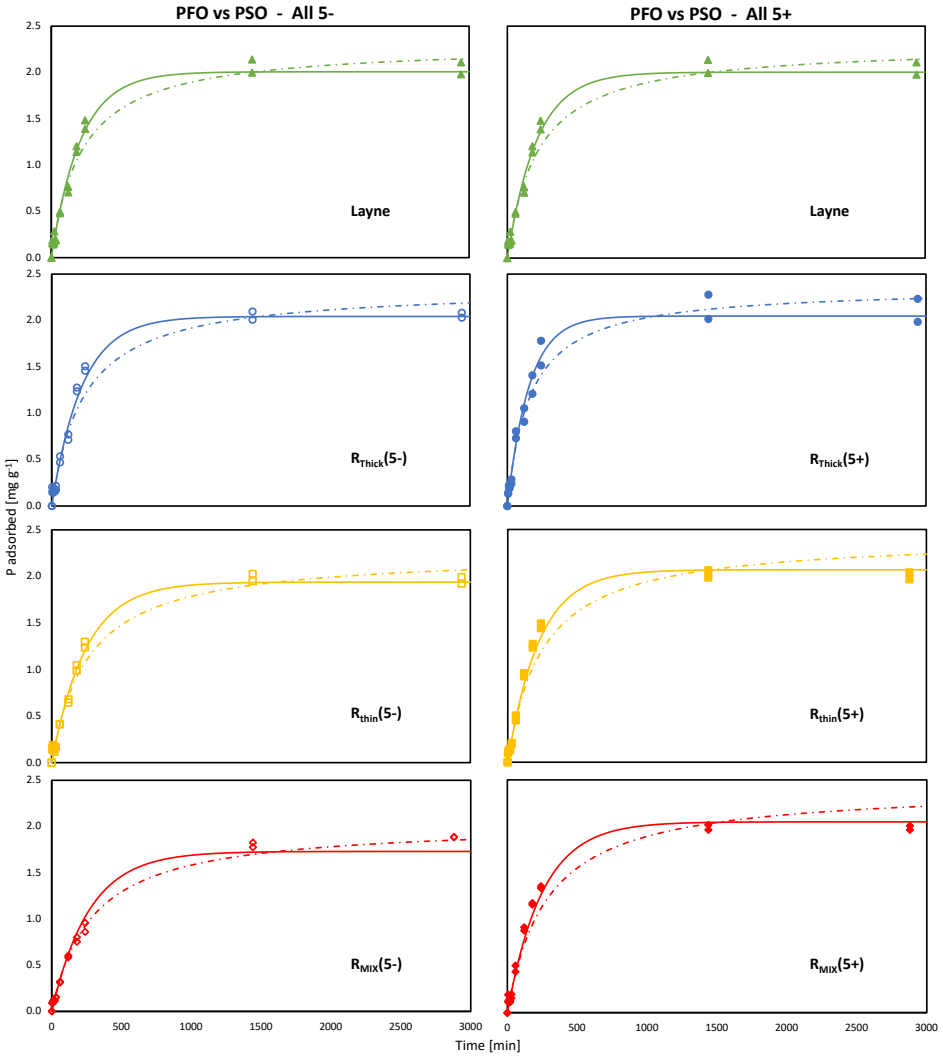

Figure 5.13: Comparison between the PFO and PSO kinetic models for Layne, $R_{Thick}(5\pm)$, $R_{thin}(5\pm)$ and $R_{MIX}(5\pm)$. The solid lines represent the PFO kinetic model curve, the dashed-dotted lines represent the PSO kinetic model curves, the full markers represent the duplicates data of Layne and the 5+ terminating layer samples, while the empty markers those of the 5- terminating layer samples.

Table 5.4: PFO kinetic models fitting results for P adsorption in the second kinetic test, in double-solute (P+Ca) synthetic solution.

PFO	k_1 (x 10^{-3}) [g mg^{-1} min^{-1}]	q_{eq} [mg g^{-1}]	t_{eq} [h]	t_{95} [h]	RMSPE
Layne	4.8	2.0	36	11	0.290
R_{Thick}(5-)	4.6	2.0	54	11	0.294
R_{Thick}(5+)	6.4	2.0	27	8	0.239
R_{thin}(5-)	4.1	1.9	45	12	0.307
R_{thin}(5+)	4.4	2.1	38	11	0.225
R_{MIX}(5-)	3.7	1.7	45	13	0.249
R_{MIX}(5+)	4.0	2.1	45	13	0.283

Table 5.5: PSO kinetic models fitting results for P adsorption in the second kinetic test, in double-solute (P+Ca) synthetic solution.

PSO	k_2 (x 10^{-3}) [g mg^{-1} min^{-1}]	q_{eq} [mg g^{-1}]	t_{95} from fit [h]	t_{95} from data [h]	RMSPE
Layne	2.0	2.3	28	69	0.285
R_{Thick}(5-)	1.9	2.4	29	73	0.295
R_{Thick}(5+)	2.6	2.4	25	51	0.234
R_{thin}(5-)	1.7	2.2	30	83	0.305
R_{thin}(5+)	1.7	2.4	30	79	0.239
R_{MIX}(5-)	1.7	2.0	31	91	0.234
R_{MIX}(5+)	1.5	2.4	31	89	0.295

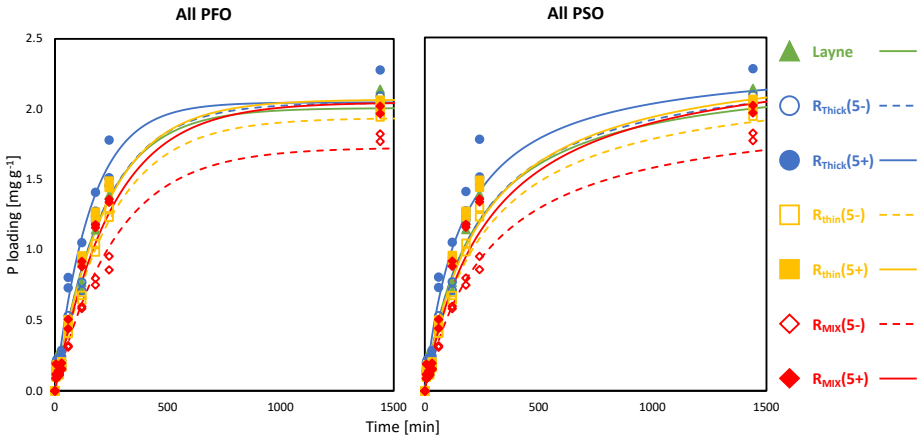

Figure 5.14: P adsorption kinetics of Layne, $R_{Thick}(5\pm)$, $R_{thin}(5\pm)$ and $R_{MIX}(5\pm)$ in double-solute (P+Ca) synthetic solution up to 25 h. The left graph shows all PFO kinetic models curves superimposed to the duplicate data for each sample, with the solid lines and full markers representing Layne and the 5+ terminating layer samples, while the dashed lines and empty markers representing the 5- terminating layer samples. Similarly, the right graph shows the PSO kinetic model results, with the dashed

5.4 Implications for PE LbL Coatings on HAIX

This study aimed to improve the selectivity of HAIX by acting on the charge and size exclusion via LbL PE coatings. However, the results did not show any evident effect in this sense. Firstly, characterizing the PSS/PDADMAC coatings on HAIX is challenging, due to the thinness of the coating layer, geometry of the medium and similar elemental composition. Secondly, the difficulty in weighing the adsorbent provide an intrinsic experimental error which hides any difference in adsorption and selectivity which might be caused by the PE coatings. Thirdly, and the main message of this investigation, batch adsorption tests to investigate selectivity with (coated) HAIX may not have been the most appropriate method to determine the efficacy. Multilayer PE coatings act on the diffusion at the boundary layer, which effect is suppressed by the time scale of equilibrium experiments and the stirring conditions. Moreover, it is surprising

that the results of the adsorption test in P-spiked ww did not show any improved organics repulsion, not even for the negative terminating layers. The results with the presented experimental design are not promising for the application of LbL coatings to improve the selectivity. Possibly better results might be obtained if the PE coated adsorbents would be tested in continuous mode, i.e., in adsorption columns. This would provide experimental conditions closer to that applied to membranes, and would allow to compare equal volumes of adsorbents, avoiding dealing with the challenging weighing procedure. Hence, these inconclusive results do not necessarily mean that PE coatings are not a suited for increasing HAIX selectivity.

Another consideration is that on the PE pair chosen, i.e., PSS and PDADMAC. When using PDADMAC, there is less control on the multilayer growth at high ionic strength, as shown (also in previous studies) by the charge imbalance between the PE pair, and the stop of the odd-even effect after a certain bilayer [219]. Probably, using a different PE in place of PDADMAC, could help in this sense. For instance, PAH (poly(allylamine hydrochloride)) allows a better control of multilayer the properties and provides a lower "pores" size cutoff, improving size selectivity [220,224]. Moreover, crosslinking of the PE layers could increase the stability and the selectivity of the coating [220,234]. Also, by using zwitterionic character to the coating, either via crosslinking [234] or directly using zwitterionic polymers could further improve the selectivity against organics [221]. Multilayer PE coatings enhance the selectivity for monovalent ions over multivalent ones [230,234,235]. Hence, a well-developed multilayer PE coating of HAIX could be applied to slightly acidic water streams, with pH between 5 and 6, where phosphate is mainly monovalent. Such surface modification would allow higher selectivity for phosphate against sulfate, which is divalent, nitrate, by playing on the hydrophobicity/hydrophilicity of the coating,

and humics, provided by the background contribution of the negatively charged PE layers.

5.5 Conclusion

Equilibrium batch experiments did not show any evident effect of the LbL PE coating of HAIX on selectivity, not even for organics rejection. P loadings of non-coated and coated HAIX remained of the same order. However, some P adsorption results showed a semblance of zig-zag trend ascribable the terminating layer effect. Also, adsorption results in ww showed visible signs (although of unclear nature) of selectivity against nitrate and silicates. These results suggest that further testing is needed to draw clear conclusions, and two alternative methodologies to investigate the effect of these coatings are recommended. First, performing continuous column experiments instead of batch tests. This would unequivocally confirm whether the experimental design or the PSS/PDADMAC coatings were inadequate for our purposes. Second, improving the coatings by changing the coating procedure (e.g., layer cross-linking), by optimizing the coating features (e.g., thickness, density, mixing), and/or by investigating other PE pairs (e.g., PSS/PAH) or zwitterionic polymers.

These further experiments would unequivocally prove whether the batch experiments are inadequate for reliable selectivity investigations, or LbL PE coating is not an efficient strategy to improve HAIX adsorption selectivity for P.

Acknowledgments

This work was performed in the cooperation framework of Wetsus, European Centre of Excellence for Sustainable Water Technology (www.wetsus.nl). Wetsus is co-funded by the Dutch Ministry of Economic Affairs and Ministry of Infrastructure and Environment, the European Union Regional Development Fund, the Province of Fryslân and the Northern Netherlands Provinces. This research received funding from the Netherlands Organization for Scientific Research (NWO) in the framework of the Innovation Fund for Chemistry, and from the Ministry of Economic Affairs and Climate Policy in the framework of the TKI/PPS-Toeslagregeling. The authors thank the participants of the research theme "Phosphate recovery" for the interest, fruitful discussions, and financial support. A special thanks goes to Wiebe de Vos for the interesting scientific discussion and support, Gladys Wangari Mutahi for the work done together.


6

6

Discussion and Outlook

6.1 Towards Effective Adsorbent Development for Eutrophication Prevention

The main objective of this thesis was to identify strategies to improve iron oxide-based adsorbents for P recovery. The improvements were related to the general properties, such as affinity for P, adsorption capacity, stability and regenerability of the adsorbent (note that the term iron oxide comprises oxides, hydroxides and oxyhydroxides, for simplicity).

The main focus was spent on the iron oxide surface properties. For this, goethite nanoparticles were synthesized and modified through doping. The potential of doping for tuning goethite properties and improving its P adsorption performances was shown. Consequently, for application purposes, these developed nanoparticles were embedded on a support, that is anion exchange resins, and tested for P recovery. This provided the so-called hybrid anion exchange adsorbents (HAIX), a highly investigated and commercially available category of Fe-based adsorbents for P recovery. These experiments highlighted some limitations of HAIX adsorbents, in particular related to the regeneration and solidity of the resins as a support for the nanoparticles. Finally, multilayer polyelectrolyte coating for improving HAIX selectivity was investigated, although it did not show promising results yet.

Based on the gathered information, observations and results throughout the different projects, the following sections will provide considerations and perspectives on how to effectively develop adsorbents for eutrophication prevention. The discussion will focus on the main steps and related crucial points for effective adsorbent development: surface properties development; functional test design; results interpretation and good practices; proper fine adsorbent characterization and monitoring; and regeneration experiments.

6.2 Investigating Functional Surfaces

For P-adsorption down to the ultra-low concentrations, it has been stressed the importance of affinity over adsorption capacity, both in previous studies [23] and in this thesis. Increasing the affinity of the adsorbent entails increasing the extent of interaction between the adsorbent, or better the surface of the adsorbent and phosphate. This is fundamental for eutrophication prevention, since the adsorbent (surface) needs to be able to adsorb phosphate, even when this is in minute concentrations, scattered within a myriad of other (competing) compounds in water. In literature, adsorbents are mainly developed with the goal to increase the specific surface area (SSA) and reach high adsorption capacities. Usually, adsorption capacity is the parameter used to evaluate the adsorbents and show their potential. However, it was shown that there is no direct relation between adsorption capacities and low equilibrium concentrations [23]. This is the research direction which should be pursued to effectively develop P adsorbents for eutrophication prevention.

The results in Chapter 2 and 3 show how doping is an effective strategy to improve goethite characteristics in this sense. The charge compensation and crystallization mechanisms can modify the surface properties in a functional way for P adsorption. It was observed that divalent cations, in our case Zn^{2+}, promote an increase in the goethite point of zero charge, providing a more positive surface for phosphate adsorption. Doping can promote changes in the crystal habit of the nanoparticles, and in the case of Zn, it promoted nanoparticles elongation, with consequent growth of some specific crystal faces. This appeared to be more favorable for P adsorption, as the Zn doped goethite nanoparticles displayed higher adsorption capacity per unit area. This suggests that a combination of surface charge and specific crystal face growth is what provides goethite with more effective surfaces for P adsorption.

On the one hand, as a continuation to this thesis work, future research can focus on systematically investigating different (preferably divalent) cations as dopants, identifying the most promising elements and optimal doping percentages. On the other hand, the basis of effective adsorbent development through doping has been set, and there is a need to bring such nanoparticles to application, identifying the optimal way to support them (see section 1.4).

6.3 The Importance of Performing Comparative Studies

When testing adsorbents for P recovery, the experimental conditions, and in particular the initial P concentration and water matrix (i.e., synthetic single solute multi-solute solutions or real wastewater), are crucial. On the one hand, these experimental conditions can have an influence on the adsorption mechanism. This stresses the importance of properly relating and discussing results and interpretations to such conditions. On the other hand, each experimental condition can highlight a specific aspect of the adsorption mechanism, providing insights on the related contribution, limiting factors, and so on. In chapter 4, experiments were performed comparing not only different water conditions, which highlighted differences in adsorption behavior, but also different adsorbents of different type. For instance, different HAIX were compared to pure anion exchange resins, providing insights on the role of the HAIX backbone. Notice that in this case, the adsorption results from experiments in highly concentrated synthetic solution showed that the anion exchange resin had adsorption capacities equal to and in some cases twice as high that of the investigated HAIX. To make a connection with what discussed in the previous section 1.1, uniquely based on the adsorption capacity, these results would suggest anion exchange resins as one of the most promising adsorbents for P recovery. However, testing different initial P concentrations and water matrices improved the understanding of the influence of the experimental conditions on the adsorption mechanism, distinguishing between physisorption dominated process and

chemisorption dominated process. This further highlighted the crucial role of the iron oxide nanoparticles for selective (chemisorption-driven) P removal, and the limitation of anion exchange resins in real-life systems. Furthermore, the synthesized HAIX were compared to a commercial HAIX, Layne^{RT}, as a reference (similarly, the experiments on goethite doping in Chapter 2 and 3 were compared to those of pure goethite nanoparticles). These comparisons provide a benchmark to better interpret the results, also in comparisons to other studies.

Hence, comparative studies not only allow for improved understanding of the adsorption mechanism and related determining/limiting factors but can also constitute a benchmark for comparing other developed or novel adsorbents. Focusing on this last point, it is highly challenging making comparisons between adsorption performances of different adsorbents form different lab-scale studies. This is due to the different experimental settings and conditions applied in each study. There is a need for experimental standards, based on the type of application (e.g., adsorption at ultra-low P concentrations, bulk P removal, etc.), consisting of either a set of short experiments, or experimental conditions, or commercially available adsorbents for reference. For instance, for adsorption at ultra-low concentrations, proof of principle adsorption equilibrium experiments in batch mode with synthetic solutions should be performed with:

- Fixed adsorbent concentrations, e.g., 2 g L^{-1}.
- Relatively low initial P concentration range, e.g., 0.1-10 mg L^{-1}.
- Buffered pH around 7.2, e.g., using 20 mM MOPS.
- Fixed temperature and shaking speed, e.g., T = 20 or 25 °C, at 120 or 150 rpm.
- A reference adsorbent for comparison, e.g., pure goethite nanoparticles, or a commercial adsorbent (Layne^{RT}, GFH, FSP, or others).

6.4 The Importance of Understanding Models and Their Limitations

An important remark on adsorption studies (but can be applied to any topic and field of research) regards the need to improve data analysis and interpretation. Properly treating and interpreting data is more important than collecting them. Data values are meaningless, until we relate their values to each other, to the conditions at which they were collected, to models and physical quantities. This process lifts the meaning of the data from a specific case (the experiment) to a more general case, improving the theoretical knowledge.

In general, for adsorption experiments, the choice of a fitting model should be determined by the adsorption mechanism, and not vice versa. For example, concluding that data agreement with the pseudo second order kinetic model entails chemisorption is wrong; concluding that data agreement with the Langmuir isotherm entails monolayer adsorption is also wrong. Still, different models could be applied as a criterion of comparison, but with good knowledge of their limitations and without too much physical interpretation. Focusing on the kinetics experiments in Chapter 4, P adsorption with HAIX showed good agreement with both the pseudo-first and the pseudo-second order kinetic models. These two models usually better describe physisorption- and chemisorption-driven processes, respectively, and in literature there is the tendency to assign the adsorption mechanism according to the fitting results. This is not a good practice and is a typical example of confusion between correlation and causation. In fact, the adsorption mechanism can only be determined by good knowledge of the adsorbent and adsorbate chemistries, and with specific analytical measurements, e.g., with FTIR, EXAFS, Mössbauer spectroscopy, calorimetry (see sections 1.2 and 1.5) [236]. Adsorption experiments with HAIX adsorbents and consequent data analysis show that distinguishing between the contributions of physisorption and chemisorption is not only challenging, but impossible. It is important

to know that iron hydroxides chemisorb phosphate while the anion exchange resins physisorb anions, and these two phenomena might happen simultaneously. Hence, attention should be paid by researchers, editors, reviewers, and readers, when mechanisms are solely interpreted my data fitting models.

Another improper practice regards the use of linearized forms of adsorption isotherms. However, linearization is a mathematical approximation method which has clear and defined conditions and limitations, and it should be applied to a small range of values (mathematically speaking, in a small neighborhood of a value). Alternatively, since adsorption kinetics and adsorption equilibrium isotherms follow sort of a combination of two linear-like trends, namely, an almost linearly ascending part and an almost linear plateau, two different linearized fitting can be applied to each portion (or subdomain). Nevertheless, linearized fittings are often applied to the entire domain, and this is wrong. Also, despite linearized forms constitute an approximation, the retrieved "linearized" parameters values are generally taken as absolute values for comparison. The inaccuracy (if not wrongness) of this practice, and related misleading results (e.g., overestimation or underestimation of fitting parameters), was already pointed out [236]. Furthermore, it is difficult to understand what the advantage of applying a linearized forms is, when dealing with relatively simple functions and data sets. Preserving the original non-linearized form of data and functions allows to directly analyze (even by eye) the different curvatures of the isotherms, providing direct insights on the higher or lower affinity of an adsorbent with respect to the adsorption capacity, and final equilibrium concentrations.

More attention and caution should be spent when choosing models and performing and interpreting data fitting results.

6.5 The Importance of Mössbauer Spectroscopy Applied to Fe-Based Adsorbents Development

When developing and investigating materials, researchers have the duty to know and define as much as possible what they are working with. Of course, this applies to Fe-based materials, and in our case, to iron oxides. There are 16 different iron oxide species, each displaying different characteristics in terms of thermodynamic stability, particle sizes, crystallinities, affinity, and capacity for phosphate, etc. Hence, it is fundamental to finely and accurately characterize iron oxide-based adsorbents. In this sense, Mössbauer spectroscopy proved to be a valuable tool, as shown in the nanoparticle characterization before and after use in this work.

In Chapter 3, Mössbauer spectroscopy was fundamental for providing a fine characterization of highly Zn-doped samples. For the 10 %at. doped sample, it revealed that the two fractions of nanoparticles of different habit (observed with TEM) consisted of two differently Zn-substituted goethites. This information could not be retrieved from XRD analysis, especially for the ultrafine nanoparticles fraction, which in literature is usually defined with the improper term "amorphous hydrous oxides", often ascribed to ferrihydrite-like phases. The adsorption results revealed that the adsorption performances are not only affected by the iron oxide phase and pzc, but also by the morphology of the nanoparticle, the presence or growth of specific crystal phases, functional to P adsorption. Without Mössbauer analysis, the different results might have been ascribed to the presence of ferrihydrite or generic amorphous iron oxide phases, leading to improper conclusions. Similarly, for the 20 %at. Zn-doped goethite, XRD suggested it to consist of zinc ferrite, without a slight presence of goethite convoluted within the pattern of zinc ferrite. Mössbauer spectroscopy revealed that the sample mainly consisted of goethite doped nanoparticles, with minor fractions of zinc ferrite and maghemite. Such information is fundamental to relate

the adsorption performances to a specific iron oxide phase and (in this case) to the effect of doping.

In this thesis, the most surprising result obtained with Mössbauer spectroscopy is the iron oxide nanoparticles speciation in HAIX of Chapter 4. HAIX adsorbents have been investigated and applied for more than 15 years. It is surprising that the contained nanoparticles, which dimension is known to be smaller than 15-20 nm, have been (almost) always characterized with XRD, which is known to face limitation in such a size range. Hence, the iron oxide phase of the nanoparticles was wrongly identified, improperly describing them as "amorphous hydrous oxides", opposed to more crystalline phases such as goethite or hematite [60,68,69,84]. In this work, Mössbauer spectroscopy revealed that these nanoparticles consist of ultrafine superparamagnetic goethite nanoparticles, and not only. It revealed that throughout multiple adsorption-desorption cycles, the nanoparticles seem to grow. Although the mechanism is still unclear (probably oriented attachment), this phenomenon is highly important since this "sintering-like" growth might affect the nanoparticles contribution to P adsorption, e.g., by downsizing the functional crystal faces.

These results bring up two considerations. First of all, on the importance of having a good knowledge of the limitations and applicability of analytical techniques (e.g., XRD and particle size), accordingly interpreting the results. It is surprising that a more thorough characterization of the nanoparticles contained in HAIX has never been attempted before. Secondly, on the importance of using more "exotic" techniques, such as Mössbauer spectroscopy or synchrotron-based techniques, to finely and fully characterize novel or developed materials. This is crucial when assigning intrinsic properties such as affinity, selectivity, and pzc, to a specific adsorbent (or in this case to a specific iron oxide phase).

6.6 *Improving the regeneration of the adsorbent*

Adsorbent regeneration is a crucial yet critical step for economic viability of adsorption technologies. The critical points on regeneration regard the adsorbent stability, since the adsorbent needs be able to sustain multiple regeneration cycles; regeneration solution losses, due to solution retainment by the porous or polymeric structure; and the purity of the recovered P-based product, linked to both adsorbent selectivity and P-desorption mechanism. However, previous studies showed that the reusing an adsorbent multiple times can highly decrease the chemical costs [23,72]. Nevertheless, adsorbent regeneration has been little investigated and in some cases the P desorption mechanism has not been fully understood, especially for HAIX.

Investigating the regeneration procedure in a similar fashion as for P adsorption would provide a definitive push for adsorption technologies toward application.

First of all, improved understanding of the desorption mechanism can provide further insights on the adsorption mechanism, and vice versa. For instance, Martin et al., 2018 [185], could estimate the chemisorption and physisorption contributions in the commercial HAIX, Layne^{RT}. Also, it can reveal whether the P removal mechanism consists of adsorption or surface precipitation, depending on what solution (acid or alkaline) causes P desorption. Simultaneously, improved understanding of the adsorption mechanism can help better designing the desorption procedure. For instance, identifying whether chemisorption or physisorption is the main mechanism can support the use of NaOH or NaCl, respectively. This can also lead to design sequential desorption systems, where different compounds are selectively desorbed (and recovered) at different stages. Fully understanding the adsorption mechanism requires an investigation on the binding energies between adsorbent and adsorbate. To investigate that,

complementary measurements, such as calorimetry, FTIR, XPS, Mössbauer spectroscopy, and others, should be performed. In particular, Mössbauer spectroscopy measurements (with ^{57}Fe impregnation) could provide information on the energy involved in the iron oxide-phosphate bond, while definitely proving the chemical nature of the adsorption mechanism. Such improved information on the bond energies can help tune the regeneration procedure, perhaps finding chemical-free options to desorb and recover P from the adsorbent.

Secondly, investigating how the regeneration solution interacts with the adsorbent and is retained within it can help developing strategies to make regeneration more efficient. The higher efficiency is related to the chemical use and losses, and avoidance of harsh regeneration steps. In terms of chemical use, for instance, the results discussed in Chapter 4 revealed the higher OH consumption required by HAIX, due to the anion exchange resin backbone, to fully desorb P. This was revealed by investigating the use of less concentrated regeneration solutions (an example of investigating desorption in a similar fashion to adsorption experiments). Improved understanding of the interaction between (in this case) the OH^- molecules, the adsorbed P, and the adsorbent active sites, can provide insights on the limitations of or alternatives for the regeneration procedure. In terms of chemical losses, multiple water-based washes are needed to release the retained regeneration solution and restore the operational pH for adsorption. Understanding how the regeneration solution interacts with the adsorbent surface and how it is retained, can help develop more efficient ways to "push out" the retained OH^-. This would prevent losing it into the water washes previously mentioned, also reducing the volume of water required for such washes.

Thirdly, a combination of the above-mentioned points would also help easing the regeneration solution. For instance, OH^- retention within the pores can promote local precipitation or surface precipitation during the following adsorption cycle. This causes pore blockage and decreases the adsorption capacity of

the adsorbent. To remove such precipitates, acid washes are needed, but these can cause adsorbent dissolution, and similarly to alkaline P desorption, they could face solution losses and high-water consumption for pH neutralization. Optimizing the alkaline wash could prevent such further steps, preserving the adsorbent for longer.

Finally, further investigation on the regeneration of the regeneration solution (excuse the pun) should be carried out. This entails designing efficient ways to both recover P, for circularity purposes, and maximize the reuse of the regeneration solution, to further decrease chemical costs. This step would definitively close the loop, making adsorption a sustainable and circular technology, in which each of its components is reused.

To conclude, further research should mainly focus on regeneration, and all related aspects. Clearly, too little focus has been spent on it in previous studies, and too little is understood on the desorption mechanism and the effects on the adsorbent. Since regeneration is crucial for the economics of the process, long term experiments on regeneration, and adsorbent stability and economic assessment are fundamental for the viability of adsorption technologies

6.7 Developing Effective Goethite Nanoparticles-Based Adsorbents for P Recovery

All the previously discussed points will help designing an effective adsorbent. In this sense, perspectives for adsorbent development are provided, based on the results of this thesis, i.e., for improved goethite-based adsorbents.

HAIX adsorbents have been widely investigated for P recovery (and As removal, which has similar chemistry with P), showing some promising results. Resins display a higher mechanical stability and faster kinetics compared to granular iron oxides [23,60]. Nevertheless, the results obtained in Chapter 4 question the potential of HAIX for P adsorption down to ultra-low

concentrations. Firstly, the active yet unspecific role of the anion exchange resin backbone in the adsorption process might affect the purity of the recovered phosphate product. Secondly, the observed active role of the anion exchange resin backbone also during the desorption process, (strongly) re-adsorbing phosphate, implies higher hydroxide (i.e., regeneration liquid) consumption for effective desorption. Thirdly, the nanoparticles growth revealed by Mössbauer spectroscopy questions the robustness of anion exchange resins as a support, and hence the long-term performances and stability of HAIX.

On the one hand, more research focused on long-term operations should unveil whether using HAIX provides actual advantages compared to granular porous adsorbents. For instance, whether the Donnan exclusion effect of the resin backbone provides any real added value to selectivity, or whether the faster adsorption kinetics of HAIX provides concrete operational advantages. If demonstrated, these advantages should exceed the regeneration related issues, i.e., the regeneration liquid overconsumption (for effective P desorption) and losses (resin swelling and liquid retention) and lower purity of the P-based recovered product. Also, the effect of nanoparticles agglomeration on the overall performances should be estimated and balanced in this overall evaluation.

On the other hand, alternative adsorbent syntheses (nanoparticles fixation) should be investigated. For instance, employing inert and more robust polymeric materials (e.g., non-charged polymers, zeolites, ceramics) as backbone for the doped nanoparticles. An inert support might prevent the P-desorption related issues observed in Chapter 4, while the higher robustness would prevent nanoparticle agglomeration/growth. Even better might be an adsorbent synthesis procedure in which nanoparticles are first developed and then embedded into a support, or the support is synthesized around the nanoparticles. This would provide higher control on the nanoparticle features, being the key component for selective P recovery. Lastly, developing granular porous adsorbents using the

improved nanoparticles as building blocks, for instance through controlled-like agglomeration.

Finally, alternative adsorbent designs for improving operational efficiency should also be investigated. The porous structure of the usually employed adsorbents, like porous iron oxide granules and HAIX (which are porous-like structures), tends to slow down diffusion kinetics and retain liquids. Especially in the case of the regeneration solution, this retainment is undesirable for the reasons explained in section 1.3 and would imply higher overall costs. Developing nanostructured adsorbents with morphologies equivalent to the "negative" (or opposite) of porous structures, e.g., extruding pillars, could represent an interesting alternative for increasing adsorbents efficiency. Such structures would provide larger "channels" of diffusion for the liquid streams, while providing the same SSA of porous adsorbents. It would also imply that during regeneration, the desorbed P would directly flow into the regeneration stream, without the hassle of wandering through and exiting from the porous structure.

6.8 *Conclusions*

The previous sections provided suggestions on research lines for effectively developing adsorbents for eutrophication prevention. Truthfully, such suggestions were focused on iron oxide-based adsorbents, based on the topic and results of this thesis. Despite that, the multiple advantages linked with Fe-based adsorbents make them extremely interesting candidates. To recall a few, iron and iron oxides are highly abundant on the Earth crust and diffuse presence in many environments. Because of this abundance, they are relatively cheap and have been widely investigated, generating a broad knowledge on their properties. Moreover, they offer versatility due to the different forms, species, and properties, and are generally easy to synthesize and manipulate. Strategies to improve iron oxide features have been widely investigated, also in this thesis.

At this point, the two main needs are: 1) developing strategies to design effective adsorbents; 2) improve the understanding and efficiency of the regeneration procedure.

Also, for future research, good practices should be carefully revised, and experimental standards defined to improve the comparability of adsorbents, and in general studies.

Nevertheless, this work will not tell that iron oxide-based adsorbents are the best for P recovery, neither that adsorption is the best technology for that. This is not the scope of this work (and should not be the scope of any work). To recall what was explained in the introduction, there is no best adsorbent or technology. It depends on the specific application. For this work, the main application was recovering P via adsorption from freshwater streams and bodies, or as a polishing step of wastewater effluents, preferably in the pH range 6-8. The results from this thesis suggest that doping of iron oxides, in particular goethite, is an effective and promising way to tune their surface properties, to obtain an efficient adsorbent for phosphate, to tackle eutrophication and recover a valuable nutrient.

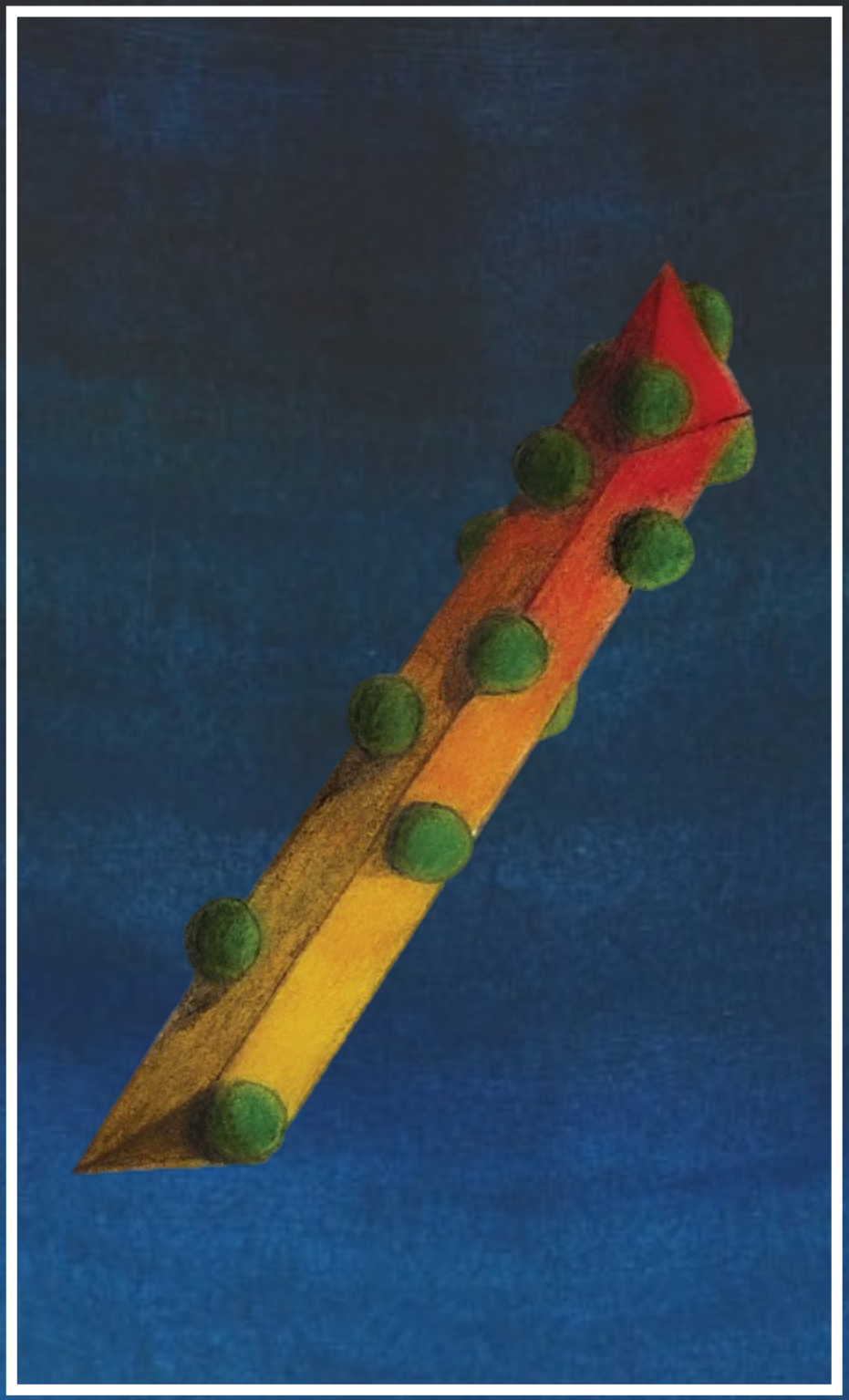

References

[1] S.H. Cohn, C.S. Dombrowski, Measurement Chlorine , By Total-Body and Neutron Calcium , Phosphorus Activation Sodium in Nitrogen , in Vivo Analysis, J. Nucl. Med. 12 (n.d.) 499–505.

[2] T. Lohman, S. Going, Z. Wang, Human body composition, (2005).

[3] D. Cordell, J.O. Drangert, S. White, The story of phosphorus: Global food security and food for thought, Glob. Environ. Chang. 19 (2009) 292–305. https://doi.org/10.1016/j.gloenvcha.2008.10.009.

[4] D.L. Childers, J. Corman, M. Edwards, J.J. Elser, Sustainability challenges of phosphorus and food: Solutions from closing the human phosphorus cycle, Bioscience. 61 (2011) 117–124. https://doi.org/10.1525/bio.2011.61.2.6.

[5] S.R. Carpenter, E.M. Bennett, Reconsideration of the planetary boundary for phosphorus, Environ. Res. Lett. 6 (2011) 14009–14021. https://doi.org/10.1088/1748-9326/6/1/014009.

[6] T. Prot, L. Korving, M.C.M. Van Loosdrecht, Ionic strength of the liquid phase of different sludge streams in a wastewater treatment 2 plant, ChemRxiv. (2020). https://doi.org/10.26434/chemrxiv.13359437.v1.

[7] D.L. Correll, The Role of Phosphorus in the Eutrophication of Receiving Waters: A Review; The Role of Phosphorus in the Eutrophication of Receiving Waters: A Review, 1998. https://doi.org/10.2134/jeq1998.00472425002700020004x.

[8] D.W. Schindler, Whole-lake eutrophication experiments with phosphorus, nitrogen and carbon, SIL Proceedings, 1922-2010. 19 (1975) 3221–3231. https://doi.org/10.1080/03680770.1974.11896436.

[9] D.W. Schindler, Recent advances in the understanding and management of eutrophication, Limnol. Oceanogr. 51 (2006) 356–363. https://doi.org/10.4319/lo.2006.51.1_part_2.0356.

[10] D.W. Schindler, S.R. Carpenter, S.C. Chapra, R.E. Hecky, D.M. Orihel, Reducing phosphorus to curb lake eutrophication is a success, Environ. Sci. Technol. 50 (2016) 8923–8929. https://doi.org/10.1021/acs.est.6b02204.

[11] L. Carvalho, C. Mcdonald, C. de Hoyos, U. Mischke, G. Phillips, G. Borics, S. Poikane, B. Skjelbred, A.L. Solheim, J. Van Wichelen, A.C. Cardoso, Sustaining recreational quality of European lakes: Minimizing the health risks from algal blooms through phosphorus control, J. Appl. Ecol. 50 (2013) 315–323. https://doi.org/10.1111/1365-2664.12059.

[12] V.H. Smith, G.D. Tilman, J.C. Nekola, Eutrophication: impacts of excess nutrient inputs on freshwater, marine, and terrestrial ecosystems, Environ. Pollut. (1999). https://doi.org/10.1016/S0269-7491(99)00091-3.

[13] I. Chorus, I.R. Falconer, H.J. Salas, J. Bartram, Health risks caused by freshwater cyanobacteria in recreational waters, J. Toxicol. Environ. Heal. - Part B Crit. Rev. 3 (2000) 323–347. https://doi.org/10.1080/109374000436364.

[14] J.N. N. Pretty, C.F. Mason, D.B. Nedwell, R.E. Hine, S. Leaf, R. Dils, Policy Analysis Environmental Costs of Freshwater Eutrophication in England and Wales, (2003). https://doi.org/10.1021/es020793k.

[15] W.K. Dodds, W.W. Bouska, J.L. Eitzmann, T.J. Pilger, K.L. Pitts, A.J. Riley, J.T. Schloesser, D.J. Thornbrugh, Eutrophication of U. S. freshwaters: Analysis of potential economic damages, Environ. Sci. Technol. 43 (2009) 12–19. https://doi.org/10.1021/es801217q.

[16] USEPA, (2015).

[17] M.F. Chislock, E. Doster, R.A. Zitomer, A.E. Wilson, Eutrophication: Causes, Consequences, and Controls in Aquatic Ecosystems, Nat. Educ. Knowl. (2013). https://doi.org/10.1002/j.1551-8833.1969.tb03755.x.

[18] D.L. Correll, Phosphorus: A rate limiting nutrient in surface waters, Poult. Sci. 78 (1999) 674–682. https://doi.org/10.1093/ps/78.5.674.
[19] A.J.P. Smolders, L.P.M. Lamers, E.C.H.E.T. Lucassen, G. Van Der Velde, J.G.M. Roelofs, Internal eutrophication: How it works and what to do about it - A review, Chem. Ecol. 22 (2006) 93–111. https://doi.org/10.1080/02757540600579730.
[20] EC, The urban waste water treatment directive, 1992.
[21] EC, WFD, 2000/60/EC, (2000).
[22] EC, Common implementation strategy guidance document on eutrophication assessment, 2009.
[23] P.S. Kumar, L. Korving, M.C.M. van Loosdrecht, G.J. Witkamp, Adsorption as a technology to achieve ultra-low concentrations of phosphate: Research gaps and economic analysis, Water Res. X. 4 (2019) 100029. https://doi.org/10.1016/J.WROA.2019.100029.
[24] W. Gleason, An introduction to phosphorus: History, production, and application, Jom. 59 (2007) 17–19. https://doi.org/10.1007/s11837-007-0071-y.
[25] R.W. Scholz, A.E. Ulrich, M. Eilittä, A. Roy, Sustainable use of phosphorus: A finite resource, Sci. Total Environ. 461–462 (2013) 799–803. https://doi.org/10.1016/j.scitotenv.2013.05.043.
[26] D.P. Van Vuuren, A.F. Bouwman, A.H.W. Beusen, Phosphorus demand for the 1970-2100 period: A scenario analysis of resource depletion, Glob. Environ. Chang. 20 (2010) 428–439. https://doi.org/10.1016/j.gloenvcha.2010.04.004.
[27] D. Cordell, S. White, Tracking phosphorus security: indicators of phosphorus vulnerability in the global food system, Food Secur. 7 (2015) 337–350. https://doi.org/10.1007/s12571-015-0442-0.
[28] M.A. de Boer, L. Wolzak, J.C. Slootweg, Phosphorus: Reserves, production, and applications, Phosphorus Recover. Recycl. (2018) 75–100. https://doi.org/10.1007/978-981-10-8031-9_5.
[29] R. El Zrelli, L. Rabaoui, N. Daghbouj, H. Abda, S. Castet, C. Josse, P. van Beek, M. Souhaut, S. Michel, N. Bejaoui, P. Courjault-Radé, Characterization of phosphate rock and phosphogypsum from Gabes phosphate fertilizer factories (SE Tunisia): high mining potential and implications for environmental protection, Environ. Sci. Pollut. Res. 25 (2018) 14690–14702. https://doi.org/10.1007/s11356-018-1648-4.
[30] EC, Communication from the Commission: Consultative Communication on the Sustainable Use of Phosphorus, Eur. Comm. Brussels, Belgium. (2013) COM no. 517. http://ec.europa.eu/environment/consultations/pdf/phosphorus/EN.pdf.
[31] MCS2021, USGS, (n.d.).
[32] EC, Critical Raw Materials, 2020. https://doi.org/10.1007/978-3-030-40268-6_9.
[33] EC, European Green Deal, 2020. https://doi.org/10.4324/9780080495781-12.
[34] EC, Circular Economy Action Plan, 2020.
[35] UN, The Sustainable Development Goals Report 2019, United Nations Publ. Issued by Dep. Econ. Soc. Aff. (2019) 64. https://unstats.un.org/sdgs/report/2022/%0Ahttps://www.un-ilibrary.org/content/books/9789210018098%0Ahttps://www.un-ilibrary.org/content/books/9789210478878.
[36] G. Crini, E. Lichtfouse, Advantages and disadvantages of techniques used for wastewater treatment, Environ. Chem. Lett. 17 (2019) 145–155. https://doi.org/10.1007/s10311-018-0785-9.
[37] M. Shafiquzzaman, S.S. Alsaleem, H. Haider, M.T. Alresheedi, H. Thabit, Experimental study for sand filter backwash water management: Low-cost treatment for recycling and residual sludge utilization for radium removal, Water (Switzerland). 13 (2021). https://doi.org/10.3390/w13202799.
[38] BAT-knowledge centre, Sand Filtration, https://emis.vito.be/en/bat/tools-overview/sheets/sand-filtration#:~:text=Sand%20filtration%20is%20used%20for,filter%2C%20it%20must%20be%20rinse d., (n.d.) 20.
[39] D. Askenaizer, Drinking Water Quality and Treatment, Encycl. Phys. Sci. Technol. (2003) 651–671. https://doi.org/10.1016/B0-12-227410-5/00186-1.
[40] F. Hammes, S. Velten, T. Egli, T. Juhna, Biotreatment of Drinking Water, Compr. Biotechnol. Second Ed. 6 (2011) 517–530. https://doi.org/10.1016/B978-0-08-088504-9.00386-X.
[41] Kemira handbook (2020). About water treatment., n.d.
[42] J.T.A. Verhoeven, B. Arheimer, C. Yin, M.M. Hefting, Regional and global concerns over wetlands and water quality, Trends Ecol. Evol. 21 (2006) 96–103. https://doi.org/10.1016/j.tree.2005.11.015.
[43] M. Lürling, M. Mucci, Mitigating eutrophication nuisance: in-lake measures are becoming inevitable in eutrophic waters in the Netherlands, Hydrobiologia. 847 (2020) 4447–4467. https://doi.org/10.1007/s10750-020-04297-9.
[44] P.C. D'Haese, G. Douglas, A. Verhulst, E. Neven, G.J. Behets, B.A. Vervaet, K. Finsterle, M.

Lürling, B. Spears, Human health risk associated with the management of phosphorus in freshwaters using lanthanum and aluminium, Chemosphere. 220 (2019) 286–299. https://doi.org/10.1016/j.chemosphere.2018.12.093.

[45] M. Zamparas, I. Zacharias, Science of the Total Environment Restoration of eutrophic freshwater by managing internal nutrient loads . A review, Sci. Total Environ. 496 (2014) 551–562. https://doi.org/10.1016/j.scitotenv.2014.07.076.

[46] M. Lürling, G. Waajen, F. Van Oosterhout, Humic substances interfere with phosphate removal by lanthanum modified clay in controlling eutrophication, Water Res. 54 (2014) 78–88. https://doi.org/10.1016/j.watres.2014.01.059.

[47] E. Worch, Adsorption Technology in Water Treatment, Fundamentals, Processes, and Modeling, De Gruyter, 2012.

[48] H.N. Tran, S.J. You, A. Hosseini-Bandegharaei, H.P. Chao, Mistakes and inconsistencies regarding adsorption of contaminants from aqueous solutions: A critical review, Water Res. 120 (2017) 88–116. https://doi.org/10.1016/j.watres.2017.04.014.

[49] P. Loganathan, S. Vigneswaran, J. Kandasamy, N.S. Bolan, Removal and recovery of phosphate from water using sorption, Crit. Rev. Environ. Sci. Technol. 44 (2014) 847–907. https://doi.org/10.1080/10643389.2012.741311.

[50] Y. Xu, J.-Q. Jiang, Technologies for Boron Removal, (2008). https://doi.org/10.1021/ie0708982.

[51] P. Wilfert, P.S. Kumar, L. Korving, G.J. Witkamp, M.C.M. Van Loosdrecht, The Relevance of Phosphorus and Iron Chemistry to the Recovery of Phosphorus from Wastewater: A Review, Environ. Sci. Technol. 49 (2015) 9400–9414. https://doi.org/10.1021/acs.est.5b00150.

[52] P.S. Kumar, W.W. Ejerssa, C.C. Wegener, L. Korving, A.I. Dugulan, H. Temmink, M.C.M. van Loosdrecht, G.-J. Witkamp, Understanding and improving the reusability of phosphate adsorbents for wastewater effluent polishing, Water Res. (2018). https://doi.org/10.1016/J.WATRES.2018.08.040.

[53] A. Bottini, L. Rizzo, Phosphorus Recovery from Urban Wastewater Treatment Plant Sludge Liquor by Ion Exchange, Sep. Sci. Technol. 47 (2012) 613–620. https://doi.org/10.1080/01496395.2011.627904.

[54] X. Huang, S. Guida, B. Jefferson, A. Soares, Economic evaluation of ion-exchange processes for nutrient removal and recovery from municipal wastewater, Npj Clean Water. 3 (2020). https://doi.org/10.1038/s41545-020-0054-x.

[55] K. Kalaitzidou, M. Mitrakas, C. Raptopoulou, A. Tolkou, P.A. Palasantza, A. Zouboulis, Pilot-Scale Phosphate Recovery from Secondary Wastewater Effluents, Environ. Process. 3 (2016) 5–22. https://doi.org/10.1007/s40710-016-0139-1.

[56] Y. Zhang, X. She, X. Gao, C. Shan, B. Pan, Unexpected Favorable Role of Ca 2+ in Phosphate Removal by Using Nanosized Ferric Oxides Confined in Porous Polystyrene Beads, Environ. Sci. Technol. 53 (2019) 365–372. https://doi.org/10.1021/acs.est.8b05177.

[57] B. Pan, J. Wu, B. Pan, L. Lv, W. Zhang, L. Xiao, Author ' s personal copy Development of polymer-based nanosized hydrated ferric oxides (HFOs) for enhanced phosphate removal from waste effluents, (n.d.). https://doi.org/10.1016/j.watres.2009.06.055.

[58] B.K. Mayer, D. Gerrity, B.E. Rittmann, D. Reisinger, S. Brandt-Williams, Innovative strategies to achieve low total phosphorus concentrations in high water flows, Crit. Rev. Environ. Sci. Technol. 43 (2013) 409–441. https://doi.org/10.1080/10643389.2011.604262.

[59] J.A. O'Neal, T.H. Boyer, Phosphate recovery using hybrid anion exchange: Applications to source-separated urine and combined wastewater streams, Water Res. 47 (2013) 5003–5017. https://doi.org/10.1016/j.watres.2013.05.037.

[60] L.M. Blaney, S. Cinar, A.K. SenGupta, Hybrid anion exchanger for trace phosphate removal from water and wastewater, Water Res. 41 (2007) 1603–1613. https://doi.org/10.1016/j.watres.2007.01.008.

[61] A. Sendrowski, T.H. Boyer, Phosphate removal from urine using hybrid anion exchange resin, Desalination. 322 (2013) 104–112. https://doi.org/10.1016/j.desal.2013.05.014.

[62] D. Pinelli, S. Bovina, G. Rubertelli, A. Martinelli, S. Guida, A. Soares, D. Frascari, Regeneration and modelling of a phosphorous removal and recovery hybrid ion exchange resin after long term operation with municipal wastewater, Chemosphere. 286 (2022) 131581. https://doi.org/10.1016/j.chemosphere.2021.131581.

[63] S. Sengupta, A. Pandit, Selective removal of phosphorus from wastewater combined with its recovery as a solid-phase fertilizer, Water Res. 45 (2011) 3318–3330. https://doi.org/10.1016/j.watres.2011.03.044.

[64] S. Guida, G. Rubertelli, B. Jefferson, A. Soares, Demonstration of ion exchange technology for phosphorus removal and recovery from municipal wastewater, Chem. Eng. J. 420 (2021) 129913. https://doi.org/10.1016/j.cej.2021.129913.

[65] A. Muhammad, A. Soares, B. Jefferson, The impact of background wastewater constituents on the selectivity and capacity of a hybrid ion exchange resin for phosphorus removal from wastewater, Chemosphere. 224 (2019) 494–501. https://doi.org/10.1016/j.chemosphere.2019.01.085.

[66] Y. Zhang, B. Pan, C. Shan, X. Gao, Enhanced Phosphate Removal by Nanosized Hydrated La(III) Oxide Confined in Cross-linked Polystyrene Networks, Environ. Sci. Technol. 50 (2016) 1447–1454. https://doi.org/10.1021/acs.est.5b04630.

[67] P. Sylvester, P. Westerhoff, T. Möller, M. Badruzzaman, O. Boyd, A Hybrid Sorbent Utilizing Nanoparticles of Hydrous Iron Oxide for Arsenic Removal from Drinking Water, 2007. www.liebertpub.com.

[68] S. Sarkar, L.M. Blaney, A. Gupta, D. Ghosh, A.K. SenGupta, Use of ArsenXnp, a hybrid anion exchanger, for arsenic removal in remote villages in the Indian subcontinent, React. Funct. Polym. 67 (2007) 1599–1611. https://doi.org/10.1016/j.reactfunctpolym.2007.07.047.

[69] Luis Cumbal, Arup K. SenGupta, Arsenic Removal Using Polymer-Supported Hydrated Iron(III) Oxide Nanoparticles: Role of Donnan Membrane Effect, (2005). https://doi.org/10.1021/es050175e.

[70] M. German, H. Seingheng, A.K. SenGupta, Mitigating arsenic crisis in the developing world: Role of robust, reusable and selective hybrid anion exchanger (HAIX), Sci. Total Environ. 488–489 (2014) 547–553. https://doi.org/10.1016/J.SCITOTENV.2013.10.092.

[71] M. Kunaschk, V. Schmalz, N. Dietrich, T. Dittmar, E. Worch, Novel regeneration method for phosphate loaded granular ferric (hydr)oxide - A contribution to phosphorus recycling, Water Res. 71 (2015) 219–226. https://doi.org/10.1016/j.watres.2015.01.001.

[72] P. Suresh Kumar, W.W. Ejerssa, C.C. Wegener, L. Korving, A.I. Dugulan, H. Temmink, M.C.M. van Loosdrecht, G.J. Witkamp, Understanding and improving the reusability of phosphate adsorbents for wastewater effluent polishing, Water Res. 145 (2018) 365–374. https://doi.org/10.1016/j.watres.2018.08.040.

[73] CRC Handbook of Chemistry and Physics, 97th edition, 2016.

[74] M. Dayah, Periodic Table - Ptable, (1997). https://ptable.com.

[75] E. Murad, MOSSBAUER SPECTROSCOPY OF ENVIRONMENTAL MATERIALS, 2004.

[76] J.W. Morgan, E. Anders, Chemical composition of Earth, Venus, and Mercury, Proc. Natl. Acad. Sci. 77 (1980) 6973–6977. https://doi.org/10.1073/pnas.77.12.6973.

[77] N.N. Greenwood, A. Earnshaw, Chemistry of the Elements, Chem. Elem. (1997) 1997. https://doi.org/10.1016/c2009-0-30414-6.

[78] R.M. Cornell, U. Schwertmann, The Iron Oxides, 2003. https://doi.org/10.1002/3527602097.

[79] P. Suresh Kumar, L. Korving, K.J. Keesman, M.C.M. van Loosdrecht, G.J. Witkamp, Effect of pore size distribution and particle size of porous metal oxides on phosphate adsorption capacity and kinetics, Chem. Eng. J. 358 (2019) 160–169. https://doi.org/10.1016/j.cej.2018.09.202.

[80] M. Kanematsu, T.M. Young, K. Fukushi, D.A. Sverjensky, P.G. Green, J.L. Darby, Quantification of the effects of organic and carbonate buffers on arsenate and phosphate adsorption on a goethite-based granular porous adsorbent, Environ. Sci. Technol. 45 (2011) 561–568. https://doi.org/10.1021/es1026745.

[81] K. Kalaitzidou, M. Mitrakas, C. Raptopoulou, A. Tolkou, P.A. Palasantza, A. Zouboulis, Pilot-Scale Phosphate Recovery from Secondary Wastewater Effluents, Environ. Process. 3 (2016) 5–22. https://doi.org/10.1007/s40710-016-0139-1.

[82] S. Sarkar, P.K. Chatterjee, L.H. Cumbal, A.K. SenGupta, Hybrid ion exchanger supported nanocomposites: Sorption and sensing for environmental applications, Chem. Eng. J. 166 (2011) 923–931. https://doi.org/10.1016/j.cej.2010.11.075.

[83] N.Y. Acelas, B.D. Martin, D. López, B. Jefferson, Selective removal of phosphate from wastewater using hydrated metal oxides dispersed within anionic exchange media, Chemosphere. 119 (2015) 1353–1360. https://doi.org/10.1016/j.chemosphere.2014.02.024.

[84] M. German, H. Seingheng, A.K. SenGupta, Mitigating arsenic crisis in the developing world: Role of robust, reusable and selective hybrid anion exchanger (HAIX), Sci. Total Environ. 488–489 (2014) 547–553. https://doi.org/10.1016/j.scitotenv.2013.10.092.

[85] X. Wang, F. Liu, W. Tan, W. Li, X. Feng, D.L. Sparks, Characteristics of phosphate adsorption-desorption onto ferrihydrite: Comparison with well-crystalline fe (Hydr)oxides, Soil Sci. 178 (2013) 1–11. https://doi.org/10.1097/SS.0b013e31828683f8.

[86] O.K. Borggaard, A.L. Gimsing, B.W. Strobel, Influence of humic substances on phosphate adsorption by aluminium and iron oxides, 127 (2005) 270–279. https://doi.org/10.1016/j.geoderma.2004.12.011.

[87] F.A. Ponce, D.P. Bour, Nitride-based semiconductors for blue and green light-emitting devices, Nature. 386 (1997) 351–359. https://doi.org/10.1038/386351a0.

[88] K. Sivula, R. Van De Krol, Semiconducting materials for photoelectrochemical energy conversion, Nat. Rev. Mater. 1 (2016). https://doi.org/10.1038/natrevmats.2015.10.

[89] K. Zhang, J. Robinson, Doping of Two-Dimensional Semiconductors: A Rapid Review and Outlook, (2019). https://doi.org/10.1557/adv.2019.391.

[90] L.F. Liotta, M. Gruttadauria, G. Di Carlo, G. Perrini, V. Librando, Heterogeneous catalytic degradation of phenolic substrates: Catalysts activity, J. Hazard. Mater. 162 (2009) 588–606. https://doi.org/10.1016/j.jhazmat.2008.05.115.

[91] D.W. Lee, M.S. Lee, J.Y. Lee, S. Kim, H.J. Eom, D.J. Moon, K.Y. Lee, The review of Cr-free Fe-based catalysts for high-temperature water-gas shift reactions, Catal. Today. 210 (2013) 2–9. https://doi.org/10.1016/j.cattod.2012.12.012.

[92] M. Zhu, I.E. Wachs, A perspective on chromium-Free iron oxide-based catalysts for high temperature water-gas shift reaction, Catal. Today. 311 (2018) 2–7. https://doi.org/10.1016/j.cattod.2017.08.042.

[93] S. Rahim Pouran, A.A. Abdul Raman, W.M.A. Wan Daud, Review on the application of modified iron oxides as heterogeneous catalysts in Fenton reactions, J. Clean. Prod. 64 (2014) 24–35. https://doi.org/10.1016/j.jclepro.2013.09.013.

[94] S. Krehula, M. Ristić, S. Kubuki, Y. Iida, L. Kratofil Krehula, S. Musić, The effects of In3+ doping on the properties of precipitated goethite, J. Alloys Compd. 658 (2016) 41–48. https://doi.org/10.1016/j.jallcom.2015.10.191.

[95] H. Liu, T. Chen, R.L. Frost, An overview of the role of goethite surfaces in the environment, Chemosphere. 103 (2014) 1–11. https://doi.org/10.1016/J.CHEMOSPHERE.2013.11.065.

[96] A. Manceau, M.L. Schlegel, M. Musso, V.A. Sole, C. Gauthier, P.E. Petit, F. Trolard, Crystal chemistry of trace elements in natural and synthetic goethite, Geochim. Cosmochim. Acta. 64 (2000) 3643–3661. https://doi.org/10.1016/S0016-7037(00)00427-0.

[97] R. Giovanoli, R.M. Cornell, Crystallization of Metal Substituted Ferrihydrites, Zeitschrift Für Pflanzenernährung Und Bodenkd. 155 (1992) 455–460. https://doi.org/10.1002/jpln.19921550517.

[98] W. Stiers, U. Schwertmann, Evidence for manganese substitution in synthetic goethite, Geochim. Cosmochim. Acta. 49 (1985) 1909–1911. https://doi.org/10.1016/0016-7037(85)90085-7.

[99] R.E. Vandenberghe, A.E. Verbeeck, E. De Grave, W. Stiers, 57Fe Mössbauer effect study of Mn-substituted goethite and hematite, Hyperfine Interact. 29 (1986) 1157–1160. https://doi.org/10.1007/BF02399440.

[100] K. Rout, A. Dash, M. Mohapatra, S. Anand, Manganese doped goethite: Structural, optical and adsorption properties, J. Environ. Chem. Eng. 2 (2014) 434–443. https://doi.org/10.1016/j.jece.2014.01.001.

[101] X. Sun, H.E. Doner, M. Zavarin, Spectroscopy study of arsenite [As(III)] oxidation on Mn-substituted goethite, 1999.

[102] X. Zhang, L. Zhang, Y. Liu, M. Li, X. Wu, T. Jiang, C. Chen, Y. Peng, Mn-substituted goethite for uranium immobilization: A study of adsorption behavior and mechanisms, Environ. Pollut. 262 (2020). https://doi.org/10.1016/j.envpol.2020.114184.

[103] P.G. Belelli, S.A. Fuente, N.J. Castellani, Phosphate adsorption on goethite and Al-rich goethite, Comput. Mater. Sci. 85 (2014) 59–66. https://doi.org/10.1016/j.commatsci.2013.12.030.

[104] E. Murad, U. Schwertmann, The influence of aluminium substitution and crystallinity on the Mössbauer spectra of goethite, Clay Miner. (1983) 301–312.

[105] E. Murad, L.H. Bowen, Magnetic ordering in Al-rich goethites: influence of crystallinity, Am. Mineral. 72 (1987) 194–200.

[106] S.A. Fysh, P.E. Clark, Aluminous goethite: A mössbauer study, Phys. Chem. Miner. 8 (1982) 180–187. https://doi.org/10.1007/BF00308241.

[107] J. Xu, L.K. Koopal, M. Wang, J. Xiong, J. Hou, Y. Li, W. Tan, Phosphate speciation on Al-substituted goethite: ATR-FTIR/2D-COS and CD-MUSIC modeling, Environ. Sci. Nano. 6 (2019) 3625. https://doi.org/10.1039/c9en00539k.

[108] A.C. Scheinost, D.G. Schulze, I. And, U. Schwertmann, Diffuse reflectance spectra of Al substituted goethite: a lingad field approach, 1999.

[109] L.-C. Hsu, Y.-M. Tzou, M.-S. Ho, C. Sivakumar, Y.-L. Cho, W.-H. Li, P.-N. Chiang, H.Y. Teah,

Y.-T. Liu, Preferential phosphate sorption and Al substitution on goethite, Environ. Sci. Nano. 7 (2020) 3497. https://doi.org/10.1039/c9en01435g.

[110] D.C. Golden, L.H. Bowen, S.B. Weed, J.M. Bigham, Mössbauer Studies of Synthetic and Soil-Occurring Aluminum-Substituted Goethites, Soil Sci. Soc. Am. J. 43 (1979) 802–808. https://doi.org/10.2136/sssaj1979.03615995004300040038x.

[111] J. Torrent, U. Schwertmann, V. Barrón, Fast and slow phosphate sorption by goethite-rich natural materials, Clays Clay Miner. 40 (1992) 14–21. https://doi.org/10.1346/CCMN.1992.0400103.

[112] C.C. Ainsworth, M.E. Sumner, Effect of Aluminum Substitution in Goethite on Phosphorus Adsorption: II. Rate of Adsorption, Soil Sci. Soc. Am. J. 49 (1985) 1149–1153. https://doi.org/10.2136/sssaj1985.03615995004900050015x.

[113] D.E. Latta, J.E. Bachman, M.M. Scherer, Fe electron transfer and atom exchange in goethite: Influence of Al-substitution and anion sorption, Environ. Sci. Technol. 46 (2012) 10614–10623. https://doi.org/10.1021/es302094a.

[114] H.D. Ruan, R.J. Gilkes, Kinteics of thermal dehydroxylation of aluminous goethite, 1996.

[115] M. Ma, H. Gao, Y. Sun, M. Huang, The adsorption and desorption of Ni(II) on Al substituted goethite, J. Mol. Liq. 201 (2015) 30–35. https://doi.org/10.1016/J.MOLLIQ.2014.11.024.

[116] W. Li, L. Wang, F. Liu, X. Liang, X. Feng, W. Tan, L. Zheng, H. Yin, Effects of Al3 + doping on the structure and properties of goethite and its adsorption behavior towards phosphate, J. Environ. Sci. (China). 45 (2015) 18–27. https://doi.org/10.1016/j.jes.2015.12.013.

[117] D.C. Champeney, G.R. Isaak, A.M. Khan, Measurement of Relativistic Time Dilatation using the Mossbauer Effect, Nature. 198 (1963) 1186–1187.

[118] H.J. Hay, J.P. Schiffer, T.E. Cranshaw, P.A. Egelstaff, Measurement of the red shift in an accelerated system using the mössbauer effect in Fe57, Phys. Rev. Lett. 4 (1960) 165–166. https://doi.org/10.1103/PhysRevLett.4.165.

[119] W. Kündig, Measurement of the Transverse Doppler Effect in an Accelerated System5, 129 (1962) 2371–2375.

[120] D.W. Schindler, Evolution of phosphorus limitation in lakes, Science (80-.). 195 (1977) 260–262. https://doi.org/10.1126/science.195.4275.260.

[121] L. Carvalho, C. Mcdonald, C. De Hoyos, U. Mischke, G. Phillips, G. Abor Borics, S. Poikane, B. Skjelbred, A.L. Solheim, J. Van Wichelen, A.C. Cardoso, Sustaining recreational quality of European lakes: minimizing the health risks from algal blooms through phosphorus control On secondment from CEH 2 to JRC 1, J. Appl. Ecol. 50 (2013) 315–323. https://doi.org/10.1111/1365-2664.12059.

[122] J.N. Pretty, C.F. Mason, D.B. Nedwell, R.E. Hine, S. Leaf, R. Dils, Environmental costs of freshwater eutrophication in England and Wales, Environ. Sci. Technol. 37 (2003) 201–208. https://doi.org/10.1021/es020793k.

[123] W.K. Dodds, W.W. Bouska, J.L. Eitzmann, T.J. Pilger, K.L. Pitts, A.J. Riley, J.T. Schloesser, D.J. Thornbrugh, Eutrophication of U. S. freshwaters: Analysis of potential economic damages, Environ. Sci. Technol. 43 (2009) 12–19. https://doi.org/10.1021/es801217q.

[124] S.R. Carpenter, Phosphorus control is critical to mitigating eutrophication, Proc. Natl. Acad. Sci. U. S. A. 105 (2008) 11039–11040. https://doi.org/10.1073/pnas.0806112105.

[125] USGS, Mineral commodity summaries 2020, 2020. https://pubs.usgs.gov/periodicals/mcs2020/mcs2020.pdf.

[126] D. Cordell, J.O. Drangert, S. White, The story of phosphorus: Global food security and food for thought, Glob. Environ. Chang. 19 (2009) 292–305. https://doi.org/10.1016/J.GLOENVCHA.2008.10.009.

[127] EC, Circular Economy Action Plan, 2020. https://doi.org/10.7312/columbia/9780231167352.003.0015.

[128] P. Suresh Kumar, T. Prot, L. Korving, K.J. Keesman, I. Dugulan, M.C.M. van Loosdrecht, G.J. Witkamp, Effect of pore size distribution on iron oxide coated granular activated carbons for phosphate adsorption – Importance of mesopores, Chem. Eng. J. 326 (2017) 231–239. https://doi.org/10.1016/j.cej.2017.05.147.

[129] M. Mohapatra, S.K. Sahoo, S. Anand, R.P. Das, Removal of As(V) by Cu(II)-, Ni(II)-, or Co(II)-doped goethite samples, J. Colloid Interface Sci. 298 (2006) 6–12. https://doi.org/10.1016/j.jcis.2005.11.052.

[130] M.A. Wells, R.W. Fitzpatrick, R.J. Gilkes, Thermal and mineral properties of A1-, Cr-, Mn-, Ni- and Ti-substituted goethite, Clays Clay Miner. 54 (2006) 176–194. https://doi.org/10.1346/CCMN.2006.0540204.

[131] S. Krehula, S. Musić, Ž. Skoko, S. Popović, The influence of Zn-dopant on the precipitation of α-FeOOH in highly alkaline media, J. Alloys Compd. 420 (2006) 260–268. https://doi.org/10.1016/J.JALLCOM.2005.10.019.

[132] M. Villacis-Garcia, M. Ugalde-Arzate, K. Vaca-Escobar, M. Villalobos, R. Zanella, N. Martinez-Villegas, Laboratory synthesis of geothite ad ferrihydrite of controlled partocel sozes, Bol. La Soc. Geol. Mex. 67 (2015) 433–446.

[133] Z. Klencsár, Mössbauer spectrum analysis by Evolution Algorithm, Nucl. Instruments Methods Phys. Res. Sect. B Beam Interact. with Mater. Atoms. 129 (1997) 527–533. https://doi.org/10.1016/S0168-583X(97)00314-5.

[134] T. Mahmood, M.T. Saddique, A. Naeem, P. Westerhoff, S. Mustafa, A. Alum, Comparison of different methods for the point of zero charge determination of NiO, Ind. Eng. Chem. Res. 50 (2011) 10017–10023. https://doi.org/10.1021/ie200271d.

[135] W.F. Tan, S.J. Lu, F. Liu, X.H. Feng, J.Z. He, L.K. Koopal, Determination of the point-of-zero charge of manganese oxides with different methods including an improved salt titration method, Soil Sci. 173 (2008) 277–286. https://doi.org/10.1097/SS.0b013e31816d1f12.

[136] Langmuir I, The adsorption of gases on plane surfaces of glass, mica and platinum, Res. Lab. Gen. Electr. Co. (1918). https://pubs.acs.org/sharingguidelines.

[137] H. Freundlich, Über die Adsorption in Lösungen, Zeitschrift Für Phys. Chemie. (1907).

[138] D.S. Tawfik, R.E. Viola, Arsenate Replacing Phosphate: Alternative Life Chemistries and Ion Promiscuity, Biochemistry. 50 (2011) 48. https://doi.org/10.1021/bi200002a.

[139] R.D. Shannon, Revised Effective Ionic Radii and Systematic Studies of Interatomic Distances in Halides and Chalcogenides, Acta Cryst. (1976). https://doi.org/https://doi.org/10.1107/S0567739476001551.

[140] E. Murad, Magnetic properties of microcrystalline iron (III) oxides and related materials as reflected in their Mössbauer spectra, Phys. Chem. Miner. 23 (1996) 248–262. https://doi.org/10.1007/bf00207766.

[141] W. Gosdy, W.J. Orville Thomas, Electronegativities of the elements, J. Chem. Phys. 24 (1956) 439–444. https://doi.org/10.1063/1.1742493.

[142] D.L. Correll, The Role of Phosphorus in the Eutrophication of Receiving Waters: A Review, J. Environ. Qual. 27 (1998) 261–266. https://doi.org/10.2134/jeq1998.00472425002700020004x.

[143] D.W. Schindler, Eutrophication and recovery in experimental lakes: Implications for lake management, Science (80-.). 184 (1974) 897–899. https://doi.org/10.1126/science.184.4139.897.

[144] T.A.H. Nguyen, H.H. Ngo, W.S. Guo, J. Zhang, S. Liang, D.J. Lee, P.D. Nguyen, X.T. Bui, Modification of agricultural waste/by-products for enhanced phosphate removal and recovery: Potential and obstacles, Bioresour. Technol. 169 (2014) 750–762. https://doi.org/10.1016/j.biortech.2014.07.047.

[145] W. Huang, X. Yu, J. Tang, Y. Zhu, Y. Zhang, D. Li, Enhanced adsorption of phosphate by flower-like mesoporous silica spheres loaded with lanthanum, Microporous Mesoporous Mater. 217 (2015) 225–232. https://doi.org/10.1016/j.micromeso.2015.06.031.

[146] K.Y. Koh, S. Zhang, J. Paul Chen, Hydrothermally synthesized lanthanum carbonate nanorod for adsorption of phosphorus: Material synthesis and optimization, and demonstration of excellent performance, Chem. Eng. J. 380 (2020) 122153. https://doi.org/10.1016/j.cej.2019.122153.

[147] W. Gu, X. Li, M. Xing, W. Fang, D. Wu, Removal of phosphate from water by amine-functionalized copper ferrite chelated with La(III), Sci. Total Environ. 619–620 (2018) 42–48. https://doi.org/10.1016/j.scitotenv.2017.11.098.

[148] A. Genz, A. Kornmüller, M. Jekel, Advanced phosphorus removal from membrane filtrates by adsorption on activated aluminium oxide and granulated ferric hydroxide, Water Res. 38 (2004) 3523–3530. https://doi.org/10.1016/j.watres.2004.06.006.

[149] J. Antelo, M. Avena, S. Fiol, R. López, F. Arce, Effects of pH and ionic strength on the adsorption of phosphate and arsenate at the goethite-water interface, J. Colloid Interface Sci. 285 (2005) 476–486. https://doi.org/10.1016/j.jcis.2004.12.032.

[150] R.J. Atkinson, A.M. Posner, J.P. Quirk, Adsorption of potential-determining ions at ferric-aqueous electrolyte interface, J. Phys. Chem. 71 (1967) 550.

[151] R.P.J.J. Rietra, T. Hiemstra, W.H. Van Riemsdijk, Interaction between calcium and phosphate adsorption on goethite, Environ. Sci. Technol. 35 (2001) 3369–3374. https://doi.org/10.1021/es000210b.

[152] R.L. Parfitt, R.J. Atkinson, Phosphate adsorption on goethite (α-FeOOOH), Nature. 264 (1976) 740–742. https://doi.org/10.1038/264740a0.

[153] R. Chitrakar, S. Tezuka, A. Sonoda, K. Sakane, K. Ooi, T. Hirotsu, Phosphate adsorption on synthetic goethite and akaganeite, J. Colloid Interface Sci. 298 (2006) 602–608. https://doi.org/10.1016/j.jcis.2005.12.054.

[154] J. Torrent, V. Barrón, U. Schwertmann, Phosphate Adsorption and Desorption by Goethites Differing in Crystal Morphology, Soil Sci. Soc. Am. J. 54 (1990) 1007–1012. https://doi.org/10.2136/sssaj1990.03615995005400040012x.

[155] S.H. Lin, H.C. Kao, C.H. Cheng, R.S. Juang, An EXFAS study of the structures of copper and phosphate sorbed onto goethite, Colloids Surfaces A Physicochem. Eng. Asp. 234 (2004) 71–75. https://doi.org/10.1016/j.colsurfa.2003.12.005.

[156] M. Li, J. Liu, Y. Xu, G. Qian, Phosphate adsorption on metal oxides and metal hydroxides: A comparative review, Environ. Rev. 24 (2016) 319–332. https://doi.org/10.1139/er-2015-0080.

[157] P.L. Sibrell, G.A. Montgomery, K.L. Ritenour, T.W. Tucker, Removal of phosphorus from agricultural wastewaters using adsorption media prepared from acid mine drainage sludge, Water Res. 43 (2009) 2240–2250. https://doi.org/10.1016/j.watres.2009.02.010.

[158] L. Zhang, Q. Zhou, J. Liu, N. Chang, L. Wan, J. Chen, Phosphate adsorption on lanthanum hydroxide-doped activated carbon fiber, Chem. Eng. J. 185–186 (2012) 160–167. https://doi.org/10.1016/J.CEJ.2012.01.066.

[159] E. Kumar, A. Bhatnagar, W. Hogland, M. Marques, M. Sillanpää, Interaction of inorganic anions with iron-mineral adsorbents in aqueous media - A review, Adv. Colloid Interface Sci. 203 (2014) 11–21. https://doi.org/10.1016/j.cis.2013.10.026.

[160] H. Bacelo, A.M.A. Pintor, S.C.R. Santos, R.A.R. Boaventura, C.M.S. Botelho, Performance and prospects of different adsorbents for phosphorus uptake and recovery from water, Chem. Eng. J. 381 (2020) 122566. https://doi.org/10.1016/j.cej.2019.122566.

[161] A. Drenkova-Tuhtan, M. Schneider, M. Franzreb, C. Meyer, C. Gellermann, G. Sextl, K. Mandel, H. Steinmetz, Pilot-scale removal and recovery of dissolved phosphate from secondary wastewater effluents with reusable ZnFeZr adsorbent @ Fe3O4/SiO2 particles with magnetic harvesting, Water Res. 109 (2017) 77–87. https://doi.org/10.1016/J.WATRES.2016.11.039.

[162] J.B. Forsyth, C.E. Johnson, P.J. Brown, The magnetic structure and hyperfine field of goethite, Philos. Mag. 10 (1968) 713–721. https://doi.org/10.1080/14786436408228489.

[163] E. de Grave, R.E. Vandenberghe, 57Fe Mössbauer effect study of well-crystallized goethite (α-FeOOH), Hyperfine Interact. 28 (1986) 643–646. https://doi.org/10.1007/BF02061530.

[164] F. van der Woude, J. Dekker, Mossbauer effect in a-FeOOH, 181 (1966).

[165] J.F. Hochepied, P. Bonville, M.P. Pileni, Nonstoichiometric Zinc Ferrite Nanocrystals: Syntheses and Unusual Magnetic Properties, J. Phys. Chem. B. 104 (2000) 905–912. https://doi.org/10.1021/jp991626i.

[166] C.N. Chinnasamy, A. Narayanasamy, N. Ponpandian, K. Chattopadhyay, The influence of Fe3 ions at tetrahedral sites on the magnetic properties of nonocrystalline ZnFe2O4, Mater. Sci. Eng. A. 304–306 (2001) 983–987. https://doi.org/10.1016/S0921-5093(00)01611-7.

[167] G.F. Goya, H.R. Rechenberg, M. Chen, W.B. Yelon, Magnetic irreversibility in ultrafine ZnFe2O4 particles, J. Appl. Phys. 87 (2000) 8005–8007. https://doi.org/10.1063/1.373487.

[168] S.J. Stewart, S.J.A. Figueroa, M.B. Sturla, R.B. Scorzelli, F. García, F.G. Requejo, Magnetic ZnFe2O4 nanoferrites studied by X-ray magnetic circular dichroism and Mössbauer spectroscopy, Phys. B Condens. Matter. 389 (2007) 155–158. https://doi.org/10.1016/j.physb.2006.07.045.

[169] E.J. Choi, Y. Ahn, K.C. Song, Mössbauer study in zinc ferrite nanoparticles, J. Magn. Magn. Mater. 301 (2006) 171–174. https://doi.org/10.1016/j.jmmm.2005.06.016.

[170] S. Ammar, N. Jouini, F. Fiévet, Z. Beji, L. Smiri, P. Moliné, M. Danot, J.M. Grenèche, Magnetic properties of zinc ferrite nanoparticles synthesized by hydrolysis in a polyol medium, J. Phys. Condens. Matter. 18 (2006) 9055–9069. https://doi.org/10.1088/0953-8984/18/39/032.

[171] V. Blanco-Gutiérrez, F. Jiménez-Villacorta, P. Bonville, M.J. Torralvo-Fernandéz, R. Sáez-Puche, Synthesis, characterization and conductivity studies of ZnFe 2 O 4 nanoparticles, J. Phys. Chem. C. (2011) 1627–1634. https://doi.org/10.1063/1.4917792.

[172] J.H. Johnston, K. Norrish, A 57fe mossbauer spectroscopic study of a selection of australian and other goethites, Aust. J. Soil Res. 19 (1981) 231–237. https://doi.org/10.1071/SR9810231.

[173] S. Mørup, D.E. Madsen, C. Frandsen, C.R.H. Bahl, M.F. Hansen, Experimental and theoretical studies of nanoparticles of antiferromagnetic materials, J. Phys. Condens. Matter. 19 (2007). https://doi.org/10.1088/0953-8984/19/21/213202.

[174] T. Möller, P. Sylvester, Effect of silica and pH on arsenic uptake by resin/iron oxide hybrid media, Water Res. 42 (2008) 1760–1766. https://doi.org/10.1016/j.watres.2007.10.044.

[175] S. Sarkar, A. Gupta, R.K. Biswas, A.K. Deb, J.E. Greenleaf, A.K. SenGupta, Well-head arsenic removal units in remote villages of Indian subcontinent: Field results and performance evaluation, Water Res. 39 (2005) 2196–2206. https://doi.org/10.1016/J.WATRES.2005.04.002.

[176] L. Cumbal, A.K. Sengupta, Arsenic removal using polymer-supported hydrated iron(III) oxide nanoparticles: Role of Donnan membrane effect, Environ. Sci. Technol. 39 (2005) 6508–6515. https://doi.org/10.1021/es050175e.

[177] Q.J. Zhang, B.C. Pan, X.Q. Chen, W.M. Zhang, B.J. Pan, Q.X. Zhang, L. Lv, X.S. Zhao, Preparation of polymer-supported hydrated ferric oxide based on Donnan membrane effect and its application for arsenic removal, Sci. China, Ser. B Chem. 51 (2008) 379–385. https://doi.org/10.1007/s11426-007-0117-6.

[178] X. Foster, C. Vaneeckhaute, Modifying the resin type of hybrid anion exchange nanotechnology (HAIX-Nano) to improve its regeneration and phosphate recovery efficiency, Npj Clean Water. 4 (2021) 1–8. https://doi.org/10.1038/s41545-021-00142-1.

[179] F.G. Donnan, Zeitschrift fuer Elektrochemie, Ang. Phys. Chem. 17 (1911) 572– 581.

[180] F.G. Donnan, Theory of membrane equilibria and membrane potentials in the presence of non-dialysing electrolytes. A contribution to physical-chemical physiology, J. Memb. Sci. 100 (1995) 45–55. https://doi.org/10.1016/0376-7388(94)00297-C.

[181] S. Sarkar, A.K. Sengupta, P. Prakash, The Donnan membrane principle: Opportunities for sustainable engineered processes and materials, Environ. Sci. Technol. 44 (2010) 1161–1166. https://doi.org/10.1021/es9024029.

[182] D. Clifford, W.J. Weber, THE DETERMINANTS OF DIVALENT/MONOVALENT SELECTIVITY IN ANION EXCHANGERS, React. Polym. 1 (1983) 77–89. https://doi.org/https://doi.org/10.1016/0167-6989(83)90040-5.

[183] S. Subramonian, D. Clifford, Monovalent/divalent selectivity and the charge separation concept, React. Polym. Ion Exch. Sorbents. 9 (1988) 195–209. https://doi.org/10.1016/0167-6989(88)90033-5.

[184] Z. Hubicki, D. Koodynsk, Selective Removal of Heavy Metal Ions from Waters and Waste Waters Using Ion Exchange Methods, Ion Exch. Technol. (2012). https://doi.org/10.5772/51040.

[185] B.D. Martin, L. De Kock, M. Gallot, E. Guery, S. Stanowski, J. MacAdam, E.J. McAdam, S.A. Parsons, B. Jefferson, Quantifying the performance of a hybrid anion exchanger/adsorbent for phosphorus removal using mass spectrometry coupled with batch kinetic trials, Environ. Technol. (United Kingdom). 39 (2018) 2304–2314. https://doi.org/10.1080/09593330.2017.1354076.

[186] K. Hristovski, P. Westerhoff, T. Möller, P. Sylvester, W. Condit, H. Mash, Simultaneous removal of perchlorate and arsenate by ion-exchange media modified with nanostructured iron (hydr)oxide, J. Hazard. Mater. 152 (2008) 397–406. https://doi.org/10.1016/j.jhazmat.2007.07.016.

[187] E. Kociołek-Balawejder, E. Stanisławska, I. Mucha, Freeze dried and thermally dried anion exchanger doped with iron(III) (hydr)oxide – Thermogravimetric studies, Thermochim. Acta. 680 (2019) 178359. https://doi.org/10.1016/j.tca.2019.178359.

[188] S. Bram, M.N. Gordon, M.A. Carbonell, M. Pink, B.D. Stein, D.G. Morgan, D. Aguilà, G. Aromí, S.E. Skrabalak, Y. Losovyj, L.M. Bronstein, Zn2+ Ion Surface Enrichment in Doped Iron Oxide Nanoparticles Leads to Charge Carrier Density Enhancement, ACS Omega. 3 (2018) 16328–16337. https://doi.org/10.1021/acsomega.8b02411.

[189] K. Govardhan, A. Nirmala Grace, Metal/metal oxide doped semiconductor based metal oxide gas sensors - A review, Sens. Lett. 14 (2016) 741–750. https://doi.org/10.1166/sl.2016.3710.

[190] H. Ito, S. Amagasa, N. Nishida, Y. Kobayashi, Y. Yamada, Wet chemical synthesis of zinc-iron oxide nanocomposite, Hyperfine Interact. 238 (2017) 1–5. https://doi.org/10.1007/s10751-017-1442-6.

[191] A. Lassoued, Synthesis and characterization of Zn-doped α-Fe2O3 nanoparticles with enhanced photocatalytic activities, J. Mol. Struct. 1239 (2021) 130489. https://doi.org/10.1016/j.molstruc.2021.130489.

[192] R. Medhi, C.H. Li, S.H. Lee, M.D. Marquez, A.J. Jacobson, T.C. Lee, T.R. Lee, Uniformly Spherical and Monodisperse Antimony- And Zinc-Doped Tin Oxide Nanoparticles for Optical and Electronic Applications, ACS Appl. Nano Mater. 2 (2019) 6554–6564. https://doi.org/10.1021/acsanm.9b01474.

[193] C.L. Warner, W. Chouyyok, K.E. Mackie, D. Neiner, L. V. Saraf, T.C. Droubay, M.G. Warner, R.S. Addleman, Manganese doping of magnetic iron oxide nanoparticles: Tailoring surface reactivity for a regenerable heavy metal sorbent, Langmuir. 28 (2012) 3931–3937. https://doi.org/10.1021/la2042235.

[194] A.K. SenGupta, US7291578B2 Patent-protocol synthesis.pdf, (2007).
[195] S. Lagergren, About the theory of so-called adsorption of soluble substances, K. Sven. Vetenskapsakademiens. 24 (2019) 1–39.
[196] S. Lagergren, Zur theorie der sogenannten adsorption gelöster stoffe, K. Sven. Vetenskapsakademiens. 24 (1898) 1–39.
[197] G. Blanchard, M. Maunaye, G. Martin, Removal of heavy metals from waters by means of natural zeolites, Water Res. 18 (1984) 1501–1507. https://doi.org/10.1016/0043-1354(84)90124-6.
[198] Q. Zhang, B. Pan, W. Zhang, B. Pan, Q. Zhang, H. Ren, Arsenate removal from aqueous media by nanosized Hydrated Ferric Oxide (HFO)-loaded polymeric sorbents: Effect of HFO loadings, Ind. Eng. Chem. Res. 47 (2008) 3957–3962. https://doi.org/10.1021/ie800275k.
[199] J. Zhang, Physical insights into kinetic models of adsorption, Sep. Purif. Technol. 229 (2019) 115832. https://doi.org/10.1016/j.seppur.2019.115832.
[200] S. Azizian, Kinetic models of sorption: A theoretical analysis, J. Colloid Interface Sci. 276 (2004) 47–52. https://doi.org/10.1016/j.jcis.2004.03.048.
[201] T. Mubita, S. Porada, P. Aerts, A. van der Wal, Heterogeneous anion exchange membranes with nitrate selectivity and low electrical resistance, J. Memb. Sci. 607 (2020) 118000. https://doi.org/10.1016/j.memsci.2020.118000.
[202] R.M. Wheaton, W.C. Bauman, Properties of Strongly Basic Anion Exchange Resins, Ind. Eng. Chem. 43 (1951) 1088–1093. https://doi.org/10.1021/ie50497a027.
[203] R.W. Slingsby, C.A. Pohl, Anion-exchange selectivity in latex-based columns for ion chromatography, J. Chromatogr. A. 458 (1988) 241–253. https://doi.org/10.1016/S0021-9673(00)90568-5.
[204] K.J. Powell, P.L. Brown, R.H. Byrne, T. Gajda, G. Hefter, S. Sjöberg, H. Wanner, Chemical speciation of environmentally significant heavy metals with inorganic ligands part 1: The Hg2+-Cl-, OH-, CO32-, so42-, and PO 43- aqueous systems (IUPAC technical report), Pure Appl. Chem. 77 (2005) 739–800. https://doi.org/10.1351/pac200577040739.
[205] Z. Fu, F. Wu, K. Song, Y. Lin, Y. Bai, Y. Zhu, J.P. Giesy, Competitive interaction between soil-derived humic acid and phosphate on goethite, Appl. Geochemistry. 36 (2013) 125–131. https://doi.org/10.1016/j.apgeochem.2013.05.015.
[206] M. Rashid, N.T. Price, M.Á. Gracia Pinilla, K.E. O'Shea, Effective removal of phosphate from aqueous solution using humic acid coated magnetite nanoparticles, Water Res. 123 (2017) 353–360. https://doi.org/10.1016/j.watres.2017.06.085.
[207] J. Antelo, F. Arce, M. Avena, S. Fiol, R. López, F. Macías, Adsorption of a soil humic acid at the surface of goethite and its competitive interaction with phosphate, Geoderma. 138 (2007) 12–19. https://doi.org/10.1016/J.GEODERMA.2006.10.011.
[208] L. Weng, W.H. Van Riemsdijk, T. Hiemstra, Factors Controlling Phosphate Interaction with Iron Oxides, J. Environ. Qual. 41 (2012) 628–635. https://doi.org/10.2134/jeq2011.0250.
[209] M.D.A. Bolland, A.M. Posner, J.P. Quirkk, Zinc adsorption by goethite in the absence and presence of phosphate, Aust. J. Soil Res. 15 (1977) 279–286. https://doi.org/10.1071/SR9770279.
[210] R.L. Penn, J.F. Banfield, Oriented attachment and growth, twinning, polytypism, and formation of metastable phases: Insights from nanocrystalline TiO2, Am. Mineral. 83 (1998) 1077–1082. https://doi.org/10.2138/am-1998-9-1016.
[211] R.L. Penn, J.F. Banfield, Imperfect oriented attachment: Dislocation generation in defect-free nanocrystals, Science (80-.). 281 (1998) 969–971. https://doi.org/10.1126/science.281.5379.969.
[212] F. Huang, H. Zhang, J.F. Banfieldt, Two-stage crystal-growth kinetics observed during hydrothermal coarsening of nanocrystalline ZnS, Nano Lett. 3 (2003) 373–378. https://doi.org/10.1021/nl025836+.
[213] M.A. Anderson, M.I. Tejedor-Tejedor, R.R. Stanforth, Influence of Aggregation on the Uptake Kinetics of Phosphate by Goethite, Environ. Sci. Technol. 19 (1985) 632–637. https://doi.org/10.1021/es00137a009.
[214] J. Zhang, Z. Lin, Y. Lan, G. Ren, D. Chen, F. Huang, M. Hong, A multistep oriented attachment kinetics: Coarsening of ZnS nanoparticle in concentrated NaOH, J. Am. Chem. Soc. 128 (2006) 12981–12987. https://doi.org/10.1021/ja062572a.
[215] H. Yang, X. Zhou, T. Tang, X. Qi, C. Wang, J. Lan, Y. Wang, Y. Yang, G. Liu, Anisotropic growth of multi-twinned goethite particles by oriented aggregation, CrystEngComm. 12 (2010) 4007–4011. https://doi.org/10.1039/c0ce00437e.
[216] T.H. Boyer, A. Persaud, P. Banerjee, P. Palomino, Comparison of low-cost and engineered materials for phosphorus removal from organic-rich surface water, Water Res. 45 (2011) 4803–4814.

https://doi.org/10.1016/j.watres.2011.06.020.
[217] M. Kunaschk, V. Schmalz, N. Dietrich, T. Dittmar, E. Worch, Novel regeneration method for phosphate loaded granular ferric (hydr)oxide - A contribution to phosphorus recycling, Water Res. 71 (2015) 219–226. https://doi.org/10.1016/j.watres.2015.01.001.
[218] E. Virga, Produced water treatment by low fouling polyelectrolyte multilayer based nanofi ltration membranes Research goals, (2012) 665874.
[219] J. de Grooth, R. Oborný, J. Potreck, K. Nijmeijer, W.M. de Vos, The role of ionic strength and odd-even effects on the properties of polyelectrolyte multilayer nanofiltration membranes, J. Memb. Sci. 475 (2015) 311–319. https://doi.org/10.1016/j.memsci.2014.10.044.
[220] M.G. Elshof, W.M. de Vos, J. de Grooth, N.E. Benes, On the long-term pH stability of polyelectrolyte multilayer nanofiltration membranes, J. Memb. Sci. 615 (2020) 118532. https://doi.org/10.1016/j.memsci.2020.118532.
[221] Y.E. Ghoussoub, H.M. Fares, J.D. Delgado, L.R. Keller, J.B. Schlenoff, Antifouling Ion-Exchange Resins, ACS Appl. Mater. Interfaces. 10 (2018) 41747–41756. https://doi.org/10.1021/acsami.8b12865.
[222] M. Pontié, S. Ben Rejeb, J. Legrand, Anti-microbial approach onto cationic-exchange membranes, Sep. Purif. Technol. 101 (2012) 91–97. https://doi.org/10.1016/j.seppur.2012.09.022.
[223] M. Schönhoff, Self-assembled polyelectrolyte multilayers, Curr. Opin. Colloid Interface Sci. 8 (2003) 86–95. https://doi.org/10.1016/S1359-0294(03)00003-7.
[224] M.A. Junker, W.M. de Vos, J. de Grooth, R.G.H. Lammertink, Relating uncharged solute retention of Polyelectrolyte Multilayer nanofiltration membranes to effective structural properties, J. Memb. Sci. 668 (2022) 121164. https://doi.org/10.1016/j.memsci.2022.121164.
[225] C. Tyagi, A. Sharma, Tailoring the optical properties of poly(diallyl dimethyl ammonium chloride) polyelectrolyte by incorporation of 2-mercaptoethanol capped CdSe nanoparticles, J. Phys. D. Appl. Phys. 49 (2016). https://doi.org/10.1088/0022-3727/49/40/405301.
[226] I.W. Mwangi, J. Catherine Ngila, P. Ndungu, A new spectrophotometric method for determination of residual polydiallyldimethylammonium chloride focculant in treated water based on a diazotization-coupledion pair, Water SA. 38 (2012) 707–714. https://doi.org/10.4314/wsa.v38i5.8.
[227] S. Mikhaylin, L. Bazinet, Fouling on ion-exchange membranes: Classification, characterization and strategies of prevention and control, Adv. Colloid Interface Sci. 229 (2016) 34–56. https://doi.org/10.1016/j.cis.2015.12.006.
[228] P. Prakash, A.K. Sengupta, Modeling Al3+/H+ ion transport in Donnan membrane process for coagulant recovery, AIChE J. 51 (2005) 333–344. https://doi.org/10.1002/aic.10312.
[229] P. Prakash, A.K. Sengupta, Selective coagulant recovery from water treatment plant residuals using donnan membrane process, Environ. Sci. Technol. 37 (2003) 4468–4474. https://doi.org/10.1021/es030371q.
[230] S. Mulyati, R. Takagi, A. Fujii, Y. Ohmukai, H. Matsuyama, Simultaneous improvement of the monovalent anion selectivity and antifouling properties of an anion exchange membrane in an electrodialysis process, using polyelectrolyte multilayer deposition, J. Memb. Sci. 431 (2013) 113–120. https://doi.org/10.1016/j.memsci.2012.12.022.
[231] C. Ba, D.A. Ladner, J. Economy, Using polyelectrolyte coatings to improve fouling resistance of a positively charged nanofiltration membrane, J. Memb. Sci. 347 (2010) 250–259. https://doi.org/10.1016/j.memsci.2009.10.031.
[232] V.D. Grebenyuk, R.D. Chebotareva, S. Peters, V. Linkov, Surface modification of anion-exchange electrodialysis membranes to enhance anti-fouling characteristics, Desalination. 115 (1998) 313–329. https://doi.org/10.1016/S0011-9164(98)00051-4.
[233] S. Hong, M. Elimelech, Chemical and physical aspects of natural organic matter (NOM) fouling of nanofiltration membranes, J. Memb. Sci. 132 (1997) 159–181. https://doi.org/10.1016/S0376-7388(97)00060-4.
[234] E. Virga, J. De Grooth, K. Žvab, W.M. De Vos, Stable Polyelectrolyte Multilayer-Based Hollow Fiber Nanofiltration Membranes for Produced Water Treatment, ACS Appl. Polym. Mater. 1 (2019) 2230–2239. https://doi.org/10.1021/acsapm.9b00503.
[235] L. Ouyang, R. Malaisamy, M.L. Bruening, Multilayer polyelectrolyte films as nanofiltration membranes for separating monovalent and divalent cations, J. Memb. Sci. 310 (2008) 76–84. https://doi.org/10.1016/j.memsci.2007.10.031.
[236] H.N. Tran, S.J. You, A. Hosseini-Bandegharaei, H.P. Chao, Mistakes and inconsistencies regarding adsorption of contaminants from aqueous solutions: A critical review, Water Res. 120 (2017) 88–116. https://doi.org/10.1016/j.watres.2017.04.014.

“You can't make everyone Happy.
You're not Pizza.”

Anonymous

Acknowledgements

The Ph.D. journey has been intense. Carrying out a Ph.D. project entails many things and involve many different aspects. Scientifically speaking, it is like a jump into the unknown, which is exciting and stimulating, but also "scary" (at times) and chaotic. Personally, it involves dealing with a lot of stressful situations, unexpected circumstances, expectations, pressure, different people and characters, and so on. Interestingly, most of these things, like pressure and expectations, originate within ourselves, meaning that a Ph.D. students have to learn how to manage people, circumstances, but also (and mostly) themselves. Hence, this Ph.D. journey made me grow both scientifically and personally, which are both great achievements. However, the thing I am most proud of and which is the most precious thing of these years are the people I met and the time I shared with them. I will try to thank everyone who was close and supported me throughout these years, in the good and in the bad times, in the easier and in the tougher moments, during work and in the private life.

I will start with a general thanks to my supervisory team, to giving me the chance to pursue the Ph.D., to providing me the proper guidance and support, both scientifically and personally, especially in the Covid19 times, and for sharing expertise and fun moments. A Ph.D. project is a team effort, a group adventure, in which failures and successes are equally shared, and I am proud to share the credit of this achievement with all of you.

First of all, thanks to thank my daily supervisor at Wetsus, **Leon Korving**. Thanks for having fate in me and supporting me throughout these years. We are definitely different persons, but you helped me making use of my strength, while improving my weaknesses. You helped me growing in all aspects, from the project (and time...) design and management, to managing people, communication and expectations, from the scientific point of view to the application point of view. You were always able to make time even when there seemed to be none. And especially, taking the helicopter, to get a broader view of the topic, especially when I was getting lost in details. Your ability to manage the Phosphate Recovery Theme, creating a pleasant environment for PhDs and researchers, and keeping the companies engaged, was inspiring, and I feel very lucky to have been part of it, and I am eager to continue this collaboration.

Thanks to my promotor **Ekkes Brück** for your availability and for putting me at ease in every meeting, with your joyful and calm approach. You always supported me with your knowledge on structure and properties of matter and tuning my research projects. You always patiently explained me concepts I was less familiar with, without making me feel ashamed for it. I will always remember your openness and support in rediscussing and rearranging the PhD project during the Covid19 breakout. I am looking forward to keeping collaborating with you.

Thanks to my other promotor **Geert-Jan Witkamp**. Your passion for "research for the sake of science" is unique. Not to mention that you still try to go to the lab to perform experiments yourself, and still have great fun! ...I find it impressive and inspiring. A pity that I could not work in close contact with you. However, you provided me lot of support, both at a scientific and personal level. We found out to have several common interests and attitude (since the Wetsus challenge). I am looking forward to visiting your playground lab one day, and to keep collaborating with you.

Thanks to my co-promotor **Iulian Dugulan**, the Mössbauer boss. Although we both had to adapt to the fact that I could not continuously be in Delft, I think we managed to find our equilibrium and eventually connect at a personal level, despite the distance. After Covid19 outbreak, you even proposed to take over the measurements for me (of course to minimize the risk of damages or making a He-powered rocket...), sparing me the hassle to "waste time" in travelling when overwhelmed with the work to recover. I will always appreciate it, as it gave me the necessary tranquility to finish my experiments at Wetsus. Also, you always patiently explained (and repeated) the basic concepts and the most intricated Mössbauer-related features. I hope I provided enough Mössbauer samples, and more are to come!

As I previously mentioned, I was part of the Phosphate Recovery theme at Wetsus. I think I could not be luckier to work with such a great research group, full of supportive, caring and stimulating people. First of all, Thomas... (ehehe need to wait). I will actually start from the old guard. **Prashanth**, my Ph.D. predecessor, with whom I shared the project topic, the haircut, and the passion for music. The way you throw yourselves into new adventures, and all you have achieved inspired me... (not to mention the pressure). Thanks for the support, for setting the starting point of my research with your work, and for the inquisitional discussion that provided be great guidance. Thanks also for all the off-topic conversations, I hope we can keep in contact, and I wish you all the best for the future! **Philipp**, although we did not spend much time together at Wetsus, thanks for the support, great advice, and the funny moments. I am happy you are in Delft now and that we have the chance to collaborate more. **Wokke**, your wisdom from the age distance between us truly inspired me. Our adventure at Wetsus started nearly at the same time, and I am happy to have the chance to work at closer contact with you. You are the king of Wetsus pilots and business challenges! Also, I am happy to share the passion for music (and drums! So happy for that!) with you, and I am looking forward to playing even more! **Nouran**, the first new entry after me, my frist "Ph.D. child" (i will always be your PhD buddy!). Your enthusiasm is incredible (I still remember your first student presentation!), as is your industriousness. Honestly... your innocence too (I know you'll hate me for this). Remember that it is perfectly normal to complain about things. Keep going as you are doing! **Ha**, you are doing a great job with your PhD, overcoming also physical challenges, and one day you will see it too! It gets a smile out to see you living (and walking) at a different pace, in yur world... A special mention for, **Samuele** (good luck with your PhD too!), the boyfriend from Padova <3... that's a plus. "...you are that b... PhD". **Jessica**, finally a lady metalhead in our P-recovery theme! You showed us how many challenges there are in P-recovery when you need to keep things alive... you taught us a lot about lakes, and we can see how much you are passionate about it. I am looking forward to your achievements and satisfactions! **Sophie**, my dear fundamentalist buddy, and cycling and M&M companion. We can count on each other laugh for fundamental nerdy jokes. Conducting fundamental investigation in manure is challenging, shitty at times. We experienced similar PhD-related challenges somehow. With your passion for science, fundamentals and interdisciplinarity, you have everything to successfully finish your PhD! **Milan**, a pity you are not at Wetsus, but with the new projects we will be "closely" collaborating. You have a lot to teach to us on the evil brother of P, As. I am sure you will do great, and I am happy you joined our group! **Simona**, an "adopted" phosphate recovery theme PhD, one of the many compatriots (found out after a whole conversation in English), with such a cheerful attitude and contagious laugh. You had such a speedy start, despite all the around challenges. There will be challenges also along the research path, but with your determination, I am sure you will have no problems dealing with them. Thanks for the nice and funny talks, and the discussion about our Bel Paese, and good luck! **Sabina**, even though you are technically not from Wetsus, it has been a pleasure to meet you and to have scientific exchanges with you, another fundamentalist. I wish you all the best with your research, looking forward to your results! I want to thank and to wish all the best to the whole **ReCaP group** too. It was a pleasure to spend a week with you and a weekend adventure on a ship. Good luck with your projects! Also, a mention to all the students who passed by the Phosphate Recovery theme. **Julie**, le petit

française. The sweetest girl of The Castle. We had so much fun, so many memories, I wish you all the best! **Lordina**, such an energetic student, good luck with your PhD! **Giulia**, "We are from Padova!", "E le nanoplastiche?", "Espressioni venete!". Always at full speed, always there to listen to a friend, to defuse situations, to provide a laugh. And always fighting, despite all the issues, hitches, and life challenges. Thanks for the support, the inspiration and good luck with your PhD. **Jacinta**, the singer in disguise, thanks for the fun! **Emmeline** and **Antoine**, the quiet Frenchies, it was fun to work together with you. And of course, a special mention to the Honour program students I had the chance to co-supervise with Thomas, for two years: **Lyssia**, **Sanne** and **Gabriel**. It has been a great and fun adventure, and very instructive for me as well. I wish you all the best for your future!

And of course, the BSc and MSc students I personally supervised during my PhD. A big thanks for your work, for trusting and accepting to work with me. You can be proud of your work, and the different parts of this thesis testify it. **Amandine**, my first ever student. You helped me refreshing my rusty French (now it's completely lost), while I pushed you to join social events. I think we had a great time together. Your hard-working attitude have really impressed me. All the best for the future. **Varad**, my second student, bright and loud. I am sure you will succeed whatever you will do, good luck with it! **Maddalena**, what a great job you manage to do, despite all the challenges we had, between the hacking and Covid19. I wish you all the best. **Gladys**, it's "Carlo Belloni" speaking! How many laughs did we have in the lab? The project was surely massive and challenging, but we did it. Asante! Good luck with your PhD. **Gwendolina**, another hard working, willing to learn student. Your learning curve was highly rewarding, and you did great. Good luck with your studies!

Of course, a big thank to all the partners of the **Phosphate Recovery theme**. Aquacare, Kemira, Waterschap Brabantse Delta, Waterschijpbedrijf Limburg, Vandcenter Syd, Aquaminerals, and Royal Haskoning DHV. Thanks for all the support, for making the meetings pleasant, with fruitful discussions, and for guiding us in understanding how things work in the real world and society. A special mention for **Koos**, **Pim**, **Raimonda**, and **Jeroen** of Aquacare, for the fruitful discussions, support and motivation you always provided me, and for making us feeling part of the Aquacare family. Also, **Outi**, **Wout**, **Ronald**, and **Bengt** from Kemira, for keeping us involved and the great moments and discussion together.

An unmeasurable thanks to who made the existence of Wetsus possible. **Cees**, **Johannes**, and **Bert**, I would like to thank you for whatever you have done and keep doing for Wetsus, for all the help, inputs, suggestions and feedback you provided me through the years. You showed how cooperation (my favorite value) can make possible the most incredible things!

Thanks to all the staff that supported me throughout these years. **Anke**, **Jan** (check later), **Nynke**, **Alexander**, **Roely**, **Marnejaeke**, **Danique** (check later), **Linda**, **Heleen**, **Hester**, **Anita**, **Jaenette**, **Jannie**, **Trienke**, **Willy**, **Rienk**, **Allard**, **Gerrit**, **Pieter** and everyone I might forget in this moment (sorry, I did my best). Thanks to the lab team and analytical team: **Jan-Willem**, **Mieke**, **Marianne**, **Jelmer**, **Lisette**, **Peter**, **Bianca**, **Agnieska**, **Jippe**, **Marta** (check later). The technical team: **Wim**, **Jan-Jurien**, **Ernst**, **Jan**, **John**, **Wiebe**, **Johan**, and of course my personal technician **Harm**. Thanks for all the support, guidance, patience in helping with my questions, requests, and discussions. Of course, thanks for all the fun moments and laughs. Thanks also to the talent team. **Marlieke** (check later). **JJ** (again!), so many fun moments, you really bring the joy in the work! **Marco**, so many inspiring discussions, you pushed me doing things I never thought I would, and always motivated me. I wish you all the best with your future!

What about office **1.18E**, by far the best office ever! I joined 1 or 2 months later for some reasons... and I felt immediately part of the group. In order of departure. **Deepikaaaaaaaaaa**, it was short, yet we had so much fun, especially when you discovered the spritz! **Elias**, it was short too,

but you always put everyone at ease, it has been a pleasure to meet you, wish all the best to your family! **Terica**, my Queen! How many adventures have we shared, from the nanoworld in the lab, to China and more! Thanks for all the help, support and fun, both at work and in life. Looking forward to more adventures! **Victor T.**, my desk neighbour, and wise guide at Wetsus. Actually... my King too? You have been a mentor, trustworthy colleague, and friend. We share many common interests; I am looking forward to having the chance to work and spend more time with you! **Sebastian**, you always kept the mood high in the office, with great laughs and incredible stories, but also wise advice. I will always remember the great barbeque parties, you always managed to bring everyone together. All the best with finalizing your work! **Ettore**, we shared many moments together, we have been office mates, house mates giving birth to The Castle, I have been your paranymphs and wedding officiant! I will always keep good memory of the many good moments we had. All the best for your new life. **Xiaoxiaaaaaa**! I think in only 5 years of PhD (actually, only counting the first year) "Xiaoxia" is the word I pronounced the most in my whole life! How many great moments have we shared together?! I still cannot believe it! You and Farid are among the closest friends (and best couple) I know. So happy we will continue at Wetsus! **Yujia**, a young Chinese, leaving the husband and children in China to pursue a PhD. And you did it! I mean... the PhD, not the rest of the story. Among the sweetest and kindest PhD in Wetsus. Happy to share more time with you! **Ruben**, our (only) Dutch office mate, watching over us (literally!). You only know how much I admire you! It was great to see how you transformed through the years, from the "I don't understand what you're talking about...", to joining the evil side, with nonsense jokes and the whole package. I wish you all the best, and hopefully we'll manage to work together longer. **Olga**, I should make a long list of compliments, since I know how much you like it. However, I am kind, so I will just do it by voice, in public. I always felt we are the same person, one raised with ravioli, the other with pierogi. I will always remember the desperate and motivational talks, but mostly the great fun moments. Happy you will stay longer at Wetsus! Ángel... espera y espera... **Antony** Antonio Cyril Mdfk Arulrajan, my friend. I still cannot believe I was at your wedding in India, and even less that I am here alive to write about it! We had so much fun, nice words, nice gifts for each other, I can hold them in one hand. Not to mention the great mutual support. Waiting for you to visit Padova, your Saint city! **Vania**, our office mate without age, but surely with lot of laughs to share! We had lot of discussion and lot of fun moments. You also pushed me to acknowledge my own achievements. Hope you will do the same with yours! Nouran (see above). **Yicheng**, the latest and great arrival to our office. It felt like you were part of the group since the very beginning. A bit unfortunate I was not in my best moment, but we will surely have more time to have fun. Good luck with your PhD, I am sure it will be a complete success! And now with the "newly" arrived, **Yizhou** (top pianist!), **Kecen**, **Jack**, keep the traditions of Office 1.18E alive!

Truthfully, my very first office was the writing room, great to start the PhD already feeling the pressure of the writing phase. There I met **Jorrit**, which helped me despite the challenges at work and in life. Eventually, we also manage to enjoy a spontaneous dive in the canals! And **Rik**, man... I will never be thankful enough for the talks, jokes, and fun we had in the beginning. And especially the random laughs at the screen.

Of course, my current office 2.09I. Zia **Cristina**. My caring and energetic Sicilian friend. We shared so many funny moments, especially with the Italian trash. Also, many supportive moments, both sides. A friend always willing to help. I am also happy to have contributed a little making your own(ed) place better. I'm looking forward for more fun moments to come! Xiaoxia (see above). **Ruizhe**, my dear friend and manager, straight to the point, trustworthy, funny, and more caring and supportive than you think. I will miss seeing you dancing or teasing people around. You were honorary member of our office 1.18E. Unfortunately, we did not spend much time in the new office, but I wish you all the best for your future! Last but not least, **Ahmed**! Since the beginning we had a great connection and shared so many interesting, funny, motivational talks. I

think you are a truly inspiring person; welcome to Wetsus, I am looking forward to sharing more time with you!

During my PhD, I have been part of the **PV2019**, best PV ever (no discussions). We organized so many wonderful borrels and activities. I had probably my best year back then. Such a great group. Thomas (again, please, wait!). Xiaoxia (see above). **Chris**, amooooreeeee. My trustworthy German friend (trust, no love). I feel so lucky to have met such a great and inspiring friend, and always available. So much fun, so many great moments. At the top, the escape room. Looking forward to following up on that! All the best for your future, break a leg (not mine... again...)! **Qingdian**, not only the kindest and sweetest PhD ever, but person! I am happy I got to know you more throughout the years and looking forward to the ones to come! **Shuyana**, if you are in the room, it is hard not to notice you, not sure if from the enthusiasm or the voice. Thanks for making the environment cheerful and for being always participatory. A big thanks from me (and whole Wetsus) for bringing the Mindfulness course in. **Mariana**, the Portuguese timebomb. I still remember how you involved me since the beginning (when you were still a student!), and all the nice evenings and moments we shared. Every moment was unpredictable. We had great fun; I will keep memory of that. **Catarina**, a quieter Portuguese, a communication style buddy. We had some great laughs and funny evenings since you were a student. All the best in Delft! **Alicia**, we started together, but different positions at the time. Good luck with finishing your PhD, and thanks for the mindfulness moments! **Jan**, a Wetsus institution. I cannot believe you are not at Wetsus anymore, but I know I have a good friend for a beer... many beers. Thanks for all the fun talks, and the great support! The canteen crew, **Gerben**, **Catharina**, **Riet** and **Karen**. You all greet newcomers by name since the first week (I think I took a year to be able to say "Gerben" decently...). You always have a kind word for everyone and bring a good cheerful mood around; you are always willing to help. Thanks for everything!

Also, I have been part of the **PhD representatives**. It has been a great experience to learn more what is happening at Wetsus, see and touch with my hands how much the board cares about the PhDs and their development. I had the chance to collaborate with many colleagues. Mariana (see above). Thomas (eheh not yet). **Steffen**, I will always remember your lunch box, your enthusiasm, your jokes (also the unintelligible ones), ethic discussions, and time with the band. Good luck with your future (cheers to Cristina)! Ruizhe (see above). **Rita**, we also shared many moments and adventures together! Trips, weddings, house moving, Eurovision nights, and aperitivi! It has been a pleasure knowing you and working with you. Hope to keep in touch for the future!

At Wetsus, I had also the luck to pursue my great music passion. For this, I want to thank the glorious Wetsus band, **Love Monsters**, and in particular to those who pushed me to join at the beginning: Victor T. (see above) and Gonçalo. **Gonçalo**, the bassist, the drummer's best friend, OMG! Thanks for all the motivational talks, funny times, great music moments and for letting me be part of such an important moment in your life, I will always remember it (obrigado Patrícia também! I wish you both a happy life!). **Fabian**, my big German friend, my drumming maestro. I am grateful for all the support, nice talks, and musical moments we shared. I did my best to honor your snare. All the best to you and your family! **Ricardo**, the Portuguese guitarist, PhD competitor (but not really...). Thanks for all the support, the laughs (especially at your bachelor party, not sure if you remember though ahaha), and I am looking forward to more musical exchanges! **Stan**, maaaan you were born with a guitar. So much fun playing with you, always a nice word and easy talks. I miss your dancing while playing! You can Stan! Steffen and Ettore (see above). **Brahzil**, thanks for being such a supportive band member, and for the team building events at your place! Looking forward to play with you again in the future! **Sofia**, another wonderful voice, unfortunately we played too little together, but I honored you keeping a bit of a more rock/metal vibe in the band. **Michele**, what an inspiring guy. Always participative, always there for everyone and anything. I still remember the first talk we had during my recruitment, and of

course, all other amazing discussions. I wish you all the best for your future and upcoming challenges (cheers to Marije)! **Maarten**, the astropiano man, the Ed Sheeran of the band! Always bringing a classical vibe to the building, and some good nerdy jokes, and we shared also nice moments in trips and with cycling. Let see what's next! Wokke and Sophie (see above... it should be the P-band!). Along the way, we also had some guest players. **Mariagiorgia**, damn, what a voice! We had great fun and pushed the band to a new level. Un saluto e in bocca al lupo! Also, **Igy** and **Jens**, thanks for joining and for the great fun! And finally, the big revolution, with the new **Materials&Methods** band! **Marlieke**, our first new singer (where were you?!). Super energetic, always in first lines for jokes and to cheer up, and make the Italian guy be on time (you need to work harder!). **Danique**, another energetic vocalist, always fun to joke with, and when starting, it is hard to stop! And we could already make jokes on that statement :P **Shuoguang**, the metalhead guitarist, the jumping like a spring, bringing extra energy (we will work on making harder songs), and never happy this the number of pedals! Thanks for the positive vibes. **Bruno**, the super chilled, super skilled, super humble guitarist, learning songs and solos on spot, with one go. A guarantee of high performance! I might subscribe to your lessons... And the last arrived singer, **Kestral**, with such a high melodious voice, what a discovery! So che potrei scrivere in italiano, but I will continue in English. We shared many great moments, dinners, cycling, thriving in India, and more to come. Thanks for this and all the support (and sorry for my English. Also, cheers to Prince **Kikko**-Meeko, Lord of Snacks, Keeper of Blankets & Protector of Mom). And finally, **Loes**, another energetic, proactive, member, drummer-to-be, orange justice dancer, and much more. Great addition for the band and for Wetsus. Keep drumming! Thanks everyone for letting me keep cultivating my passion for music, weekly escaping from the PhD reality.

Of course, the whole Old Guard of PhDs! Within couple of borrels you made me feel welcomed and part of the group! The first one I ever met: **Nimmy**. You have been my guide during the Wetsus challenge, always kind... well... maybe not really ahaha but we always had great fun. All the best to you and your family! **Rebeca**, such a great fighter in the lab. Thanks for being always supportive and kind (at an impressive word-pace). Thanks of course for having me at your wedding, I will always keep great memory of it! **Raquel**, a great come back at Wetsus. What an inspiration have you been! I will keep telling the story of you PhD as a true inspiration. Also, thanks all the support. **Karine**, you have been the lab police in my first year, but mostly, you also welcomed me since the very beginning and have always been kind and supportive, especially job-wise. Thanks for all of this, and all the fun within and outside Wetsus (cheers also to **Laurens**, the big, chilled giant. Thanks for the nice easy talks) **Andrew**, I will never thank you enough for having taught of the impostor syndrome and Dunning-Kruger effect since the beginning. This truly helped a lot. Not to mention the moments of fun (and excessive humor). **Paulina**, thanks for the great laughs and great advice! I will keep you posted with the Nobel thingy. **Hector**, the man and The Laugh. My flat mate at the Graspop. Thanks for all the funny moments. Maybe we'll have some horror nights one day! **Hakan**, HaKan, K... You know what I mean. I swear, with a "hand on my heart" (...chest at least), I am happy to have such a great friend. So many jokes, so many fun moments, so many inspiring talks. Keep it up with your Italian! **Kaustub**, brooooh, what'sup?! We had so much fun and so many laughs at Wetsus. We also enjoyed a really cool concert together, sharing opinions movie and soundtrack-wise. See you in Delft again! **Jaap**, always bringing a happy mood, crazy funny guy. Thanks for the support and funny moments. **Victor A.**, ciao bello! Ciao Amico! Such a hard worker and inspirational guy. Thanks for all the great laughs in the lab and the motivational talks. **Natascha**, thanks for all the fun moments, the supportive and motivational talks, the cheerful attitude, and for always being there! **Sandra**, grazie per tutto! Thanks to you as well for the support, for the nice evenings, the great tips, and the crazy stories! Na zdravie! **Mariana** the Mexican ahaha, always with a kind word for everyone, energetic, cheerful (cheers also to **Mark** and the **party-kiddo** ahaha), thanks for it! **Gerwin**, another great, humble musician, and spectrophotometry expert. I will always keep memory of the nice events at your

place, with Brahzil (up!). **Diego**, another Italian PhD-traveling companion. Apparently silent and wise, but we had some great funny talks. Your journey was truly inspiring! **Zexin**, the same goes for you. I wish you and your family all the best. **Ilse**, thanks for always being cheerful and easy to talk with. **Antoine**, thanks for your open smiles and nice talks. **Suyash**! Always kind, with a smile. I will always remember the great times together, especially those in India. All the best to you and your family (cheers to **Indresh**!). **Louis**, the only other French PhD with Thomas, great scientist, great pianist, great to talk to. Thanks for the nice moments at Wetsus, and all the best for you and your family! **Gijs**, what a crazy dude. With all sorts of crazy (and controversial) jokes, but always there to help. I really appreciate the support you gave me, all the best for your future! **Caspar**, the modelling guy, the best animations and simulations I have ever seen in a presentation! Thanks for supporting the PhDs with the programming courses, and thanks for the nice talks during lunches and breaks. **Antonino**, I will count you as old guard, even though you were a visitor. So much fun, exchanging so much knowledge, from trash culture, dialectal expressions... eventually scientific stuff. Cool thing that we will meet at least 3 times a year now. Amala!

A big thanks to all the PhD colleagues met throughout these years. **Emadiiiiii**, one of the Castle's King, the Yemeni Carlo Conti! Man, what a time we spent together, since **Frank**'s house (best house lord in the universe, thanks for all the fun and help, always!), and with **Mark** (hope you are doing fun, also thanks for the support and inspiring talks!). "Is this a cimitery?!" ahahah so many memories man, thanks for having always been there for me, for the inspiring talks, the laughs. All the best with your new adventure, and with your family!!! **Ragne**, also known as "Estonia". From student to researcher to PhD! So many memories, so much fun through these years, especially with your dry humor. Also, thanks for the info about Mexico, for teaching me the Estonian 12 years, for showing me your T-shirt in the most uncomfortable way! **Danieleee**, carissimo, un po' di φ qua? Un piacere ospite to have you at Wetsus. Always bringing great fun wherever you go. Thanks for the many laughs, and the supportive and motivational talks. I swear, I will make that damn pizza one day! **Saaaaam**, heel erg bedankt for your support over these years, really, I owe you a lot for that. Thanks for keeping an eye on this old and random Italian guy. We shared so many adventures man, "that's freaking dope!". Looking forward to new adventures and to perhaps to work together longer... the prodigy guy, give him a PhD project, he will excel, give him a bike, he will cross continents on it without a drop of sweat, and so on... **Jolanda**, the meteo girl, buongiorno! Always impressed by the complexity of your work, thanks for the cheerfulness and mindfulness. **Nandini**, thanks a lot for the nice laughs, and for your inputs and advice for the Indian trip. The whole group owes you for that ahah. Speaking of which, **Sebastian**, que tal? We made it to survive India! One who does not like spicy but can survive it; the other who does like it but cannot survive it. Always there for jokes and chit-chats, and a good amount of good humor. A mention for **Marko**, man, I thought we would have lost you back there in India. Your attitude to try everything was both scary and inspiring... but I surely enjoyed the show. Great musical taste though, all the best! **Elfy**, my second "PhD child", fun, nice and easy to talk to, and always participative. I wish you all the best with your PhD! **Rose**, we started together, I still remember your first question "is it true that Iranians look like Italians?" ahah. Such a hard worker, and always there for a cheerful talk, thanks! **Barbara**, so calm and easy to talk with, thanks for the nice chit-chats, the mindfulness moments. And also, fun to see your comments on the Dutch culture you embraced ahaha. Thanks for always being there for a relaxed talk. **Sara**, kind, always willing to help, always giving out smiles, despite all the challenges you faced. Thanks for that, I wish you all the best of luck for your future! **Lester**, the calm guy you would not expect to hack Wetsus (indeed, he did not... but...). So nice talking and joking with you! **Mu** Lin, the entertainer guy! keep organizing stuff and moving people, you have the skills for that. Thanks for the nice talks and for always checking on everyone. **Roman**, I still remember your hard work to assemble your setup, and now it's shiny and sparkling, literally! So many laughs, so many beers. I wish you the best! **Shih-Shuan**, the machine man, cycling the Elfstedentocht with a one gear bike... kind, quiet, but with the party spirit inside. **Liang-Shin**, always participative and there for a good laugh.

Thanks for the fun! **Edward**, another calm, humble, prodigy guy, always smiling, always easy to talk with. Keep it up Edward! And what about de kleine **Joris** en **Lourens**, two unnoticeable definitely not Dutch guys, but funny as hell. Looking forward to spending more borrels and drink more biertjes with you! **Mirvahid**, providing always positive mood around, available for jokes, but also for interesting talks, from **Farady**, to some overrated cities... Speaking of which, **Talie**! Always interesting discussing about nanoparticles and measurement techniques about your challenging project and talking about music (you have great taste!). All the best of luck! **Berke** and **Pamela**, you are now almost one thing (watch out for these two! ahah), always ready to laugh together and bringing a smile, thanks for that! **Asala**, such a passionate researcher and fighter, highly caring person. Looking forward to learning more from you, thanks for the interesting insights and radiant attitude. **Rodrigo**, always in for hanging out and for some funny moments, perfectly integrated since the very first day (PV trip... I mean...). Thanks for the fun! **Marco**, you have been with us for a little, but you managed to leave quite an impression. Always with a joke, willing to help, highly supportive, ready to rattusing ahah. All the best for your future! And the visiting PhDs, **Giulia** and **Vincenzo** (un altro interista!). Nice to have lunches and talks with you both, despite the unfortunate times.

A big thanks also to all other PhDs I did not have the chance to spend much time with, but I still managed to have for the nice breaks, lunches, talks and laughs, and the more or less newly arrived, which embraced the Wetsus culture: **Gosia**, **Tania**, **Emanuel**, **Antoine**, **Naghme**, **Casper**, **Enas**, **Swarupa**, **Weicher**, **Yang Lei**, **Rutger**, **Sam**, **Ana**, **Ruixuan**, **Arunitha**, **Cao Vinh**, **Olga B.**, **Xiao**, **Dhyana**, **Elorm**, **Evelyn**, **Marijah**, **Mithat**. Looking forward to catching up though!

Thanks to all the postdocs and researchers for the great time together, inside and outside of Wetsus, for all the fun and the support. **Amanda**, such a big heart, always willing to help, super patient, always joking and laughing. **Sara**, we both are not great conversation starter, but eventually we get there ahah, easy to talk and joke with, and slowing down the pace of life. **Carlos** ("Carlos!"), thanks for making things more confusing after 4 years of trying to make people not calling me the Hispanic way. Jokes apart, always fun joking with you. **Sanjay**, so calm, relaxed, it is great to talk to you and to get to know you more! **Roeèl**, thanks for helping me talk about myself ahaha next step is to read about myself... thanks for the fun talks. **Alex**, chers... ches... chees... cheers! I will never be sorry enough for my English, surely not sorry for the EuroCup. Always great fun talking to you!

Thanks to all the supervisors at "the upper floor" (my neighbors now). Thanks for motivating and guiding us (or at least me), each of you with a nice word or advice. First of all, a special thanks to **Renata**, thanks for supporting me during my research and for showing so much interest in my work. **Valentina**, another Italian companion! Humble, fun, all over the place (like me), thanks for the support and for bringing an easy approach to life! **Roel** (great support on work, music, cycling, beers, everything!), **Philipp** (you are my cycling manager now!), **Annemerel** (looking forward to future collaborations!), **Alan** (always amazing inspiring talks), **Slawomir** (always joking, always having a great laugh in the lab), **Tom** ("Remember that PhDs and supervisors are both on the same side"), **Erik** (nice and cheerful talks), **Martijn B.** (crazy jokes and "pecorino"), **Martijn W.** (I love what you do, thanks for the advice on my follow-up), **Doekle** (the audio-tech guy, always there for a nice chit-chat on anything), **Maarten** (modelling expert, sharp and precise, nice to talk to you!), **Luewton** (amazing research, I hope we can play music together some day!), **Caroline** (the glovebox master), **Michel** (Any question? So knowledgeable, so inspiring, so cheerful!), **Lucia** (your laugh precedes you, thanks for being supportive), **Pawel** (alias, Pablo de Romano!), Adam (still my savior, you know!), **Olivier** (you knew Padova... unfortunately maybe... and gave the most epic goodbye of all!), **Inez** (approachable and amazing glass work!), **Jan** (always there for a carrer/life talk), **Elmar** (kind and artistic), **Henk** (nice talks and discussions).

A big thanks to all the students who shared many moments throughout my journey, making it more interesting and funnier. **Laura C.** (eye of the tiger), **Laris(ssss)sa** (and **Andreas**, spaghetti carbonaraaa), **Julie** (up!), **Veronica** (**Monicaaaaa**, chef carbonara!), **Elena** (the fighter), **Inigo** (indigo!), together with Ettore and Emadi, the famous **Castle crew**. We shared many trips and adventures, fun moments, we always supported each other. You made the time we spent together wonderful. I will never thank you enough for that! Hope to see you soon in the future, I wish you all the best in life! Speaking of the Castle, cheers also for **Enrique**, it was short, thanks for the fun, and the great Dutch language exchange ahah. **Felipe** and **Thayse**, a wonderful couple, thanks for all the support, for the nice (and easy) talks, for always being there. I am extremely happy you will be around longer! **Sarahì** and **Sifis**, another great couple, so fun, so unpredictable talks ahaha (pajaretes changed my life). **Nike**, mia compatriota veneta, thanks for the great fun, your honesty and friendship (and fooooood). **Matteo**, er mejo der Colosseo, such a fun, unpredictable, caring and supportive friend, you can achieve everything in life! **Iole** and **Alessandra**, such wonderful and supportive uaglione! I think I need to thank you for something too ehehe. I wish you all the best in life, hope to see you soon! **Amaya**, always welcoming and there to talk about anything, with ease. **Paraschos**, always nice to talk to you, about anything. **Advait** (great fun, and great sufferance in football ahaha, congrats for your PhD!) **Beatriz** (super fun and fastest speaker I know), **Magali** ("Magari magari!", lot of fun and burrate), **Cesar** (your Italian rulez!), **Elena** (compaesana!), **Pauline**, **Lydia**, **Angelo**, **Jeffrey**, **Mark**, **Nick**, **Kevin**, **Anna**, **Hana**, **Emily**, **Alejandro**, **Owen**, **Geert-Jan**, **Sara**, **Filipi**, **Maria**, **Indah**, **Clara**, **Patricìa**, **André**, **Joao**, **José**, **Deimanté**, **Laura C.**, **Laura V.**, **Daniela**, **Michela**, **Gauthier**, **Giulia**, **Antonella**, **Marrit**, **Gabriele**, **Adriana**, **Vanessa**, **Mafalda**, and many, many more. Pricless memories.

Of course, the French Graspop crew, **Laure**, high energy in a confined space, thanks for all the fun. **Jordan**, more calmness in more space, thanks for the fun a being a more chilled anchor when Thomas and Laure are full on! xD

Thanks also to **Ronald** for the guidance in the business-related courses. Also, **Sinead**, which I met at the business development course. It was great working with you, all the best for your future! **Ingrid**, thanks for your commitment in the self-development courses. **Tieneke**, grazie mille for providing me solid bases of Dutch, I have to work way more on it, but I am sure I will succeed eventually! **Uche**, we still need to find an economic agreement! ahaha thanks for the fun talks, and the career advice! **Joost**, thanks for believing in me (us, with Ettore), for the nice business lesson, for putting me at ease at the most stressful and challenging networking event of my life (so far).

A big thank to the academic colleagues who helped me out in different occasion: **Maxim**, my Mössbauer PhD mentor, thanks for always supporting and involving me, helping me not feel a lost stranger at the RID. All the best to you with your life! Also, **Luke**, **Anika**, **Tammo**, and **Mike**, for the support, advice, and involving me with the few hang outs I could join. **Michel**, thanks for the support, for showing me around, the football talks, for always being there. **Kees**, the XRD institution, my only regret is not having worked with you more. Thanks for always being available. **Anton**, **Robert**, **Wiel**, **Jouk**, **Laura R.**, thanks for the technical support and Thanks to **Ilse** and **Nicole**, for supporting me, especially being so far from the RID. **Mark**, thanks for both the fun and inspiring discussions, and all the support. **Miquel**, always kind words, ironic presentations, thanks for helping me out at my first conference! **Wiebe**, your availability to talk and ease of interaction is more unique than rare. I will never thank you enough for your support.

Time pressure and memory might easily trick my forgetful mind. To everyone I might have forget, which crossed my path during my PhD, I want to thank you.

And now, the mighty paranymphs.

Angel, or shall I say Castel Sant'Angelo! We shared so much throughout these years: the office, the house, the parties, dinners and lunches, trips, football games and injuries, football games on tv, cycling adventures and knees pain... climbing was maybe too much at that point... Jokes aside, I feel lucky to have had such an office mate, house mate, and mostly friend to support me and to share fun moments. With you, The Castle finally became a home (thanks also to the tips of the padrino!). You helped me rationalizing the hard moments, pushed me to finally start cycling... I definitely need a push, always. Thanks for the great meals, I will great memory of the many cocido's and fabada's. We had definitely a lot of food ahah and surely lot of fun. Could have been even more epic, but given the circumstance, I think things worked out more than great... I would say "complete scuccess!". Thanks for the support, for being a great host (hola y gracias a toda la familia!), a great colleague and a great friend!

Thomas, mon ami, tutti frutti, sacco di... amoooore! I will never thank you enough. We started talking about everything, well... mostly music, since the recruitment challenge. You gave an immense help to this random and indecisive Italian guy since the very beginning. You pushed me a lot to go out of my comfort zone (for instance, organizing events... you know I'm a great follower... definitely not an initiator...), always providing great support. We also shared a lot of moments throughout the years: parties, dinners, trips, football and volleyball games, concerts, the Graspop... You let me be your paranymph and come to your wedding. I feel grateful for this! We always supported each other, and I think that a consistent part of this work, especially mentally and motivation wise, you can feel it as your own. I am looking forward to continuing working with you and sharing more and more fun events. Allez les Bleus!

I would like to thank all my friends who believed in me and supported me from far throughout these years, both during the easy moments and the toughest ones, and for the great fun/funny moments. The London crew: **David**, **Federica**, **Justine**. I feel I have a second home in London, we shared so many adventures... **Cristina**, per il supporto e la pazienza. Ai colleghi e amici dell'università: **Giulia** & **Marco**, **Michele**, **Mirko**, **Ceci**, **Cesco**, **Michela**, **Giorgio R.**, **Giovanni**, **Dario**, **Mario**, **Roberto**, **Giorgio C.**, **Federica**, **Ionut**, **Boris**, **Diego**, **Carlo**, **Niccolò**, **Giovanni**, **Chiara**, **Tiziana**, e tutti quelli che son stati parte dei miei anni di studi (e sudore... soprattutto sudore...). Gli amici di vecchia data, **Leo**, **Lorenzo**, **Simone**, **Ama**, **Alex**, **Nesa**, **Zanna**, **Marilisa**, grazie del vostro supporto, con voi, una birretta è sempre d'obbligo! Un grazie anche ai famigerati **Winter Dust**, i ragazzi del **Fanta**, del calcetto: **Marco** (Vezz), **Marco** (Mak), **Marco** (Lezze), **Fabio** (Gazzal), **Giulia**, **Dimiz**, **Lej**, **Ratanni**, **Tutric**, **Rozin**, **Glo**, **Giady**, **Caps**, **Denny**, **Gabe**, **Leo**, **Pez**, **Filone**. Grazie di non esservi scordati della vostra montagna... Agli amici di una vita, della famosa **JCK**: **Cellu** & **Paola**, **Kekky** & **Angy**, **Kelfo** & **Reebbhaa**, **Ary**, **Nick** & **Chiarezza**, **Vale**, **Tone**, **Ricky**, grazie per il vostro supporto, per aver creduto in me, ma soprattutto perché ogni volta che ci vediamo, mi sembra di ripartire dal momento in cui sono partito per l'Olanda. E ovviamente i grandissimi momenti svacco e la demenza che ci contraddistingue. **Filippo**, mi conosci da quando sono nato. Grazie per il supporto, le gran chiacchierate, e per le megarisate grasse, i disegni bravi e i bene. Bravi tutti! **Ale Big**! Cuginone, sempre pronti a farci gran risate al telefono e spararne a mille... semo de fameja... A **Marisa**, grazie per le gran chiacchierate e belle parole che hai sempre speso per me, ti devo molto! A tutti gli **amici** che son troppi da nominare: grazie a tutti!

Un immenso grazie ai miei **parenti** e alla mia **famiglia**. Ai miei genitori per avermi supportato e aver creduto in me in tutti questi anni, soprattutto i difficili anni universitari, o quando ho deciso di dedicarmi alla ricerca. Grazie per non avermi mai fatto mancare nulla. Questa tesi la dedico anche ai miei nonni e parenti, vi voglio bene! E anche ai miei fratelli, coi quali condivido il nostro unico neurone. Grazie per il sostegno e i momenti megasvacco. Avere dei fratelli così credo sia tra le più grandi fortune che ho. Detto questo, possiamo tornare a menarci quando ci vediamo! :)

E infine la mia **Laura**, amoooore! "Italiana?" Il più bel regalo che questi anni di PhD mi hanno dato, la mia più grande conquista. Grazie per avermi supportato, ma soprattutto sopportato questi anni, e ancor di più accettato per come sono. Abbiamo passato momenti incredibili insieme, ma abbiamo anche già superato mille disavventure, e questo mi da grandi convinzioni e fiducia per il nostro futuro. Abbiamo superato alla grandissima la convivenza forzata durante il Covid19, fin dall'inizio, abbiamo imparato a conoscere i nostri difetti e limiti aiutandoci a vicenda. Per me, soprattutto la mia memoria e cognizione del tempo... (i limiti dialettali poi...). Mi hai sempre lasciato i miei spazi e incoraggiato in qualunque cosa facessi, dal dottorato alla musica, dallo sport alla dieta (ehm ehm...). Son sicuro che negli anni a venire ci toglieremo ancor più soddisfazioni insieme. Grazie infinite. Ti amo tanto!

PS: Un grazie anche a me, perché sì!

List of publications

Prot, T., Pannekoek, W., **Belloni, C.**, A.I. Dugulan, A.I., Hendrikx, R., Korving, L., van Loosdrecht, M.C.M., 2022, *Efficient formation of vivianite without anaerobic digester: Study in excess activated sludge*, Journal of Environmental Chemical Engineering, 10, 107473.

Submitted: **Belloni, C.**, Korving, L., Witkamp, G.J., Brück, E., Dugulan, A.I., 2023, *Effect of goethite doping using elements with different preferential oxidation states for improved reversible phosphate adsorption*, Journal of Environmental Chemical Engineering.

Submitted: **Belloni, C.**, Korving, L., Witkamp, G.J., Brück, E., Dugulan, A.I., 2023, *Zn induced surface modification of stable goe-thite nanoparticles for improved regenerative phosphate adsorption*, Journal of Colloid and Interface Science.

In submission: **Belloni, C.**, de Jager, P., Korving, L., Witkamp, G.J., Brück, E., Dugulan, A.I., 2023, *FeOOH- and (Fe,Zn)OOH-based hybrid anion exchange adsorbents for phosphate recovery: a thorough determination of Fe-phases and adsorption-desorption mechanisms*.

About the author

Carlo Belloni was born on December 24th in Camposampiero, in the Province of Padova, Italy. He completed his bachelor in Physics in 2014, and the master in Experimental Physics in 2018, both at the Università degli Studi di Padova. The studies covered all of the different Physics branches, from Physics of Matter to Nuclear Physics, from Astrophysics to Fluid Dynamics, and so on. The master graduation thesis *"Plasmonic NanoHole Arrays for label-free Biosensors"* was an experimental investigation on nanostructured biosensors, from synthesis to application, combining the fields of nanophotonics and plasmonics with that of chemistry and biology. After graduation, he worked as a substitute teacher at the professional institute ENAIP in Dolo (Italy), teaching Science.

In 2018, he started the PhD project *"Improved recovery of phosphorus through manipulation of iron phosphorus chemistry using Mössbauer spectroscopy"* under TU Delft, and pursued mainly at Wetsus, in the Phosphate Recovery theme, and at the Reactor Institute Delft, under the supervision of Leon Korving, Ekkes Brück, Geert-Jan Witkamp and Iulian Dugulan. In 2022, at the European Water Technology Week, he was awarded with the by the Wetsus advisory board with the Marcel Mulder Award, for the outstanding achievements in research resulting into a patent application.

The results of his research are presented in this thesis.

“So long, and thanks for all the fish.”

The Hitchhiker's Guide to the Galaxy,
Douglas Adams